PAUL SCHERRER INSTITUT

PSI Proceedings 96-03
November 1996
ISSN 1019-6447

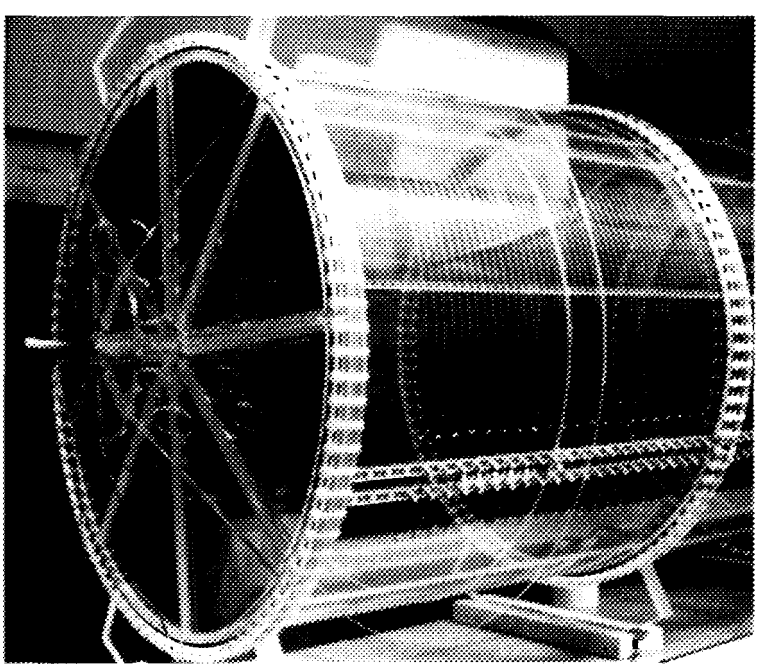

Proceedings of the Summer School on Physics with Neutrinos

Zuoz (Engadin), Switzerland
August 04-10, 1996

PSI-Proceedings 96-03
November 1996

PAUL SCHERRER INSTITUT

Proceedings of the Summer School on Physics with Neutrinos

Zuoz (Engadin), Switzerland

August 4 - 10, 1996

edited by

Milan P. Locher

Sponsored by the

Paul Scherrer Institut

Villigen, PAUL SCHERRER INSTITUT, 1996

PSI-Proceedings 96-03
ISSN 1019-6447
November 1996

Photograph:
Time Projection Chamber of the *MUNU* Collaboration
(courtesy J. Busto)

This publication is available from:
Paul Scherrer Institute
Christine Kunz
Würenlingen and Villigen
CH-5232 Villigen PSI
Switzerland
Telephone: +41 56 310 21 11
Telefax +41 56 310 32 94
E-mail Christine.KUNZ@PSI.CH

EDITOR'S NOTE

The Summer School on PHYSICS WITH NEUTRINOS concentrated on a particularly rewarding topic on the intersection between particle and astrophysics. Although the neutrino has been postulated as early as 1930 in the famous letter by Pauli the intriguing particle poses challenging problems to the present day. The speakers did not spare any effort in creating an atmosphere of stimulating scientific exchange and all those which have contributed to these proceedings are sincerely thanked for taking on the extra burden of writing everything up. The participants young and old enjoyed the presence of Jack Steinberger who presented a talk on the history of the neutrino and contributed in many other ways to the meeting. Apart from the lectures and seminars that are mostly reflected in these proceedings there were also a number of extra seminars on topics ranging from special nuclear reactions to the extinction of life in the universe, adding to the breadth of the presentations.

ACKNOWLEDGEMENT

We are grateful to the directorate of the Paul Scherrer Institute for supporting the long-standing tradition of the Zuoz schools. In setting up the programme the help of R. Rosenfelder (scientific secretary), N. Straumann, F. Thielemann and D. Wyler has been much appreciated. The Lyceum Alpinum helped making us feel at home by offering its traditionally excellent infrastructure. We thank the director, Dr. L. Thali, the administrator A. Pitsch and the staff for continuous hospitality. All the administrative burden connected with the school, including the preparation of the Proceedings has been assumed professionally by our secretary, Christine Kunz. Without her assiduous efforts nothing would have worked.

October 22, 1996 Milan P. Locher

Table of Contents

NEUTRINOS BEYOND THE STANDARD THEORY

S.T. Petcov [1]

Scuola Internazionale Superiore di Studi Avanzati, and
Istituto Nazionale di Fisica Nucleare, Sezione di Trieste, I-34013 Trieste, Italy

ABSTRACT

The current status of the neutrino mass problem is discussed. The established neutrino properties and the existing experimental limits on the intrinsic neutrino properties (mass, electric charge, magnetic moment) are reviewed. The general implications of the nonzero neutrino mass and lepton mixing hypothesis are considered. These include the existence of: neutrino oscillations, lepton flavour changing neutral current (FCNC) processes, neutrinoless double beta decay, and distortion of the ^{3}H β—decay spectrum. The achieved sensitivity in the searches for these processes and effects and the existing indications of lepton mixing are briefly considered. The general theory of neutrino mass generation is reviewed. More specifically, the following topics are discussed: i) Dirac mass term, ii) Majorana mass term, iii) properties of massive Majorana neutrinos, iv) nonstandard massive Dirac and pseudo-Dirac neutrinos, v) Dirac + Majorana mass term (the see-saw mechanism). Examples of neutrino mass generation in the gauge theories of electroweak interaction are given. The theory of neutrino oscillations in vacuum is reviewed. The results of the searches for vacuum oscillations of terrestrial (reactor, accelerator, etc.) and atmospheric neutrinos are presented. The atmospheric neutrino problem and the evidence for neutrino oscillations reported by the LSND experiment are briefly reviewed. Future long base-line oscillation experiments designed to test the neutrino oscillation solution of the atmospheric neutrino problem are considered. Neutrino oscillations in matter are discussed in detail.

---

[1] Also at: Institute of Nuclear Research and Nuclear Energy, Bulgarian Academy of Sciences, 1784 Sofia, Bulgaria.

Most of the material covered in the lectures can be found in published reviews, books and recent articles. A suggestive but incomplete list is given below.

The closest in content and spirit to my lectures is the review article:

1. S.M. Bilenky and S.T. Petcov, "Massive Neutrinos and Neutrino Oscillations", Rev. Mod. Phys. 59 (1987) 671.

A beautiful discussion of neutrino oscillations is given in:

2. S.M. Bilenky and B. Pontecorvo, Phys. Rep. 41 (1978) 225.

A detailed discussion of the general theory of neutrino mass generation and of the properties of massive Dirac and massive Majorana neutrinos can be found also in:

3. B. Kayser, "The Physics of Massive Neutrinos", World Scientific, Singapore, 1989.

4. R.N. Mohapatra and P. Pal, "Massive Neutrinos in Physics and Astrophysics", World Scientific, Singapore, 1991.

For an extensive and rather complete discussion of the current status of the atmospheric neutrino problem see, e.g.:

5. T.K. Gaisser, F. Halzen and T. Stanev, Phys. Rep. 258 (1995) 173.

The results of the LSND collaboration have been published in:

6. C. Athanassopoulos et al., Phys. Rev. Lett. 75 (1995) 2650, and Los Alamos Nat. Lab. report LA-UR-96-1326; see also: J.E. Hill, Phys. Rev. Lett. 75 (1995) 2654.

A rather complete discussion of the long base-line neutrino oscillation experiments can be found in:

7. P. Monacelli, "Long Base Line Neutrino Oscillation Experiments at Accelerators", and A. Baldini, "Long Base Line Neutrino Experiments at Reactors", in Proc. of the 7th Int. Workshop on Neutrino Telescopes, February 26 – March 1, 1996, Venice, Italy (ed. M. Baldo Ceolin, Univ. of Padua, 1996), pp. 351 and 359.

There exist numerous review articles on the current status of the solar neutrino problem. See, for example:

8. W. Haxton, Ann. Rev. Astr. Astrophys. 33 (1995) 459; S.T. Petcov, Nucl. Phys. B (Proc. Suppl.) 43 (1995) 12.

For a detailed discussion of the matter-enhanced neutrino oscillations as well as of the analytic description of the MSW effect for the solar neutrinos see, e.g., ref. [2] from the above list as well as, e.g.,

9. S.P. Mikheyev and A.Yu. Smirnov, Prog. Part. Nucl. Phys. 23 (1989) 41; S.T. Petcov, Nucl. Phys. B (Proc. Suppl.) 13 (1990) 527 and the articles quoted therein.

The possible interpretation of the solar neutrino data, atmospheric neutrino anomaly and/or the LSND results in terms of neutrino matter-enhanced (MSW) transitions and/or vacuum oscillations has been discussed by many authors; see, for example:

10. S.T. Petcov and A.Yu. Smirnov, Phys. Lett. 322B (1994) 109; D.O. Caldwell and R.N. Mohapatra, Phys. Lett. 354B (1995) 371, Phys. Rev. D48 (1993) 3259 and D50 (1994) 3477; G.L. Fogli et al., Phys. Rev. D49 (1994) 3626 and D52 (1995) 5334, Astropart. Phys. 4 (1995) 177; G. Raffelt and J. Silk, Phys. Lett. 366B (1996) 429; S.M. Bilenky et al., Phys. Rev. D54 (1996) 4432.

Finally, for the current limits on the neutrino intrinsic properties, lepton FCNC processes, neutrinoless double beta decay and neutrino oscillation parameters consult the latest edition of the Particle Data Group.

STANDARD PHYSICS SOLUTION TO THE SOLAR NEUTRINO PROBLEM ?

Arnon Dar
Department of Physics
and
Asher Space Research Institute
Technion-Israel Institute of Technology
Haifa 32000, Israel

November 4, 1996

Abstract

The ^{8}B solar neutrino flux predicted by the standard solar model (SSM) is consistent within the theoretical and experimental uncertainties with that observed at Kamiokande. The Gallium and Chlorine solar neutrino experiments, however, seem to imply that the ^{7}Be solar neutrino flux is strongly suppressed compared with that predicted by the SSM. If the ^{7}Be solar neutrino flux is suppressed, still it can be due to astrophysical effects not included in the simplistic SSM. Such effects include short term fluctuations or periodic variation of the temperature in the solar core, rotational mixing of ^{3}He in the solar core, and dense plasma effects which may strongly enhance p-capture by ^{7}Be relative to e-capture. The new generation of solar observations which already look non stop deep into the sun, like Superkamiokande through neutrinos, and SOHO and GONG through acoustic waves, may point at the correct solution. Only Superkamiokande and/or future solar neutrino experiments, such as SNO, BOREXINO and HELLAZ, will be able to find out whether the solar neutrino problem is caused by neutrino properties beyond the minimal standard electroweak model or whether it is just a problem of the too simplistic standard solar model.

1 Introduction

Solar neutrinos have been detected on Earth in four pioneering solar neutrino ($\nu_\odot$) experiments, in roughly the expected numbers, demonstrating that the sun is indeed powered by fusion of hydrogen into helium. However the precise counting rates in the $\nu_\odot$ experiments (e.g., Hampel, this proceedings) are approximately one half that predicted by the Standard Solar Model (SSM). This discrepancy, which has persisted for 30 years, has become known as the solar neutrino problem (SNP). It has attracted much attention of both astrophysicists and particle physicists for two main reasons. First, astrophysicists were surprised to find out that the sun, and in particular the nuclear reactions in its core, are not accurately described by the simple SSM. Second, particle physicists found that natural extensions of the minimal standard electroweak model (SEM) can solve elegantly the SNP. However when astronomers had a closer look at the sun through helioseismology, X-ray and UV observations it turned out to be "a bewildering turmoil of complex phenomena", showing unexpected features and behavior at any scale. It has a strange complex internal rotation, unexplained magnetic activity with unexplained 11 year cycle, unexpected anomalies in its surface elemental abundances, unexplained explosions in its atmosphere and unexplained mechanism that heats its million degree corona and accelerates the solar wind. Perhaps the surface of the sun is complex because we can see it and the center of the sun is not only because we cannot? Perhaps the SSM which has been improved continuously over the past three decades (see e.g., Clayton 1968, Bahcall 1989), which still assumes an exact spherical symmetry, no mass loss or mass accretion, no angular momentum loss or gain, no differential rotation and zero magnetic field through the entire solar evolution, is a too simplistic picture and does not provide a sufficiently accurate description of the core of the sun and/or the neutrino producing reactions there?

Indeed, here I will show that the solar neutrino problem does not provide solid evidence for neutrino properties beyond the SEM and that standard physics solutions to the SNP are possible. In particular I will argue that:
1. There is no ^{8}B solar neutrino problem.
2. Only observations of spectral distortions and/or flavor change of $\nu_\odot$'s in future $\nu_\odot$ experiments, like Superkamiokande, SNO, Borexino and HELLAZ may establish that neutrino properties beyond the SEM are responsible for

the SNP.
3. There is no solid evidence for a real deficit of ^{7}Be solar neutrinos
4. A real deficit of ^{7}Be solar neutrinos, if there is one, may still be explained by standard physics and/or astrophysics.
5. The major three new solar observatories, which are already running and looking into the solar interior, the Superkamiokande solar neutrino observatory that began taking data on April 1, 1996, the solar heliospheric observatory (SOHO) that was launched on December 2, 1995 and is now observing the sun non stop, and the ground based telescopes in the Global Oscillations Network Group (GONG) which have just begun observing solar oscillations around the clock, may very soon point at the correct solution to the SNP (for general reviews see Science, 31 May 1996).

2 Is There a ^{8}B Solar Neutrino Problem?

Table I presents a comparison between the solar neutrino observations and the SSM predictions of Bahcall and Pinsonneault 1995 (BP95) and of Dar and Shaviv 1996 (DS96). Although BP (and some other similar SSM calculations) predict a ^{8}B solar neutrino flux that is approximately 2.4 larger than observed by Kamiokande (see Hampel, this proceedings), DS predict a flux consistent with that observed by Kamiokande. The differences between BP and DS are summarized in Table II (for details see Dar and Shaviv 1996). The difference between the predicted ^{8}B flux are mainly due to the use of updated nuclear reaction rates by DS, differences in the calculated effects of diffusion, differences in the initial solar composition assumed in the two calculations and the use of an improved equation of state by DS. They reduce the predicted ^{8}B flux by approximate factors of 0.55, 0.81, 0.95 and 0.96, respectively (the remaining differences are mainly due to inclusion of partial ionization effects, premain sequence evolution and deviations from complete nuclear equilibrium by DS which were neglected by BP, and due to different numerical methods, fine zoning and time steps used in the two calculations):
Nuclear Reaction Rates: The uncertainties in the nuclear reaction rates at solar conditions are still large due to (1) uncertainties in the measured cross sections at laboratory energies, (2) uncertainties in their extrapolations to solar energies, (3) uncertainties in dense plasma effects (screening, correlations and fluctuations) on reaction rates. Rather than averaging mea-

sured cross sections that differ by many standard deviations, DS used for the extrapolation only the most recent and consistent measurements of the relevant nuclear cross sections. Because sub-Coulomb reactions take place when the colliding nuclei are far apart, the Optical Model and the Distorted Wave Born Approximation give a reliable description of their energy dependence. DS have used them for extrapolating measured sub-Coulomb cross sections to solar energies. BP preferred to rely on published extrapolations of averaged cross sections based on energy dependences calculated from sophisticated microscopic nuclear reaction models (e.g. Johnson et al 1992). Similar screening corrections (which by accidental cancellation have a very small net effect on $\phi_{\nu_\odot}(^8\mathrm{B})$) have been used by DS and BP. The updated "astrophysical S factors" which were used by DS are listed in Table II. They reduce the BP predictions by approximately a factor of 0.55 .

Diffusion: Diffusion, caused by density, temperature, pressure, chemical composition and gravitational potential gradients play an important role in the sun since it modifies the local chemical composition in the sun. The relative changes in SSM predictions due to diffusion of all elements are summarized in Table III. While BP found a rather large increases in the predicted ^{7}Be, ^{8}B, ^{13}N, ^{15}O and ^{17}F solar neutrino fluxes; 14%, 36%, 52%, 58%, and 61% which result in 36%, 33%, 9% increases in their predicted rates in Kamiokande, Homestake, and in GALLEX and SAGE, respectively, DS found only a moderate increase due to diffusion, 4%, 10%, 23%, 24% and 25%, respectively, in the above fluxes, which result in 10%, 10% and 2% increase in the predicted rates in Kamiokande, Homestake, and in GALLEX and SAGE, respectively. Although the two diffusion calculations assumed a different initial solar chemical composition (see below) and BP approximated the diffusion of all elements heavier than ^{4}He by that of fully ionized iron (the DS calculations followed the diffusion of each element separately and used diffusion coefficients calculated for the actual ionization state of each element at each shell in the sun as obtained from solving the local Saha equations), these cannot fully explain the above large differences. Recent independent diffusion calculations by Richard et al. (1996) obtained similar results to those obtained by DS as can be seen from Table III (we interpolated the results from the two models of Richard et al. to the initial chemical composition assumed by DS).

Initial Chemical Composition: The initial chemical composition influences significantly the solar evolution and the present density, chemical com-

position and temperature in the solar core, which determine the solar neutrino fluxes. In particular, the calculated radiative opacities, which in turn determine the temperature gradient in the solar interior, are very sensitive to the heavy elements abundances (the heavy elements are not completely ionized in the sun). Apart from the noble gases, only a few elements such as H, C, N and O, which were able to form highly volatile molecules or compounds, have escaped complete condensation in primitive early solar system meteorites (see, e.g., Sturenburg and Holweger 1990). Thus, the initial solar abundances of all other elements are expected to be approximately equal to those found in type I carbonaceous chondrites as a result of their complete condensation in the early solar system. Since the chemical composition of the solar surface is believed to have changed only slightly during the solar evolution (by nuclear reactions during the Hayashi phase, by diffusion and turbulent mixing in the convective layer during the main sequence evolution, and by cosmic ray interactions at the solar surface) it has been expected that the photospheric abundances of these elements are approximately equal to those found in CI chondrites. Over the past decades there have been many initial disagreements between the meteoritic and photospheric abundances. In nearly all cases, when the atomic data were steadily improved and the more precise measurements were made, the photospheric values approached the meteoritic values. The photospheric abundances are now as a rule in very good agreement with the meteoritic values (Grevesse and Noels 1991; 1993). Since the meteoritic values represent the initial values and are known with much better accuracy (often better than 10%) than the photospheric ones, DS assumed that the initial solar heavy metal abundances are given approximately by the meteoritic (CI chondrites) values of Grevesse and Noels (1993) and adjusted the initial CNO and Ne abundances to reproduce their observed photospheric abundances. Also the unknown initial ^{4}He solar abundance has been treated as an adjustable parameter. DS "predicted" its present photospheric mass fraction to be $Y = 0.238 \pm 0.05$ in good agreement with the ^{4}He surface mass fraction inferred from helioseismology: $Y_s = 0.242 \pm 0.003$ (Hernandez and Christensen-Dalsgaard 1994. However, their formal error is highly misleading because of the great sensitivity of the result to the model of the solar atmosphere, the equation of state there and the atmospheric opacities. We estimate that at present the ^{4}He mass fraction at the solar surface is not known from helioseismology better than $Y_s = 0.242 \pm 0.010$). BP adjusted the initial solar composition to reproduce the present day surface

abundances which, except for the CNO and the nobel gases, were assumed to be represented by their meteoritic values.

The photospheric abundances of ^{7}Li, ^{9}Be and ^{11}B are smaller by a factor of nearly 150, 3 and 10, respectively, than their meteoritic abundances. The origin of such large differences is still not clear. They cannot be explained by nuclear burning during the Hayashi phase although significant Lithium burning does takes place during this phase. They may be explained by rotational mixing (e.g., Richard et al 1996). Although the initial solar (meteoritic) abundances of Lithium, Beryllium and Boron are very small and do not play any significant role in solar evolution their depletion perhaps can provide a clue to the real history of the convection zone and the sun.

Equation of State: The equation of state is used to calculate the local density and temperature required to balance the gravitational pressure in the sun. Since the neutrino producing reactions in the sun depend strongly on temperature, their predicted fluxes depend strongly on the equation of state. DS have used an updated equation of state which is described in detail in DS96. It is consistent with the new OPAL equation of state (Rogers et al. 1996) The use of an improved equation of state reduce significantly our 1994 solar neutrino fluxes and improves the agreement between the sound speed in the solar core that we calculated from our SSM and the sound speed that is extracted from helioseismology. The agreement with the updated sound speed from helioseismology (Christensen Dalsgaard, 1996) is better than 2×10^{-3}, as is demonstrated in Fig. 1. It is significantly better than the agreement obtain/reported by other SSM calculations.

3 Evidence For ν_e Properties Beyond the Minimal SEM?

Counting rates in $\nu_\odot$ experiments are formally given by

$$R = N_A \Sigma_i \phi_{\nu_\odot}(i) \int_{E_0} (dn_{\nu_i}/dE) \sigma_{\nu A}(E) dE \qquad (1)$$

where N_A is the number of "active" atoms in the detector, $\sigma_{\nu A}(E)$ is their cross section for neutrinos with energy E, dn_{ν_i}/dE is the normalized energy spectrum of neutrinos from reaction i in the sun and $\phi_{\nu_\odot}$ is their total flux.

Both, dn_{ν_i}/dE and $\sigma_{\nu A}$ follow directly from the standard electroweak theory and are independent of the sun. (dn_{ν_i}/dE is practically the standard β-decay spectrum for the β-decays $2p \rightarrow De^+\nu_e$, $^8B \rightarrow 2\alpha e^+\nu_e$, $^{13}N \rightarrow ^{13}Ce^+\nu_e$ and $^{15}O \rightarrow ^{15}Ne^+\nu_e$ and is a δ-function for the electron captures $e^7Be \rightarrow \nu_e^7Li$ and $pep \rightarrow D\nu_e$.) Thus *conclusive evidence* for new electroweak physics can be provided only by detecting at least one of the following signals:

1. Spectral distortion of the fundamental β-decay spectrum.
2. Solar neutrino flavors other than ν_e.
3. A clear violation of the luminosity sum rule.
4. Rates which require negative $\phi_{\nu_\odot(i)}$.

So far, no such clear evidence has been provided by the $\nu_\odot$ experiments.

Spectral Distortions: Until recently, only Kamiokande could test whether the spectrum of their detected $\nu_\odot$'s is consistent with the ν_e spectrum from β-decay of ^8B. Kamiokande observed an electron recoil spectrum from $\nu_\odot e$ interactions which is consistent, within their limited statistics, with that expected from an undistorted ^8B solar neutrino spectrum. Superkamiokande, which has been running since April 1, 1996, will soon have much larger statistics (See Hampel these proceedings).

Neutrino Oscillations: Neutrino oscillations or neutrino helicity flip can explain the solar neutrino observations (see Petcov, this proceedings). However, no time variation which is predicted by a magnetic helicity flip has been detected by the $\nu_\odot$ experiments, nor could the experiments detect (Homestake, GALLEX and SAGE) or distinguish (Kamiokande) between different neutrino flavors. Superkamiokande will soon examine with a high level of sensitivity (real time, high statistics) whether the ^8B solar neutrino flux is time dependent while only future experiments like SNO will be able to detect other neutrino flavors (the sensitivity of Superkamiokande to temporal variation in the solar neutrino flux will be demonstrated by measuring the annual variation of the flux due to the annual variation of the distance of Earth from the sun).

The Solar Luminosity Sum Rule: If the sun derives its energy from fusion of Hydrogen into Helium and *if it is in a steady state* where its nuclear energy production rate equals its luminosity, then conservation of baryon number, electric charge, lepton flavor and energy requires that the total solar neutrino

flux at Earth satisfies (e.g., Dar and Nussinov 1991):

$$\phi_{\nu_\odot} = \frac{2L_\odot}{Q - 2\bar{E}_\nu} \frac{1}{4\pi D^2} \geq 6.52 \times 10^{10}\ cm^{-2}s^{-1}\ , \qquad (2)$$

where $D \approx 1.496 \times 10^{13}\ cm$ is the distance to the sun, $Q = 26.733\ MeV$ is the energy released when four protons fuse into Helium, $\bar{E}_\nu = \sum E_{\nu_i}\phi_{\nu_i} / \sum \phi_{\nu_i}$ is the average energy of solar neutrinos and $\bar{E}_\nu \geq 0.265\ MeV$ if the pp reaction in the sun produces $\nu_\odot$'s with the smallest average energy. Eq. (2) can be rewritten as a luminosity sum rule:

$$\Sigma_i (Q/2 - \bar{E}_{\nu_i})\phi_{\nu_i} = S, \qquad (3)$$

where $S = L_\odot / 4\pi D^2 = 1367\ W\ m^{-2}$ is the solar "constant". A clear Violation of eq. (2) or the solar luminosity sum rule, can prove that lepton flavor is not conserved. In this conference the Gallium experiments with the low energy threshold of 233 keV, which makes them sensitive to almost all the SSM neutrinos, reported updated time-averaged capture rates of $70 \pm 8\ SNU$ in GALLEX (Hampel, this proceedings) and $72 \pm 12\ SNU$ in SAGE (see Hampel, this proceedings). These new smaller rates are still consistent within the experimental uncertainties with $76 \pm 2\ SNU$, the "minimal" signal expected from eq. (2) and $\sigma_{Ga} = (1.18 \pm 0.02) \times 10^{45}\ cm^{-2}$, if all the $\nu_\odot$'s were pp ν's. However, the ^{8}B solar neutrino flux measured in Kamiokande, $\phi_{\nu_\odot} = (2.8 \pm 0.4) \times 10^6\ cm^{-2}$, contributes another $7 \pm 2\ SNU$ which increase the minimal expected signal in Gallium to 83 ± 3 SNU. This somewhat larger rate is still consistent within 2σ with the capture rates measured by GALLEX and SAGE, in particular if their rates are "recalibrated" by their new Cr source experiments (see Hampel, this proceedings). But the Gallium experiments leave no room for significant (SSM-like) contributions from ^{7}Be and CNO solar neutrinos. This confirms the combined results from the Chlorine experiment at Homestake (see Hampel, this proceedings) and the Kamiokande experiment (see Hampel, this proceedings):

The Missing $\nu_\odot$'s: Althogh the ^{37}Cl experiment with an energy threshold of 814 keV is completely blind to the pp solar neutrinos it is sensitive to both the ^{8}B neutrinos and the lower energy *pep*, CNO and ^{7}Be neutrinos. However, while the expected signal from a ^{8}B solar neutrino flux alone as measured by Kamiokande is $3.08 \pm 0.53\ SNU$, the time-averaged counting rate in the ^{37}Cl experiment is $2.56 \pm 0.25\ SNU$ (see Hampel, these proceedings. Although

the ^{37}Cl experiment has not been "calibrated" with a neutrino source, the Cr source experiments of GALLEX and SAGE suggest that the accuracy of the radiochemical experiments is probably of the order of 10%, or better. Consequently, although the joint results from Homestake and Kamiokande do not provide solid evidence for "new electroweak physics" (e.g., Bahcall and Bethe 1991) they do indicate that the combined contributions from ^{7}Be, CNO and pep solar neutrinos is strongly suppressed in ^{37}Cl compared with their SSM estimated contribution.

4 Are ^{7}Be Solar Neutrinos Missing?

Electron capture by ^{7}Be into the ground state of ^{7}Li produces 862 keV neutrinos. The threshold energy for neutrino absorption by ^{37}Cl is 814 keV. Thus, absorption of ^{7}Be neutrinos by ^{37}Cl produces 48 keV electrons. The maximum energy of the pp solar neutrinos is 420 keV. The threshold energy for neutrino absorption in ^{71}Ga ($3/2^-$) is 233 keV into the ground state ($1/2^-$) and 408 into its first excited state ($5/2^-$). The produced electrons have therefore energies below 187 and 12 keV, respectively. If the theoretical cross sections for neutrino absorption near threshold overestimate significantly their true values then the predicted rates will significantly overestimate the expected signals in the Chlorine and Gallium experiments.

An indication that final state interactions effects are not completely understood is provided by Tritium β-decay. Although final state interactions in Tritium β-decay have been studied extensively, they do not explain well the end-point β-decay spectrum ($E_e \sim 18.6\ keV$). In all recent measurements, the measured spectrum yields a negative value for the fitted squared mass of the electron neutrino (see, e.g., Holzschun, this proceedings). Final state interactions effects (screening of the nuclear charge by atomic electrons, exchange effects, radiative corrections, nuclear recoil against the electronic cloud, etc) in neutrino captures near threshold in ^{37}Cl and ^{71}Ga may be much larger because their Z values are much larger and because the de Broglie wave lengths of the produced electrons are comparable to the Bohr radii of the atomic K shells in Cl and Ga. If final state interactions reduce considerably the near threshold absorption cross sections of pp neutrinos in ^{71}Ga (making room for the expected contribution of ^{7}Be solar neutrinos in Gallium) and

of ^{7}Be neutrinos in ^{37}Cl, perhaps they can make the solar neutrino observations of Kamiokande and the Homestake experiment compatible. Such an explanation of the solar neutrino problem implies that experiments such as BOREXINO and HELLAZ will observe the full ^{7}Be solar neutrino flux.

5 Astrophysical Solutions To The SNP

Even if the ^{7}Be solar neutrino flux is strongly suppressed, it does not eliminate standard physics solutions to the solar neutrino problem:

The ratio between the fluxes of ^{7}Be and ^{8}B solar neutrinos is given by

$$R = \frac{\phi_{\nu_\odot}(^7\mathrm{Be})}{\phi_{\nu_\odot}(^8\mathrm{B})} = \frac{\int n_e n_7 < \sigma v >_{e7} 4\pi r^2 dr}{\int n_p n_7 < \sigma v >_{p7} 4\pi r^2 dr}. \quad (4)$$

Because of the decreasing temperature and Be7 abundance as function of distance from the center of the sun on the one hand, and the $\sim r^2$ increase in radial mass on the other, the production of ^{7}Be and ^{8}B solar neutrinos in the SSM peaks around an effective radius, $r_{eff} \approx 0.064 R_\odot$ (r_{eff} is approximately the radius within which 50% of the flux is produced) . The SSM also predicts a ratio of electron to proton densities near the center of the sun, $n_e/n_p \sim 2$, consistent with helioseismology observations. Consequently, the SSMs predict

$$R \approx \frac{2 < \sigma v >_{e7}}{< \sigma v >_{p7}} \approx 4.4 \times 10^{-17} S_{17} T_7^{1/6} e^{47.625/T_7^{1/3}}, \quad (5)$$

where T_7 is the temperature in $10^7 K$ at the effective radius and S_{17} is in eV *barn* units. The SSMs yield $T_7(r_{eff}) \approx 1.45$. Using $S_{17}(0) = 17\ eV\ b$ and $\phi_\odot(^8\mathrm{B}) = 2.8 \times 10^6\ cm^{-2}\ s^{-1}$ as observed by Kamiokande, one can reproduce the SSM prediction (e.g., Dar and Shaviv 1996)

$$\phi_{\nu_\odot}(^7\mathrm{Be}) = R\phi_{\nu_\odot}(^8\mathrm{B}) \approx 3.7 \times 10^9\ cm^{-2}\ s^{-1}. \quad (6)$$

Astrophysical solutions of the solar neutrino problem aim towards suppressing the value of R. Three alternatives are currently investigated:

Plasma Physics Effects: The effects of the surrounding plasma on nuclear reaction rates in dense stellar plasmas, and in particular on proton and electron capture by ^{7}Be in the sun are known only approximately. In order to

explain the deficit of ^{7}Be solar neutrinos, without much affecting the SSM, plasma screening effects must reduce/enhance considerably electron/proton capture by ^{7}Be, respectively, relative to the predictions of the weak screening theory (Salpeter and Van Horne 1969). This possibility is currently studied, e.g., by Shaviv and Shaviv (1996) using numerical methods and by Brown and Sawyer (1996) using quantum statistical mechanics techniques. Because of accidental cancellations the screening corrections to the rates of all nuclear reactions do not change the predicted ^{8}B solar neutrino flux, but perhaps a more exact treatment of screening may change R considerably.

In principle, collective plasma physics effects, such as very strong magnetic or electric fields near the center of the sun, may polarize the plasma electrons, and affect the branching ratios of electron capture by ^{7}Be (spin $3/2^-$) into the ground state (spin $3/2^-$, $E_{\nu_e} = 0.863\ MeV$, BR=90%) and the excited state (spin $1/2^-$, $E_{\nu_e} = 0.381\ MeV$, BR=10%) of ^{7}Li. Since solar neutrinos with $E_{\nu_e} = 0.381\ MeV$ are below the threshold (0.81 MeV) for capture in ^{37}Cl and have a capture cross section in ^{71}Ga that is smaller by about a factor of 6 relative to solar neutrinos with $E_{\nu_e} = 0.863\ MeV$, therefore a large suppression in the branching ratio to the ground state can produce large suppressions of the ^{7}Be solar neutrino signals in ^{37}Cl and in ^{71}Ga. However, such an explanation require anomalously large fields near the center of the sun.

Temporal and Spatial Variations in T:

Davis (1996) has been claiming persistently that the solar neutrino flux measured by him and his collaborators in the ^{37}Cl radiochemical experiment is varying with time. Because of the possibility that neutrinos may have anomalous magnetic moments, much larger than those predicted by minimal extensions of the standard electroweak model, which can solve the solar neutrino problem (see Ould-Saada, these proceedings), attention has been focused on anticorrelation between the solar magnetic activity (the 11 year cycle) and the $\nu_\odot$ flux (see, e.g., Davis 1996). Also a day-night effect (e.g., Cribier et al 1986; Dar and Mann 1987) due to resonant conversion of the lepton flavor of solar neutrinos which cross Earth at night before reaching the solar neutrino detector was not found by Kamiokande. However, the basic general question whether the solar neutrino flux varies on a short time scale, has not been fully answered, mainly because of the limited statistics of the first generation of solar neutrino experiments.

The SSM predict no significant variation of the solar neutrino flux on

time scales shorter than millions of years. However, the sun has a differential rotation. It rotates once in ~ 25 days near the equator, and in ~ 33 days near the poles. Moreover, the observed surface rotation rates of young solar-type stars are up to 50 times that of the sun. It suggest that the sun has been loosing angular momentum over its lifetime. The overall spin-down of a sun-like star by mass loss and electromagnetic radiation is difficult to estimate from stellar evolution theory, because it depends on delicate balance between circulations and instabilities that tend to mix the interior and magnetic fields that retard or modify such processes. It is quite possible that the differential rotation extends deep into the core of the sun and causes there spatial and temporal variations in the solar properties due to circulation, turbulences and mixing. Since R is very sensitive to the temperature, even small variations in temperature can affect R significantly without affecting significantly the pp solar neutrino flux (the ^{7}Be and ^{8}B solar neutrinos will come mainly from temperature peaks, while the pp neutrinos will reflect more the average temperature).

In fact, a cross correlation analysis of the various data sets from the Homestake, Kamiokande, GALLEX and SAGE, shows an unexpected correlation: If arbitrary time lags are added to the different solar neutrino experiments, the cross correlation is maximal when these time lags vanish. Moreover, a power spectrum analysis of the signals shows a peak around 21 days, suggesting a periodical variation (Sturrock and Walther 1996). The effect may be a statistical fluke. However, it can also indicate a real short time scale variation in the solar core. Fortunately, Superkamiokande will soon provide the answer to whether the ^{8}B solar neutrino flux is time-dependent or not. Relevant information may come soon also from SOHO and GONG.

Mixing of ^{3}He:

The SSM ^{3}He equilibrium abundance increases sharply with radius. Cumming and Haxton (1996) have recently suggested that the ^{7}Be solar neutrino problem could be circumvented in models where ^{3}He is transported into the core in a mixing pattern involving rapid filamental flow downward. We note that if this mixing produces hot spots (due to enhanced energy release) they can increase the effective temperature for p capture by ^{7}Be in a cooleenvironment, reducing R while keeping the ^{8}B solar neutrino flux at the observed level. Perhaps, helioseismology will be able to test that.

Cummings and Haxton (1996) also noted that such mixing will have other astrophysical consequences. For example, galactic evolution models predict

^{3}He abundances in the presolar nebula and in the present interstellar medium (ISM) that are substantially (i.e., a factor of five or more) in excess of the observationally inferred values. This enrichment of the ISM is driven by low-mass stars in the red giant phase, when the convective envelope reaches a sufficient depth to mix the ^{3}He peak, established during the main sequence, over the outer portions of the star. The ^{3}He is then carried into the ISM by the red giant wind. The core mixing lowers the main sequence ^{3}He abundance at large r.

6 The MSW Solution

Standard solar models, like the one calculated by Dar and Shaviv (1996), perhaps can explain the results reported by Kamiokande. However, if the neutrino absorption cross sections used by the radiochemical experiments are correct, then standard physics cannot explain an ^{37}Ar production rate in ^{37}Cl smaller than that expected from the solar ^{8}B neutrino flux measured by Kamiokande (assuming that both results are correct). If the experimental results of Kamiokande and Homestake are interpreted as an evidence for such a situation (e.g., Bahcall 1994; 1995), they do imply new physics beyond the standard particle physics model (Bahcall and Bethe 1991). In that case an elegant solution to the solar neutrino anomaly is resonant neutrino flavor conversion in the sun, first proposed by Mikheyev and Smirnov (1986) (see also Wolfenstein 1978; 1979). It requires only a natural extension of the minimal standard electroweak theory and it is based on a simple quantum mechanical effect. Many authors have carried out extensive calculations to determine the neutrino mixing parameters which can bridge between the predictions of the standard solar models and the solar neutrino observations. They found that a neutrino mass difference $\Delta m^2 \sim 0.7 \times 10^{-5}\ eV^2$ and a neutrino mixing of $sin^2 2\theta \approx 0.5 \times 10^{-2}$ can solve the solar neutrino problem (see Petcov, these proceedings). These parameters, however, cannot explain the neutrino-oscillation-like signal which was reported by the LSND experiment (see Caldwell, these proceedings).

7 Conclusions

The solar neutrino problem may be an astrophysical problem. An indication for that may come from observation of unexpected temporal variability of the solar neutrino flux by Superkamiokande or from helioseismology observations by SOHO and GONG. An indication may also come from cross correlation analysis of the time dependent of the counting rates in GALLEX and Sage and of the counting rates of Kamiokande and Homestake. Such cross correlation analysis may test whether the time variation of the counting rates is statistical or physical. Deviations of the experimental results from those predicted by the standard solar models may reflect the approximate nature of the models (which neglect angular momentum effects, differential rotation, magnetic field, angular momentum loss and mass loss during evolution and do not explain yet, e.g., solar activity and the surface depletion of Lithium, Berilium and Boron relative to their meteoritic values, that may or may not be relevant to the solar neutrino problem). Improvements of the standard solar model should continue. In particular, dense plasma effects on nuclear reaction rates and radiative opacities, which are not well understood, may affect the SSM predictions and should be further studied, both theoretically and experimentally. Relevant information may be obtained from studies of thermonuclear plasmas in inertial confinement experiments. Useful information may also be obtained from improved data on screening effects in low energy nuclear cross sections of ions, atomic beams and molecular beams incident on a variety of gas, solid and plasma targets.

Better knowledge of low energy nuclear cross sections is badly needed. Measurement of crucial low energy nuclear cross sections by new methods, such as measurements of the cross sections for the radiative captures $p + {}^7Be \rightarrow {}^8B + \gamma$ and ${}^3He + {}^4He \rightarrow {}^7Be + \gamma$ by photodissociation of ${}^8B$ and ${}^7Be$ in the coulomb field of heavy nuclei are badly needed in order to determine whether there is a ${}^8B$ solar neutrino problem.

The ${}^{37}Ar$ production rate in ${}^{37}Cl$ indeed may be smaller than that expected from the flux of standard solar neutrinos as measured by electron scattering in the Kamiokande experiment. In that case neutrino oscillations, and in particular the MSW effect, may be the correct solution to the solar neutrino problem. Only future experiments, such as SNO, Superkamiokande, BOREXINO and HELLAZ, will be able to supply a definite proof that Nature has made use of this beautiful effect.

Acknowledgement: The author would like to thank M. Locher for his invitation to attend the Zuoz summer school and for his kind hospitality. This talk is based on an ongoing collaboration with Giora Shaviv. It was supported in part by the Technion fund for the promotion of research.

8 REFERENCES

Anders, E. and Grevesse, N., 1989, Geochim. Cosmochim. Acta , **53**, 197.
Bahcall, J.N. 1989, *Neutrino Astrophysics* (Cambridge Univ. Press 1989).
Bahcall, J.N. & Bethe, H. 1991, Phys. Rev. D. **44**, 2962.
Bahcall, J.N. & Pinsonneault, M. 1995, Rev. Mod. Phys., (submitted).
Caldwell, D. 1996, these proceedings
Brown, L.S. & Sawyer, R.F. 1996, preprint astro-ph 9610256
Clayton, D. 1968, *Princ. of Stellar Evolution & Nucleosyn.* (McGraw-Hill)
Christensen-Dalsgaard, J. 1996, Nucl. Phys. B (Proc. Suppl.) **48**, 325
Christensen-Dalsgaard, J. 1996a, private communication to G. Shaviv
Cummings, A. & Haxton, W. 1996, preprint nucl-th 9608045
Cribier, M. et al. 1986, Phys. Lett. **B182 2**, 89
Dar, A. and & Mann, A. 1987, Nature **325**, 790
Dar, A. and Nussinov, S. 1991, Particle World **2**, 117
Dar, A.. & Shaviv, G., 1996, ApJ, **468**, 933
Dar, A. & Shaviv G. 1994, Proc. VI Int. Conf. on Neutrino Telescopes (ed.. M. Baldo-Ceolin) p. 303.
Davis, R. Jr. 1996, Nucl. Phys. B (Proc. Suppl.) **48**, 284
Dzitko, H. et al., 1995, ApJ. **447**, 428 (1995)
Grevesse, N., 1991, A&A, **242**, 488
Grevesse, N. & Noels, A., 1993, in *Origin and Evolution of the Elements* (eds. N. Prantzos et al., Cambridge Univ. Press) p. 15
Grevesse, N. & Noels, A., 1993, Phys. Scripta **T47** , 133
Hampel, W. 1996, these proceedings and references therein.
Hata, N. et al., 1994, Phys. Rev. D **49**, 3622
Hata, N. & Langacker, P., (1995), Phys. Rev. D **52**, 420
Hernandez, E.P. & Christensen-Dalsgaard, J., (1994), MNRAS **269**, 475
Holzschun, E. 1966, these proceedings and references therein.
Johnson, C.W. et al. 1992, ApJ. **392**, 320
Kovetz, A. & Shaviv, G., 1994, ApJ. **426**, 787
Mikheyev, P. & Smirnov, A. Yu. 1985, Yad. Fiz. **42**, 1441
Petcov, S. 1996, these proceedings and references therein.
Richard, O. et al. 1996, Submitted to A&A, preprint astro-ph 9601136
Rogers, F.J. et al. 1996, ApJ, **456**, 902
Salpeter, E.E. & Van Horne, H.M. 1969, ApJ, **155**, 183
Shaviv, G. & Shaviv, N., 1996, ApJ, **468**, 433

Sturenburg, S. & Holweger, H., 1990, A&A **237**, 125
Sturrock, P.A. and Walther, G. 1996, report astro-ph 9609152
Wolfenstein, L. 1978, Phys. Rev. **D17**, 2369
Wolfenstein, L. 1979, Phys. Rev. **D20**, 2634

Figure Caption: Comparison between the sound speed in the core of the sun as extracted from recent helioseismology studies (Christensen Dalsgaard 1996a) and the sound speed calculated from the standard solar model of Dar and Shaviv (1996).

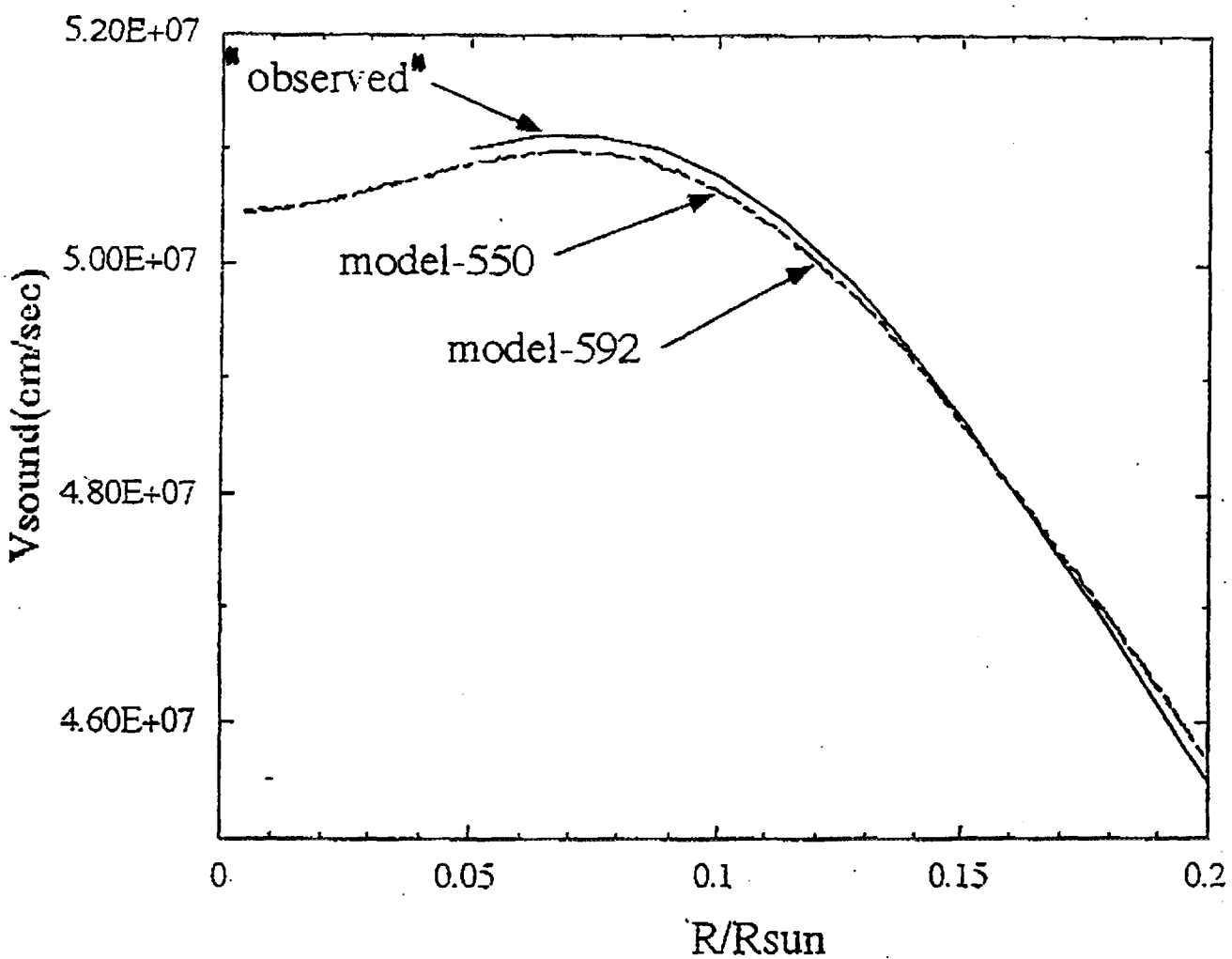

Table Ia: Comparison between the solar neutrino fluxes predicted by the SSM of BP95 and of DS96, and measured by the four solar neutrino experiments.

ν Flux	BP95	DS96	Observations	Experiment
$\phi_\nu(pp)$ $[10^{10} cm^{-2} s^{-1}]$	5.91	6.10		
$\phi_\nu(pep)$ $[10^{8} cm^{-2} s^{-1}]$	1.39	1.43		
$\phi_\nu(^7Be)$ $[10^{9} cm^{-2} s^{-1}]$	5.18	3.71		
$\phi_\nu(^8B)$ $[10^{6} cm^{-2} s^{-1}]$	6.48	2.49	2.80 ± 0.40	Kamiokande
$\phi_\nu(^{13}N)$ $[10^{8} cm^{-2} s^{-1}]$	6.4	3.82		
$\phi_\nu(^{15}O)$ $[10^{8} cm^{-2} s^{-1}]$	5.15	3.74		
$\phi_\nu(^{17}F)$ $[10^{6} cm^{-2} s^{-1}]$	6.48	4.53		
$\Sigma(\phi\sigma)_{Cl}$ $[SNU]$	9.3 ± 1.4	4.1 ± 1.2	2.56 ± 0.25	Homestake
$\Sigma(\phi\sigma)_{Ga}$ $[SNU]$	137 ± 8	115 ± 6	70 ± 8	GALLEX
$\Sigma(\phi\sigma)_{Ga}$ $[SNU]$	137 ± 8	115 ± 6	72 ± 12	SAGE

Table Ib Characteristics of the BP95, DS94, and DS96 Solar Models in Table Ia (c=center; s=surface; bc=base of convective zone; $\bar{\mathrm{N}} = \log([\mathrm{N}]/[\mathrm{H}]) + 12$).

Parameter	BP95	DS94	DS96
T_c $[10^7 K]$	1.584	1.554	1.561
ρ_c $[g\ cm^{-3}]$	156.2	155.3	155.4
X_c	0.3333	0.3462	0.3424
Y_c	0.6456	0.6359	0.6380
Z_c	0.0211	0.01950	0.01940
R_{conv} $[R/R_\odot]$	0.712	0.7105	0.7130
T_{bc} $[10^6 \mathrm{K}]$	2.20	2.10	2.105
X_s	0.7351	0.7243	0.7512
Y_s	0.2470	0.2597	0.2308
Z_s	0.01798	0.01574	0.0170
$\overline{N}_s(^{12}C)$	8.55	8.50	8.55
$\overline{N}_s(^{14}N)$	7.97	7.92	7.97
$\overline{N}_s(^{16}O)$	8.87	8.82	8.87
$\overline{N}_s(^{20}Ne)$	8.08	8.03	8.08
T_{eff} [K]		5920	5803

Table II: Comparison between the SSM of Bahcall and Pinsonneult (1995) and of Dar and Shaviv (1996).

	BP95	DS96
$M_\odot$	$1.9899 \times 10^{33}\ g$	$1.9899 \times 10^{33}\ g$
$L_\odot$	$3.844 \times 10^{33}\ erg\ s^{-1}$	$3.844 \times 10^{33}\ erg\ s^{-1}$
$R_\odot$	$6.9599 \times 10^{10}\ cm$	$6.9599 \times 10^{10}\ cm$
$t_\odot$	$4.566 \times 10^{9}\ y$	$4.57 \times 10^{9}\ y$
Rotation	Not Included	Not Included
Magnetic Field	Not Included	Not Included
Mass Loss	Not Included	Not Included
Angular Momentum Loss	Not Included	Not Included
Premain Sequence Evolution	Not Included	Included
Initial Abundances :		
^{4}He	Adjusted Parameter	Adjusted Parameter
C, N, O, Ne	Adjusted Photospheric	Adjusted Photospheric
All Other Elements	Adjusted "Photospheric"	Meteoritic
Photospheric Abundances :		
^{4}He	Predicted	Predicted
C, N, O, Ne	Observed	Observed
All Other Elements	= Meteoritic	Predicted
Radiative Opacities	OPAL 1994	OPAL 1996
Equation of State	Straniero 1988?	DS 1996
Partial Ionization Effects	Not Included	Included
Diffusion of Elements :		
H, ^{4}He	Included	Included
Heavier Elements	Approximated by Fe	All Included
Partial Ionization Effects	Not Included	Included
Nuclear Reaction Rates :		
$S_{11}(0)$	3.896×10^{-22} keV $\cdot$ b	4.07×10^{-22} keV $\cdot$ b
$S_{33}(0)$	$4.99 \times 10^{3}\ keV \cdot b$	$5.6 \times 10^{3}\ keV \cdot b$
$S_{34}(0)$	$0.524\ keV \cdot b$	$0.45\ keV \cdot b$
$S_{17}(0)$	$0.0224\ keV \cdot b$	$0.017\ keV \cdot b$
Screening Effects	Included	Included
Nuclear Equilibrium	Imposed	Not Assumed

Table III: Fractional change in the predicted $\nu_\odot$ fluxes and counting rates in the $\nu_\odot$ experiments due to the inclusion of element diffusion in the SSM calculations of Bahcall and Pinsonneault (1996), Dar and Shaviv (1994, 1996) and Richard, Vauclair, Charbonnel and Dziembowski (1996). The results of models 1 and 2 of RVCD were extrapolated to the initial solar composition which was used in DS96.

$\phi_{\nu_\odot}$	BP95	DS96	RVCD
pp	− 1.7%	− 0.3%	− 0.8%
pep	− 2.8%	− 0.3%	− 0.4%
^{7}Be	+13.7%	+4.2%	+ 6.5%
^{8}B	+36.5%	+11.2%	+10.7%
^{13}N	+51.8%	+22.7%	+19.8%
^{15}O	+58.0%	+24.0%	+20.8%
^{17}F	+61.2%	+24.9%	+21.8%
Rates			RVCD
H2O	+36.5%	+11.2%	+13.3%
Cl	+32.9%	+ 9.5%	+12.3%
Ga	+ 8.7%	+ 2.6%	+ 3.7%

SOLAR NEUTRINO EXPERIMENTS

W. Hampel
Max-Planck-Institut für Kernphysik
P.O. Box 103980, 69029 Heidelberg, Germany

Abstract

The present status of experimental solar neutrino research is reviewed. Updated results from the Homestake, Kamiokande, GALLEX and SAGE detectors all show a deficit when compared to recent standard solar model calculations. Two of these detectors, GALLEX and SAGE, have recently been checked with artificial ^{51}Cr neutrino sources. It is shown that astrophysical scenarios to solve the solar neutrino problems are not favoured by the data. There is hope that the results of forthcoming solar neutrino experiments can provide the answers to the open questions.

1. Introduction

Experiments which can observe the neutrinos produced in the fusion reactions in the interior of the Sun provide the only direct way to test the theories of energy generation in stars. A second motivation arises from particle physics: solar neutrino experiments may be the only way to obtain information on neutrino properties which reveal themselves only over astronomical distances between neutrino source and detector.

The spectrum of solar neutrinos produced in the proton-proton reaction chain as predicted by Standard Solar Models (SSM) is displayed in Figure 1 along with the energy thresholds of the running experiments (see below), gallium (Ga), chlorine (Cl) and Kamiokande (K). Table 1 gives the fluxes of the different solar neutrino sources according to the SSM of Bahcall and Pinsonneault [1] (BP 95). Other SSMs have been calculated by Turck-Chièze and Lopes [2] (TCL) and by Dar and Shaviv [3] (DS). The resulting fluxes for the pp, ^{7}Be and ^{8}B neutrinos predicted by these models are listed in Table 2 along with the values of the BP 95 SSM [1]. The table also includes the predictions from an earlier SSM of Bahcall and Pinsonneault [4] (BP 92), because in the past this model has often been used as a reference model. Differences in the neutrino fluxes predicted by the various models are small for the

Table 1: Solar neutrino fluxes and capture rates for the Chlorine and Gallium detectors [1].

Neutrino source and energy [MeV]		Flux at earth [10^{10}cm^{-2}sec^{-1}]	Production rate [SNU]	
			^{37}Cl experiment	^{71}Ga experiment
pp	≤ 0.42	5.91	–	69.7
pe$^-$p	1.44	0.014	0.22	3.0
^{7}Be	0.38, 0.86	0.515	1.24	37.7
^{8}B	< 15	0.000662	7.36	16.1
^{3}He p	≤ 18.77	$1.21 \cdot 10^{-7}$	0.005	0.01
^{13}N	≤ 1.20	0.0618	0.11	3.8
^{15}O	≤ 1.73	0.0545	0.37	6.3
^{17}F	≤ 1.74	0.000648	0.005	0.06
Total		6.56	9.3	137

pp neutrinos (a few percent), 20 to 35 % for the ^{7}Be neutrinos, and up to a factor of two for the ^{8}B neutrinos. This is mainly due to different choices on some of the solar model input parameters, especially the astrophysical S_{17} factor (see Dar [5]).

Four solar neutrino detectors have been in operation during the past few years: the

Table 2: Solar neutrino fluxes and capture rates for different Standard Solar Models.

Solar Model	BP 92	TCL	BP 95	DS
Reference	[4]	[2]	[1]	[3]
pp flux (10^{10} cm^{-2}s^{-1})	6.00 ± 0.12	6.02	5.91 ± 0.06	6.10
^{7}Be flux (10^9 cm^{-2}s^{-1})	4.89 ± 0.88	4.33	$5.15 \pm^{0.31}_{0.36}$	3.71
^{8}B flux (10^6 cm^{-2}s^{-1})	5.70 ± 0.82	4.4 ± 1.1	$6.62 \pm^{0.93}_{1.13}$	2.49
^{37}Cl signal [SNU]	8.0 ± 1.0	6.4 ± 1.4	$9.3 \pm^{1.2}_{1.4}$	4.1 ± 1.2
^{71}Ga signal [SNU]	132 ± 7	122.5 ± 7.0	$137 \pm^{8}_{7}$	115 ± 6
Kamiokande signal	$\equiv 1.0$	0.77 ± 0.19	$1.16 \pm^{0.16}_{0.20}$	0.44

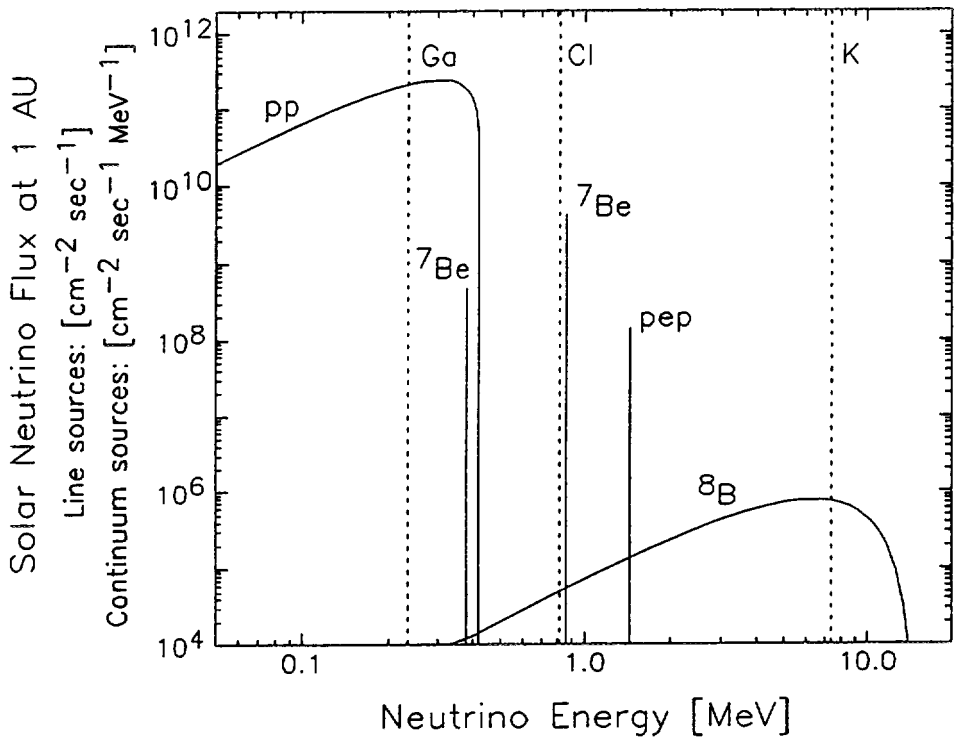

Fig. 1: Energy spectrum of solar neutrinos produced in the pp chain. The vertical dashed lines indicate the energy thresholds for the Gallium (Ga), Chlorine (Cl) and Kamiokande (K) experiments.

Homestake radiochemical detector utilizing neutrino capture in chlorine, the Kamiokande water Cherenkov detector and two radiochemical experiments based on neutrino capture in gallium, GALLEX and SAGE. Section 2 provides updated results from all four experiments. Results on the ^{51}Cr neutrino source experiments which recently have been performed for GALLEX and SAGE are reported in section 3. Section 4 compares the experimental results with the solar model predictions and discusses possible reasons for the observed discrepancies. Finally, the status of the upcoming new solar neutrino experiments is presented in section 5.

2. Results of running or stopped experiments

2.1 Homestake detector

The Homestake radiochemical chlorine detector [6,7], located at the Homestake gold mine at a depth of 1480 meters underground (4200 ± 100 meters water equivalent) in Lead, South Dakota (USA), is based on the neutrino capture reaction $^{37}Cl(\nu,e^-)^{37}Ar$ ($T_{1/2}$ = 35 d). The threshold for this reaction is 814 keV. After an exposure time of 1 to 3 months, the ^{37}Ar atoms are extracted from the target liquid (615 tons tetrachloroethylene, C_2Cl_4) and counted by observing their radioactive decay in a proportional counter.

The ^{37}Ar production rate measured in 108 individual runs (runs 18 to 133) covering the time period from 1970 to 1994 is plotted in Figure 2 [7]. The rate averaged over these 108 runs is [2.54 ± 0.14 (stat.) ± 0.14 (syst.)] SNU (1 SNU ≡ 1 neutrino reaction per second in

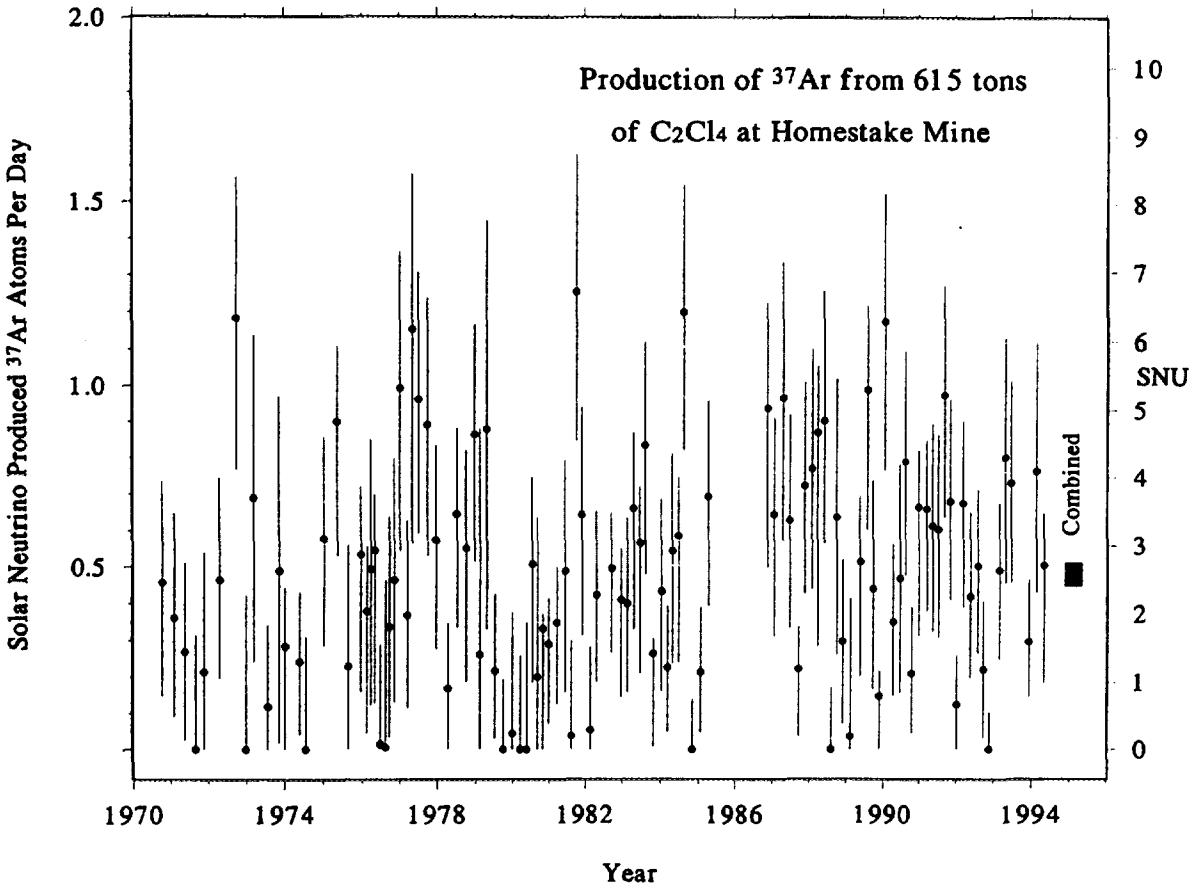

Fig. 2: Results of 108 individual runs from the Homestake experiment. The filled rectangle labeled "combined" represents the production rate averaged over all 108 runs (from Cleveland et al. [7]).

10^{36} target atoms). This is considerably lower than the SSM predictions: almost a factor of 4 if compared to the BP 95 model, and still a factor of 1.6 if compared to the DS model (see Table 2). This implies that the flux of ^{8}B neutrinos which give the overwhelming contribution to the Cl detector signal (see Table 1) must be smaller than the SSM predictions, a fact which has long been known as the "Solar Neutrino Problem" (SNP).

2.2 Kamiokande detector

Since 1987 there exist experimental data from a second experiment, the Kamiokande detector located in the Kamioka mine in Japan [8,9]. This experiment measures the Cherenkov light emitted by relativistic electrons produced in elastic collisions between solar neutrinos and electrons in the inner fiducial 680 tons of a large tank filled with a total of 2180 tons of water. For background reduction, the threshold has to be set to a rather high electron recoil energy (7.0 MeV total electron energy), therefore the detector is sensitive only to the upper end of the ^{8}B neutrino spectrum (see Figure 1). After 1043 days of data taking, solar neutrino measurements were interrupted in 1990 for 9 months (end of Kamiokande-II) in order to

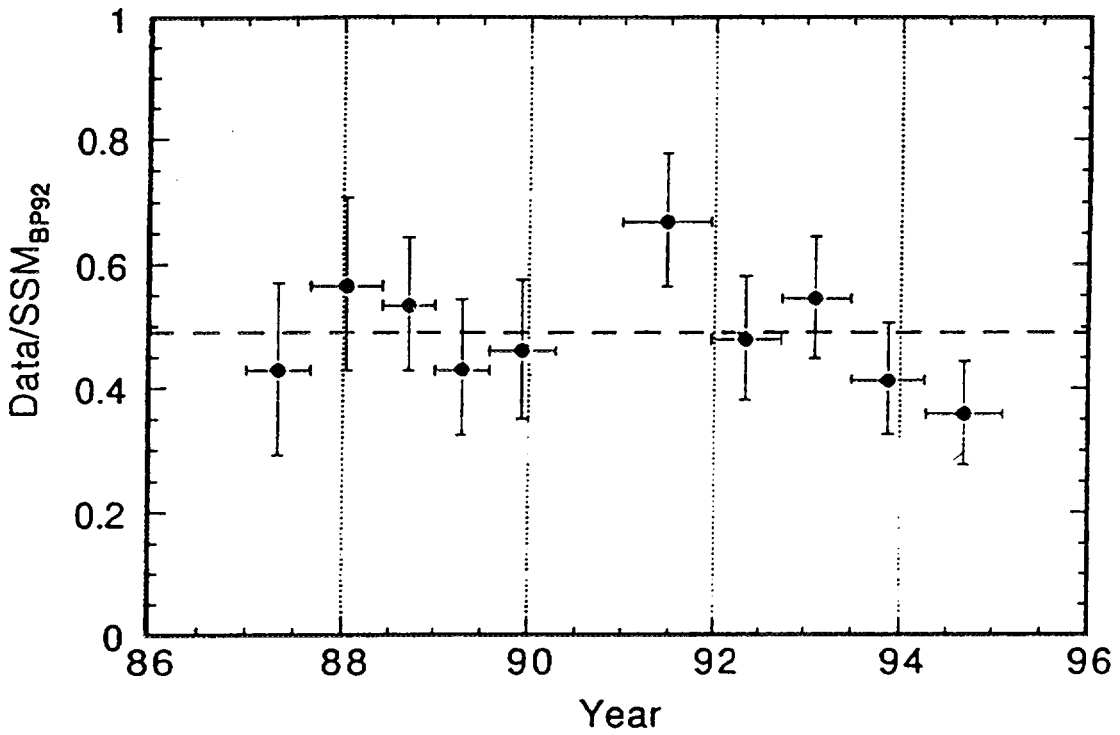

Fig. 3: Results of the Kamiokande detector for ten different time periods (from Suzuki [9]).

replace dead photomultipliers, to implement new electronics and to add reflective mirrors for better light collection. Data taking was resumed in December 1990 (start of Kamiokande-III). Since then the detector monitored the solar ^{8}B neutrino flux for an additional 1036 days. Solar neutrino data taking ended in February 1995.

Figure 3 depicts all Kamiokande II and III data (10 periods with a cumulative live time of 2079 days) [9]. The average ^{8}B neutrino flux, when expressed in units of the BP 92 SSM [4], is [0.492 ± 0.033 (stat.) ± 0.060 (syst.)], or if expressed as an absolute flux: (2.80 ± 0.39) × 10^6 cm^{-2} s^{-1}. This result is more than a factor of 2 lower than the BP 95 prediction [1], but in agreement with the DS model [3] (see Table 2).

2.3 GALLEX detector

The radiochemical GALLEX detector [10,11], located at the Gran Sasso Underground Laboratory in Italy, is based upon neutrino capture in gallium, i.e. on the reaction ^{71}Ga(ν_e,e$^-$)^{71}Ge. The energy threshold (233.2 keV) is well below the maximum energy of the pp neutrinos, 420 keV (see Figure 1). ^{71}Ge decays back to ^{71}Ga by electron capture with a halflife of 11.43 d.

The last column of Table 1 lists the gallium detector capture rates for the different solar neutrino sources according to the BP 95 SSM [1]. The total rate of 137 SNU is dominated by 73 SNU from the pp and pe$^-$p neutrinos resulting from the basic fusion reaction in the pp chain. Predictions by the two other SSM calculations give slightly lower values, 115 SNU (DS) [3] and 122.5 SNU (TCL) [2], respectively (see Table 2).

The experimental procedure for GALLEX is as follows. 30.3 tons of gallium in form of a

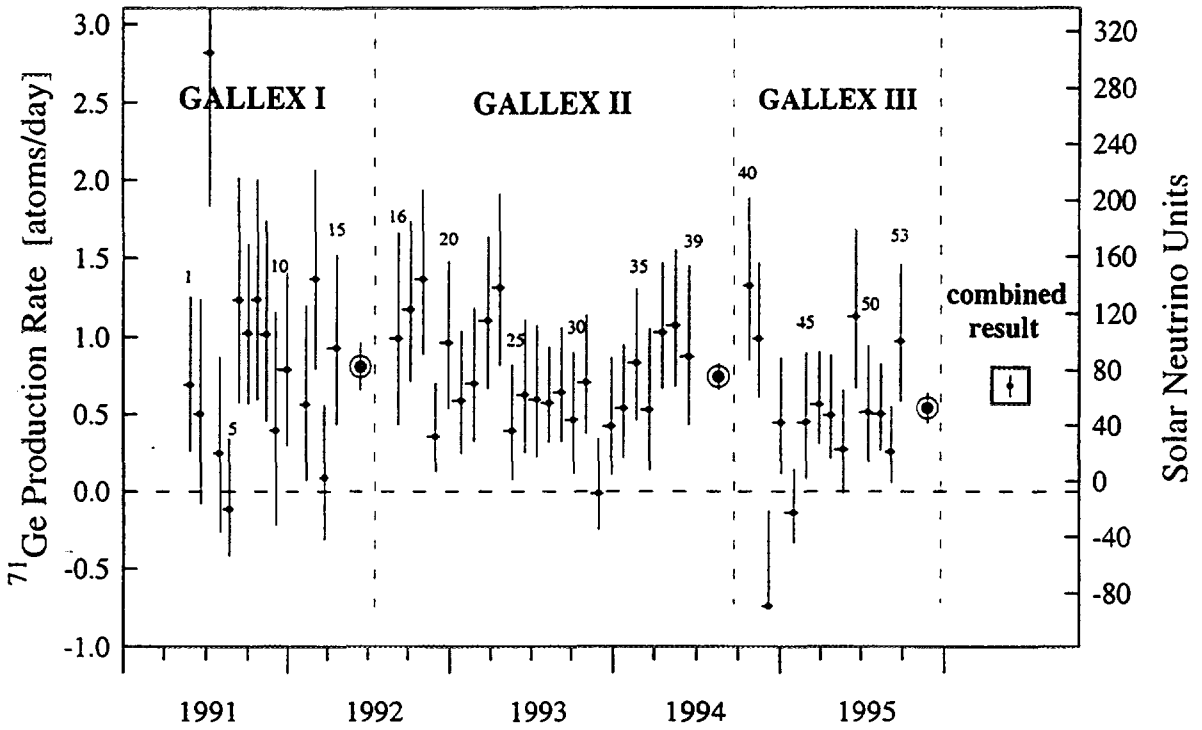

Fig. 4: Results of 53 individual GALLEX runs obtained in the data taking periods GALLEX I, II and III [11].

concentrated $GaCl_3$-HCl solution are exposed to solar neutrinos. In $GaCl_3$-HCl solution, the neutrino induced ^{71}Ge atoms (as well as the inactive Ge carrier atoms added to the solution at the beginning of a run) form the volatile compound $GeCl_4$, which at the end of an exposure is swept out of the solution by means of a gas stream (nitrogen). The nitrogen is then passed through a gas scrubber where the $GeCl_4$ is absorbed in water. The $GeCl_4$ is finally converted to GeH_4, which together with xenon is introduced into a proportional counter in order to determine the number of ^{71}Ge atoms by observing their radioactive decay.

The results of 53 individual GALLEX runs corresponding to the data taking periods GALLEX I, II and III are plotted in Figure 4. Since in a single run on the average only 4.5 solar neutrino events are observed, there are rather large statistical fluctuations from run to run. If all 53 runs are combined, a ^{71}Ge production rate of [69.7 ± 6.7 (stat.) +3.9/−4.5 (syst.)] SNU is obtained [11] (data point labeled "combined result" in Figure 4). This is between 51 and 61% of the SSM predictions and accounts just for the pp neutrino flux alone (see Tables 1 and 2).

2.4 SAGE detector

The second gallium solar neutrino experiment is carried out by the Russian-American SAGE Collaboration [12,13]. Their detector uses gallium in its metallic form (melting point 29°C). Except for the first 8 runs in which 27 tons were used, the total available amount of gallium is 57 tons. The SAGE detector is located in the Baksan Neutrino Observatory in the Northern

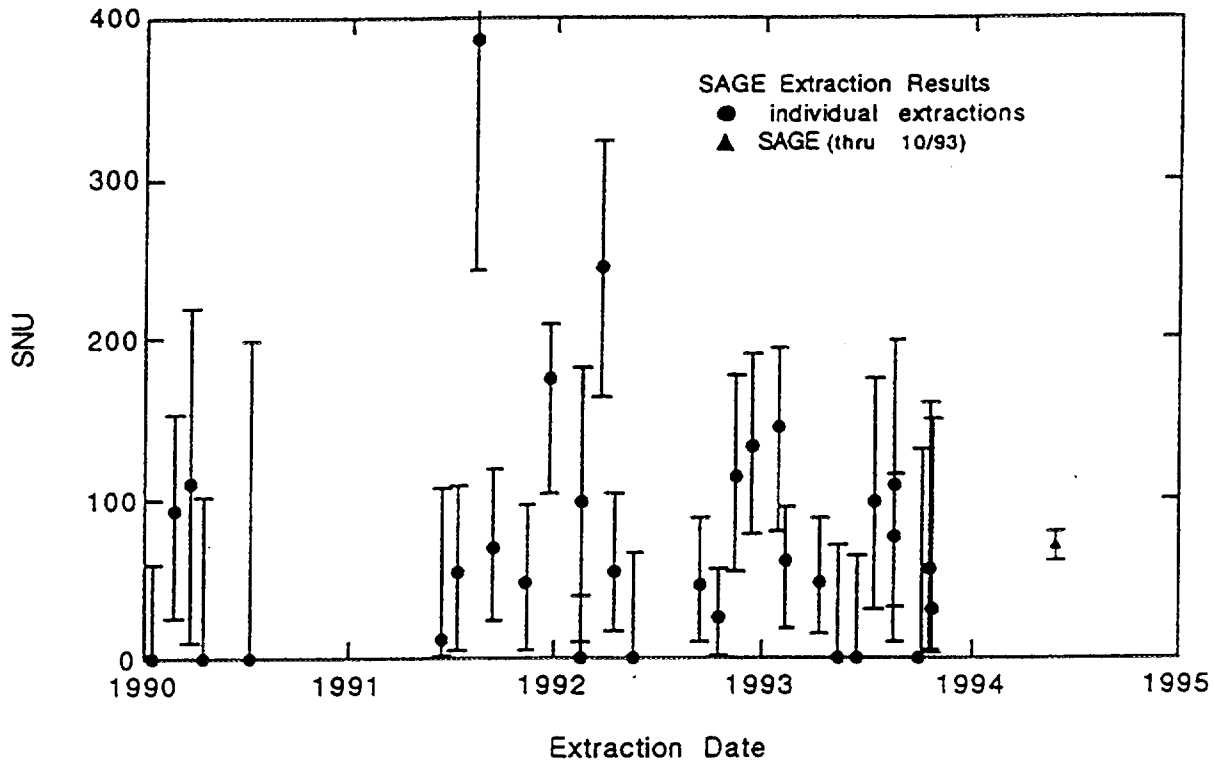

Fig. 5: Solar neutrino production rates of 31 individual SAGE runs. The combined result is indicated by the solid triangle on the right hand side (from Gavrin [13]).

Caucasus mountains at a shielding depth of 4715 meter water equivalent. Apart from the first additional step employed in the chemical extraction (in which germanium is removed from the gallium metal by a liquid-liquid extraction into a HCl-H_2O_2 phase) the experimental procedure in SAGE is very similar to that of GALLEX (see section 2.3).
Initially, SAGE reported rather low ^{71}Ge production rates, see for instance Figure 3 in Anselmann et al. [14]. On the other hand, the most recent SAGE average [13] based on 31 individual runs (see Figure 5) is [72 +12/−10 (stat.) +5/−7 (syst.)] SNU which is very in good agreement with the GALLEX result reported above.

2.5 Molybdenum experiment

A few so-called geochemical solar neutrino experiments have been suggested in the past [15]. A large amount of a natural ore or salt deposit exposed to solar neutrinos over geological time scales is used as a target for this kind of neutrino detectors. One of these geochemical experiments has actually been carried out [15]. It is based on the neutrino capture reaction $^{98}Mo(\nu_e,e^-)^{98}Tc^* \rightarrow {}^{98}Tc$ (halflife 4.2 $\times$ 10^6 a). The effective threshold is 1.74 MeV. Of the order of 10^8 solar neutrino induced ^{98}Tc atoms have been separated out of 40,000 tons of molybdenite ore from the Henderson mine in Colorado (USA). The ^{98}Tc atoms have been detected as TcO_4^- by negative ion mass spectrometry. The ^{98}Tc production rate expected from the ^{8}B neutrino flux of the BP 95 SSM is about 20 SNU [1,27]. Unfortunately, the measured

signal was about three times this value which probably was caused by a contamination of the ore processing installation with cosmic ray produced ^{98}Tc [16].

3. ^{51}Cr neutrino source experiments

The radiochemical solar neutrino detection method is based on the removal of a few neutrino induced atoms from large quantities (of the order of 100 tons) of target material. This corresponds to separation factors of the order of 10^{29} ! There has always been some skepticism about whether such a separation is indeed possible with a high and sufficiently well known efficiency, even though numerous tests have been performed in the various radiochemical experiments without any evidence for problems in this respect.

The most straightforward check, however, is the exposure of a radiochemical solar neutrino detector to an artificial neutrino source with known intensity and neutrino energy. Such a demonstration of the reliability of the radiochemical method has recently been performed for GALLEX and SAGE. In both cases an intense man-made ^{51}Cr neutrino source has been produced. ^{51}Cr decays with a halflife of 27.7 days by electron capture to the ground state (90.14%) and to the first excited state (9.86%) of ^{51}V, which subsequently decays by emission of a 320 keV γ ray to the ground state. Because of the L/K electron capture branching, there are in total four monoenergetic neutrino lines produced in the ^{51}Cr decay: 746 keV (81%), 751 keV (9%), 426 keV (9%) and 431 keV (1%).

3.1 The GALLEX ^{51}Cr source experiment

GALLEX has performed two ^{51}Cr neutrino source experiments [17,18], the first one between the solar neutrino data taking periods GALLEX II and III, the second one after GALLEX III (see Figure 4). The sources have been produced in the Siloe reactor, Grenoble (France), by neutron irradiation of 36 kg chromium powder enriched to 38.6% in the isotope ^{50}Cr. Source strengths of 62.5 PBq for the first and 68.7 PBq for the second source have been achieved. These source activities are equivalent to production rates of 1310 and 1440 SNU, respectively.

The results are expressed in terms of R, the ratio of the ^{71}Ge production rate measured with the ^{51}Cr source to the rate expected from the known source strength. This ratio R came out to be 1.00 ± 0.11 for the first experiment (11 individual extractions). A preliminary value for R obtained in the second source experiment (7 individual extractions) is 0.83 ± 0.10 [18]. The combined fit for both experiments gives $R = 0.92 \pm 0.08$. This result provides an overall check of the GALLEX detector. Unknown systematic errors on a level of 10% or larger are excluded. It follows that the solar neutrino deficit measured with GALLEX (section 2.3) cannot be an experimental artefact.

3.2 The SAGE ^{51}Cr source experiment

The ^{51}Cr source used in SAGE has been produced by neutron irradiation of 510 g chromium rods (enriched to 93% in the isotope ^{50}Cr) in the fast breeder reactor in Aktau, Kazakhstan. The source was placed for 5 months into a tank containing 13.1 tons of gallium metal. A source strength of 19.1 PBq was obtained, this corresponds to a production rate of 3700 SNU [13]. The ratio R, the ^{71}Ge production rate directly measured with the source relative to the rate expected from the source strength was determined in 8 individual exposures. The result is $R = 0.95 \pm 0.11$ [13]. This demonstrates also for SAGE that the observed deficit in the solar neutrino measurements cannot be attributed to unknown problems in the the detector performance.

4. Interpretation of the data

4.1 Time variations of the solar neutrino flux

The rate given for the Homestake detector in section 2.1 is a time-averaged rate, yet it has been speculated (see for instance [6]) that the individual data are not randomly distributed in time but exhibit an anticorrelation with the eleven-year sun spot cycle. Spin precession for Dirac neutrinos [19] or spin-flavour conversion for Majorana neutrinos [20,21] with a large magnetic moment ($\mu_\nu > 10^{-11}\mu_{Bohr}$) in the time-dependent magnetic fields of the solar convective zone have been proposed as explanation for such a time variation. However, the significance for this anticorrelation in the Homestake data has decreased since 1989 (see Figure 2 in [6]). Some authors have tried other parameters as indicators of the solar activity, for instance the intensity of the green coronal line [22] or the solar wind flux [23]. On the other hand, Kamiokande [9] and GALLEX [11] do not show a dependence of their signal on sun spot numbers. The final answer to this question must come from experiments with higher statistics, such as Super-Kamiokande [9] (see section 5.1).

4.2 Astrophysical solutions

As mentioned in section 2, all four solar neutrino experiments show substantial deficits in the observed signal if compared to recent SSM calculations. The largest of these deficits exists for the Homestake detector, a fact which is well known since more than 20 years (SNP). There have been many attempts to construct so-called non-standard solar models which in most cases were tailored to yield a lower core temperature, thus resulting in a much lower ^{8}B neutrino flux (see Dar [5]). However, recent improvements in the field of helioseismology exclude this possibility, since measurements of the oscillation frequencies of the sun are in very good agreement with the predictions from SSMs [24].

Even more difficult to resolve with non-standard solar models (see below) is the fact that there is no room for a sizeable ^{7}Be neutrino contribution in the measured signals. This so-

Table 3: Combined χ^2 fit for ^{7}Be and ^{8}B neutrino fluxes (see text).

Experiments included in the fit (a)	Percentage of cases (b)	Percentage of cases (c)	^{8}B flux (d)
H K	5.4	0.6	0.39 ± 0.03
H G	3.1	0.1	0.37 ± 0.03
H G S	1.9	< 0.1	0.36 ± 0.04
K G	2.1	< 0.1	0.48 ± 0.07
K G S	1.2	< 0.1	0.47 ± 0.07
H K G	0.7	< 0.1	0.39 ± 0.03
H K G S	0.5	< 0.1	0.39 ± 0.03

(a) H = Homestake, K = Kamiokande, G = GALLEX, S = SAGE
(b) best fit yields a non-negative ^{7}Be flux
(c) best fit overlaps with solar model region (see Fig. 6)
(d) in units of the BP 92 SSM

called "^{7}Be problem", has been realized a few years ago from the gallium detector results when their statistical errors (especially that of the GALLEX result) became sufficiently small [10]. It should be noted, however, that the ^{7}Be problem in principle became apparent already in 1990, see the comparison of the Homestake and Kamiokande results with solar model calculations [25].

There have been a large number of publications in the past few years in which the experimental solar neutrino data have been confronted with possible astrophysical solutions, see for instance Hata et al. [26]. We apply here a similar and rather straightforward procedure in order to extract information about the fluxes of the different solar neutrino sources from the updated experimental results by performing a χ^2 minimization. The expected signals for each of the solar neutrino detectors are calculated as a function of the solar pp, pep, ^{7}Be and ^{8}B neutrinos fluxes and then compared to the measured values. The neutrino fluxes are chosen by a Monte Carlo technique, with no constraints from solar models except that the resulting energy production in the sun is required to be consistent with the observed solar luminosity (luminosity constraint, see Bahcall [27]) and that the pp-pe$^-$p branching in the starting reaction of the hydrogen fusion chain is the same as given in SSMs. Errors of the experimental results as well as of the neutrino reaction cross sections are properly taken into account. The CNO branch is set to zero, since any CNO cycle contribution to the energy production in the sun would exaggerate the ^{7}Be neutrino problem.

The results are presented in Figure 6 and in Table 3. Figure 6 displays the predictions for ^{7}Be and ^{8}B neutrino fluxes of about 130 solar models (standard and non-standard) which have been published over the last 25 years (open circles). The SSMs mentioned in section 1

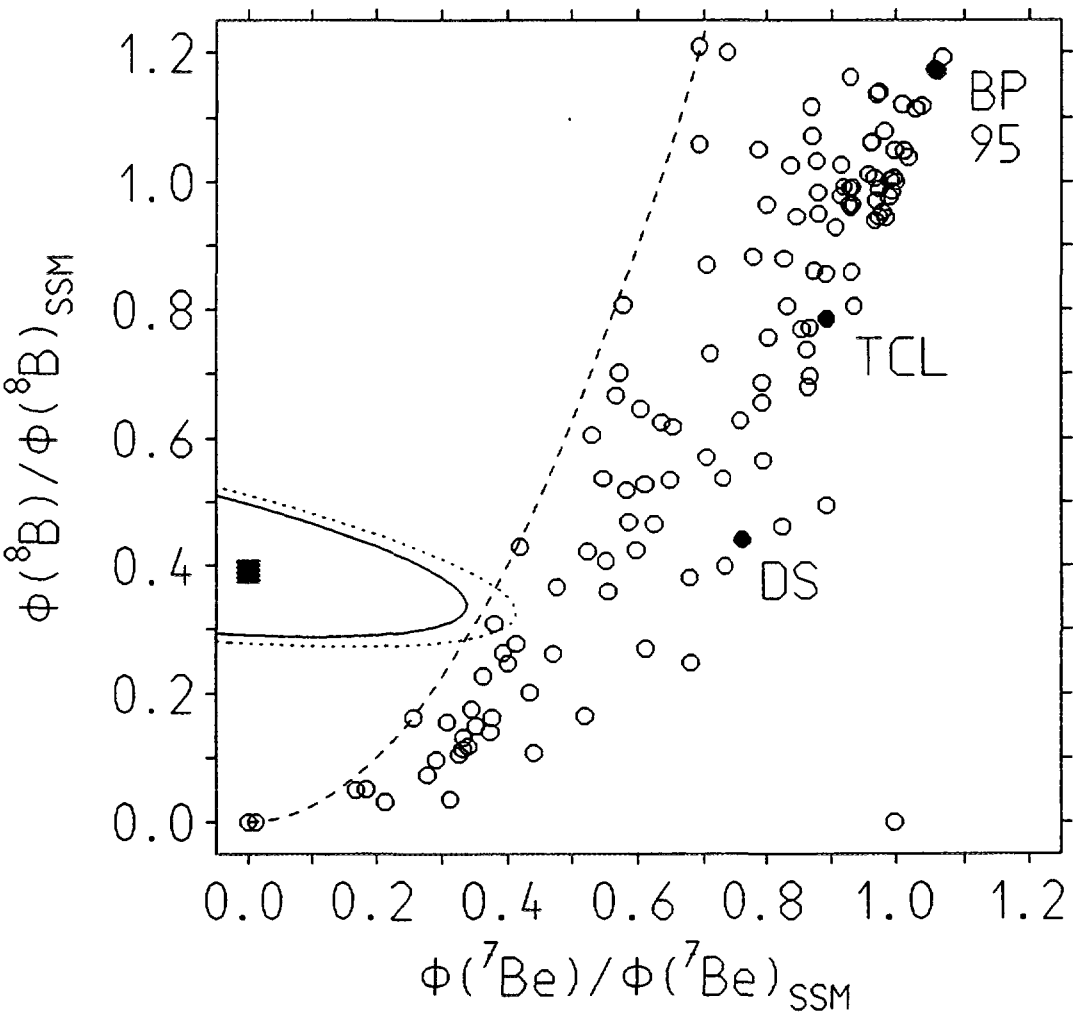

Fig. 6: Comparison between the best fit of the results of all four experiments (solid square) with standard and non-standard solar models (circles) in the ^{7}Be-^{8}B plane (see text).

(labeled BP 95 [1], TCL [2] and DS [3]) are indicated by solid circles. All fluxes are expressed in units of the BP 92 model [4]. Note that because ^{7}Be and ^{8}B neutrinos are produced by either electron or proton capture on the same nucleus (^{7}Be), their fluxes are related to each other. This leads to the fact that there are no models located to the left of the dashed line in Figure 6. There has been an attempt titled "Last hope for an astrophysical solution to the solar neutrino problem" by Berezinsky et al. [28] to construct solar models to the left of the dashed line in Figure 6 (using non-standard values for the astrophysical S_{33}, S_{34} and S_{17} factors), without success. The last sentence in their paper reads: "Thus, the last hope turned out to be a no-hope case".

The χ^2 minimizations presented here lead to the same conclusion: the measured data do not favour an astrophysical solution to the solar neutrino problems. The best fit including all four experiments (indicated in Figure 6 by the solid square) is far away from any realistic

solar model prediction and yields zero for the ^{7}Be neutrino flux and $(2.2 \pm 0.2) \times 10^6$ cm^{-2}s^{-1} for the ^{8}B neutrino flux (equivalent to 39% of the BP 92 SSM flux [4]). The error ellipses around the best fit include 90% (solid line) and 95% (dotted line), respectively, of all MC simulations. Table 3 summarizes the results of the different χ^2 minimizations, in which the data of 2, 3 or all 4 experiments are used. The best fit for the ^{7}Be neutrino flux is in all cases zero, whereas the ^{8}B flux comes out between 36 and 48% of the BP 92 SSM [4] (last column in Table 3). The percentage of cases in which the best fit reaches into the region of standard and non-standard solar models, i.e. is located to the right of the dashed curve in Figure 6, is always very small ($\leq$ 0.6%, see column (*c*) in Table 3). If negative ^{7}Be fluxes are allowed in the χ^2 minimization, the results in column (*b*) are obtained: only a small fraction of all simulations gives a non-negative ^{7}Be flux, the overwhelming part requires negative (thus unphysical) ^{7}Be fluxes, indicating that the model applied does not adequately describe the measured data. All these conclusions are virtually independent of the experiments included in the fit, i.e. they do not change if one or even two of the experimental results were omitted from the fit.

4.3 Neutrino mixing

The overall conclusion from section 4.2 leaves the other widely discussed solution to the solar neutrino problems, neutrino mixing, as the more likely candidate. Here one considers especially the matter enhanced neutrino oscillations, the Mikheyev-Smirnov-Wolfenstein (MSW) effect (see [29–31]). If mixing is restricted to the two-neutrino case, then the expected suppression factors (relative to the SSM predictions) for the Homestake, Kamiokande and gallium experiments can be calculated as a function of two parameters, Δm^2 (the difference of the squared masses of the two mixing neutrino eigenstates) and $\sin^2 2\theta$ (where θ is the mixing angle).

It is well known that there are (at the 95% confidence level) two consistent MSW solutions for all experiments: the so-called "small angle solution" at $\sin^2 2\theta \sim 0.006$ and $\Delta m^2 \sim 6 \times 10^{-6}$ eV^2, and the "large angle solution" at $\sin^2 2\theta \sim 0.7$ and$\Delta m^2 \sim 10^{-5}$ eV^2 (see for instance [29–31]).

For completeness it should be noted that there is also a solution for vacuum neutrino oscillations which can accomodate (within error limits) the results of all four experiments [30]. In this case Δm^2 must be close to 10^{-10} eV^2 (which corresponds to an oscillation length of 1.65 Astronomical Units for a 10 MeV neutrino) and mixing must be nearly maximal ($\sin^2 2\theta \simeq 1$).

5. Upcoming experiments

At present, the problems with solar neutrinos are still not finally solved, though there are now much more constraints on possible solutions than a few years ago. The final answer, especially the decision of whether or not new physics is required to explain the measured data must come from a new generation of solar neutrino experiments.

5.1 Super-Kamiokande

It has already been mentioned (section 2.2) that the Kamiokande detector has stopped solar neutrino measurements in February 1995. However, Super-Kamiokande, a 50,000 ton water Cherenkov detector viewed by 11,2000 photomultiplier tubes, has started to take solar neutrino data in April 1996 [9]. The anticipated fiducial mass for solar neutrino measurements is 22,000 tons, about 30 times larger than Kamiokande. With an energy threshold of 5 MeV, the expected solar neutrino event rate is 24 per day (assuming the ^{8}B flux observed with Kamiokande). This much higher rate obtained with Super-Kamiokande may allow to observe the change in the energy spectrum of the recoil electrons if the MSW effect is at work.

5.2 Sudbury Neutrino Observatory

The Sudbury Neutrino Observatory (SNO) is a 1,000 ton heavy water Cherenkov detector surrounded by 7,000 tons of light water and viewed by 9,500 photomultiplier tubes. SNO is presently being built in a nickel mine near Sudbury, Canada [32,33]. The acrylic vessel for the D_2O and the photomultiplier tube structure are about half completed (August 1996). SNO intends to measure the electron neutrino content of the ^{8}B neutrinos as well as the total (flavor-independent) flux via their charged-current ($\nu_e + d \rightarrow e^- + p + p$) and neutral-current ($\nu_x + d \rightarrow \nu_x + p + n$) interactions with deuterium. Solar neutrino measurements will start in 1997.

5.3 Borexino

Borexino aims at the detection of ^{7}Be neutrinos via neutrino-electron scattering in 300 tons of liquid scintillator (fiducial mass 100 tons) viewed by 2000 photomultipliers [34,35]. A measurement of the ^{7}Be neutrino line intensity would be extremely useful since it would allow the unambiguous interpretation of the results from the Cl and Ga detectors. There are huge problems concerning the radiopurity of the scintillator and its surroundings. However, measurements with a pilot installation (Counting Test Facility, CTF) have yielded very encouraging results. The conceptual design of Borexino implemented in the CTF has been shown to work. The internal activity of the liquid scintillator could be reduced from initially 600 events per day to a rate consistent with zero. Borexino is expected to be in full scale operation in 1999.

5.4 Iodine experiment

A new radiochemical detector based on the neutrino capture reaction $^{127}I(\nu_e,e^-)^{127}Xe^* \rightarrow {}^{127}Xe$ (halflife 36.4 d, effective threshold 0.79 MeV) is under preparation [32,36]. A pilot experiment using 100 tons of ^{127}I in form of a NaI solution is presently installed at the Homestake gold mine in Lead, South Dakota (USA). The final detector size will be 1,000 tons of ^{127}I. The advantage of the iodine detector as compared to the chlorine detector is the higher rate (41

SNU versus 9.3 SNU for the BP 95 SSM [1]), the larger sensitivity to ^{7}Be neutrinos and the much faster extraction (99% extraction efficiency in one hour) which in principle would allow to measure a possible MSW day-night effect. On the other hand, the neutrino capture cross sections on ^{127}I are not well known. For instance, a measurement of the cross section for ^{7}Be neutrinos can be achieved only by means of an artificial ^{37}Ar neutrino source.

References

[1] J.N. Bahcall and M.H. Pinsonneault, Rev. Mod. Phys. **67** (1995) 781-808.

[2] S. Turck-Chièze and I. Lopes, Ap. J. **408** (1993) 347.

[3] A. Dar, and G. Shaviv, Ap. J. **468** (1996) 933.

[4] J.N. Bahcall and M.H. Pinsonneault, Rev. Mod. Phys. **64** (1992) 885-926.

[5] A. Dar, these proceedings.

[6] R. Davis Jr., Nucl. Phys. B (Proc. Suppl.) **48** (1996) 284-298.

[7] B.T. Cleveland, T. Daily, R. Davis Jr., J.R. Distel, K. Lande, C.K. Lee and P.S. Wildenhain, submitted to The Astrophysical Journal, April 1996.

[8] Y. Totsuka, ICRR-Report 359-96-10 (March 1996), Institute for Cosmic Ray Research, Univ. of Tokyo, Japan.

[9] Y. Suzuki, Talk presented at the XVIIth Int. Conf. on Neutrino Physics and Astrophysics, Helsinki, Finland (June 1996). To be published in the Conference Proceedings.

[10] P. Anselmann et al. (GALLEX collaboration), Phys. Lett. **B357** (1995) 237-247.

[11] W. Hampel et al. (GALLEX collaboration):"GALLEX Solar Neutrino Observations: Results for GALLEX-III", (July 1996), to be published in Physics Letters B.

[12] J.N. Abdurashitov et al., Nucl. Phys. B (Proc. Suppl.) **48** (1996) 299-303.

[13] V. Gavrin, Talk presented at the XVIIth Int. Conf. on Neutrino Physics and Astrophysics, Helsinki, Finland (June 1996). To be published in the Conference Proceedings.

[14] P. Anselmann et al. (GALLEX collaboration), Phys. Lett. **B327** (1994) 377-385.

[15] K. Wolfsberg and G.E. Kocharov, in: The Sun in Time, C.P. Sonett, M.S. Giampapa, M.S. Matthews (eds.), University of Arizona Press, Tuscon (1991) 288-313.

[16] K. Wolfsberg, priv. communication (1992).

[17] P. Anselmann et al. (GALLEX collaboration), Phys. Lett. **B342** (1995) 440-450.

[18] W. Hampel et al. (GALLEX collaboration): "Preliminary results from the second ^{51}Cr neutrino source experiment in GALLEX", GALLEX internal note GX-90, (July 1996).

[19] M.B. Voloshin, M.I. Vysotskii and L.B.Okun, Soviet Phys. JETP **64** (1986) 446.

[20] C.S. Lim and W.J. Marciano, Phys. Rev. **D37** (1988) 1368.

[21] E. Akhmedov, Phys. Lett. **B213** (1988) 64.

[22] S. Massetti, M. Storini and J. Sykora, Proceedings of the 4th Int. Topical Workshop on New Trends in Solar Neutrino Physics, May 2-4, 1996, Gran Sasso, L'Aquila (Italy), 277-284.

[23] R.L. McNutt, Science **270** (1995) 1635-1639.

[24] J. Christensen-Dalsgaard, Nucl. Phys. B (Proc. Suppl.) **48** (1996) 325-334.

[25] W. Hampel, Physics World **3** (1990) 20-21.

[26] N. Hata, S. Bludman and P. Langacker, Phys. Rev. D**49** (1994) 3622-3625.

[27] J.N. Bahcall, Neutrino Astrophysics, 567 pages, Cambridge University Press (1989).

[28] V. Berezinsky, G. Fiorentini and M. Lissia, Phys. Lett. **B365** (1996) 185-192.

[29] S.T. Petcov, these proceedings.

[30] P.I. Krastev and S.T. Petcov, Nucl. Phys. B**449** (1995) 605-627.

[31] N. Hata and P. Langacker, Phys. Rev. D**50** (1994) 632-660.

[32] A.B. McDonald, Nucl. Phys. B (Proc. Suppl.) **48** (1996) 357-362.

[33] A.B. McDonald, Talk presented at the XVIIth Int. Conf. on Neutrino Physics and Astrophysics, Helsinki, Finland (June 1996). To be published in the Conference Proceedings.

[34] R.B. Vogelaar, Talk presented at the XVIIth Int. Conf. on Neutrino Physics and Astrophysics, Helsinki, Finland (June 1996). To be published in the Conference Proceedings.

[35] G. Bellini, Nucl. Phys. B (Proc. Suppl.) **48** (1996) 363-369.

[36] K. Lande, Talk presented at the XVIIth Int. Conf. on Neutrino Physics and Astrophysics, Helsinki, Finland (June 1996). To be published in the Conference Proceedings.

LSND RESULTS AND THEIR IMPLICATIONS

David O. Caldwell
Physics Department, University of California,
Santa Barbara, CA 93106-9530, USA
E-mail: caldwell@slacvx.slac.stanford.edu

The combined 1993, 1994, and 1995 data from the LSND experiment shows a statistically compelling excess of events of the type expected for $\bar{\nu}_\mu \to \bar{\nu}_e$ neutrino oscillations. An electron between 36 and 60 MeV is identified by Cherenkov and scintillation light from $\bar{\nu}_e p \to e^+ n$, and if a γ is tightly constrained to be correlated with it from $np \to d\gamma$ (2.2 MeV), then 22 such events are observed, but only 4.6 ± 0.6 are expected from backgrounds. The probability that this is a fluctuation is $< 10^{-7}$. If subsequent analysis shows a similar effect from the independent channel $\nu_\mu \to \nu_e$, then this would imply a neutrino mass difference which would contribute significantly to the dark matter of the universe. Explaining also the solar and atmospheric neutrino deficits results in a neutrino mass pattern which gives a cold + hot dark matter mix which fits the structure of the universe on all scales and requires a critical density universe and a universe age compatible with that of the oldest stars. This mass pattern involves a sterile neutrino, evidence for which may come from the need for it in producing heavy elements by supernovae and for blowing off the supernova mantle.

1 LSND Experiment

The existence of neutrino mass would have profound effects on particle physics, since that is outside the Standard Model, and on cosmology, since the $\sim 10^2$ relic neutrinos/cm^3 of each type would contribute significantly to the mass of the universe and hence to the formation of its structure. Evidence for neutrino mass comes from the LSND (Large Scintillator Neutrino Detector) experiment, which uses 800-MeV protons from the Los Alamos Meson Physics Facility accelerator. The protons produce eight times as many π^+ as π^- in water target, and $\sim$ 3% of the pions decay in flight ($\pi^+ \to \mu^+ \nu_\mu$), giving a ν_μ beam of up to about 180 MeV which goes into a tank 8.3 m long by 5.7 m in diameter. About 97% of the pions come to rest in a beam stop, and the resulting decay muons give a $\bar{\nu}_\mu$ beam via $\mu^+ \to e^+ \nu_e \bar{\nu}_\mu$ of maximum energy 52.8 MeV into the 200 tons of mineral oil in the tank 30 m away. A small amount of scintillator is added to the oil so that the 1220 8-inch-diameter photomultiplier tubes (25% coverage) can detect both rings of Cherenkov and the slower scintillation light. Events from the two beams are separated because of their energy difference. Thus although $\nu_\mu \to \nu_e$ is being searched for via the decay-in-flight beam, and ν_e's are produced in the decay at rest, the latter are of too low an energy to produce electrons in the search window. The $\bar{\nu}_e$

background for the $\bar{\nu}_\mu$ beam comes mainly from the symmetrical decay chain starting with a π^-, but this is suppressed by the π^-/π^+ ratio, by 95% of the π^- being absorbed and not decaying, and by 88% of the μ^- being captured, giving a relative yield of only $(1/8)(0.05)(0.12) = 8 \times 10^{-4}$.

The more difficult analysis looking for $\nu_\mu \to \nu_e$ oscillations has not yet produced a useful outcome, but results from the 1993+1994 data for $\bar{\nu}_\mu \to \bar{\nu}_e$ oscillations have already been published,[1] and the newer developments discussed here have been accepted for publication.[2] LSND detects $\bar{\nu}_e$ by $\bar{\nu}_e p \to e^+ n$, followed by a γ from $np \to d\gamma$ (2.2 MeV). Requiring an energy above 36 MeV eliminates most of the accidental background from $\nu_e\, ^{12}\mathrm{C} \to e^- X$ (the detector not distinguishing between e^+ and e^-), while the upper energy requirement of 60 MeV allows for the $\bar{\nu}_\mu$ endpoint plus energy resolution.

The first step in searching for $\bar{\nu}_e$ interactions is to select electrons, and by far the biggest background is from cosmic rays. The hadronic component is eliminated by a 2 kg/cm^2 overburden, and a liquid scintillator veto shield enclosing all but the bottom of the detector rejects muons efficiently. To eliminate decay $e^\pm$ from muons, a veto is imposed on any event occurring too soon after even low-level activity in the detector or veto shield; a hardware cut of $\approx$ 7 muon lifetimes is extended in software to as much as $\approx$ 18 muon lifetimes. Electrons are distinguished from neutrons and residual muons by both Cherenkov and scintillation light. The Cherenkov ring and ratio of late (scintillation) to early (Cherenkov) light selects electrons, but further cosmic ray events are reduced by eliminating those having track centers closer than 35 cm to the phototube faces and removing events near the outer parts of the tank and headed inward. Any remaining cosmic ray background is well measured because about 14 times as much data are collected outside of the beam spills as inside.

Cosmic rays also serve a useful purpose, however. The very large sample of decay $e^\pm$ from stopped cosmic ray muons covers exactly the right energy range to provide an energy calibration, a means of measuring energy resolution, and a mechanism for tuning cuts in an unbiased manner. These decay electrons can be compared with the muons from which they were created and with cosmic ray neutrons, identified by their 2.2-MeV capture γ rays and initial small signal.

The second step in searching for $\bar{\nu}_e$ interactions is to require a correlated 2.2 MeV γ within a reconstructed distance, $\Delta r < 2.5$ m from the e^+, having a relative time, $\Delta t < 1$ ms, and a number of hit phototubes $21 \leq N_\gamma \leq 50$. To determine if such a γ is correlated with the e^+, a function R of Δr, Δt, and N_γ is defined to be the ratio of approximate likelihoods for it to be correlated (by comparing with distributions from the cosmic neutron sample) to its being accidental (using accidental photons seen with laser calibration events).

Using a strict criterion for reducing accidentals to a 0.6% rate (i.e., $R >$ 30), and eliminating events with more than one γ, 22 events were observed for beam on and $36 \times 0.07 = 2.5$ events for beam off. The estimated beam-related background consisted of 1.72 ± 0.41 events with correlated neutrinos and 0.41 ± 0.06 without. The probability that the beam-on events are due entirely to a statistical fluctuation of the 4.6 ± 0.6 event expected total background is 4×10^{-8}. Figure 1(a) shows the energy distribution of all electrons before requiring a correlated photon (i.e., $R \geq 0$), and Fig. 1(b) shows that distribution when requiring $R > 30$.

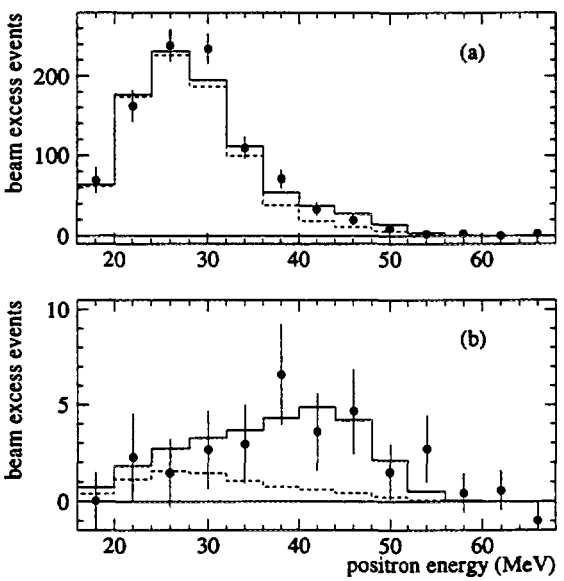

Figure 1: The energy distribution for positron events (a) without requiring a correlated γ ($R \geq 0$) and (b) with a tight requirement ($R > 30$) for a correlated γ. Shown in the figure are the beam-excess data, estimated neutrino background (dashed), and expected distribution for neutrino oscillations at large Δm^2 plus estimated neutrino background (solid).

While there are considerably more $R > 30$ events now than in the published report,[1] this is due more to changes in the analysis procedure than to additional data. Using the previous criteria,[1] there would be 13 events with an expected background of 4.3 ± 0.5, for which the probability of a fluctuation is

1×10^{-3}. Although Kolmogorov tests indicate no problem with the spatial distributions of the events, if the 55% of the tank volume is eliminated where the backgrounds are most intense, 6 events remain, whereas 1.7 ± 0.3 are expected, giving a fluctuation probability of 1×10^{-2}.

Statistically these events indicate the existence of neutrino oscillations. One may then ask whether these events have characteristics of oscillations. While a real proof of this would require changing the source-to-detector distance, Fig. 1 at least shows that the energy distribution of the $R > 30$ events is compatible with that expected from oscillations. Furthermore, Fig. 2, which shows the distribution in angle between the incident neutrino and the outgoing positron, is also oscillation like. The significance of this plot is enhanced by comparison with the quite different angular distributions provided by $\nu_e C \rightarrow e^- X$ and ν_e scattering.

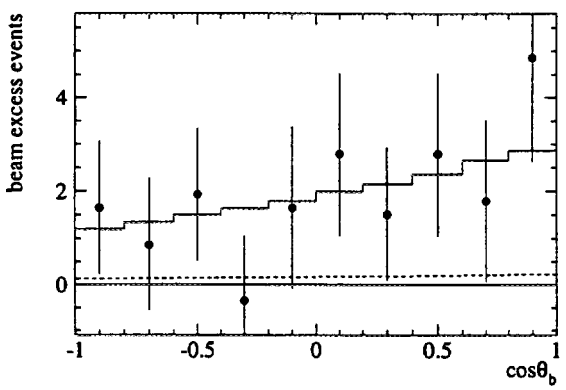

Figure 2: The $\cos\theta_b$ distribution for beam-excess data events with $36 < E_e < 60$ MeV and $R > 30$ and that expected for neutrino oscillations at large Δm^2 (solid). The dashed curve is the estimated neutrino background. θ_b is the e^+ angle with respect to the neutrino direction.

Assuming oscillations are being observed, one may use the simplification of a two-generation neutrino oscillation probability

$$P = (\sin^2 2\theta) \sin^2(1.27\Delta m^2 L/E)$$

to describe the results. To determine favorable ranges of the mass-squared difference, Δm^2, as a function of the mixing angle, θ, between the two neutrino mass eigenstates, a fit is made to the observed event energy E, the neutron

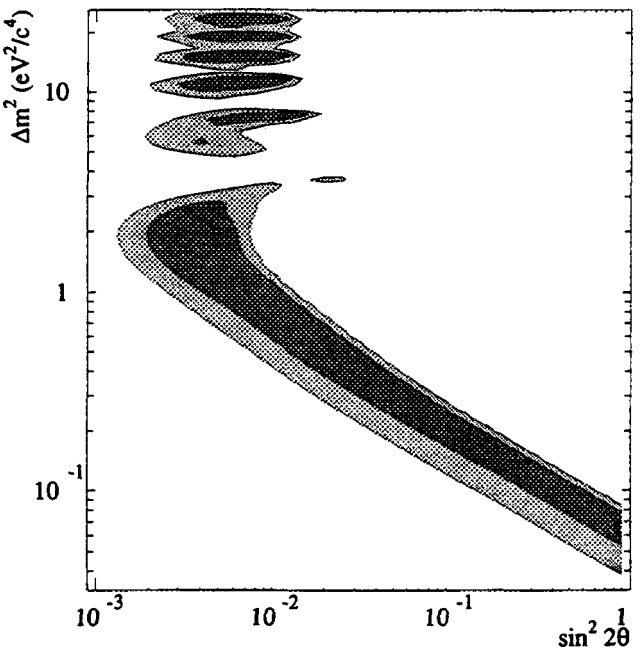

Figure 3: Mass-squared difference (Δm^2) vs. degree of mixing ($\sin^2 2\theta$) assuming a two-neutrino oscillation explanation of the LSND beam-excess data. Shown are regions of Δm^2 favored by a fit using the energy (from 20 to 60 MeV) and distance from the source of each event.

likelihood ratio R, the direction of the electron relative to the neutrino, and the distance of the event from the source L. In order to increase the range of L/E, values of E down to 20 MeV were used. Figure 3 shows favored regions of Δm^2, with contours at 2.3 and 4.5 log-likelihood units from the maximum. If this were a gaussian distribution, which it is not, the contours would correspond to 90% and 99% likelihood levels, but in addition they have been smeared to account for some systematic errors. Comparison to the KARMEN experiment,[3] which presents results in a similar way, shows no conflict, but if limits are plotted (as they are in Ref. 2) on this graph from E776 at BNL [4] and the Bugey reactor experiment,[5] then one might conclude that the only allowed Δm^2 region is 0.2–3 eV^2. If instead an 80% confidence level band is calculated to compare with the 90% confidence level limits of those experiments using, as they do, just numbers of events (i.e., not using the L/E information) and using only the 36–60 MeV region with its much lower background, then there is no conflict with other experiments above 0.2 eV^2.

If the same effect is seen in $\nu_\mu \rightarrow \nu_e$, then the case for neutrino mass is very strong, since the different detection mechanism ($\nu_e\,{}^{12}\mathrm{C} \rightarrow e^- X$) and the higher energy makes these two determinations essentially independent. The ν_e analysis is made more difficult because of the single signal of an e^- and because there is no calibration process like the $e^\pm$ from stopped muon decays for that high energy e^-. If $\nu_\mu \rightarrow \nu_e$ eventually shows an excess similar to that for $\bar{\nu}_\mu \rightarrow \bar{\nu}_e$, however, this would require that the observation is being made near an oscillation maximum, such as the 2, 6, and 10 eV^2 regions of Fig. 3. The maxima for the higher energy $\nu_\mu \rightarrow \nu_e$ are near 6, 18, ... eV^2, so a likely overlap is about 6 eV^2. These are rough numbers, and 6 could as well be 8, for example.

2 Possible Cosmological Consequences

While the LSND $\bar{\nu}_\mu \rightarrow \bar{\nu}_e$ result could imply a range of $\Delta m^2 > 0.2$ eV, let us examine the consequences if $\nu_\mu \rightarrow \nu_e$ is also seen and Δm^2 is in the 6–8 eV^2 range. If, for definiteness, $\Delta m^2 = 6$ eV^2, either the ν_μ or ν_e is ≥ 2.4 eV, a value which would contribute $\gtrsim 10\%$ to the mass of the universe for critical density ($\Omega = 1$). This is a contribution to Ω equivalent to as much baryonic matter as nucleosynthesis permits and is more than an order of magnitude more than the baryonic matter observed so far. Models of the universe which utilize a density lower than critical (typically $\Omega \leq 0.3$) would then not have enough cold dark matter to produce sufficiently early structure formation, since the 2.4 eV neutrinos (hot dark matter) would wash out density fluctuations.[6] The only other models which come close to fitting the observed structure of the universe on all scales have $\Omega = 1$, so such a neutrino likely forces critical density, a requirement for an era of inflation and the only time-stable value for no cosmological constant.

One species of 2.4 eV neutrino would not provide a cold plus hot dark matter model which would fit structure information well. These models were created because the cold dark matter model (CDM), which was a fair approximation to the structure of the universe, when normalized to the COBE data, produced too much structure on small scales, since baryons readily clump around the cold dark matter. The first cold + hot dark matter models (CHDM) had $\sim 30\%$ neutrinos and fit structure on all scales very well[7] because the free streaming of the neutrinos reduced density fluctuations on small scales. Unfortunately, this damping of density perturbations also caused structure to form too late. Reducing the neutrino content to $\sim 20\%$ allowed early enough structure formation.[8] With all the mass in one neutrino species, this otherwise successful model (CνDM) overproduced clusters of galaxies. In other words,

the CνDM model worked well at all distance scales except $\sim 10h^{-1}$Mpc, where h is the Hubble constant in units of 100 km·s^{-1}·Mpc^{-1}. If $h = 0.5$ and $\Omega = 1$, the mass of the neutrino required in the CνDM model is $94h^2\Omega F_\nu = 4.7$ eV, for a neutrino fraction of Ω, $F_\nu = 0.20$. If instead this mass is divided between two nearly degenerate neutrino species, the motivation for which will be discussed shortly, then this Cν^2DM model turned out to have a remarkable property.[6] While 4.7 eV in one neutrino species or two makes essentially no difference at very large or very small scales, at $\sim 10h^{-1}$Mpc the larger free-streaming length of the 2.4 eV neutrinos tends to wash out fluctuations and lowers the abundance of clusters. Thus the model (Cν^2DM) with two, 2.4 eV neutrinos fits structure information on all scales.

The Cν^2DM model works only if $\Omega = 1$ and if $h \lesssim 0.6$. The sets of determinations of h have been grouped near 0.5 and 0.7–0.8, with the latter being incompatible with $\Omega = 1$ and the age of the oldest stars. Recently there has been some convergence, with the upper values moving down and the lower values being more like 0.55, which for $F_\nu = 0.20$ would correspond to 2.8 eV neutrino mass or $\Delta m^2 = 8$ eV^2 for LSND. Should LSND determine Δm^2 and the masses needed for the Cν^2DM model be bourne out, then terrestrial experiments will have settled the long-disputed and all-important cosmological parameters Ω and h.

3 Possible Neutrino Mass Patterns

The reason the large-scale simulations for the Cν^2DM model were tried was a scenario[9] for neutrino masses designed to account for three hints of neutrino mass, one of which is the need for some hot dark matter. Of the other two, one is the deficit of ν_es from the sun observed by four experiments of three types. Of those three types, two have to be making incorrect observations in order for an astrophysical explanation of the deficit to work.[10] A solution in terms of neutrino oscillations requires that the mass-squared difference between the ν_e and whatever it turns into be no more than $\Delta m^2_{ei} \sim 10^{-5}$ eV^2. The second indication for neutrino mass results from evidence for a deficit of ν_μs relative to ν_es in atmospheric secondary cosmic rays. There are compatible results from three experiments[11] and further information from Kamiokande.[12] The latter includes accelerator confirmation of the ability to separate ν_e and ν_μ events, as well as an independent higher energy data set giving not only a ν_μ/ν_e ratio agreeing with the lower energy data, but also a zenith-angle (hence source-to-detector) dependence compatible with oscillations requiring $\Delta m^2_{\mu i} \sim 10^{-2}$ eV^2. The explanation of the observations in terms of the oscillation $\nu_\mu \to \nu_e$ is almost excluded by data from the Bugey[5] and Krasnoyarsk[13] reactor

oscillation experiments. Also, in the higher energy Kamiokande data,[12] the muons display the zenith-angle dependence, whereas the electrons do not, as would be expected if the ν_μ were affected by oscillations, but the ν_e were not. Finally, the calculated ν_e and ν_μ fluxes—backed by measurements of μ fluxes—agree with the ν_e data but show a ν_μ deficit.[14] Thus $\nu_\mu \to \nu_\tau$ oscillations are favored as an explanation of this atmospheric ν_μ deficit.

If the solar ν_e and atmospheric ν_μ deficits and the need for some hot dark matter arise from the existence of neutrino mass, then there are basically two patterns of those masses.[9] Other schemes[15] are essentially rearrangements of those two patterns, and if LSND's evidence is correct, then one of those two patterns is ruled out. Invoking three-neutrino oscillations has difficulty in accommodating the three distinct mass differences needed,[16] and it appears likely that introducing a fourth (sterile) neutrino is necessary, as was done in the remaining one of the two mass patterns[9] just mentioned. The sterile neutrino, ν_s, which does not have the normal weak interactions and hence does not contribute to the width of the Z^0 boson, must still not exceed the limit on the number of relativistic species at the time of nucleosynthesis. This limitation, perhaps 3.5–4 — a subject of current controversy — can be avoided for the favored small mixing angle MSW or the vacuum oscillation solution for solar $\nu_e \to \nu_s$, since any other use of a light ν_s would bring it into equilibrium in the early universe. The ν_μ and ν_τ then provide the atmospheric ν_μ deficit and share the dark matter, making $m_{\nu_\mu} \approx m_{\nu_\tau} \approx 2.4$–$2.8$ eV. A combination of the SNO and SuperKamiokande experiments will be able to demonstrate $\nu_e \to \nu_s$ to check this mass pattern, which is consistent with the LSND oscillation result.

4 Supernovae Information

There is, however, a possible conflict between the $\bar{\nu}_\mu \to \bar{\nu}_e$ interpretation of the LSND data and information from supernovae. It is believed that much of heavy element production occurs in the outer neutrino-heated ejecta of Type II supernovae, where rapid interactions with the large number of neutrons can take place, the so-called r process. A limitation on the mixing of ν_μ and ν_e comes about because energetic ($\langle E \rangle \simeq 25$ MeV) ν_μ could convert via an MSW transition to ν_e inside the region where the r process is believed to occur. Such converted ν_e would have a much higher energy than the thermal ν_e ($\langle E \rangle = 11$ MeV), because the latter have charged current interactions with electrons and hence emerge from farther out in the supernova. Since the cross section for $\nu_e n \to e^- p$ rises rapidly with energy, the energetic ν_e would deplete the neutrons, stopping the r process. Calculations[17] of this effect limit $\sin^2 2\theta$ for $\nu_\mu \to \nu_e$ to $\lesssim 10^{-4}$ for $\Delta m^2_{\mu e} \gtrsim 2$ eV^2, apparently in conflict with the

LSND results.

Recently problems have been found with the r process itself which would require the region in which it takes place to be even more neutron rich, exacerbating the LSND conflict. A possible solution to these issues comes from inverting the neutrino mass hierarchy,[15] but a more likely solution is provided by the sterile neutrino, which produces two effects.[18] First, there is a zone outside the neutrinosphere but inside the $\nu_\mu \to \nu_e$ MSW region where the ν_μ interaction potential goes to zero, so a $\nu_\mu \to \nu_s$ transition can occur, reducing the dangerous high-energy $\nu_\mu s$. Second, because of the reduction in $\nu_\mu s$, the dominant process in the MSW region reverses, becoming $\nu_e \to \nu_\mu$, which reduces the ν_e flux into the r-process region, making it more neutron rich because of fewer $\nu_e n \to e^- p$ reactions.

The sterile neutrino may have two further uses in supernovae. While the r process goes on at rather late times ($\sim$ 10 s post bounce), another nucleosynthesis process goes on at early times ($\sim$ 1 s) and requires a proton-rich region. This p process could be aided by two regions where the ν_e interaction potential goes to zero, one inside the core and the other outside the neutrinosphere. The first converts $\nu_e \to \nu_s$, which then escape the dense core and reconvert at the second, producing high energy ν_es which produce protons via $\nu_e n \to e^- p$. These regions are effective only at these very early times and may provide the needed extra energy deposit to blow off the supernova mantle, since in present calculations the shock is stalled at an early time (0.15 s post bounce) close to the radius at which the $\nu_s \to \nu_e$ reconversion would occur at that time.

Thus there may be evidence for the sterile neutrino which had to be invoked in a rather ad hoc fashion to provide the small mass difference scale needed to explain the solar ν_e deficit, if the other active neutrinos are needed for the atmospheric ν_μ/ν_e ratio and both the hot dark matter component and the LSND result.

5 Conclusions

The LSND observation of 22 events of the type $\bar{\nu}_e p \to e^+ n$, $np \to d\gamma$, whereas 4.6 ± 0.6 were expected, is statistically strong evidence for $\bar{\nu}_\mu \to \bar{\nu}_e$ oscillations. If this is confirmed by a similar observation in the essentially independent $\nu_\mu \to \nu_e$ channel, then this will be the first laboratory violation of the Standard Model of particle physics and will likely provide evidence for a neutrino of 2–3 eV. Such a neutrino ensures that low-Ω models of the universe do not work, making it very likely that the universe has critical density ($\Omega = 1$). If the solar ν_e and atmospheric ν_μ deficits are also a result of neutrino mass, then the former can be explained by $\nu_e \to \nu_s$ (a sterile neutrino) and the latter by $\nu_\mu \to$

ν_τ. The ν_μ and ν_τ almost equally share the needed 5–6 eV for a cold + hot dark matter model of the universe which fits the structure on all scales, and besides requiring $\Omega = 1$, also needs a low value of the Hubble constant, eliminating problems of the universe age. Evidence for this pattern of neutrino masses may also be coming from the production of heavy elements in supernovae, since the ν_s may play a crucial role there. Thus the lightest elementary particle which can have mass and which has remarkably little interaction with other matter likely has profound effects in particle physics, astrophysics, and cosmology.

Acknowledgments

The author's work was supported in part by the U.S. Department of Energy. Appreciation is due to the extensive contributions to this work provided by the LSND collaboration, R.N. Mohapatra, J.R. Primack, G.M. Fuller, Y.-Z. Qian, A. Klypin, and J. Holtzman.

References

1. C. Athanassopoulos et al., *Phys. Rev. Lett.* **75**, 2650 (1995).
2. C. Athanassopoulos et al., to appear in both *Phys. Rev. Lett.* and *Phys. Rev. C.*
3. G. Drexlin, *Prog. in Part. and Nucl. Phys.* **32**, 375 (1994); B. Armbruster et al., *Nucl. Phys. (Proc. Suppl.)* **B38**, 235 (1995).
4. L. Borodovsky et al., *Phys. Rev. Lett.* **68**, 274 (1992).
5. B. Achkar et al., *Nucl. Phys.* B **434**, 503 (1995).
6. J.R. Primack et al., *Phys. Rev. Lett.* **74**, 2160 (1995).
7. A. Klypin et al., *Astrophys. J.* **416**, 1 (1993).
8. A. Klypin et al., *Astrophys. J.* **444**, 1 (1995).
9. D.O. Caldwell, *Perspectives in Neutrinos, Atomic Physics and Gravitation*, Gif-sur-Yvette, France: Editions Frontières, 1993, p. 187; D.O. Caldwell and R.N. Mohapatra, *Phys. Rev.* D **48**, 3259 (1993); *ibid.* **50**, 3477 (1994); J.T. Peltoniemi and J.W.F. Valle, *Nucl. Phys.* B **406**, 409 (1993); Z. Shi et al., *Phys. Rev.* D **48**, 2563 (1993).
10. J.N. Bahcall, *Phys. Lett.* B **338**, 276 (1994); P.I. Krastev and A. Yu. Smirnov, *Phys. Lett.* B **338**, 282 (1994); V. Berezinsky et al., *Phys. Lett.* B **365**, 185 (1996); N. Hata and P. Langacker, *Phys. Rev.* D **52**, 420 (1995).
11. K.S. Hirata et al., *Phys. Lett.* B **280**, 146 (1992); R. Becker-Szendy et al., *Phys. Rev.* D **46**, 3720 (1992); P.J. Litchfield, in *Proc. Int. Europhys. Conf. on High Energy Physics*, Gif-sur-Yvette, France: Editions

Frontières, 1993, p. 557.
12. Y. Fukuda et al., *Phys. Lett.* B **335**, 237 (1994).
13. G.S. Vidyakin et al., *JETP Lett.* **59**, 390 (1994).
14. G. Barr et al., *Phys. Rev.* D **39**, 3532 (1989); W. Frati et al., *Phys. Rev.* D **48**, 1140 (1993); D.H. Perkins, *Astroparticle Physics* **2**, 249 (1994).
15. G.M. Fuller, J.R. Primack, and Y.-Z. Qian, *Phys. Rev.* D **52**, 1288 (1995); D.O. Caldwell and R.N. Mohapatra, *Phys. Lett.* B **354**, 371 (1995); G. Raffelt and J. Silk, *Phys. Lett.* B **366**, 429 (1996).
16. C.Y. Cardall and G.M. Fuller, *Phys. Rev.* D **53**, 4421 (1996).
17. Y.-Z. Qian et al., *Phys. Rev. Lett.* **71**, 1965 (1993); Y.-Z. Qian and G.M. Fuller, *Phys. Rev.* D **51**, 1479 (1995); G. Sigl, *Phys. Rev.* D **51**, 4035 (1995).
18. D.O. Caldwell, G.M. Fuller and Y.-Z. Qian, in preparation; the use of $\nu_\mu \to \nu_s$ to avoid the bound on LSND has been noted also by S. Petcov (private communication) and by J.T. Peltoniemi, Univ. of Helsinki preprint HU-TFT-95-69 (1995, unpublished).

Neutrino Oscillation Experiments

Leslie Camilleri
CERN, 1211 Geneva 23, Switzerland

Abstract

Neutrino oscillation experiments ($\nu_\mu \rightarrow \nu_e$ and $\nu_\mu \rightarrow \nu_\tau$) currently being performed at accelerators are reviewed. Future plans for short and long base-line experiments are summarized.

1 Introduction

Under the assumption that neutrinos are massive and that mixing in the lepton sector can be described by a unitary matrix U_{fk} similar to the Cabibbo-Kobayashi Maskawa matrix [1] in the quark sector, then the weak eigenstates ν_e, ν_μ, ν_τ are related to the mass eigenstates ν_1, ν_2, ν_3 by the transformation:

$$|\nu_f >= \sum_{k=1}^{3} U_{fk}|\nu_k > \qquad k = 1,2,3 \qquad f = e, \mu, \tau$$

This allows oscillations [2] to occur. In the case of two-neutrino mixing, such as ν_μ and ν_τ, the probability for finding a ν_τ having started with a ν_μ is given by $P_{\mu\rightarrow\tau} = \sin^2 2\theta \sin^2 2\pi L/\lambda$ where θ = mixing angle which characterizes the strength of the oscillation, L (km) = distance between source and detector, λ = oscillation length = $5E_\nu(\text{GeV})/\Delta m^2(\text{eV}^2)$ with E_ν = neutrino energy, $\Delta m^2 = m^2_{\nu_1} - m^2_{\nu_2}$.

For the probability of oscillation to be significantly different from zero the smallness of Δm^2 must be compensated by a large L or a small E_ν. For small λ (small E_ν or large Δm^2) several oscillations can occur within the detector and $\sin^2(2\pi L/\lambda)$ averages to $\frac{1}{2}$ yielding

$$P_{\mu\rightarrow\tau} = \frac{1}{2}\sin^2 2\theta.$$

The present state of the exclusion plot for $\nu_\mu \rightarrow \nu_\tau$ is shown in Fig. 1. The best limit at high $\Delta m^2, \sin^2 2\theta < 5 \times 10^{-3}$ at 90% CFL, is set by E531 [3] at Fermilab. Similar limits are set by CHARM II [4] and CCFR [5].

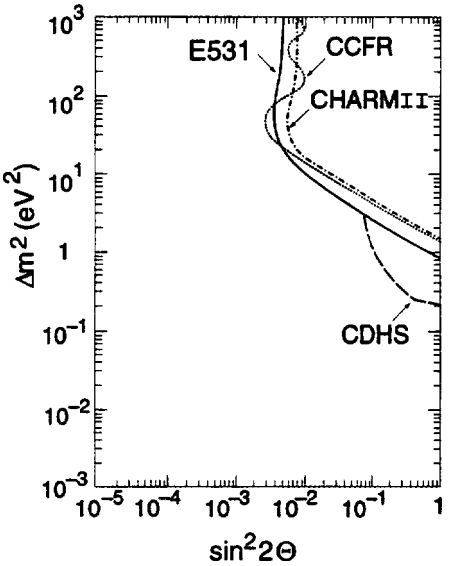

Figure 1: Present state of the $\nu_\mu \rightarrow \nu_\tau$ exclusion plot

2 Observations that Could Benefit from Massive Neutrinos

2.1 Dark matter

If the flat rotational curve of galaxies [6] is interpreted as pointing to the existence of Dark Matter and if this dark matter is identified with the fossil neutrinos left over from the Big Bang, from the density of those neutrinos, 100 $(\nu + \overline{\nu})$ of each flavour per cm^3 and the dark matter density needed to explain the velocity curves, one can infer a neutrino mass of 10 eV/c^2.

2.2 Solar neutrinos

Several experiments [7] have measured the flux of solar neutrinos on earth and found a deficit. The results of the four experiments, combined with the measured luminosity of the sun, indicate that all the pp neutrinos 43% of the boron neutrinos and none of the beryllium neutrinos are observed. This is difficult to understand in terms of a deficiency of the solar models [8] since the beryllium and the boron neutrinos have the same "origin". One possible explanation is that ν_e neutrinos produced in the sun oscillate, on the way to earth, to other types of neutrinos, to which the experiments are not as sensitive. In particular Mikheyev, Smirnov and Wolfenstein (MSW) have proposed a model [9], in which the mixing angle in matter θ_m is related to the mixing angle in vacuum θ_v, the density of the sun, ρ_{SUN}, and the neutrino energy E_ν by:

$$\tan 2\theta_m = \frac{\sin 2\theta_v}{\cos 2\theta_v - \frac{0.76\times10^{-7}\rho_{Sun}E_\nu}{\Delta m^2}}$$

Maximal mixing happens when the denominator goes to zero. If this happens at the energy of the beryllium neutrinos then a value of Δm^2 of 10^{-5} eV^2 is obtained. If the oscillation is attributed to $\nu_e \rightarrow \nu_\mu$ and assuming that $m_{\nu e} \sim 0$, one can then estimate the mass of the ν_τ through the see-saw mechanism [10] that relates the neutrino masses to the quark masses

$$m_{\nu_e} : m_{\nu_\mu} : m_{\nu_\tau} = m_u^2 : m_c^2 : m_t^2$$

yielding $m_{\nu_\tau} \sim 33$ eV^2.

2.3 Atmospheric neutrinos

Atmospheric neutrinos produced in the decays of pions and kaons themselves produced in the interaction of cosmic rays in the upper atmosphere, have been observed [11] in the Kamiokande experiment and others. The expected ratio of ν_μ's to ν_e's is observed to be close to 1 whereas a ratio of 2 is expected. This also could point to oscillations. A measurement of this ratio as a function of zenith angle for higher energy neutrinos has also been performed by Kamiokande [12]. It indicates that the ν_μ/ν_e ratio is most different from expectations for neutrinos entering the detector from below, that is for neutrinos produced 12 000 km away. If this disagreement with expectations is attributed to $\nu_\mu \rightarrow \nu_\tau$ oscillations then $\Delta m^2 = 1.6 \times 10^{-2}$ eV^2 and $\sin^2 2\theta = 1.0$. To probe this region of Δm^2 would require long baseline experiments.

3 The Experiments

The experiments running or approved to run are listed in Table 1.

Table 1:

Experiment	Accel.	Beam	Typical energy	Distance	Mode	Status start-up
KARMEN	ISIS (Rutherford)	ν_μ $\overline{\nu}_\mu$	0.1 GeV	17 m	$\nu_e, \overline{\nu}_e$ Appear	Running 1990
LSND	LAMPF (Los Alamos)	ν_μ $\overline{\nu}_\mu$	0.1 GeV	27 m	$\nu_e, \overline{\nu}_e$ Appear	Running 1993
CHORUS	SPS (CERN)	ν_μ	30 GeV	800 m	ν_τ Appear	Running 1994
NOMAD	SPS (CERN)	ν_μ	30 GeV	800 m	$\nu\tau$ Appear	Running 1995
E803	MAIN INJ. (Fermilab)	ν_μ	10 GeV	470 m	ν_τ Appear	Approved 2000
ICARUS	CERN → GRAN SASSO	ν_μ	10 GeV	732 km	ν_μ Disap. ν_e Appear.	
MINOS	FERMILAB → SOUDAN	ν_μ	10 GeV	732 km	ν_μ Disap. ν_e Appear.	2000
SUPER KAMIOKANDE	KEK 12 GeV (50 GeV) → Super K	ν_μ	1 GeV	250 km	ν_μ Disap. ν_e Appear.	1998 (2003)

3.1 The KARMEN [13] and LSND [14] experiments

The principle of these two experiments is the same. An 800 MeV proton beam is incident on a target in which the pions produced come to rest. The π^+ (at rest) $\rightarrow$ μ^+ (at rest) $\rightarrow$ e^+ decay chain produces ν_μ's, $\overline{\nu}_\mu$'s and ν_e's. The experiments look for the oscillation of $\overline{\nu}_\mu$'s into $\overline{\nu}_e$'s. These are then observed through the $\overline{\nu}_e p \rightarrow e^+ n$ reaction in which the positron is in the $37 < E_e < 50$ MeV range. The $\overline{\nu}_e$'s in the $\pi^- \rightarrow \mu^- \nu_\mu, \mu^- \rightarrow e^- \nu_\mu \overline{\nu}_e$ chain are suppressed by the π^+/π^- ratio of ~ 8, most (95%) of the π^-'s coming to rest in the beam-stop undergoing capture before decaying, the μ^-'s produced by the 5% of the π^-'s that do decay before capture being themselves mostly (88%) captured from atomic orbits before decay. Altogether the relative yield of these is 7.5×10^{-4}. The two experiments do not use a magnetic field and therefore cannot measure the charge of the observed e^-/e^+.

The KARMEN detector consists of a 56 ton segmented liquid scintillator calorimeter. The energy is measured by pulse height and the position by the cell size. The neutron is identified through photons (8 MeV) it emits in its interaction with gadolinium located on foils placed between the calorimeter cells. The neutron travels typically 1 m before interacting and the photons are emitted within 250 μs of the positron detection time. The detector is located 17 m from the target and at 90° to the incident beam direction. The time structure of the KARMEN machine, two 100 ns pulses separated by 330 ns, and a repetition rate of 50 Hz, results in the $\overline{\nu}_e$'s being expected mostly at a time of no accelerator activity, the muon lifetime being 2.3 μs.

The candidate events for $\overline{\nu}_e$'s do not exhibit a time distribution relative to the beam on target time characteristic of the muon lifetime thus leading KARMEN to conclude that no $\overline{\nu}_\mu \rightarrow \overline{\nu}_e$ oscillations are observed at the level of $\sin^2 2\theta < 7.5 \times 10^{-3}$ at large Δm^2. The experiment also sets a limit of $\sin^2 2\theta < 3.8 \times 10^{-2}$ for $\nu_\mu \rightarrow \nu_e$ oscillations through the non observation of $\nu_e C \rightarrow e^- N$ in the E_{e^-} range 60 $\rightarrow$ 180 MeV. KARMEN is currently being upgraded with a better veto shield which will allow its sensitivity to be improved by a factor of 10 within a few years.

The LSND detector consists of a 180 ton tank of liquid scintillator. The energy is measured both through the pulse height of the scintillator light and the radius of the Čerenkov ring emitted by the electron, both being detected by photomultipliers lining the inner surface of the tank. The position of the particles is determined using phototube timing. The neutron is identified as in KARMEN except that the photons are emitted through its interaction with the protons in the scintillator: $np \rightarrow d\gamma (E_\gamma = 2.2$ MeV). The detector is located 27 m from the target at an angle of 17° to the beam. The time structure of the LAMPF accelerator, a 500 μs continuous spill repeated every 8.3 ms makes the detection of the expected $\overline{\nu}_e$'s coincident with accelerator activity, unlike KARMEN. Because of this long spill the requirement that the events be observed with the characteristic muon lifetime distribution relative to beam on target time, cannot be used by LSND. They discriminate between background events and signal events using a likelihood: R, computed for each event and based on the difference in position between the positron and the photon, the difference in time between the positron and the photon and the photon pulse height. The positron energy distribution for events with $R > 30$ is shown in fig. 2 together with the expected background.

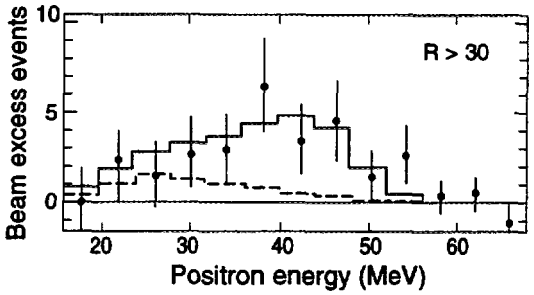

Figure 2: The positron energy distribution obtained by LSND for the likelihood R (defined in the text) greater than 30.

A total of 22 events are seen in the interval $36 < E_e < 60$ MeV, where 2.5 background events are expected from non-beam sources and 2.14±0.4 from beam-related sources. A fit of the overall likelihood distribution for events with $20 < E_e < 60$ MeV, to a sum of correlated and uncorrelated neutron-positron distributions yields a total of $51.8^{+18.7}_{-16.9}$ candidate events and an oscillation probability of $(0.31^{+0.11}_{-0.10} \pm 0.05)\%$. The expected energy distribution including an oscillation contribution with large Δm^2 is also shown in fig. 2. The regions of 90% and 99% CFL obtained by LSND are shown in fig. 3 together with the limits set by KARMEN, E776 [15] and the Bugey [16]. There is a region at $\Delta m^2 < 2 - 3eV^2$ that could still satisfy all the experiments.

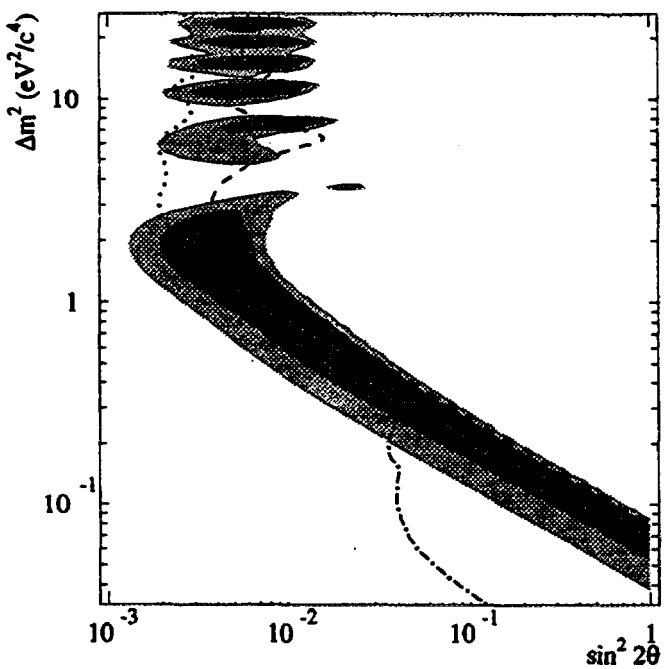

Figure 3: The LSND Δm^2 vs $\sin^2 2\theta$ favoured regions. The darkly shaded and lightly shaded regions are the 90% and 99% likelihood regions. Dashed curve: KARMEN, Dotted curve: E776, dot-dashed curve: Bugey.

3.2 The neutrino oscillation experiments at CERN

There are two experiments, the CERN Hybrid Oscillation Research Apparatus (CHORUS) [17] and the Neutrino Oscillation Magnetic Detector (NOMAD) [18]. Both are looking for $\nu_\mu \rightarrow \nu_\tau$ oscillations through the appearance of ν_τ's in a ν_μ beam. The ν_τ is searched for through its charged current interaction $\nu_\tau N \rightarrow \tau^- X$.

The 450 GeV/c protons accelerated by the SPS are directed onto a target to produce pions and kaons which subsequently decay giving neutrinos. The target is made of beryllium, a low atomic number material, to reduce multiple scattering and avoid widening of the beam. The target has a small diameter (3 mm) to avoid reinteraction of secondaries and therefore degradation of the energy spectrum, and is long enough (1.1 m) to allow 93% of the protons to interact. The secondaries of a given sign are focused into a parallel beam by two magnetic horns. These horns consisting of two coaxial current sheets providing a toroidal field run at currents of 100 kA. They must therefore be pulsed. For this reason and in order to reduce cosmic ray background, the protons are delivered to the target in two 6 ms long spills at each SPS cycle. The horns are followed by a 290 m long evacuated decay tunnel. The muons are bent away by a magnetic iron toroid and ranged out by shielding. About 2.5×10^{13} protons are incident on the beryllium target every 14.4 s. The beam composition is $\nu_\mu : \overline{\nu}_\mu : \nu_e : \overline{\nu}_e = 1 : 0.054 : 0.009 : 0.002$.

The intrinsic fraction of ν_τ's in the beam, coming from the decay of D_S mesons produced in the target is estimated [19] to be $\sim 5 \times 10^{-6}$ which is negligibly small. CHORUS started running in 1994 and has collected 3.1×10^{19} protons on target (pots) whereas NOMAD started in 1995 and has collected 1.8×10^{19} pots. Both experiments will run until the end of 1997.

NOMAD (fig. 4) intends to distinguish $\nu_\tau N \rightarrow \tau^- X$ events from background using kinematical cuts such as missing P_T, angular correlations etc. To do so very good energy, momentum and angular resolutions are needed. The τ is detected through its $e\,\overline{\nu}_e\nu_\tau$, $\mu\overline{\nu}_\mu\nu_\tau$, $\pi^-\nu_\tau$, $\rho^-\nu_\tau$, $\pi^+\pi^-\pi^-(n\pi^0)\nu_\tau$ decay modes for a total of 83% of its branching ratio. The target consists of the walls of the drift chambers used for momentum measurement: 132 planes spread over 4 m amounting to 3 tons in mass and to only 1 radiation length in total. The experiment reuses the UA1 magnet inside which the drift chambers are placed. The momentum resolution, $\sigma(p)/p$, for an average length track varies between 3 and 5% over the momentum range relevant to the measurement. The electromagnetic calorimeter needed to identify electrons and measure photons consists of lead glass and has an energy resolution of $\sigma(E)/E = 0.04/\sqrt{E} + 0.01$.

The discrimination between electrons and pions is provided by 9 transition radiation modules each consisting of 350 foils of polypropylene followed by a plane of 176 straw tubes containing a xenon-methane mixture to detect the transition radiation X-rays. A preshower consisting of a lead sheet followed by two planes of proportional tubes provides further e/π separation. Chambers behind walls of iron provide muon identification. Some of this iron has been instrumented to provide a hadron calorimeter.

As an example of the type of cuts used in the analysis, the electronic decay of the τ will be considered.

$$\nu_\tau N \rightarrow X\tau^- \rightarrow e^-\overline{\nu}_e\nu_\tau$$

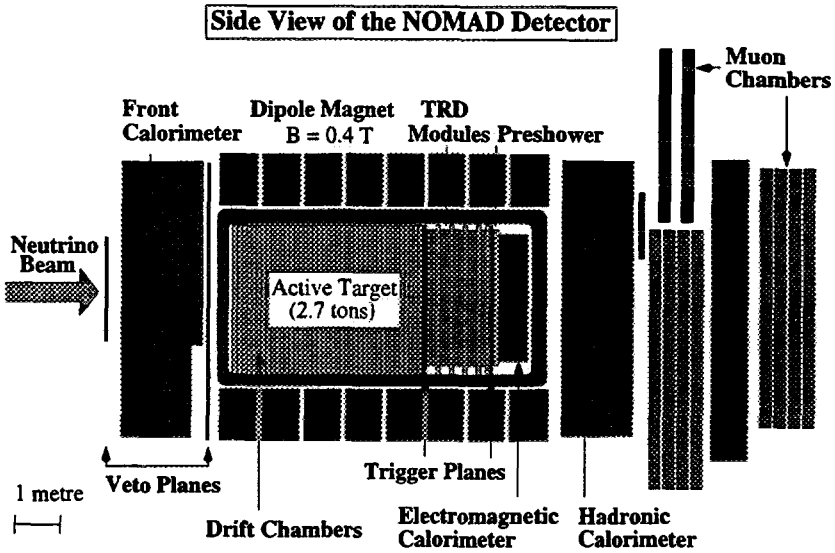

Figure 4: The NOMAD detector

The major background to this channel is caused by charged current interactions of the $\sim 1\%$ ν_e component of the beam $\nu_e N \rightarrow Xe^-$.

In the plane perpendicular to the beam direction, angles between the electron and the resultant hadron vector, ϕ_{eh}, and between the missing P_T and the resultant hadron vector, ϕ_{mh}, are defined (fig. 5a,b). For the background reaction, since the electron and the hadrons are the only particles in the reaction, the Monte Carlo distribution for ϕ_{eh} is sharply peaked at π (fig. 5c). For the τ reaction, the τ is back to back to the hadrons, but the electron from its decay will not be necessarily back to back with the hadron (fig. 5d). In the background reaction any missing P_T will arise either from missed particles or from mismeasurements resulting in a flat ϕ_{mh} distribution (fig. 5e). In the τ reaction the missing P_T will be due to the two missing neutrinos and will be centered on the τ direction, resulting in a peak in ϕ_{mh} at π (fig. 5f). The ϕ_{eh} and ϕ_{mh} distributions are quite different for the background and signal.

The number of events expected to be seen by NOMAD for an exposure of 2.4×10^{19} pots, should oscillations occur just at the present limit of $\sin^2 2\theta = 5 \times 10^{-3}$ is listed in Table 2, together with the number of background events expected in each of the τ decay modes. With these numbers NOMAD will be able to set a limit of $\sin^2 2\theta < 3.8 \times 10^{-4}$ at 90% CFL for high Δm^2. Note that should any significant number of candidates be observed, they will have to be distributed among the various decay channels according to the various branching ratios and efficiencies.

NOMAD has very good electron identification and can therefore make a thorough study of ν_e CC events coming from the small (1%) ν_e content of the beam. By studying the $E_{vis} (= E_e + E_{hadrons} = E_\nu)$ distribution of these ν_e CC events and comparing it to the one expected, an additional contribution due to $\nu_\mu \rightarrow \nu_e$ oscillations can be looked for. The difficulty of this measurement is that it requires a very good knowledge of the "standard" ν_e component of the beam. It is expected that significant oscillations limits could be set at the high Δm^2 end of the LSND favoured region.

The principle used by CHORUS (fig. 6a) to recognise the presence of a τ meson is to observe the finite path of the τ meson before it decays. Because τ decay paths are < 1 mm at these energies the target must be active and have very good spatial resolution. This has led to the use of emulsions. A total of 800 kg will be used amounting to 4 radiation lengths. A detail of the target area is shown in Fig. 6b.

Table 2:

Channel	Expected number of events $\sin^2 2\theta = 5 \times 10^{-3}$ and large Δm^2	Background events
$\tau \rightarrow e\nu\nu$	39	4.6
$\mu\nu\nu$	11	2.0
$\pi\nu$	3	< 0.2
$\rho\nu$	7	< 0.2
$3\pi\nu + (\geq 0\pi^0)$	18	< 0.2
Total	78	7

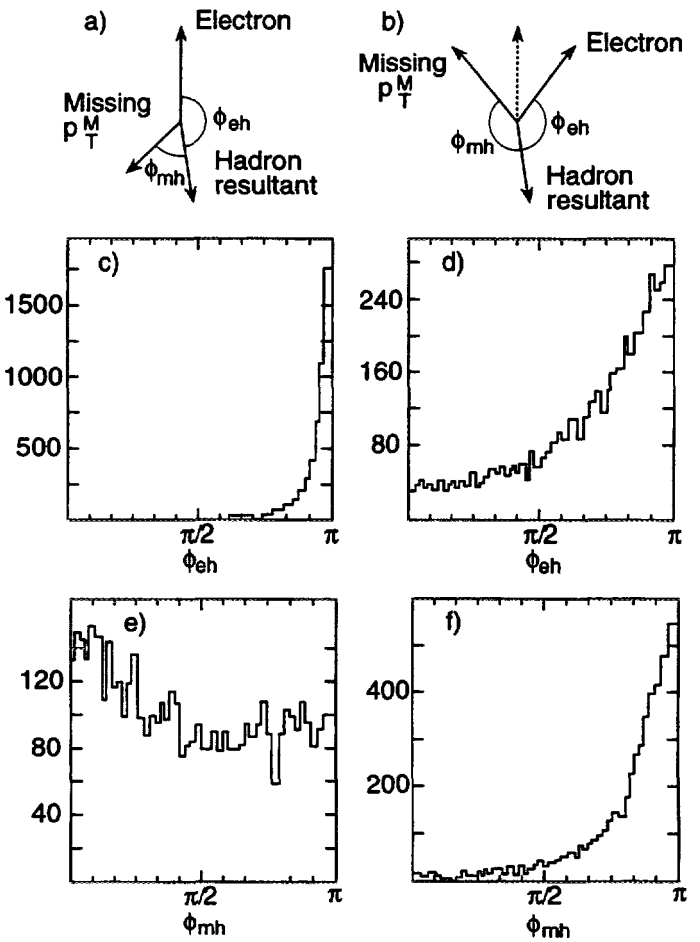

Figure 5: Definition of ϕ_{eh} and ϕ_{mh} and representative Monte Carlo distributions of these variables for ν_e CC and $\nu_\tau(\tau \rightarrow e)$ events

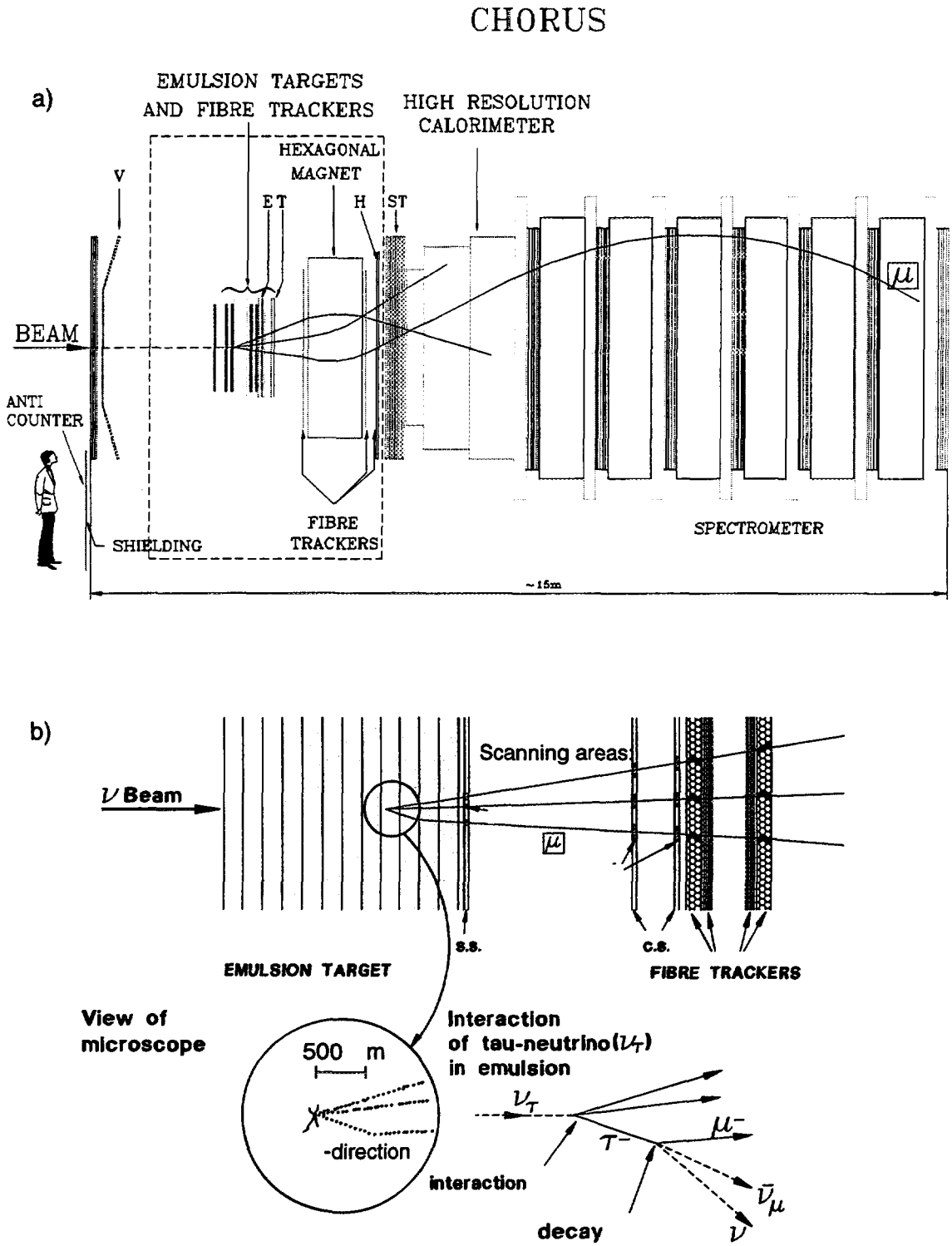

Figure 6: a) The CHORUS detector b) A detail of the CHORUS emulsions

A bulk emulsion stack which remains in place for two years is followed by sheets which are changed more often and will therefore have less occupancy and by scintillation fiber trackers. An hexagonal magnet giving a toroidal field provides a momentum resolution of 16% at 2 GeV/c rising to 23% at 10 GeV/c. The spectrometer is followed by an electromagnetic calorimeter and by a muon detector.

The number of events to be scanned is reduced by a factor of 10 by applying loose kinematics cuts of the type used by NOMAD. In the surviving events, tracks reconstructed in the spectrometer are extrapolated to the emulsions in order to determine where to scan. These tracks are followed into the emulsions to look for a kink with a P_T relative to the candidate τ direction of at least 0.24 GeV/c. The magnitude of this kink P_T is determined using the momentum of the track as determined by the spectrometer and the angle of the kink as determined by the tracking in the emulsion. A charm decay observed in the CHORUS emulsion is shown in fig. 7.

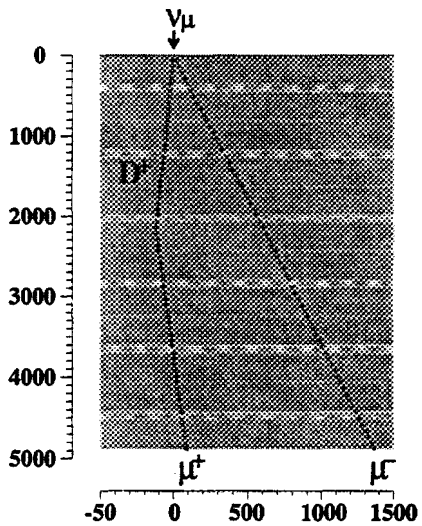

Figure 7: A charm decay observed in CHORUS

The major background to the muonic channel comes from the semileptonic decays of negative charmed particles produced by the $\overline{\nu}_\mu$ and $\overline{\nu}_e$ components of the beam coupled with missing the accompanying μ^+ or e^+. The finite travel of the D^- before its decay can thus simulate a τ decay.

In the $\tau^- \rightarrow \pi^- \nu_\tau$ channel, the major background is due to hadrons from a neutral current interaction scattering close to the vertex without any visible recoil activity. These "white star" kinks are very much reduced by requiring the P_T of the kink to be at least 0.24 GeV/c. Further background reduction can be obtained by comparing the direction of the hadronic momentum vector as calculated using the spectrometer with the direction of the τ candidate track as measured in the emulsions. For genuine τ decays these two vectors must be back to back in the plane transverse to the beam. Although the neutrinos from the τ decays are not observed, enough kinematic variables are measured to be able to estimate the ν_τ energy for each candidate event. If enough candidates are recorded the shape of the $E_{\nu\tau}$ distribution will provide a measure of Δm^2. If oscillations occur at the E531 limit 64 events

are expected with 0.4 background events. The expected sensitivity of CHORUS after a four year run will be $\sin^2 2\theta < 2 \times 10^{-4}$ at 90% CFL for high Δm^2.

3.3 E803 (COSMOS)

This experiment [20] will run at Fermilab with the new main injector. The detector, fig. 8, is very similar to CHORUS. Emulsion stacks comprising both fixed bulk emulsions and changeable sheets are followed by fibre trackers, a magnet, drift chambers, an electromagnetic calorimeter and a muon detector. However the high repetition rate of the main injector should allow E803 to collect 1.3×10^{21} protons on target as opposed to 4.5×10^{19} for CHORUS. The background in E803 is similar to that described for CHORUS. However, the better momentum resolution of E803 (3%) should allow a better rejection of the background: for the $\tau^- \rightarrow \pi^- \nu_\tau$ mode, a plot of the kink P_T relative to the τ direction should display the characteristic Jacobian peak at $\sim m_\tau/2$ (fig. 9). A limit of 2.8×10^{-5} in $\sin^2 2\theta$ is expected to be set by E803.

The expected exclusion plot for the three $\nu_\mu \rightarrow \nu_\tau$ oscillation experiments is shown in Fig. 10. Over the next 10 years the E531 limit on $\sin^2 2\theta$ at large Δm^2 should be improved by more than two orders of magnitude and at large mixing, the Δm^2 limit will be improved by about a factor of 5 down to the 1 eV^2 range.

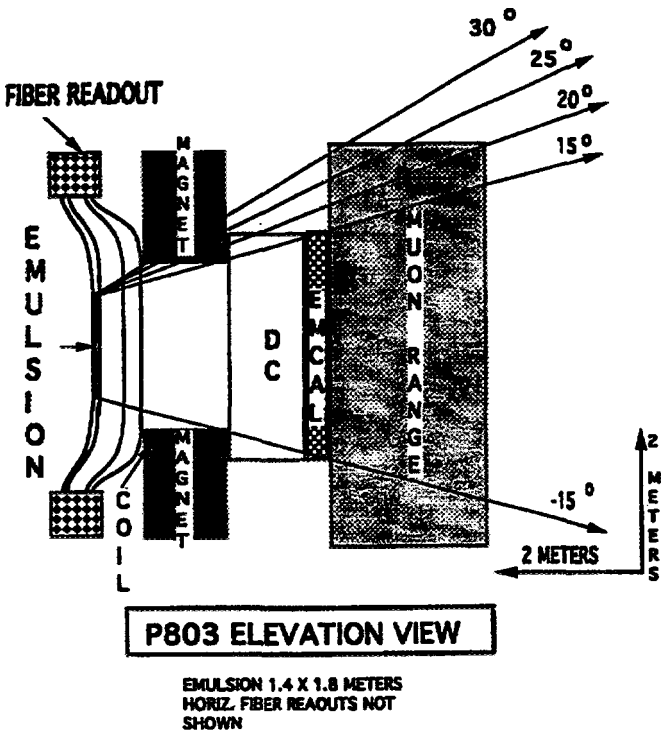

Figure 8: The E803 detector

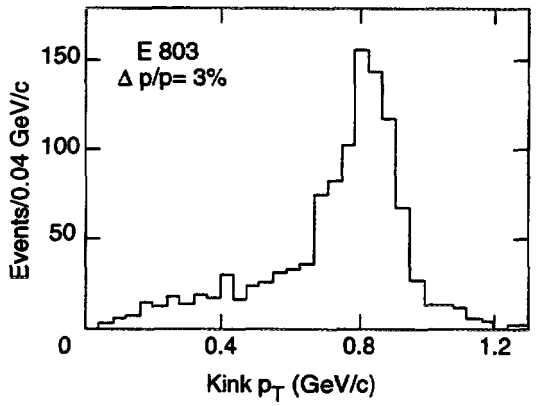

Figure 9: The Jacobian peak in the P_{TKINK} distribution expected from $\tau \rightarrow \pi\nu$ decays

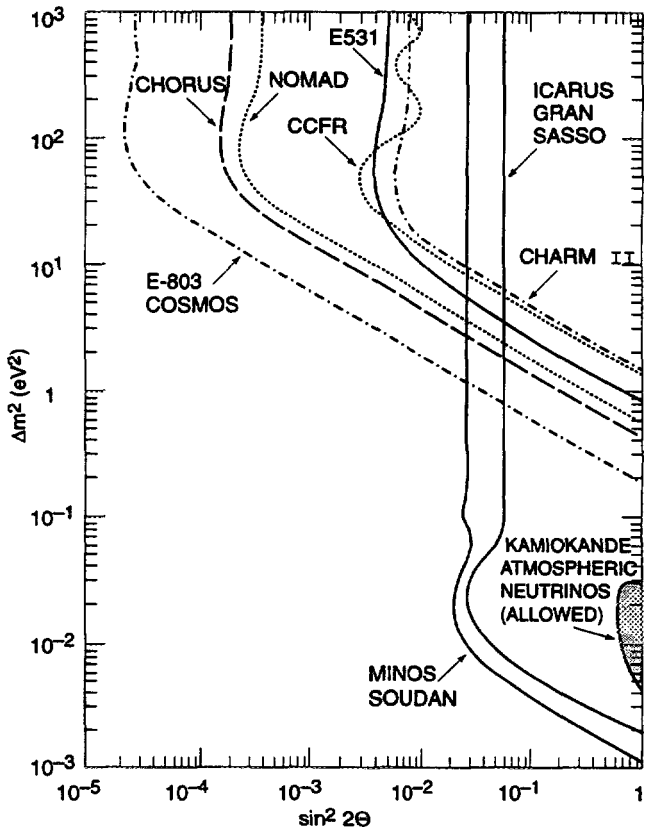

Figure 10: The regions of the $\Delta m^2 - \sin^2 2\theta$ plot expected to be excluded by NOMAD, CHORUS, E803, ICARUS and MINOS

3.4 Future ideas at CERN

Meetings between CHORUS, NOMAD and other interested physicists, including the proponents of an Argon TPC neutrino experiment ALADINO [21] and of a water Čerenkov counter experiment [22] are currently taking place. One possibility would be to combine the good kinematical discrimination of NOMAD with the good spatial resolution of CHORUS.

Such a detector could consist of an active target weighing 900 kg and consisting of planes of silicon (40 m^2 in total) interleaved with passive material such as boron carbide [23]. The active target would be followed by a spectrometer such as the one used by NOMAD. The silicon planes would provide a measurement of the impact parameter at the primary vertex for candidate pions from $\tau \rightarrow \pi^- \nu_\tau$ decays or displaced vertex identification for $\tau \rightarrow 3\pi\nu_\tau$ candidate decays. These additional constraints would allow much looser kinematic cuts to be applied thus greatly improving the τ detection efficiency and hence the sensitivity of the experiment. A four-year run could reach a sensitivity of $\sin^2 2\theta < 1.9 \times 10^{-5}$ at 90% CFL.

A prototype of such a detector [24] is currently being built and will be installed in NOMAD in time for the 1997 run. It should provide enough neutrino interactions to allow the measurement of the resolution function for the impact parameter and displaced vertex under realistic conditions. Two variants on this scheme are also being studied.

- Replacing the silicon by 20 μm capillaries filled with liquid scintillator and read by image intensifiers. This technique is currently being studied in CHORUS.

- Replacing the boron carbide with emulsion sheets [25]. Here the silicon impact parameter capabilities would only be used for a fast selection of events of interest which would then be scanned. This reduction of the number of events to be scanned would allow an increase in the total emulsion mass used.

ALADINO [21] is a proposal to install a 400 ton liquid argon TPC in the present neutrino beam line behind CHORUS and NOMAD. The optics of the beam would be changed to provide a lower neutrino energy and a narrower energy distribution. The physics addressed is $\nu_\mu \rightarrow \nu_\tau$ oscillations through the detection of quasi-elastic ν_τ CC interactions with the subsequent electronic decay of the τ. The experiment would also measure $\nu_\mu \rightarrow \nu_e$ oscillations again using quasi-elastic events. The expected snsitivities at high Δm^2 are $\sin^2 2\theta < 6 \times 10^{-5}$ for $\nu_\mu \rightarrow \nu_\tau$ oscillations and $\sin^2 2\theta < 6.4 \times 10^{-4}$ for $\nu_\mu \rightarrow \nu_e$ oscillations.

3.5 Long base-line experiments

This involves sending neutrino beams produced at an accelerator to an underground detector located several hundred kilometres away. Three such projects are currently under way or being considered.

1) Sending a beam from KEK to the Superkamiokande detector located 250 km away [26]. The present accelerator can provide a neutrino beam of mean energy 1 GeV. This will happen in 1998 and the first priority is to look for $\nu_\mu \rightarrow \nu_e$ oscillations and check the atmospheric neutrino results. A 50 GeV synchrotron is currently being planned at KEK. A neutrino beam from this machine and directed at Superkamiokande would allow $\nu_\mu \rightarrow \nu_\tau$ oscillation experiments as well starting in 2003.

2) A beam from the SPS, different from the present neutrino beam, could be directed at detectors located in the Gran Sasso laboratory, 732 km away. Detectors based on a liquid argon TPC (ICARUS)[27] or on an iron filings + scintillator calorimeter (NOE) [28] are being discussed. An ICARUS prototype module weighing 600 tons will be installed in the Gran Sasso laboratory in 1998. The final design would probably involve 10 such modules.

3) It has been decided to direct a Fermilab neutrino beam to a detector located in the

SOUDAN mine, MINOS,[29] again 732 km away. The experiment intends to look for $\nu_\mu \rightarrow \nu_\tau$ oscillations and is best done in conjunction with a near detector. The technique is based on a different ratio of charged current (CC) to all events being measured at the two locations. Assuming the oscillation wavelength is comparable to 700 km, the near detector would then measure the "correct" CC/ALL ratio. However if ν_μ's oscillate to ν_τ's only 17% of the ν_τ's decay to muons and would look like charged current events, whereas 83% would look like neutral currents. Therefore

$$\frac{CC}{ALL}|_{FAR} < \frac{CC}{ALL}|_{NEAR}.$$

When including the future long base-line results, the $\nu_\mu - \nu_\tau$ exclusion plot would then look as shown in fig. 10-. As can be seen a large fraction of the area pointed to by the current "anomalous" results will have been covered. As can also be noted the field is exceedingly active, with experiments running, being built and being proposed on many continents.

References

[1] M.Kobayashi and M.Maskawa, Progr. Theor. Phys. **49** (1973) 652.

[2] B.Pontecarvo, Zh. Eksp. Theor. Fiz. **33** (1957) 549 and **34** (1958) 247.

[3] N.Ushida et al,. Phys. Rev. Lett. **57** (1986) 2897.

[4] M.Gruwé et al., Phys. Lett. **B309** (1993) 463.

[5] K.S.McFarland et al., Phys. Rev. Lett. **75** (1995) 3993.

[6] S.F.Shandarin. Massive Neutrinos and Cosmology in Neutrino Physics edited by Klaus Winter (Cambridge Monographs on Particle Physics, Nuclear Physics and Cosmology) p. 645 and references therein.

[7] HOMESTAKE: R.Davis, Prog. Part. Nucl. Phys. **32** (1994) 13;
KAMIOKANDE: Y.Suzuki et al., Nucl. Phys. B (Proc. Suppl) **38** (1995) 54;
SAGE: J.N.Abdurashitov et al., Phys. Lett. **B328** (1994) 234;
GALLEX: P.Anselmann et al., Nucl. Phys. (Proc. Suppl.) **B38** (1995) 68.

[8] J.N.Bahcall and R.K.Ulrich, Rev. Mod. Phys. **60** (1988) 297 and references therein;
J.N.Bahcall and M.H.Pinsonneault, Rev. Mod. Phys. **64** (1992) 885;
S.Turck-Chieze and I.Lopes, Astrophys. J. **408** (1993) 347.

[9] L.Wolfenstein, Phys. Rev. **D17** (1978),2369;
S.P.Mikheyev and A.Y.Smirnov, Sov. J. Nucl. Phys. **42** (1985) 913.

[10] M.Gell-Mann, P.Ramond and R.Slansky *in* Supergravity, eds. P.van Nieuwenhuizen and D.Freeman (North Holland, Amsterdam, 1979) p. 315;
T.Yanagida, Progr. Theor. Phys. **B135** (1978) 66.

[11] K.S.Hirata et al., Phys. Lett. **B280** (1992) 146;
D.Casper et al., Phys. Rev. Lett. **66** (1991) 2561.

[12] Y.Fukuda et al., Phys. Lett. **B335** (1994) 237.

[13] B.Armbruster et al., Nucl. Phys. (Proc. Suppl.) **38** (1995) 235.

[14] C.Athanassapoulos et al., Phys. Rev. Lett **B75** (1995) 2650.

[15] L.Borodovsky et al., Phys. Rev. Lett. **68** (1992) 274.

[16] B.Achkar et al., Nucl. Phys. **B434** (1995) 503.

[17] CERN Hybrid Oscillation Research Apparatus (CHORUS). A new search for $\nu_\mu \rightarrow \nu_\tau$ oscillation, CERN PPE/93–131 and CERN-SPSLC/90–42 SPSC P254.

[18] Neutrino Oscillation Magnetic Detector (NOMAD). Search for the Oscillation $\nu_\mu \rightarrow \nu_\tau$ CERN-SPSLC/91–121 SPSC P261 (1991) and CERN-SPSLC/93–31 SPSLC M525 (1993).

[19] Prompt ν_τ background in Wide Band ν_μ beams. B.Van de Vyver and P.Zuccheli, CERN-PPE 96–113. Submitted to Nucl. Instrum. Methods;
Prompt ν_τ Fluxes in Present and Future Tau Neutrino Experiments. M-C.Gonzalez-Garcia and J-J.Gomez-Cadenas, CERN-PPE 96–114. Submitted to Phys. Rev. D.

[20] COSMOS - Muon Neutrino to Tau Neutrino Oscillations Experiment at Fermilab (E803).

[21] Letter of Intent for a short-baseline experiment with a Liquid Argon TPC, CERN SPSLC 95–37 SPSLC/I205.

[22] T.Ypsilantis et al., Nucl. Instrum. Methods **A371** (1996) 330.

[23] J-J.Gomez-Cadenas et al., Nucl. Instrum. Methods **A378** (1996) 196.

[24] A prototype of an Instrumented Target for the NOMAD detector, CERN SPSLC/96–2, SPSLC/P261/Add.3.

[25] Study of a new experiment for the search for $\nu_\mu - \nu_\tau$ oscillations. A.Ereditato et al., CERN PPE/96–106.

[26] Long Base Line Neutrino Oscillation Experiment (E362) using KEK-PS and Super-Kamiokande.

[27] ICARUS II. A Second Generation Proton Decay Experiment and Neutrino Observatory at the Gran Sasso Laboratory, Proposal by the ICARUS Collaboration (1993).

[28] M.Ambrosio et al., Nucl. Instrum. Methods **A363** (1995) 604.

[29] MINOS: Main Injector Neutrino Oscillation Search (Fermilab E-875).

CH9700119

Neutrino Masses in Astrophysics and Cosmology

Georg G. Raffelt
Max-Planck-Institut für Physik, Föhringer Ring 6, 80805 München, Germany
(October 28, 1996)

Astrophysical and cosmological arguments and observations give us the most restrictive constraints on neutrino masses, electromagnetic couplings, and other properties. Conversely, massive neutrinos would contribute to the cosmic dark-matter density and would play an important role for the formation of structure in the universe. Neutrino oscillations may well solve the solar neutrino problem, and can have a significant impact on supernova physics.

I. INTRODUCTION

Within the standard model of elementary particle physics, neutrinos play a special role in that they are the only fermions that appear with only two degrees of freedom per family, which are massless, and which interact only by the weak force apart from gravitation. If neutrinos had masses or anomalous electromagnetic interactions, or if right-handed (sterile) neutrinos existed, this would constitute the long-sought "physics beyond the standard model." Hence the enthusiasm with which experimentalists search for neutrino oscillations, neutrinoless double-beta decay, a signature for a neutrino mass in the tritium beta decay spectrum, or for neutrino electromagnetic dipole or transition moments.

Over the years, many speculations about hypothetical neutrino properties and their consequences in astrophysics and cosmology have come and gone. I shall not pursue the more exotic of those conjectures such as strong neutrino-neutrino interactions by majoron and other couplings, small neutrino electric charges, the existence of low-mass right-handed partners to the established sequential flavors, and so forth. Any of them can be significantly constrained by astrophysical and cosmological methods [1], but currently there does not seem to be a realistic way to positively establish physics beyond the standard model on such grounds. Therefore, I will focus on the more conservative modifications of the standard-model neutrino sector, namely on neutrino masses and mixings. Surely, the discovery of a nonvanishing mass is the holy grail of neutrino physics, and one that actually may be established to exist in the near future.

Arguably the most important astrophysical information about neutrino properties is the cosmological mass limit of about 40 eV which, in the case of ν_τ, improves the direct experimental limit by about six orders of magnitude. If neutrinos decay, this limit can be circumvented. However, the only standard-model decay that would be fast enough is $\nu_\tau \to e^+e^-\nu_e$ if $m_{\nu_\tau} \gtrsim 2m_e$. This mode can be constrained by the absence of γ rays from the supernova (SN) 1987A and other arguments to be far too slow than needed to evade the cosmological mass limit. Therefore, its violation requires fast invisible neutrino decays, i.e. rather exotic physics beyond the standard model. These issues are explored in Sec. II.

Currently favored models for the formation of structure in the universe exclude neutrinos as a dark-matter candidate. Still, neutrinos with a mass of a few eV could play an important positive role in mixed hot plus cold dark matter scenarios. The chances for a signature of such scenarios in future cosmic microwave background maps has been assessed (Sec. III).

Big-bang nucleosynthesis (BBN) has long been used to constrain the number of light neutrino species [2], which however is now well established to be 3 from precision measurements of the Z^0 decay width. More recently, the BBN argument has been revived to constrain a ν_τ mass in the MeV range [3]. However, the assumption of a neutrino mass in excess of the cosmological limit of about 40 eV is rather forced as it would require unmotivated neutrino interactions beyond the standard model.

The existence of three massless or nearly massless two-component neutrino flavors is compatible with standard BBN, even though there is some current debate about the interpretation of certain observations which imply somewhat incompatible or inconsistent primordial light element abundances [4]. However, what is at stake is not so much any serious implication for neutrino physics, but rather the precise value of the baryon content η of the universe. I expect that the current problems with these observations will sort themselves out so that a consistent and uncontested value for η will eventually emerge.

Therefore, even though BBN used to be a classic topic for neutrino cosmology, I think that as such it has outlived its usefulness. Pragmatically, with the laboratory input of three low-mass neutrino families, BBN is now for the most part a unique probe for η. BBN is not sensitive to those nonstandard neutrinos properties that realistically one may hope to find in nature, i.e. small masses and mixings. Therefore, I do not want to embark here on any further discussion of BBN.

A positive identification of neutrino masses most likely will come from the discovery of neutrino oscillations. Current indications for this phenomenon include the solar neutrino problem, the atmospheric neutrino anomaly, and the LSND excess counts of $\overline{\nu}_e$'s. As these issues are discussed by other speakers at this School, I will give only the briefest of summaries at the beginning of Sec. IV. For the most part, that section will be dedicated to the impact of neutrino oscillations on SN physics.

II. MASS LIMITS

A. Cosmological Mass Limit

The most important cosmological contribution to neutrino physics is the mass limit which arises from the requirement that the universe is not "overclosed" by neutrinos [2]. In the framework of the big-bang scenario of the early universe one expects about as many cosmic "black-body neutrinos" as there are microwave photons. In detail, the cosmic energy density in massive neutrinos is found to be $\rho_\nu = \frac{3}{11} n_\gamma \sum m_\nu$ with n_γ the present-day density in microwave background photons. The sum extends over the masses of all sequential neutrino flavors. In units of the critical density this is

$$\Omega_\nu h^2 = \sum \frac{m_\nu}{93\,\mathrm{eV}}, \tag{1}$$

where h is the present-day Hubble expansion parameter in units of $100\,\mathrm{km\,s^{-1}\,Mpc^{-1}}$. The observed age of the universe together with the measured expansion rate yields $\Omega h^2 \lesssim 0.4$ so that for any of the known families

$$m_\nu \lesssim 40\,\mathrm{eV}. \tag{2}$$

If one of the neutrinos had a mass near this bound it would be the main component of the long-sought dark matter of the universe.

The importance of this result is illustrated in Fig. 1 which shows the mass spectrum of the quarks and charged leptons, and the direct experimental neutrino mass limits. Except for ν_e, the cosmological limit is far below the experimental ones which implies that neutrino masses (except for ν_e) cannot be detected by direct experimental methods. It also implies that if neutrinos have masses at all, they are very much smaller than those of the other fundamental fermions. Therefore, neutrinos play a very special role, even if they were to carry nonvanishing masses after all, a hypothesis which is entertained by a majority of all particle physicists.

B. Decaying Neutrinos

The cosmological mass limit is based on the assumption that neutrinos are stable which most likely they are not if they have masses. Sufficiently early decays into nearly massless daughter particles would allow the energy stored in the massive neutrinos to be redshifted enough so that the universe would not be "overclosed" after all. In Fig. 2 the range of neutrino masses and lifetimes that remains forbidden is shown by the shaded area marked "Mass Density." A detailed construction of this plot is found in Ref. [5].

A "decaying neutrino cosmology" actually has some attractive features for the formation of structure in the cosmic matter distribution. In Sec. III B below I will discuss that the standard cold dark matter cosmology has the problem of producing too much power in the density-fluctuation spectrum on small scales, and that a mixed hot plus cold dark-matter scenario is one way of fixing this problem. Another way is with decaying neutrinos because the universe would become matter dominated when the massive neutrino becomes nonrelativistic, would return to radiation domination when it decays, and

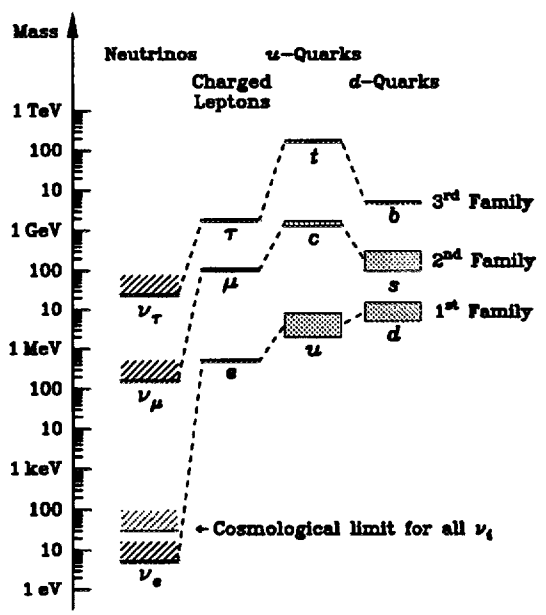

FIG. 1. Mass spectrum of elementary fermions. For neutrinos, the direct experimental mass limits as well as the cosmological limit are shown.

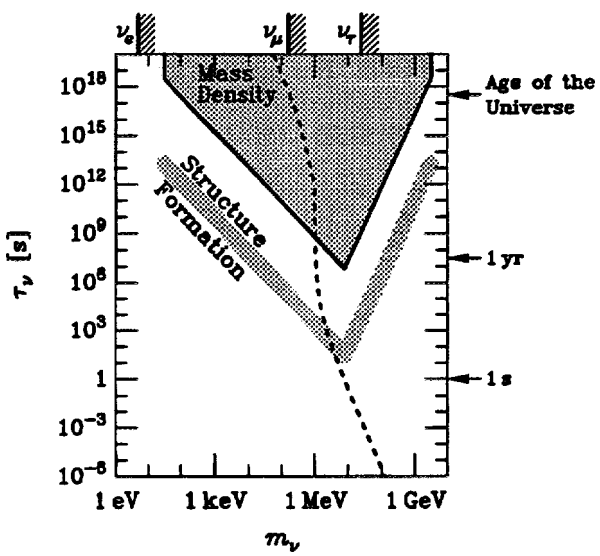

FIG. 2. Cosmological bounds on neutrino masses and lifetimes. The experimental mass limits are shown above the main panel. The dashed line is the lifetime for $\nu_\tau \to \nu_e\gamma$ and $\nu_\tau \to \nu_e e^+ e^-$ under the assumption of maximum ν_e-ν_τ-mixing.

would become matter dominated again at a later time. As structure grows by gravitational instability only in phases of matter domination, one has two more parameters at hand (the neutrino mass and lifetime) to tune the final density fluctuation spectrum. For neutrino parameters in the shaded band marked "Structure Formation" in Fig. 2 this mechanism could at least partially solve the problems of the cold dark matter cosmology [6].

The snag with this sort of scenario is that within the particle-physics standard model even massive neutrinos cannot decay fast enough. Even mixed, massive neutrinos cannot decay at tree-level by processes of the sort $\nu_\tau \to \nu_e \overline{\nu}_e \nu_e$ because of the absence of flavor-violating neutral currents. Therefore, only radiative decays of the sort $\nu_\tau \to \nu_e \gamma$ are possible. Because they proceed through a one-loop amplitude, and because of their so-called GIM suppression, their rate is exceedingly slow. Even if the radiative mode were enhanced by some unknown mechanism, radiative decays can be excluded in a large range of masses and lifetimes because the final-state photons would appear as contributions to the cosmic photon backgrounds [2]. Therefore, decaying-neutrino cosmologies as well as a circumvention of the cosmological mass bound require "fast invisible decays," i.e. fast decays with final-state neutrinos or with new exotic particles such as majorons. Put another way, if neutrinos were found to violate the cosmological mass bound of 40 eV, this would be a signature for physics "far beyond" the standard model. It would require novel ingredients other than neutrino masses and mixings.

There is one exception to this reasoning if ν_τ had a mass exceeding $2m_e$ because then the decay $\nu_\tau \to \nu_e e^+ e^-$ is kinematically possible. Assuming maximum mixing between ν_τ and ν_e, the lifetime of ν_τ as a function of its mass is plotted in Fig. 2 as a dashed line. (For $m_{\nu_\tau} < 2m_e$ the rate is dominated by $\nu_\tau \to \nu_e \gamma$.) Evidently, even without exotic extensions of the standard model, a heavy ν_τ could escape the cosmological mass limit.

This loophole can be plugged by a combination of laboratory and astrophysical arguments. First, there are numerous laboratory limits on the ν_τ-ν_e mixing angle. In Fig. 3 I show exclusion areas under the assumption that $\nu_\tau \to \nu_e e^+ e^-$ is the only available decay channel which is open due to ν_τ-ν_e mixing. The hatched area marked "Cosmic Energy Density" is the corresponding exclusion area taken from Fig. 2.

It is thought that in a SN collapse the gravitational binding energy of the newborn neutron star is emitted almost entirely in the form of neutrinos, and that this energy of about 3×10^{53} ergs is roughly equipartitioned between the (anti)neutrinos of all flavors. Even if m_{ν_τ} were as large as allowed by laboratory experiments (about 24 MeV) the ν_τ emission process would not be significantly suppressed by threshold effects. Therefore, supernovae are powerful ν_τ sources. The positrons from the subsequent $\nu_\tau \to \nu_e e^+ e^-$ decay would be trapped in the galactic magnetic field and would have a lifetime against annihilation of about 10^5 yr. Therefore, the

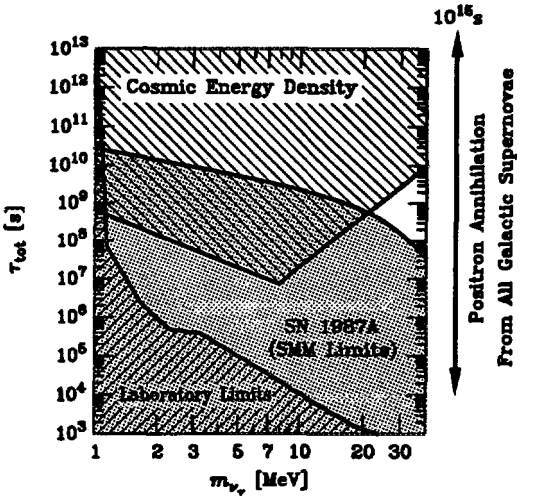

FIG. 3. Exclusion areas for the ν_τ mass and lifetime if $\nu_\tau \to \nu_e e^+ e^-$ is the only available decay channel. The "Cosmic Energy Density" region is taken from Fig. 2.

galactic positron flux integrated over all supernovae over such a period would far exceed the observed value unless the ν_τ's either decay very fast (very close to the SN), or else they live so long that they escape from the galaxy before decaying. The excluded range of lifetimes according to Ref. [7] is indicated in Fig. 3 by a vertical arrow.

A particulary important exclusion range arises from SN 1987A which is the first and only supernova from which neutrinos were observed. The gamma-ray spectrometer (GRS) on the solar maximum mission (SMM) satellite which was operational at the time did not observe any excess photon counts in coincidence with the neutrino signal, allowing one to derive restrictive limits on neutrino radiative decays [1]. For the present discussion it is most interesting that the absence of observed γ-rays also allows one to restrict the innner bremsstrahlung process $\nu_\tau \to \nu_e e^+ e^- \gamma$ and thus the $\nu_\tau \to \nu_e e^+ e^-$ channel [8]; the excluded parameter range is shaded in Fig. 3.

Interestingly, this SN 1987A exclusion range can be extended by new γ-ray observations. The time-of-flight delay of MeV-mass neutrinos from SN 1987A is so large that one could still observe γ-rays today; one does not depend on the SMM observations which were coincident with the neutrino signal. The COMPTEL γ-ray telescope has been used for that purpose with two dedicated viewing periods in 1991 with a total observation time of 6.82×10^5 sec [9]. Thus far, only an analysis for the $\nu_\tau \to \nu_e \gamma$ channel has been presented. However, for MeV-mass ν_τ's one would expect a dramatic improvement of the limits on the $\nu_\tau \to \nu_e e^+ e^- \gamma$ channel as well; such an analysis is in progress [10].

In summary, if one extends the particle-physics standard model only with neutrino masses and mixings, the cosmological mass bound remains firm as there is no vi-

able neutrino decay channel which is both fast enough and "invisible." Conversely, if neutrino masses in excess of about 40 eV were to show up in experiments, this would indicate novel neutrino interactions far outside of what is expected by the standard model. In this case decaying neutrinos could also play a useful role for the formation of structure in the universe.

C. Supernova Mass Limits

For the sake of completeness, two mass limits deserve mention which were derived from the SN 1987A neutrino signal. First, the absence of a discernible time-of-flight dispersion of the observed $\overline{\nu}_e$ burst gave rise to $m_{\nu_e} \lesssim 20\,\mathrm{eV}$ [11]. This limit is now obsolete in view of the improved experiments concerning the tritium β decay endpoint spectrum. Even though these results seem to be plagued with unidentified systematic errors, a ν_e mass as large as 20 eV does not seem to be viable.

Second, if neutrinos had Dirac masses, helicity-flipping collisions in the dense inner core of a SN would produce right-handed states. Because these sterile neutrinos are not trapped they carry away the energy directly which otherwise escapes by a diffusion process to the neutrino sphere from where it is radiated by standard left-handed neutrinos. Therefore, the energy available for standard neutrino cooling would be diminished, leading to a shortening of the SN 1987A $\overline{\nu}_e$ burst. Because the burst duration roughly agrees with theoretical expectations, this scenario can be constrained, leading to $m_\nu \lesssim 30\,\mathrm{keV}$ on a possible Dirac mass for the ν_μ and ν_τ [1]. Of course, such a large mass would violate the cosmological limit and thus is only of interest if there are fast invisible decays beyond the standard model. Typically, even "invisible" decay channels would involve (left-handed) final-state neutrinos which could become visible in the detectors which registered the SN 1987A signal. Because the sterile neutrinos which escape directly from the SN core would have higher energies than those emitted from the neutrino sphere, these events would stick out from the observed SN 1987A signal. This allows one to derive additional limits on certain decay channels of Dirac-mass ν_μ's and ν_τ's [12].

Of course, much improved mass limits could be derived if one were to observe a future galactic supernova. In a detector like the proposed Supernova Burst Observatory (SNBO) one could observe ν_μ's and ν_τ's by a coherently enhanced neutral-current nuclear dissociation reaction of the type $\nu + (Z,N) \to (Z,N-1) + n + \nu$. In principle, one could be sensitive to time-of-flight signal dispersion effects corresponding to neutrino masses of a few 10 eV for ν_μ or ν_τ, especially if the SNBO neutral-current signal were analysed in conjunction with the charged-current $\overline{\nu}_e p \to n e^+$ signal expected for the Superkamiokande detector [13].

III. NEUTRINOS AS DARK MATTER

A. Galactic Phase Space

Cosmology implies a mass limit of about 40 eV on all sequential neutrinos. If this limit were saturated by one of the neutrinos, say the ν_τ, it would constitute the dark matter of the universe. Is this possible and plausible? The current standard answer is "no" because neutrinos as dark matter candidates fare poorly on two main grounds.

The first is a well-known problem with neutrinos filling the dark-matter haloes of galaxies. By definition, galactic dark-matter neutrinos would be gravitationally bound to the galaxy so that their velocity would be bound from above by the galactic escape velocity v_{esc}, yielding an upper limit on their momentum of $p_{\max} = m_\nu v_{\mathrm{esc}}$. Because of the Pauli exclusion principle the maximum number density of neutrinos is given when they are completely degenerate with a Fermi momentum $p_{\max}$, i.e. it is $n_{\max} = p_{\max}^3/3\pi^2$. Therefore, the maximum local mass density in dark-matter neutrinos is $m_\nu n_{\max} = m_\nu^4 v_{\mathrm{esc}}^3/3\pi^2$. As this value must exceed a typical galactic dark matter density, one obtains a *lower* limit on the necessary neutrino mass. A refinement of this simple derivation is known as the Gunn-Tremaine limit [14]. For typical spiral galaxies it is in the range of a few 10 eV.

Therefore, dark-matter neutrino masses are squeezed between the upper limit from the overall cosmic mass density, and the lower limit from the galactic phase-space argument. They are squeezed, but perhaps not entirely squeezed out. Neutrinos could not constitute the dark matter of dwarf galaxies where a mass of a few 100 eV is required by the Gunn-Tremaine argument. However, perhaps the dark matter in dwarf galaxies is of a different physical nature. At any rate, the galactic phase-space argument surely disturbs any simple-minded fantasy about neutrinos being the dark matter on all scales.

B. Structure Formation

The main argument against neutrino dark matter arises from current scenarios of how structure forms in the cosmic matter distribution. One pictures a primordial power spectrum of low-amplitude density fluctuations which are later amplified by the action of gravity. The expected final distribution of galaxies then depends on both the nature of the dark matter and the original fluctuation spectrum. The result of this sort of reasoning are often displayed in a plot like Fig. 4 where the Fourier transform of the matter distribution is shown as a function of wave-number or length scale. The data are derived from the analysis of observed galaxy distributions.

Inflationary models of the early universe predict a roughly scale-invariant primordial fluctuation spectrum (Harrison-Zeldovich-spectrum). At the time of matter-radiation decoupling its amplitude is normalized by the

IV. NEUTRINO OSCILLATIONS

A. Evidence So Far

While neutrino masses would play a very important role in cosmology, it appears unlikely that cosmological arguments or observations alone will be able to prove or disprove this hypothesis anytime soon. Therefore, the only realistic and systematic path to search for neutrino masses is to search for neutrino oscillations as explained by other speakers at this school. Unsurprisingly, a vast amount of experimental effort is dedicated to this end. While large regions of neutrino mass differences and mixing angles have been excluded (Fig. 6) there is yet no uncontestable positive signature for oscillations. However, there exist a number of experimental "anomalies" that could well point to oscillations.

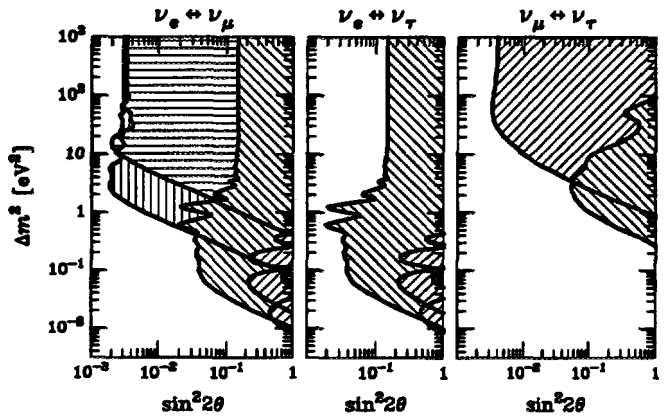

FIG. 6. Limits on neutrino masses and mixing angles from laboratory experiments. For detailed references see Refs. [1,20].

The most recent example is a pure laboratory experiment at Los Alamos where neutrinos are produced in a proton beam dump. The secondary positive pions decay according to $\pi^+ \to \mu^+ + \nu_\mu$ and the muons according to $\mu^+ \to e^+ + \overline{\nu}_\mu + \nu_e$. In the Liquid Scintillator Neutrino Detector (LSND) about 30 meters downstream, a significant number of excess $\overline{\nu}_e$ counts was obtained [21] which cannot be due to the primary source which does not produce $\overline{\nu}_e$'s. These excess counts can be interpreted as the appearance of oscillated $\overline{\nu}_\mu$'s (Fig. 7). If this interpretation were correct, the ν_e-ν_μ mass difference could be of order 1 eV or more, pointing to cosmologically significant neutrino masses. At the present time one has to wait and see if more LSND data and other experiments such as KARMEN will confirm this rather tentative finding.

Another indication for oscillations arises from the atmospheric neutrino anomaly. The production process by high-energy cosmic-ray protons is very similar to the LSND experiment, except that the higher-energy protons produce both positively and negatively charged pions and kaons in roughly equal proportions so that one expects about equally many neutrinos as antineutrinos,

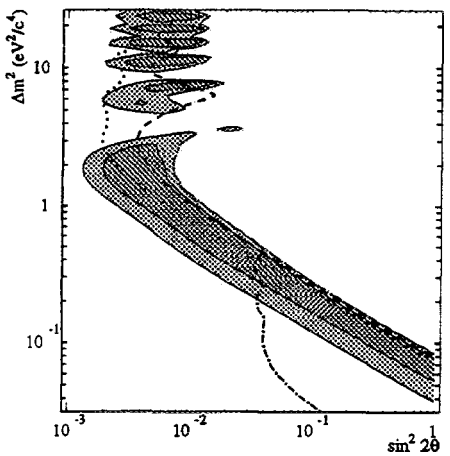

FIG. 7. The LSND favored mixing parameters [21]. The shaded areas are the 90% or 99% likelihood regions. Also shown are 90% C.L. limits from KARMEN (dashed curve), BNL-E776 (dotted curve), and the Bugey reactor experiment (dot-dashed curve).

and a $\nu_\mu : \nu_e$ flavor ratio of about 2 : 1. However, the Kamiokande detector has observed a flavor ratio more like 1 : 1 [22]. Further, Kamiokande has seen an angular dependence of the flavor ratio as expected for oscillations due to the different path lengths through the Earth from the atmosphere to the detector [23]. In principle, these observations can be explained by either ν_μ-ν_e oscillations, or by ν_μ-ν_τ ones (Fig. 8). Either way, nearly maximum mixing is required with a mass difference of about 10^{-1} eV. However, for ν_μ-ν_e oscillations the favored range of parameters is excluded entirely by the

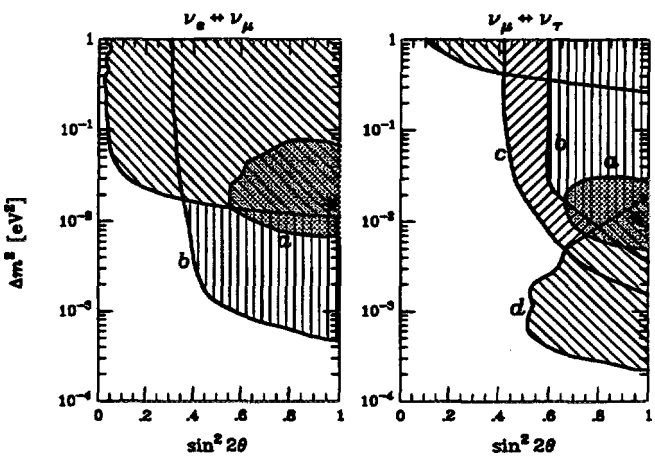

FIG. 8. Limits on neutrino masses and mixing angles from atmospheric neutrinos. (a) The shaded area is the range of masses and mixing angles required to explain the ν_e/ν_μ anomaly at Kamiokande [23]; the star marks the best-fit values. The hatched areas are excluded by: (b) ν_e/ν_μ ratio at Fréjus [24]. (c) Absolute rate and (d) stopping fraction of upward going muons at IMB [25]. Also shown are the parameter regions excluded by laboratory experiments.

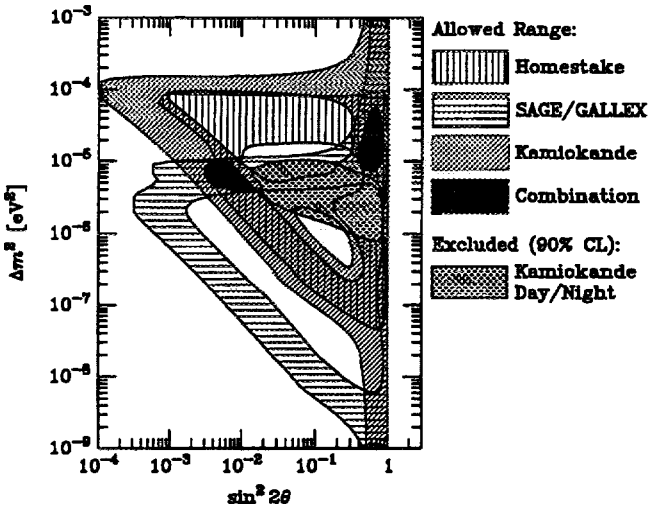

FIG. 9. MSW solutions to the solar neutrino problem according to Ref. [26] if the flux deficit relative to the Bahcall and Pinsonneault (1995) solar model is interpreted in terms of neutrino oscillations.

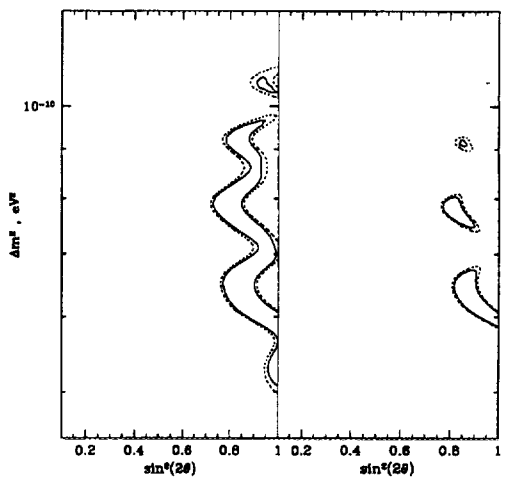

FIG. 10. Vacuum solutions to the solar neutrino problem at 90 and 95% C.L. according to Ref. [27] for ν_e-ν_μ or ν_e-ν_τ oscillations. The two panels represent somewhat different versions of the statistical analysis.

nonobservation of a flavor anomaly in Fréjus [24], while the ν_μ-ν_τ case is only partially excluded. Further inconsistencies seem to exist with certain IMB measurements of the stopping fraction of upward-going muons [25]. One may hope that the new Superkamiokande detector will soon clarify this confusing situation.

Probably the most convincing tentative evidence for neutrino oscillations arises from the solar neutrino problem which has been amply covered by other speakers at this school. If the measured flux deficits are interpreted in terms of matter-induced oscillations (MSW-effect) one obtains the favored mixing parameters for ν_e-ν_μ or ν_e-ν_τ oscillations as indicated in Fig. 9. A consistent interpretation in terms of "long-wavelength" vacuum oscillations is also possible; the favored mixing parameters obtained from a typical analysis are shown in Fig. 10. If any of these solutions will indeed bear out from future solar neutrino experiments remains to be seen. Certainly, at the present time there is no plausible alternate explanation on the market.

These indications for neutrino oscillations require three different mass differences which are not compatible with each other. Therefore, not all of these results can indeed indicate neutrino oscillations unless one appeals to the existence of neutrino degrees of freedom beyond the known sequential flavors, i.e. to the existence of sterile neutrinos. It remains to be seen which (if any) of these results will withstand closer scrutiny by better data.

Meanwhile it remains of interest to look for other scenarios where neutrino oscillations could be important. Neutrinos dominate the dynamics of the early universe and so it is natural to wonder if oscillations could have significant effects there. However, because all flavors are in thermal equilibrium with each other, the usual flavor oscillations would not change anything. Oscillations into sterile neutrinos would be a nontrivial effect, but since there is little theoretical or experimental motivation to speculate about the existence of low-mass right-handed neutrinos, I will not discuss neutrino oscillations in the early universe any further.

B. Supernova Physics

Concentrating on flavor oscillations between sequential neutrinos, supernovae are natural environments to scrutinize for nontrivial consequences. A type II supernova occurs when a massive star ($M \gtrsim 8\,M_\odot$) has reached the end of its life. At this point it consists of a degenerate iron core, surrounded by several shells of different nuclear burning phases. Because iron is the most tightly bound nucleus, it cannot gain further energy by nuclear fusion so that no further burning phase can be ignited at the center. As the iron core grows in mass because nuclear burning at its surface produces more "ashes," it eventually reaches its Chandrasekhar limit of about $1.4\,M_\odot$, i.e. the maximum mass that can be supported by electron degeneracy pressure. The subsequent core collapse is halted only when nuclear densities are reached where the equation of state stiffens. At this point a shock wave forms at the edge of the inner core, i.e. at the edge of that part of the iron core which collapses subsonically and thus is in good hydrodynamic "communication" with itself. This shock wave advances outward, and eventually expels the mantle and envelope of the collapsed object, an event which is observed as the optical supernova explosion. Essentially, the gravitational implosion of the core is transformed into an explosion of the outer parts of the star by the "shock and bounce" mechanism.

Virtually all of the binding energy of the newly formed

compact star (about 3×10^{53} ergs) is radiated away by neutrinos. However, because the collapsed core is so hot and dense that even neutrinos are trapped, this process takes several seconds which corresponds to a neutrino diffusion time scale from the center of the core to the "neutrino sphere" at its surface from where these particles can escape freely. It is thought that the released energy is roughly equipartitioned between all (anti)neutrino flavors, and that it is emitted with roughly thermal spectra.

In spite of the approximate flavor equipartition of the emitted energy, neutrino oscillations can have important consequences for supernova physics because the spectra are different between the different flavors. Various studies find that the average expected neutrino energy from a SN is [28]

$$\langle E_\nu\rangle = \begin{cases} 10\text{–}12\,\text{MeV} & \text{for } \nu_e, \\ 14\text{–}17\,\text{MeV} & \text{for } \overline{\nu}_e, \\ 24\text{–}27\,\text{MeV} & \text{for } \nu_{\mu,\tau} \text{ and } \overline{\nu}_{\mu,\tau}, \end{cases} \tag{3}$$

i.e. typically $\langle E_{\nu_e}\rangle \approx \frac{2}{3}\langle E_{\overline{\nu}_e}\rangle$ and $\langle E_\nu\rangle \approx \frac{5}{3}\langle E_{\overline{\nu}_e}\rangle$ for the other flavors. The different mean energies are explained by the different main reactions which trap neutrinos, namely $\nu_e n \to pe^-$, $\overline{\nu}_e p \to ne^+$, and $\nu N \to N\nu$ with $N = n$ or p. Because the charged-current reactions have larger cross sections than the neutral-current ones, and because there are more neutrons than protons, the ν_e's have the hardest time to escape and thus emerge from the farthest out and thus coldest layers. Still, the radii of the layers from which the different flavors escape are not too different so that the relatively large variation of the spectral temperatures between the flavors and the equipartition of the emitted energy appears to contradict the Stefan-Boltzmann law. An explanation for this apparent paradox is given in Ref. [29].

It is conceivable that (resonant) oscillations occur outside of the neutrino sphere so that the spectra between two flavors can be swapped. Two possible consequences of such a spectral exchange have been discussed in the literature.

The first has to do with the explosion mechanism for type II supernovae which does work quite as simple as described above. Because the shock wave forms at the edge of the subsonic inner core, not at the edge of the iron core, it moves through a layer of iron before reaching the stellar mantle. By dissociating iron it loses energy and stalls after a few 100 ms in typical calculations. The deposition of energy by neutrinos which emerge from the inner core is thought to revive the shock wave so that it resumes its outward motion and eventually explodes the outer star. However, this "delayed explosion mechanism" still does not seem to work in typical calculations because the transfer of energy from the neutrinos to the shock wave is not efficient enough. Recently the importance of convection both within the neutron star and between the neutron star and the shock wave has been recognized to play some role at helping to transfer more energy to the shock wave, but even then successful explosions are not guaranteed.

If neutrinos follow a "normal" mass hierarchy so that ν_e is dominated by the lighest mass eigenstate, one can have MSW-type resonant oscillations between, say, ν_e and ν_τ. If this occurs between the neutrino sphere and the stalling shock wave, the ν_e's reaching the shock wave are really oscillated ν_τ's and thus have the higher spectral energies characteristic for that flavor. The total energy flux in both flavors is about the same, but the absorption cross sections are larger for larger energies so that more energy is transferred to the shock wave [30]. Because the MSW transition must occur rather close to the neutrino sphere where the matter densities are large, neutrino mass differences in the cosmologically interesting regime are required for this effect to operate. In Fig. 11 the approximate range of masses and mixing angles is shown where neutrino oscillations would help to explode supernovae.

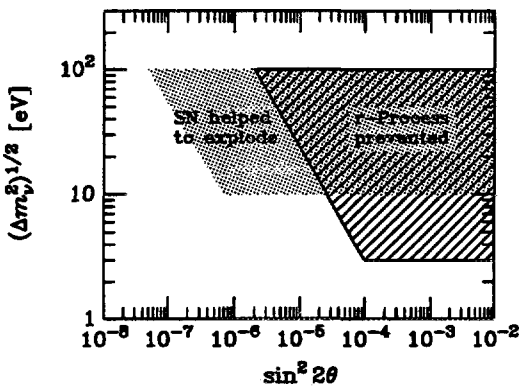

FIG. 11. Mixing parameters between ν_e and ν_μ or ν_τ where a spectral swap by resonant oscillations would be efficient enough to help explode supernovae (schematically after Ref. [30]), and where it would prevent r-process nucleosynthesis (schematically after Ref. [31]).

A second consequence of oscillations is their possible impact on nucleosynthesis. It has long been thought that the isotopes with $A \gtrsim 70$ are formed by neutron capture which thus requires a neutron-rich environment. It is now thought that an ideal site for the r-process is the high-entropy "hot bubble" in a SN between the young neutron star and the advancing shock wave a few seconds after collapse. The neutrino-driven wind in this dilute environment is shifted to a neutron-rich phase by β processes and because of the energy hierarchy $\langle E_{\nu_e}\rangle < \langle E_{\overline{\nu}_e}\rangle$. However, if oscillations would cause a spectral swap between, say, ν_e and ν_τ then this energy hierarchy would be inverted and the wind would be shifted to a proton-rich phase, preventing the occurrence of r-process nucleosynthesis [31]. Because this argument applies to a later phase than the explosion argument above, the neutron star has thermally settled so that the matter gradients at its surface are much steeper than before. This makes it harder to meet the adiabaticity condition for the MSW effect,

reducing the range of mixing angles where this effect operates (Fig. 11).

At the present time it is not certain if r-process nucleosynthesis indeed occurs in supernovae so that the hatched are in Fig. 11 cannot be taken as a serious exclusion plot for neutrino mixing parameters. Still, it is fascinating that cosmologically interesting neutrino masses would have a nontrivial impact on SN physics. At any rate, there is a significant range of small mixing angles where supernovae could be helped to explode by oscillations, and r-process nucleosynthesis could still proceed unscathed.

C. SN 1987A Signal Interpretation

Neutrinos from a collapsing star were observed for the first and only time from SN 1987A which occurred in the Large Magellanic Cloud on 23 February 1987. Naturally, the observed signature would be different if oscillations had occurred between the source and the detectors. Two observable effects have been discussed in the literature.

The first relates to the so-called neutronization ν_e burst which precedes the main cooling phase. It is produced when the shock wave breaks through the surface of the iron core, allowing the sudden release of ν_e's from the reactions $e^- p \to n\nu_e$ from a layer encompassing perhaps a few $0.1\,M_\odot$ of matter. Most of the core is deleptonized and thus neutronized only during the relatively slow subsequent cooling phase. In the water Cherenkov detectors IMB and Kamiokande which registered the SN 1987A signal, the $\nu_e e \to e\nu_e$ scattering reaction would have produced forward-peaked electrons as a signature for this burst, although one would have expected only a fraction of an event. As the first event in Kamiokande does point in the forward direction, it has often been interpreted as being due to the neutronization burst.

If resonant oscillations in the SN mantle and envelope had occurred, the deleptonization ν_e's would have arrived as ν_μ's or ν_τ's instead which have a much smaller scattering cross section on electrons, thus reducing the observable signal. In Fig. 12 the shaded triangle shows the mixing parameters for which the oscillation probability would have exceeded 50%, assuming a normal neutrino mass hierarchy. For orientation, the MSW triangle for solar neutrinos in the Kamiokande detector and the MSW solution to the solar neutrino problem are also shown. Evidently, the small-angle MSW solution would not be in conflict with the interpretation that the first SN 1987A Kamiokande event was indeed ν_e scattering. Of course, this single event does not allow one to reach the opposite conclusion that the large-angle MSW solution was ruled out.

Most or probably all of the 19 events at Kamiokande and IMB must have been due to the $\overline{\nu}_e p \to n e^+$ reaction. Assuming again a normal neutrino mass hierarchy, resonant oscillations could not have swapped the $\overline{\nu}_e$ spectra

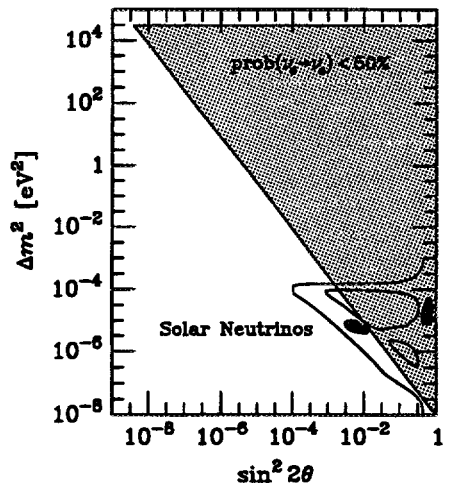

FIG. 12. Mixing parameters between ν_e and ν_μ or ν_τ where the prompt SN neutronization burst of ν_e's would have resonantly oscillated into another flavor (after Ref. [32]). A normal mass hierarchy is assumed where ν_e is dominated by the lightest mass eigenstate. For orientation, the Kamiokande solar MSW triangle and the MSW solutions to the solar neutrino problem are also shown.

with some other flavor; they could have affected only the ν_e spectrum. Therefore, the observed events represent the initial $\overline{\nu}_e$ spectrum at the source unless the mixing angle is large, allowing for significant non-resonant oscillation effects. Large mixing angles in the neutrino sector are motivated by the large-angle MSW and the vacuum solution to the solar neutrino problem as well as by the oscillation interpretation of the atmospheric neutrino anomaly.

One way of interpreting the observed SN 1987A events is to use the data to derive best-fit values for the total binding energy E_b and the spectral temperature of the observed $\overline{\nu}_e$'s which is defined by $T_{\overline{\nu}_e} = \frac{1}{3}\langle E_{\overline{\nu}_e}\rangle$. Assuming certain mixing parameters and certain relative spectral temperatures $\tau \equiv T_{\overline{\nu}_\mu}/T_{\overline{\nu}_e}$ between the flavors the results from such an analysis are shown in Figs. 13 and 14 according to Ref. [33]. In the case $\tau = 1$ oscillations have no effect so that this is identical to the standard no-oscillation scenario. Apparently the measured signal characteristics are nearly incompatible with the theoretical predictions which are indicated by the hatched rectangle in Figs. 13 and 14. This effect is due to the surprisingly low energies of the events in the Kamiokande detector.

According to Eq. (3) a typical value for the relative spectral temperature is $\tau = 1.7$. According to Fig. 13 this would be inconsistent with the vacuum solution to the solar neutrino problem because the expected event energies in the detector would have been even larger than in the standard case, contrary to the relatively low energies that were actually observed. Put another way, if the vacuum solution to the solar neutrino problem is borne out by future experiments, there is a serious conflict between the

SN 1987A observations and theoretical predictions.

For the large-angle MSW solution the conflict is less severe (Fig. 14). For such mixing parameters the flavor evolution is adiabatic in the supernova envelope so that propagation eigenstates emerge from the surface which do not oscillate between the SN and us. However, on the path through the Earth to the detectors, matter-induced "regeneration effects" partly undo the spectral mixture that emerged from the supernova, i.e. partly restore the original source spectra, reducing the overall impact of neutrino oscillations.

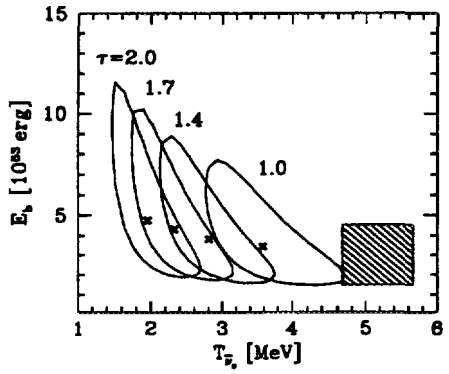

FIG. 13. 95% confidence contours for the neutron star binding energy and temperature of the primary $\bar{\nu}_e$ spectrum for the marked values of $\tau = T_{\bar{\nu}_\mu}/T_{\bar{\nu}_e}$ [33]. For the neutrino mixing parameters typical values for the solar vacuum oscillation solution were chosen ($\Delta m^2 = 10^{-10}\,\mathrm{eV}^2$, $\sin^2 2\Theta = 1$). In the case $\tau = 1$ oscillations do not change the spectra so that this contour corresponds to the absence of oscillations. The hatched area represents the range of theoretical predictions.

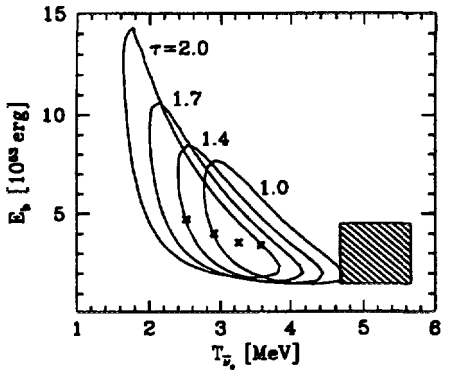

FIG. 14. Same as Fig. 13 for neutrino mixing parameters which are typical for the solar large-angle MSW solution ($\Delta m^2 = 10^{-5}\,\mathrm{eV}^2$, $\sin^2 2\Theta = 0.8$).

In summary, the comparison of the SN 1987A neutrino observations with theoretical predictions disfavor the large-angle solutions to the solar neutrino problem, even though the data are too sparse to reach this conclusion "beyond reasonable doubt."

V. DISCUSSION AND SUMMARY

The minimal picture of neutrinos as espoused by the particle-physics standard model is still compatible with all established experimental, astrophysical, and cosmological evidence. Of course, even such minimal neutrinos would play a dominant role for the dynamics of the early universe, of supernova explosions, and for the energy loss of evolved stars. In the absence of any compelling theoretical reason for neutrinos to be truly massless it is commonplace to assume that they do carry small masses and that the flavors mix. Cosmology provides by far the most restrictive limit of about 40 eV on the mass of all sequential flavors. This limit cannot be circumvented by decays unless neutrinos interact by new forces which allow for "fast invisible" (i.e. nonradiative) decays. Therefore, the assumption of neutrino masses in excess of about 40 eV is tantamount to the assumption of a significant extension of the standard model in the neutrino sector, an extension for which there is no compelling theoretical motivation. If neutrinos have masses at all, I think it is a safe bet to assume that their masses obey the cosmological limit.

Neutrinos are unfashionable dark matter candidates because of the well-known problems of a hot dark matter cosmology if one assumes that structure forms by gravitational instability from something like a Harrison-Zeldovich spectrum of initial density perturbations. For the time being, the standard cold dark matter picture works impressively well even though it appears to overproduce structure on small scales. This problem can be patched up by a number of different modifications, one of them being a hot plus cold dark matter scenario with a neutrino component corresponding to $m_{\nu_e} + m_{\nu_\mu} + m_{\nu_\tau} \approx 5\,\mathrm{eV}$. However, it looks unlikely that this sort of scenario can be unambiguously identified by cosmological methods alone. Even the most ambitious future cosmic microwave sky maps probably will not be able to identify this model unambiguously in view of the remaining uncertainty in other cosmological parameters.

Depending on the exact mixing parameters, neutrino oscillations can have very severe consequences for supernova physics and the signal interpretation of SN 1987A or a future galactic supernova. Especially for neutrino masses in the cosmologically interesting regime, oscillations may affect the explosion mechanism and r-process nucleosynthesis in the hot bubble between the neutron star and the advancing shock wave. However, the current understanding of SN physics is too uncertain and the SN 1987A data are too sparse to tell if neutrino oscillations are either required or excluded. Still, it remains fascinating that a neutrino mass as small as a few eV has *any* significant consequences outside of cosmology.

In summary, even though massive neutrinos may play an important role in cosmology and supernova physics, realistically we will know if this is indeed the case only by more direct measurements. With the possible exception of neutrinoless double β decay experiments, the only fair

chance to positively identify neutrino masses is by oscillation experiments. In principle, oscillations can explain the atmospheric neutrino anomaly, the LSND $\overline{\nu}_e$ excess counts, and especially the solar neutrino problem. However, a simultaneous explanation of all three phenomena by oscillations is barely possible and surely implausible. Unless the ongoing laboratory experiments come forth with a surprise result, the current round of solar neutrino experiments holds the most realistic promise of producing uncontestable evidence for neutrino physics beyond the narrow confines of the standard model.

---

[1] G. G. Raffelt, Stars as Laboratories for Fundamental Physics (University of Chicago Press, Chicago, 1996).

[2] E. W. Kolb and M. S. Turner, The Early Universe (Addison-Wesley, Reading, Mass.).

[3] G. M. Fuller and R. A. Malaney, Phys. Rev. D 43 (1991) 3136. E. W. Kolb et al., Phys. Rev. Lett. 67 (1991) 533. K. Enqvist and H. Uibo, Phys. Lett. B 301 (1993) 376. A. D. Dolgov and I. Z. Rothstein, Phys. Rev. Lett. 71 (1993) 476. M. Kawasaki et al., Nucl. Phys. B 419 (1994) 105. A. D. Dolgov, K. Kainulainen, and I. Z. Rothstein, Phys. Rev. D 51 (1995) 4129. B. D. Fields, K. Kainulainen, and K. A. Olive, HEP-PH/9512321 (1995). S. Hannestad and J. Madsen, Phys. Rev. Lett. 76 (1996) 2848 and Erratum, E-Print HEP-PH/9606452, submitted to Phys. Rev. Lett. (1996). A. D. Dolgov, S. Pastor, and J. W. F. Valle, E-Print HEP-PH/9602233 (1996).

[4] A few references concerning the current BBN debate are: N. Hata et al., Phys. Rev. Lett. 75 (1995) 3977. B. D. Fields and K. A. Olive, Phys. Lett. B 368 (1996) 103. P. J. Kernan and S. Sarkar, Phys. Rev. D 54 (1996) 3681. J. C. Copi, K. A. Olive and D. N. Schramm, Report Fermilab-Pub-96-158-A, submitted to Astrophys. J. Lett. (1996). M. Rugers and C. J. Hogan, ASTRO-PH/9603084. S. Burles and D. Tytler, E-Print ASTRO-PH/9603070. D. Tytler, X.-M. Fan and S. Burles, E-Print ASTRO-PH/9603069. D. Tytler and S. Burles, E-Print ASTRO-PH/9606110.

[5] D. A. Dicus, E. W. Kolb and V. L. Teplitz, Phys. Rev. Lett. 39 (1977) 169.

[6] G. Steigman and M. S. Turner, Nucl. Phys. B 253 (1985) 253. J. Bardeen, J. Bond, and G. Efstathiou, Astrophys. J. 321 (1987) 28. L. M. Krauss, Phys. Lett. B 263 (1991) 441. J. R. Bond and G. Efstathiou, Phys. Lett. B 265 (1991) 245. S. Dodelson, G. Gyuk, and M. S. Turner, Phys. Rev. Lett. 72 (1994) 3754. M. White, G. Gelmini, and J. Silk, Phys. Rev. D 51 (1995) 2669.

[7] A. Dar, J. Goodman, and S. Nussinov, Phys. Rev. Lett. 58 (1987) 2146. For an update see Ref. [1].

[8] A. Dar and S. Dado, Phys. Rev. Lett. 59 (1987) 2368. For an update see Ref. [1].

[9] R. S. Miller, Doctoral Thesis (University of New Hampshire, 1995). R. S. Miller, J. M. Ryan and R. C. Svoboda, Contributed Paper to Neutrino 96 (unpublished).

[10] R. S. Miller, work in progress (1996).

[11] T. J. Loredo and D. Q. Lamb, in: Fourteenth Texas Symposium on Relativistic Astrophysics, edited by E. J. Fenyves, Ann. N.Y. Acad. Sci. 571 (1989) 601. P. J. Kernan and L. M. Krauss, Nucl. Phys. B 437 (1995) 243.

[12] S. Dodelson, J. A. Frieman and M. S. Turner, Phys. Rev. Lett. 68 (1992) 2572.

[13] L. M. Krauss et al., Nucl. Phys. B 380 (1992) 507. D. Cline et al., Phys. Rev. D 50 (1994) 720.

[14] J. E. Gunn and S. Tremaine, Phys. Rev. Lett. 42 (1979) 407.

[15] P. J. Steinhardt, E-print ASTRO-PH/9502024.

[16] R. Brandenberger, "Modern Cosmology and Structure Formation," Lectures given at Theoretical Advanced Study Institute in Elementary Particle Physics (TASI 94): CP Violation and the limits of the Standard Model, Boulder, CO, 29 May - 24 Jun 1994. Proceedings edited by John F. Donoghue (World Scientific, Singapore, 1995).

[17] J. R. Primack et al., Phys. Rev. Lett. 74 (1995) 2160. D. Pogosyan and A. A. Starobinsky, Astrophys. J. 447 (1995) 465. D. H. Lyth et al., Mon. Not. R. Astron. Soc. 281 (1996) 531.

[18] J. R. Primack, E-Print HEP-PH/9610321, to appear in the Proceedings of the XVII International Conference on Neutrino Physics and Astrophysics, Helsinki, Finland, 13–19 June 1996, edited by K. Enqvist, K. Huitu and J. Maalampi (World Scientific, Singapore, 1997).

[19] S. Dodelson, E. Gates and A. Stebbins, E-Print ASTRO-PH/9509147, submitted to the Astrophysical Journal (1995).

[20] Particle Data Group, Phys. Rev. D 50 (1994) 1173.

[21] C. Athanassopoulos et al., Report LA-UR-96-1582 (May 1996), E-Print NUCL-EX/9605003, and Report LA-UR-96-1326 (May 1996), E-Print NUCL-EX/9605001.

[22] K. S. Hirata et al., Phys. Lett. B 280 (1992) 146.

[23] Y. Fukuda et al., Phys. Lett. B 335 (1994) 237.

[24] Fréjus Collaboration, Phys. Lett. B 245 (1990) 305 and Z. Phys. C 66 (1995) 417. K. Daum, Report WUB 94-9, Contributed paper to Neutrino 94 (unpublished).

[25] R. Becker-Szendy et al., Phys. Rev. Lett. 69 (1992) 1010.

[26] N. Hata and W. Haxton, Phys. Lett. B 353 (1995) 422.

[27] P. I. Krastev and S. T. Petcov, Phys. Rev. Lett. 72 (1994) 1960.

[28] H.-T. Janka, in: Proc. Vulcano Workshop 1992 "Frontier Objects in Astrophysics and Particle Physics," edited by F. Giovanelli and G. Mannocchi, Conf. Proc. Vol. 40 (1993) (Soc. Ital. Fis.).

[29] H.-T. Janka, Astropart. Phys. 3 (1995) 377.

[30] G. M. Fuller et al., Astrophys. J. 389 (1992) 517.

[31] Y.-Z. Qian et al., Phys. Rev. Lett. 71 (1993) 1965. Y.-Z. Qian and G. M. Fuller, Phys. Rev. D 51 (1995) 1479.

[32] D. Nötzold, Phys. Lett. B 196 (1987) 315.

[33] B. Jegerlehner, F. Neubig and G. Raffelt, Phys. Rev. D 54 (1996) 1194.

Neutrinos from type-II supernovae and the neutrino-driven supernova mechanism[1]

H.-Thomas Janka

Max-Planck-Institut für Astrophysik
Karl-Schwarzschild-Str. 1, D-85740 Garching, Germany
email: thj@mpa-garching.mpg.de

ABSTRACT

Supernova 1987A has confirmed fundamental aspects of our theoretical view of type-II supernovae: Type-II supernovae are a consequence of the collapse of the iron core of a massive evolved star and lead to the formation of a neutron star or black hole. This picture is most strongly supported by the detection of electron antineutrinos in the IMB and Kamiokande II experiments in connection with SN 1987A (Bionta et al. 1987, Hirata et al. 1987). However, the mechanism causing the supernova explosion is not yet satisfactorily understood.
In this paper the properties of the neutrino emission from supernovae and protoneutron stars will be reviewed; analytical estimates will be derived and results of numerical simulations will be shown. It will be demonstrated that the spectral distributions of the emitted neutrinos show clear and systematic discrepancies compared with thermal (black body-type) emission. This must be taken into account when neutrino observations from supernovae are to be interpreted, or when implications of the neutrino emission on nucleosynthesis processes in mantle and envelope of the progenitor star are to be investigated. Furthermore, the influence of neutrinos on the supernova dynamics will be discussed, in particular their crucial role in causing the explosion by Wilson's neutrino-driven delayed mechanism. Possible implications of convection inside the newly born neutron star and between the neutron star surface and the supernova shock will be addressed and results of multi-dimensional simulations will be presented.

1. Introduction

Massive stars with $8M_\odot \lesssim M \lesssim 25M_\odot$ are expected to end their lives in spectacular type-II supernova outbursts. The source of energy for these most powerful cosmic events after the Big Bang is gravitational binding energy, set free, when the

[1] reprint from: Conference Proceedings Vol. 40: *"Frontier Objects in Astrophysics and Particle Physics"*, eds. F. Giovannelli and G. Mannocchi, Workshop in Vulcano, Italy, 18–23 May 1992, Italian Physical Society, Bologna, Italy (1993), p. 345–374

star's central regions collapse due to their own gravitational pull. After iron group elements, the most tightly bound nuclei, have been formed in the center of the star in successive nuclear burning phases, no more energy gain by nuclear fusion reactions is possible, and contraction sets in. As the density grows, electron captures on nuclei and on free protons as well as photodisintegration of heavy nuclei reduce the pressure with increasing speed. The stellar iron core, its mass being close to the Chandrasekhar mass

$$M_{\rm Ch} \approx 5.8 \cdot Y_e^2 M_\odot \approx 1.2 ... 1.5 M_\odot \qquad (1)$$

(Y_e is the electron concentration, i.e. the number of electrons per baryon), cannot escape gravitational collapse on dynamical time scales. Persistent capture of electrons on protons and nuclei produces neutrinos, which, at least initially, leave the star nearly unhindered. The collapse does not stop until the equation of state becomes stiff at the moment nuclear matter densities are reached.

This is the moment of 'core bounce', when a shock wave is formed at the interface of the subsonically, 'homologously', collapsing inner part and the supersonically falling outer layers of the stellar iron core. The shock wave starts to propagate outwards, as well in mass as in radius. If there were no energy losses, this shock might well travel outwards into the mantle and envelope of the star and cause the disruption of the star in the type-II supernova outburst. However, the shock experiences strong energy losses, initially by photodisintegration of heavy nuclei in the hot matter behind the shock front. Another source of energy loss is due to neutrinos, which are amply produced in the electron rich, hot, shocked stellar gas. When the shock front reaches neutrino transparent layers, there is a huge outburst of electron neutrinos with peak luminosities close to 10^{54} erg/s. All current supernova calculations agree that this additional loss of energy means the death of the prompt shock (see e.g. Hillebrandt 1987; Bruenn 1989a,b; Myra et al. 1987; Myra and Bludman 1989; Bruenn 1992): Only a few milliseconds after shock formation the velocities behind the prompt shock become very small or even negative, and the shock transforms into a standing accretion shock, nearly stationary in radius. Matter is falling through the shock and is slowly settling onto the newly formed compact object inside the collapsed star, the protoneutron star.

This hot remnant looses lepton number and energy by radiating neutrinos of all kinds, thus getting more compact, and, on short time scales, even hotter. The matter accreted onto the newly formed neutron star during a phase of several hundred milliseconds after core bounce increases the final mass of the remnant and adds neutrinos to the fluxes diffusing out from deeper layers. On a time scale of several seconds up to some ten seconds the emission of neutrinos drives the evolution of the hot, lepton rich, extended protoneutron star to the final cool and neutronized neutron star (Burrows and Lattimer 1986; Hecht 1989; Suzuki 1989). This scenario of the events occuring deep inside the supernova hours before the first light from the supernova outburst can be 'seen', was nicely confirmed by the 19 neutrino events recorded in the IMB and Kamiokande II detectors in conncetion with SN 1987A (Bionta et al. 1987, Hirata et al. 1987). Total energy loss, time scales, neutrino energetics, and radial extension of the neutrino source agree well with the core collapse/neutron star picture (see e.g. Sato and Suzuki 1987a,b; Suzuki and Sato 1987; Bludman and Schinder 1987; Lamb et al. 1987; Bahcall et al. 1987; etc., etc.). The same

holds for the neutrino events possibly recorded in the Baksan laboratory (Alexeyev et al. 1988). However, there is definite trouble with the events reported by the Mont Blanc experiment (Aglietta et al. 1987). Time and spectral characteristics as well as total energy necessary to explain these events by neutrinos from a supernova in the Large Magellanic Cloud let a connection with SN 1987A appear very unlikely (for a detailed discussion see e.g. Sato 1989, Schramm and Brown 1990, Hillebrandt and Höflich 1989). One would have to construct an extreme non-standard scenario to explain *both* the Mont Blanc observations on the one hand and the IMB and Kamiokande II observations on the other.

Neutrinos certainly may open an important and useful window to observe the physics happening deep inside the supernova core and to learn about the mechanism which leads to the explosion of the star. Unfortunately, the few neutrino events did not allow for any conclusion on this point. Still the detailed sequence of events causing the supernova outburst is not satisfactorily understood. Currently the most promising scenario is the 'delayed explosion mechanism', originally discovered by Wilson (1985; also: Bethe and Wilson 1985, Wilson et al. 1986). Here neutrino energy deposition plays a crucial role to restart the shock front and to power the final explosion of the star in the type-II supernova event. On time scales of several hundred milliseconds up to about one second, much longer than the propagation time scale of the prompt hydrodynamical shock, which is of the order of milliseconds, net cooling of the post-shock matter is superseded by net heating: The neutrinos streaming up from deeper regions are supposed to deposit a small fraction of their energy in the matter between the increasingly compact protoneutron star and the shock, 'sitting' at typical radii of 100 to several hundred kilometers.

Wilson's delayed mechanism has the desirable property that it might yield supernova explosions much less sensitive to small changes of the core collapse physics. The hydrodynamical prompt shock mechanism, if it works at all, turns out to lead to successful explosions only in case of very special, not to say extreme, assumptions about the structure and size of the stellar core prior to collapse and about the characteristics of the equation of state around and beyond nuclear matter densities. Both crucially determine the energetics of the prompt shock and its chance to travel out into the stellar mantle (see e.g. Bruenn 1989a,b). On the other hand the neutrino heating mechanism, by its nature, depends on the properties of the neutrino emission during the first several hundred milliseconds after core bounce, and, at least in the initial phase of shock revival, seems to be rather sensitive to changes of the neutrino fluxes and spectra. Therefore, it is still controversial, whether the neutrino luminosities and neutrino energies are sufficient for strong enough heating to revive the stalled shock wave (see in particular Bruenn 1992). Convective processes in the collapsed stellar core and in the region between protoneutron star and shock seem to play an important role to get the desired high neutrino luminosities and to transport energy from the neutrino heated region into the shock front (see Mayle 1985, Burrows 1987, Burrows and Lattimer 1988, Bethe 1990, Herant et al. 1992). This is supported by the contradictory results of the calculations by Mayle and Wilson (e.g. Wilson et al. 1986), who include a parameterized description of effects due to neutron finger instabilities in their one-dimensional simulations, and by Bruenn (e.g. 1992), who does not mimic any convective processes in his computations.

In the following Section 2 generic features of the neutrino emission from supernovae and newly born neutron stars will be discussed in detail by deriving simple analytical estimates and refering to results from numerical simulations. In the first part of Section 3 one-dimensional computations will be presented, which follow the neutrino energy deposition between protoneutron star and shock over a time scale of more than 10 seconds and allow for conclusions on the energetics of type-II supernova explosions by Wilson's delayed mechanism. The second part of Section 3 will address fundamental changes of the idealized spherically symmetric picture when convective processes are taken into account. First results of simulations in two and three dimensions will be shown. A summary and conclusions will close the paper in Section 4.

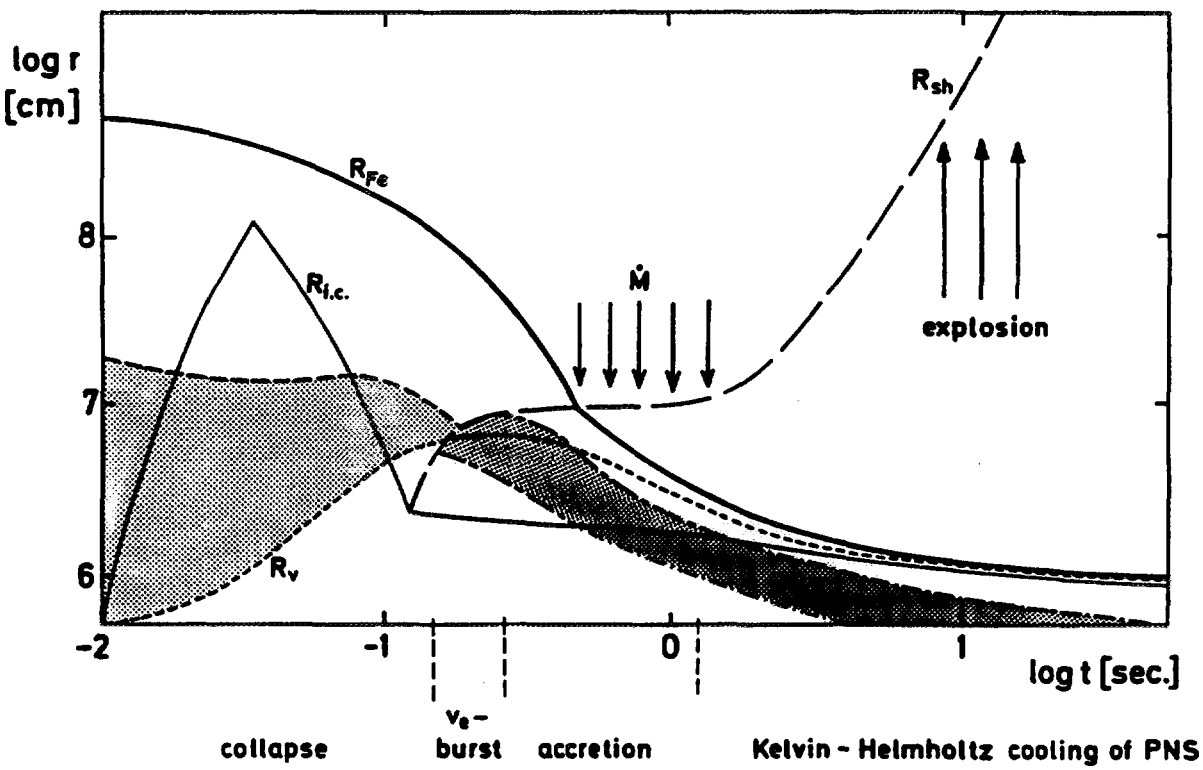

Figure 1. Schematic picture of stellar core collapse, formation of the neutron star remnant and start of the supernova explosion. The figure shows particular radial positions in the star's central region as they evolve in time. The shaded region indicates those layers where most of the neutrino emission comes from. The evolution can be divided into the collapse phase, the phase of prompt shock propagation, the matter accretion phase, and the protoneutron star cooling phase. $R_{\rm Fe}$ is the radius of the stellar iron core, R_ν means the position of the 'neutrino sphere', which separates the regions of neutrino diffusion and neutrino transparency. For ${}_{10}\log(t) < -1$ the line $R_{\rm ic}$ marks the size of the subsonically collapsing inner part of the stellar core, at later times it encompasses the settled, compact inner region of the nascent neutron star. The supernova shock ($R_{\rm sh}$) is formed at core bounce, stagnates for several hundred milliseconds, and is revived by neutrino heating to propagate outwards into the stellar mantle with some time delay.

2. Neutrino emission from supernovae and protoneutron stars

2.1 Emission phases and neutrino luminosities

Refering to the scenario of stellar core collapse and post bounce evolution as described in Section 1 the neutrino emission from a type-II supernova will be discussed now. As "usual" in the supernova context neutrinos will be assumed to be massless (or nearly so). Possible implications of non-standard effects like neutrino vacuum or matter mixing will be mentioned at some places, or references will be given, where more information can be found.

Figure 1 shows a graphical summary and overview of physical events occuring in the center of a massive star between the onset of core collapse and the formation of the young neutron star on the one side, and the start of the explosion and later ejection of the mantle and envelope of the star on the other side. The graph shows the radial positions of special mass shells as functions of time, the time is plotted logarithmically and measured in seconds from the beginning of core collapse. Figure 2 displays the corresponding variation of the neutrino luminosities during the different phases of the evolution as discriminated in Figure 1. The thick solid line ($R_{\rm Fe}$) in Fig. 1 marks the surface of the stellar iron core, the thin solid line ($R_{\rm ic}$) indicates an inner part, which falls coherently ('homologously'). Initially this part grows as well in mass as in radius, containing the region where sound waves are able to communicate that the center has started to undergo collapse. The maximum mass of this region is always close to the present Chandrasekhar mass according to Eq. (1), determined by the average value of the electron concentration Y_e in the core. Since emission of electron neutrinos continuously reduces Y_e, there is a point when this inner part of the core will begin to shrink in mass. $R_{\rm ic}$ also separates the subsonically infalling inner layers from the supersonically collapsing outer region. Therefore, it gives the approximate position where the shock wave is formed at core bounce.

During collapse the neutrino emission is by far dominated by electron neutrinos, copiously produced in electron captures on free protons and nuclei

$$e^- + p \longrightarrow \nu_e + n\,, \qquad e^- + (A,Z) \longrightarrow \nu_e + (A,Z-1)\,. \qquad (2\,\mathrm{a,b})$$

The region where most neutrinos stem from is roughly indicated by the shaded area in Fig. 1. It is bounded at the lower side by an inner zone where the high densities let the matter be opaque to neutrinos on collapse (in general: on the relevant) time scales. The transition region between neutrino opaque core or neutrino diffusion region and the neutrino transparent layers above is called 'neutrino sphere' and marked by R_ν. In the outer region of the stellar iron core the neutrino emission becomes negligible, because at low densities the capture time scale for electrons is very long.

The shock position as a function of time is indicated by $R_{\rm sh}$ in Fig. 1. Right after formation the shock front propagates quickly outward, however transforms into a standing accretion shock at about 100–200 km soon after it passes the neutrino sphere and an outburst of electron neutrinos (see Fig. 2) from the hot matter behind the shock yields a significant energy sink and causes a pressure reduction in the shocked matter. Over time scales of several 10 to several 100 milliseconds neutrino emission from post shock layers dominates and the burst phase is followed by

a plateau phase in the neutrino luminosities (Fig. 2). Neutrinos of all kinds are now produced by thermal neutrino processes in the high-temperature material and their luminosities get close to the electron neutrino flux. Additional considerable neutrino losses from the matter accreted onto the newly formed neutron star during the phase of shock stagnation may impose temporal variations onto the neutrino luminosities, and Fig. 2 displays just a simplification of the true situation. This intermediate period of high neutrino luminosities must also be the time of shock revival. If the neutrino energy deposition below the shock is sufficiently high, the post shock material starts to expand and develops positive velocities. This causes the end of the matter accretion onto the newly formed neutron star, naturally shut down when the supernova explosion goes off. The protoneutron star deleptonizes, cools, and shrinks in the quasistatic Kelvin-Helmholtz phase, accompanied by roughly exponentially decaying neutrino luminosities, which are dominated by neutrinos diffusing out from successively deeper layers of the young remnant (Fig. 1).

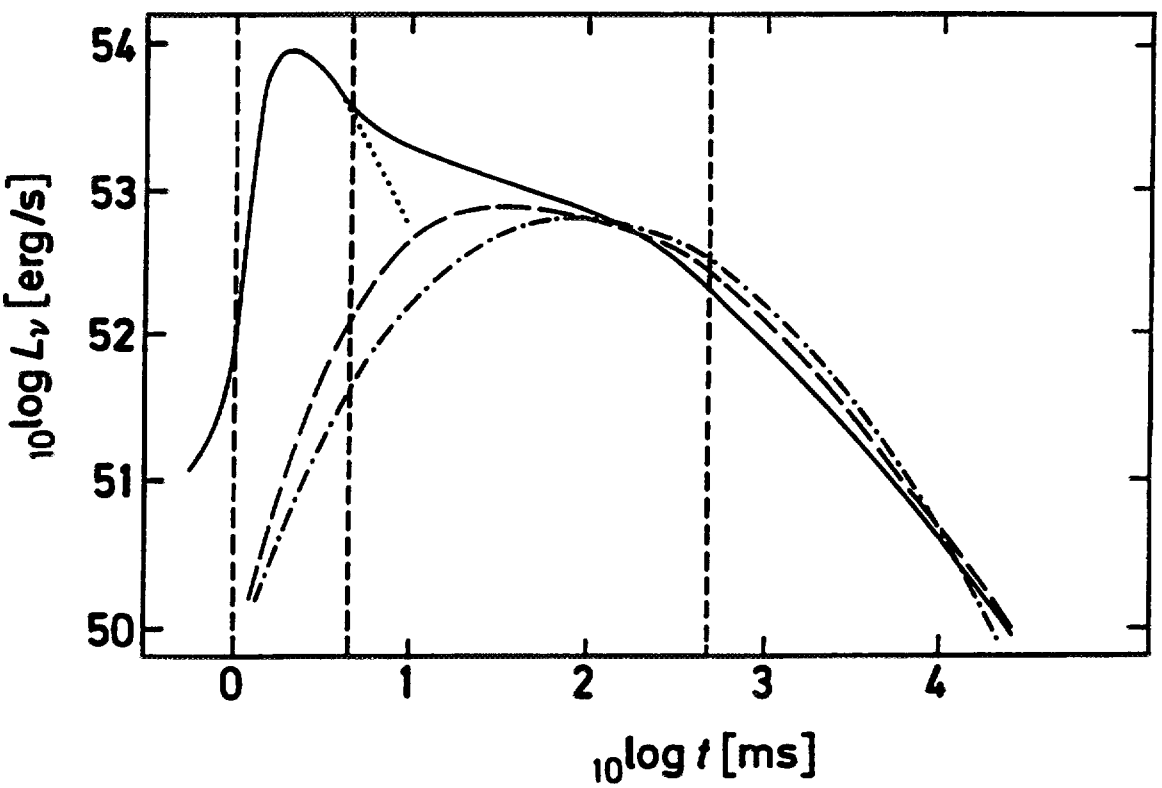

Figure 2. Schematic representation of neutrino 'light' curves during stellar core collapse, shock propagation and shock breakout, accretion phase, and protoneutron star cooling, the different phases separated by vertical short-dashed lines. The solid curve corresponds to ν_e, the long dashed line marks $\bar{\nu}_e$-emission, the dashed-dotted curve indicates the luminosity in each of the neutrino kinds ν_μ, $\bar{\nu}_\mu$, ν_τ, and $\bar{\nu}_\tau$. Time is measured in milliseconds with $_{10}\log(t) = 0$ positioned at the moment of core bounce.

Let us derive orders of magnitude estimates for the energy being emitted from the supernova in the different evolution phases described above. Basically one

can distinguish between 'neutronization neutrinos', ν_e, carrying lepton number and energy out of the star, and 'cooling neutrinos', neutrinos of all flavours and kinds, ν_i and $\bar{\nu}_i$ with $i = e, \mu, \tau$, radiating away energy from the stellar gas. ν_e-luminosities dominate by far during collapse and burst phases. Considering a star of mass M and an average change of its lepton content ΔY_e one can write for the energy emitted in these neutrinos

$$\Delta E \approx 2 \cdot 10^{51} \cdot \frac{M}{M_\odot} \frac{\Delta Y_e}{0.1} \frac{\langle \epsilon_\nu \rangle_{\rm esc}}{10\,{\rm MeV}} \ {\rm erg}\,, \tag{3}$$

when $\langle \epsilon_\nu \rangle_{\rm esc}$ is the mean energy of the neutrinos when they leave the star.

(1) *Collapse* phase: During the collapse phase numerical simulations give an average deleptonization of the inner part of the stellar iron core with $M \lesssim 1 M_\odot$ of roughly $\Delta Y_e \approx 0.06$–0.08. In the still transparent material the average neutrino energy equals the average energy of a captured electron, $\langle \epsilon_\nu \rangle_{\rm esc} \approx \frac{5}{6}\mu_e \approx 10$–$12\,{\rm MeV}$; ($\mu_e$ is the chemical potential of the degenerate electrons). One gets with the collapse time scale being a multiple of the free fall time scale $\Delta t = \alpha \cdot t_{\rm ff} \approx 10$–$100\,{\rm ms}$:

$$\Delta E_{\nu_e} \approx 10^{51}\ {\rm erg}\,, \qquad L_{\nu_e} \lesssim 10^{52}\ {\rm erg/s}\,. \tag{4}$$

(2) *Shock breakout* phase: At shock breakout the shock heated material of $M \approx 0.5\,M_\odot$ looses a lepton fraction $\Delta Y_e \approx 0.2$ within quite a short time scale of $\Delta t \approx \Delta r / 0.1c \approx 10\,{\rm ms}$, where Δr is the radial extension of the region, and the effective propagation speed of neutrinos is around $\frac{1}{10}$ of the speed of light. In the shock heated region neutrinos are present according to local chemical equilibrium, thus $\langle \epsilon_\nu \rangle_{\rm esc} \approx T \cdot \mathcal{F}_3(\eta_\nu)/\mathcal{F}_2(\eta_\nu) \approx 12$–$15\,{\rm MeV}$. $\mathcal{F}_k(y)$ denotes the Fermi integrals for extremely relativistic particles,

$$\mathcal{F}_k(y) \equiv \int_0^\infty {\rm d}x \, \frac{x^k}{1 + \exp(x - y)}\,, \tag{5}$$

$\eta_\nu = \mu_\nu / k_{\rm B} T$ is the degeneracy parameter of neutrinos in local chemical equilibrium. One ends up with

$$\Delta E_{\nu_e} \approx 2...3 \cdot 10^{51}\ {\rm erg}\,, \qquad L_{\nu_e} \lesssim 10^{54}\ {\rm erg/s}\,. \tag{6}$$

During accretion phase and Kelvin-Helmholtz cooling of the protoneutron star neutrinos of all kinds are emitted with similar luminosities. For an order of magnitude estimate the luminosity can be described by black body radiation from the surface of the emitting object:

$$L_\nu \approx 3 \cdot 10^{52} \cdot \left(\frac{R}{50\,{\rm km}}\right)^2 \left(\frac{T}{4\,{\rm MeV}}\right)^4 \ {\rm erg/s}\,, \tag{7}$$

T and R being temperature and radius at the radiating surface. (Here as in the following T always denotes the product of the temperature and Boltzmann's constant and is measured in MeV.)

(3) *Accretion and hot mantle cooling* phase: The total energy lost during this phase can be estimated from the average temperature $T \approx 5$–$8\,\mathrm{MeV}$ and the mass of the cooling matter $M \approx 0.5\,M_\odot$ to be about

$$\Delta E \approx E_{\mathrm{th}} \approx 2 \times 1.5 \cdot 10^{52}\,\frac{M}{M_\odot}\,\frac{T}{5\,\mathrm{MeV}}\,\mathrm{erg}\,, \qquad (8\,\mathrm{a})$$

when equal total energies in relativistic electrons and the nonrelativistic baryonic gas component are assumed. For typical radii around 50 km one finds

$$L_\nu \approx 5...10 \cdot 10^{52}\,\mathrm{erg/s}\,, \quad \Delta t \gtrsim 100\,\mathrm{ms}\,. \qquad (8\,\mathrm{b})$$

(4) *Kelvin-Helmholtz cooling* phase: During this phase the newly born neutron star with a radius of 10–15 km looses most of its gravitational binding energy

$$\Delta E \approx \frac{3}{5}\frac{GM^2}{R} \approx 1.6 \cdot 10^{53}\left(\frac{M}{M_\odot}\right)^2\left(\frac{R}{10\,\mathrm{km}}\right)^{-1}\,\mathrm{erg}\,, \qquad (9\,\mathrm{a})$$

which is initially stored as internal energy in the degenerate lepton gases. With a diffusion time scale of typically

$$t_{\mathrm{diff}} \cong \frac{R^2}{c\langle\lambda\rangle} \approx 2 \cdot \frac{M}{M_\odot}\left(\frac{R}{10\,\mathrm{km}}\right)^{-1}\frac{\langle\epsilon_\nu^2\rangle}{(20\,\mathrm{MeV})^2}\;\mathrm{s}\,,$$

where the averages mean average values over the whole star, and ϵ denotes the neutrino energy, one can derive numbers for the lepton loss time scale $t_{\mathrm{L,loss}} \cong (Y_{\mathrm{L}}/Y_\nu)\,t_{\mathrm{diff}} \approx (3...5) \cdot t_{\mathrm{diff}}$ and for the energy loss time scale $t_{E,\mathrm{loss}} \cong (E/E_\nu)\,t_{\mathrm{diff}} \approx (5...10) \cdot t_{\mathrm{diff}}$. In the latter two expressions the ratios account for the difference of the lepton content in the neutrino gas and in the stellar gas and for the energy stored in the stellar matter, respectively. Finally, one ends up with typical neutrino luminosities of the protoneutron star of about

$$L_\nu \approx 2...30 \cdot 10^{51}\,\mathrm{erg/s}\,. \qquad (9\,\mathrm{b})$$

One-dimensional numerical simulations of stellar core collapse and protoneutron star cooling with neutrino transport (e.g. Mayle 1985, Bruenn 1987, Mayle 1990, Myra and Bludman 1989, Burrows and Lattimer 1986, Suzuki 1989) yield detailed neutrino luminosity curves, the generic structure of which can well be interpreted within the framework developed above. Note, however, that the individual computations strongly differ from each other with respect to details of the employed physics. Variations due to differences in the core structure of the used progenitor star models are unavoidable. Also, the equation of state describing matter around and beyond nuclear matter density determines the supernova dynamics and the structure of the newly formed neutron star, both of which must have influences on details of the neutrino emission. Some of the listed computations include effects due to convective processes (mimiced in a parameterized description in course of the one-dimensional simulations), some disregard the accretion process onto the newly formed neutron star, etc. Moreover, the numerical description of the neutrino transport (in some

cases 'neutrino heat conduction' schemes or 'flux-limited diffusion' methods) causes discrepancies between results from different groups. Finally, non-standard neutrino properties might change the picture described above. Burrows et al. (1992) has considered effects on the neutrino signal from the supernova and the young neutron star by neutrino matter or vacuum oscillations.

How will the neutrino emission be distributed among the different neutrino kinds ν_e, $\bar{\nu}_e$, and ν_x ($x \equiv \mu, \bar{\mu}, \tau, \bar{\tau}$)? Again one can quite easily derive limits for the possible range of variation. All neutrino transport simulations agree in the point that electron neutrinos leave the star with smaller average energies than electron antineutrinos, while the latter are less energetic than heavy lepton neutrinos. This can easily be understood in the following way: A large part of the opacity of the stellar gas for ν_e results from absorption processes onto free neutrons; in case of $\bar{\nu}_e$ absorption onto free protons plays the dominant role in most of the collapsed stellar core. Now, since the neutron concentration in the matter is larger than the proton concentration — this difference increasing in time as the neutronization of the gas continues — ν_e are more strongly interacting with the stellar gas than $\bar{\nu}_e$ and decouple farther out at lower temperature, while $\bar{\nu}_e$ leave the star from deeper, thus hotter, layers. This effect is even stronger for ν_x (ν_μ, $\bar{\nu}_\mu$, ν_τ, and $\bar{\nu}_\tau$ interact with the stellar gas in nearly the same way): They are not absorbed by baryonic matter particles. Thus they come from even deeper regions. As time goes on and an increasing fraction of protons combines with electrons to form neutrons, the energetics of $\bar{\nu}_e$ and ν_x should become more similar. Numerical simulations of neutrino transport (Mayle 1985; Mayle et al. 1987; Janka 1987; Janka and Hillebrandt 1989a,b; Janka 1990; Bruenn 1987; Myra and Bludman 1989; Myra and Burrows 1990; compare also the overview graph in Burrows 1988) give typically:

$$\begin{aligned} \langle \epsilon_{\nu_e} \rangle &\approx 10...12\,\mathrm{MeV}\,, \\ \langle \epsilon_{\bar{\nu}_e} \rangle &\approx 14...17\,\mathrm{MeV} \approx 1.5 \cdot \langle \epsilon_{\nu_e} \rangle\,, \\ \langle \epsilon_{\nu_x} \rangle &\approx 24...27\,\mathrm{MeV} \approx (2...2.5) \cdot \langle \epsilon_{\nu_e} \rangle\,. \end{aligned} \tag{10}$$

Considering a total lepton loss ΔY_e of the collapsed stellar core with baryon number $N_B = \mathcal{A} \cdot M$ ($\mathcal{A}$ is Avogadro's constant) and a total energy loss of ΔE, one can write down three equations for the energies E_{ν_e}, $E_{\bar{\nu}_e}$, and E_{ν_x} transported away by the different neutrino kinds:

$$N_B \cdot \Delta Y_e = \frac{E_{\nu_e}}{\langle \epsilon_{\nu_e} \rangle} - \frac{E_{\bar{\nu}_e}}{\langle \epsilon_{\bar{\nu}_e} \rangle}\,, \tag{11a}$$

$$\Delta E = E_{\nu_e} + E_{\bar{\nu}_e} + 4 \cdot E_{\nu_x}\,, \tag{11b}$$

$$4 \cdot E_{\nu_x} \approx \left(\tfrac{1}{2}...\tfrac{2}{3}\right) \cdot \Delta E\,, \tag{11c}$$

where the last equation gives the approximate possible range of variation found in numerical simulations, and Eq. (11b) assumes thermal equipartition of the energy reservoir. Combining all three equations one derives

$$E_{\nu_e} = \tfrac{1}{5}\left(\tfrac{2}{3}...1\right) \cdot \Delta E + \tfrac{3}{5} \langle \epsilon_{\nu_e} \rangle N_B \cdot \Delta Y_e\,, \tag{12a}$$

$$E_{\bar{\nu}_e} = \tfrac{1}{5}\left(1...\tfrac{3}{2}\right) \cdot \Delta E - \tfrac{3}{5} \langle \epsilon_{\nu_e} \rangle N_B \cdot \Delta Y_e\,. \tag{12b}$$

With $M = 1.5\,M_\odot$, $\Delta Y_e = 0.4$, and $\langle \epsilon_{\nu_e} \rangle = 10\,\mathrm{MeV}$ this gives $E_{\bar{\nu}_e}/E_{\nu_e} \approx 1...1.25$, and one finds that the energy transported away in the different neutrino types is roughly within the following bounds:

$$E_{\nu_e}: \ 17\%.....22\%\,; \quad E_{\bar{\nu}_e}: \ 17\%.....28\%\,; \quad E_{\nu_x}: \ 66\%.....50\%\,. \qquad (13)$$

Once again, if neutrino oscillations occur, this simple picture might change, and observations of supernova neutrinos would have to be interpreted in a different way (Burrows et al. 1992).

2.2 Neutrino spectra

The energetic distributions of neutrinos emitted from supernovae and protoneutron stars are important for an interpretation of supernova neutrino detections as well as for the investigation of neutrino induced nucleosynthesis processes in the mantle and envelope layers of the exploding star. Moreover, as we shall see below, a determination of the neutron star radius, which is better than an order of magnitude estimate, requires knowledge about the spectral character of the neutrino emission.

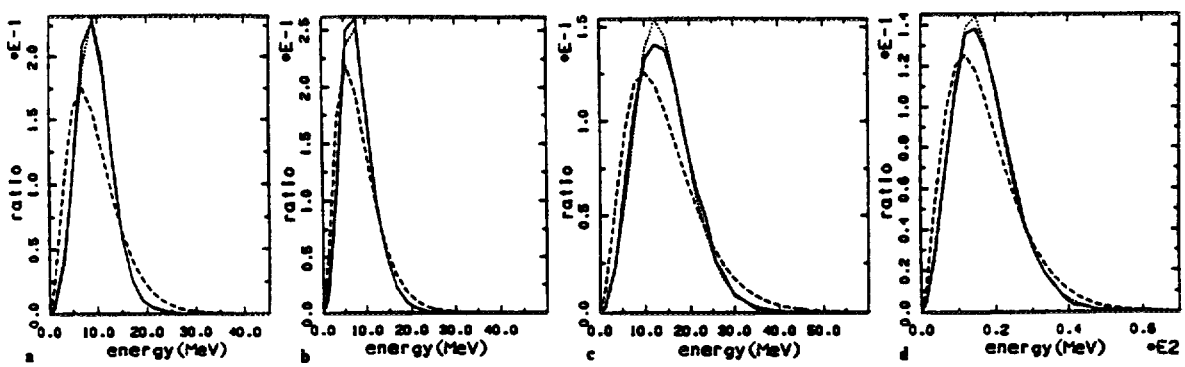

Figure 3. Spectra of neutrinos from a supernova (from Janka and Hillebrandt 1989b). The left two figures give results for ν_e at 12 milliseconds and 315 milliseconds after core bounce, respectively, Fig. 3c shows the $\bar{\nu}_e$-spectrum, Fig. 3d corresponds to ν_x ($x \equiv \mu, \bar{\mu}, \tau, \bar{\tau}$) at the later stage of the supernova evolution. The spectra plotted as solid lines were obtained by Monte Carlo simulations of neutrino radiative transfer, the dashed lines show the 'thermal' or 'black body' spectra (i.e. $\eta_\nu = 0$) with the same average energy, the dotted lines represent fits with non-vanishing neutrino degeneracy parameter $\eta_\nu^{\mathrm{eff}} \neq 0$. Note that the Monte Carlo spectra show significant depletion at low and high energies compared with the thermal spectra. The average spectral energies are 9.5 MeV, 8.2 MeV, 14.4 MeV, and 17.2 MeV in Figs. 3a–d, respectively.

Before we turn to results of elaborate numerical simulations of neutrino transport in supernovae and protoneutron stars, let us first develop a qualitative feeling of the effects we expect to see. Very roughly, neutrino opacities vary like the square of the neutrino energy ϵ: $\kappa \propto \sigma \propto \epsilon^2$. This quite strong energy dependence immediately implies that in general neutrinos will not be emitted from a well defined surface, but

will decouple from the stellar gas within a radially extended region, where gradients of the state variables T, μ_e, ρ, etc. are present. High energy neutrinos, having larger reaction cross sections, will interact with the stellar gas until far out in the star, while low energy neutrinos should decouple from the stellar surroundings deeper inside the star. Therefore the emitted neutrino spectra will in general not be thermal.

If we assume that neutrinos of energy ϵ stay in thermodynamical equilibrium with the stellar gas until they decouple at their decoupling radius $r(\epsilon)$, we can write for the neutrino luminosity at the energy ϵ

$$l(\epsilon) \equiv \frac{L(\epsilon)}{\epsilon^3} \propto r^2(\epsilon) \cdot \frac{1}{1+\exp\left(\epsilon/T\left[r(\epsilon)\right]\right)} , \tag{14}$$

where $T[r(\epsilon)]$ is the matter temperature at radius $r(\epsilon)$, and the neutrino chemical potential μ_ν was neglected in the Fermi-Dirac distribution function for reasons of simplicity, but could in principle be carried through the now following considerations. One already sees that at the low energy end of the spectrum, $\epsilon/T \lesssim 1$, one gets $l(\epsilon_1) < l(\epsilon_2)$ for $\epsilon_1 < \epsilon_2$, because in this case we expect $r(\epsilon_1) < r(\epsilon_2)$. Therefore, the emitted neutrino spectra will be depleted on the low energy side compared with thermal spectra. (Of course, here we neglect that farther out neutrinos might be downscattered from higher energies and fill this depletion at low energies; downscattering can be disregarded as long as absorption and emission processes or pair production/annihilation reactions dominate over non-isoenergetic scatterings.) High energetic neutrinos, $\epsilon/T \gg 1$, decouple from the stellar gas farther out, where the gas temperatures are smaller. With the exponential term in Eq. (14) now determining the variations we deduce $l(\epsilon_2)/l(\epsilon_1) \propto \exp\left[-\epsilon_2/T(\epsilon_2) + \epsilon_1/T(\epsilon_1)\right] < \exp\left[-(\epsilon_2-\epsilon_1)/T(\epsilon_1)\right]$ for $\epsilon_2 > \epsilon_1$, since $T(\epsilon_2) < T(\epsilon_1)$. That means that we also expect a suppression of the high energy tails of the spectra.

Considering a model atmosphere with power law profiles of density and temperature, $\rho \propto r^{-\alpha}$ and $T \propto r^{-\beta}$, respectively, we can determine the neutrino decoupling radius $r(\epsilon)$ as a function of the neutrino energy ϵ from the optical depth $\tau(\epsilon)$ by inverting the expression

$$1 = \tau(\epsilon) = \int_{r(\epsilon)}^{\infty} \mathrm{d}r\, \kappa(r,\epsilon) \propto \epsilon^2\, r^{1-\alpha} . \tag{15}$$

One gets $r(\epsilon) \propto \epsilon^{2/(\alpha-1)}$. Introducing this into the expression for $T(r)$ leads to $T[r(\epsilon)] \propto \epsilon^{-2\beta/(\alpha-1)}$. With $r(\epsilon)$ and $T[r(\epsilon)]$ Eq. (14) yields

$$L(\epsilon) \propto \frac{\epsilon^\gamma}{1+\exp\left(a\cdot\epsilon^\delta\right)} \quad \text{with} \quad \gamma = \frac{4}{\alpha-1}+3 \quad \text{and} \quad \delta = \frac{2\beta}{\alpha-1}+1 , \tag{16}$$

and a being a constant. Inserting typical numbers $\alpha \approx 3$ and $\beta \approx 1$ we find $L(\epsilon) \propto \epsilon^5 / \left[1+\exp(a\cdot\epsilon^2)\right]$. This demonstrates the effect we discussed qualitatively above.

Detailed Monte Carlo simulations of neutrino transport with all relevant neutrino-matter reactions carefully included (Janka 1987; Janka and Hillebrandt 1989a,b; Janka 1990) confirm these considerations. Due to 'inelastic' (actually: not isoenergetic) scatterings of neutrinos off electrons the depletion of the spectra at low energies

and high energies is not as dramatic as suggested by Eq. (16). However, the pinching of the spectra is clearly present for all types of neutrinos, and has consequences when the interactions of neutrinos with target nuclei in the star and in laboratory experiments are investigated, since the corresponding reaction rates sensitively depend on the high energy parts of the spectra (see below).

Figures 3a,b,c show spectra of ν_e, $\bar{\nu}_e$, and ν_x for the neutrino emission from a supernova at times between ten and several hundred milliseconds after core bounce (Janka and Hillebrandt 1989b). The spectra computed with the Monte Carlo transport (solid lines) are compared with 'thermal' spectra, i.e. neutrino distributions according to Fermi-Dirac functions with chemical potential $\mu_\nu = 0$ and temperatures such that the average energy of the true spectrum is reproduced. The pinched shape of the real spectra relative to the thermal distributions (dashed lines) is clearly visible. Figures 4a,b,c give spectra for all types of neutrinos at three different times during the protoneutron star cooling phase (about 3.3, 5.8, and 7.8 seconds after core bounce) (Janka 1990). They also show the suppression in the high energy tails. Note that for an observer at infinity these spectra have to be redshifted by 10–20%, the exact number depending on the size of the neutron star and the stage of the evolution.

An approach based on Eq. (16) does in general not allow to fit the computed spectra with physically meaningful temperatures (see Janka and Hillebrandt 1989b). Instead, good fits with 'reasonable' fit parameters are possible with a Fermi-Dirac ansatz:

$$\frac{\mathrm{d}L}{\mathrm{d}\epsilon} = \frac{L_\nu}{T_\nu^4\,\mathcal{F}_3(\eta_\nu^{\mathrm{eff}})} \cdot \frac{\epsilon^3}{1+\exp\left(\epsilon/T_\nu - \eta_\nu^{\mathrm{eff}}\right)} \,. \tag{17}$$

The product $T_\nu^4 \cdot \mathcal{F}_3(\eta_\nu^{\mathrm{eff}})$ with $\mathcal{F}_3(\eta_\nu^{\mathrm{eff}})$ being the integral defined in Eq. (5) appears in the denominator for reasons of normalization. The two fit parameters, 'neutrino temperature' T_ν and 'effective neutrino degeneracy' η_ν^{eff}, are chosen such that two energy moments of the true non-thermal spectrum, the averge neutrino energy $\langle\epsilon\rangle$ and the average squared energy $\langle\epsilon^2\rangle$, are correctly reproduced by the fit spectrum, i.e. the mean value and the width $\sqrt{\langle\epsilon^2\rangle - \langle\epsilon\rangle^2}$ of the computed spectrum and the fit spectrum are equal (for details see Janka and Hillebrandt 1989b). Note that a third parameter, which appears as a scaling factor in Eq. (17), is used to ensure the correct absolute size of the neutrino luminosity. In Figs. 3a–c the corresponding fits are shown by the dotted lines. The neutrino temperature, of course, varies with time as the energies of the emitted neutrinos do and depends on the particular structure of the supernova model (density, temperature, etc.) and on the phase of the supernova evolution. The degeneracy parameter η_ν^{eff}, however, turns out to be much less sensitive and can be chosen quite generally. Typical values for ν_e, $\bar{\nu}_e$, and ν_x found in our transport simulations are

$$\eta_{\nu_e}^{\mathrm{eff}} \approx 5\ldots3\,, \quad \eta_{\bar{\nu}_e}^{\mathrm{eff}} \approx 2.5\ldots2\,, \quad \eta_{\nu_x}^{\mathrm{eff}} \approx 2\ldots0\,, \tag{18}$$

where the change with time during the supernova event and the protoneutron star history (see also Myra and Burrows 1990, Suzuki 1989) is indicated by ordering the bounds of the range of possible variation in the chosen way.

One can easily convince oneself that an ansatz according to Eq. (17) with $\eta_\nu > 0$ yields the desired reduction of the low *and* high energy parts and thus the

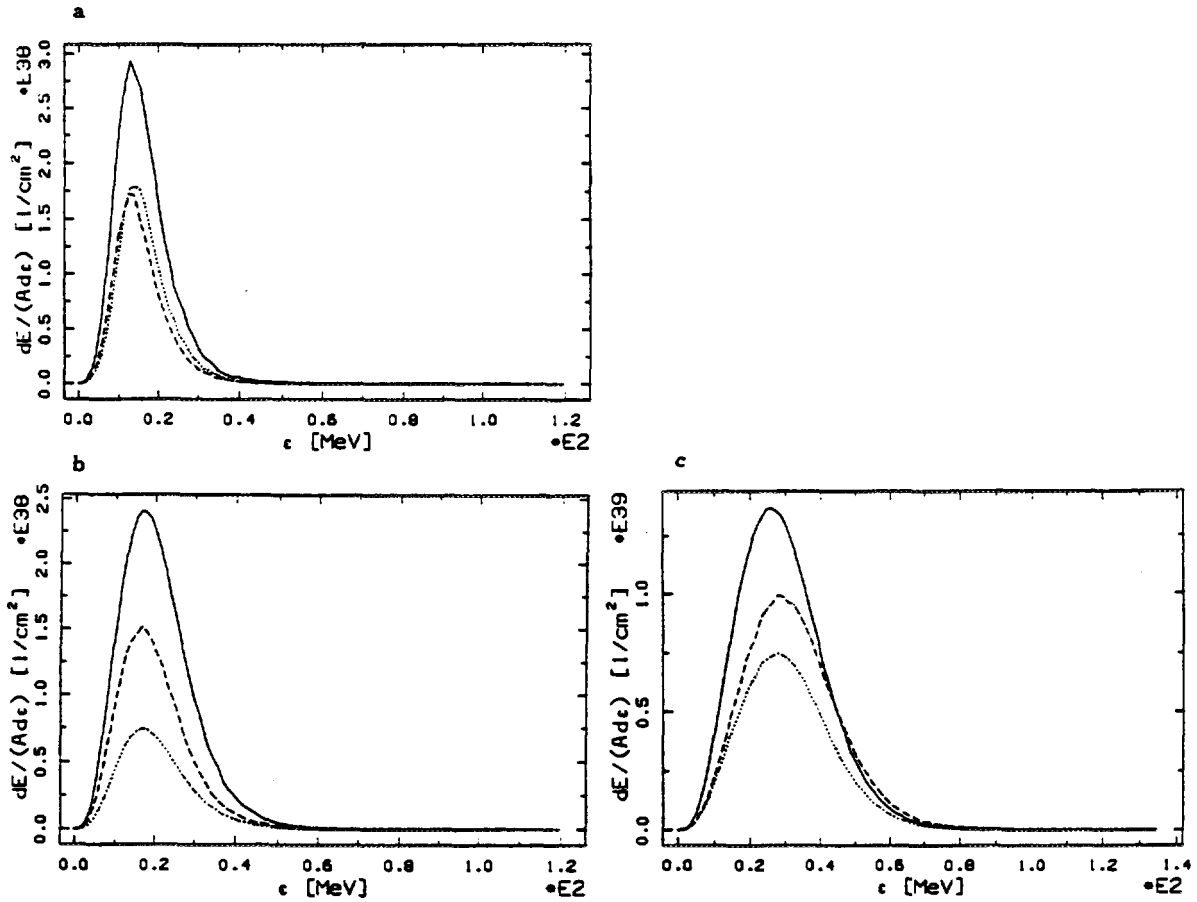

Figure 4. Neutrino spectra during protoneutron star cooling (Janka 1990). The graphs give spectral distributions of the energy radiated in ν_e (Fig. 4a), $\bar{\nu}_e$ (Fig. 4b), ν_x (Fig. 4c) per energy interval and per unit area at the neutron star surface, integrated over the time periods during which the neutrino transport was followed by Monte Carlo simulations (approx. 1 ms). Solid lines correspond to a model at about 3.3 s after core bounce (radius of the neutron star $R_{\rm NS} = 16\,{\rm km}$), the dashed lines to a model at 5.8 s after bounce ($R_{\rm NS} = 12.8\,{\rm km}$), the dotted lines represent the emission at 7.8 s post bounce ($R_{\rm NS} = 11.8\,{\rm km}$). The average spectral energies are 12–13 MeV for ν_e, about 16 MeV for $\bar{\nu}_e$, and 24–27 MeV for ν_x. For an observer at infinity these energies have to be redshifted by roughly 10–20%.

pinched shape of the neutrino spectrum. (Here and in the following we shall write η_ν instead of $\eta_\nu^{\rm eff}$ and mean the fit parameter in Eq. (17).) We have to compare the two cases with the choices $T_\nu = T_1$, $\eta_\nu = 0$ and $T_\nu = T_2$, $\eta_\nu = \eta_2 > 0$, respectively. For fixed $\eta_\nu = 0$ the spectrum of Eq. (17) only guarantees correct representation of the neutrino luminosity and the average neutrino energy. Requiring $\langle\epsilon\rangle$ to be equal in both cases relates the temperatures T_1 and T_2. Using

$$\langle\epsilon\rangle \;=\; T_\nu \cdot \frac{\mathcal{F}_3(\eta_\nu)}{\mathcal{F}_2(\eta_\nu)} \tag{19}$$

one gets

$$\frac{T_1}{T_2} \;=\; \frac{\mathcal{F}_3(\eta_2)/\mathcal{F}_2(\eta_2)}{\mathcal{F}_3(0)/\mathcal{F}_2(0)} \;>\; 1 \quad \text{for} \quad \eta_2 > 0\,. \tag{20}$$

In the limit of small energies, $\epsilon \lesssim \eta_2 \cdot T_2$ and $\epsilon \lesssim T_1$, we derive

$$\frac{dL_2/d\epsilon}{dL_1/d\epsilon} \lesssim 2\left(\frac{T_1}{T_2}\right)^4 \left(\frac{\mathcal{F}_3(0)}{\mathcal{F}_3(\eta_2)}\right) = 2\left(\frac{\mathcal{F}_3(\eta_2)}{\mathcal{F}_3(0)}\right)^3 \left(\frac{\mathcal{F}_2(0)}{\mathcal{F}_2(\eta_2)}\right)^4 , \qquad (21)$$

where the second transformation uses Eq. (20). For typical values $\eta_2 \gtrsim 3$ we arrive at

$$\frac{dL_2/d\epsilon}{dL_1/d\epsilon} \lesssim 0.39 < 1 .$$

At high energies, $\epsilon \gg T_1$ and $\epsilon/T_2 - \eta_2 \gg 1$, we find

$$\frac{dL_2/d\epsilon}{dL_1/d\epsilon} \approx \left(\frac{T_1}{T_2}\right)^4 \frac{\mathcal{F}_3(0)}{\mathcal{F}_3(\eta_2)} \cdot \exp\left[-\frac{T_1 - T_2}{T_1 T_2}\epsilon + \eta_2\right] , \qquad (22)$$

which is smaller than unity for sufficiently high energies.

2.3 Implications for neutrino observations

As mentioned above the suppression of the high energy tail of the spectra has consequences for the interpretation of supernova neutrino observations as well as for neutrino induced nucleosynthesis processes in the outer layers of the progenitor star. We shall estimate the size of these effects in this section.

Given the spectral density of the neutrino particle flux in terms of the spectral luminosity $dL/d\epsilon$,

$$\frac{d\Phi_\nu}{d\epsilon} = \frac{1}{4\pi r^2\,\epsilon} \cdot \frac{dL}{d\epsilon} \quad [\mathrm{cm^{-2}s^{-1}MeV^{-1}}] , \qquad (23)$$

the number of neutrino interactions N_ν occuring in a volume V at distance r from the neutrino source and the energy E_ν absorbed in the volume V during time Δt can be calculated as the moments

$$\begin{aligned} M^{(m)} &= \int_0^\infty d\epsilon \int_0^{\Delta t} dt \int_V dV \, \frac{d\Phi_\nu}{d\epsilon} \epsilon^m \, n_T \sigma(\epsilon)\chi(\epsilon) \\ &= N_T \cdot \int_0^\infty d\epsilon \, \frac{d(\Phi_\nu \cdot \Delta t)}{d\epsilon} \epsilon^m \sigma(\epsilon)\chi(\epsilon) . \end{aligned} \qquad (24)$$

It is $N_\nu \equiv M^{(0)}$, $E_\nu \equiv M^{(1)}$, if each neutrino deposits its whole energy ϵ in the matter. Here N_T is the number of target particles in volume V, σ the reaction cross section, and χ the energy dependent detector efficiency. The notation $(\Phi_\nu \Delta t)$ is introduced as an abbreviation of the time integral of Φ_ν. Setting $\chi \equiv 1$ leaves us with integrals which describe the interaction of the neutrino fluxes in the ambient stellar material far away from the neutron star.

Now, supposed the neutrino luminosity L from the star and the average energy $\langle\epsilon\rangle$ of the emitted neutrinos are given, how does the neutrino-matter interaction differ, when the spectra have an effective degeneracy instead of being black body spectra? Equation (24) allows us to estimate the consequences. Let us consider a reaction with

cross section proportional to the n-th power of neutrino energy: $\sigma(\epsilon) \propto \epsilon^n$. We set $\chi \equiv 1$ for simplicity in Eq. (24), which is correct when we investigate the interactions of neutrinos in the stellar gas and ensures an underestimation of effects due to the spectral shape in case of the response in a neutrino experiment. Equation (24) has to be evaluated with the spectrum Eq. (17) with $\eta_\nu = 0$ and $T_\nu = T_1$ on the one hand and $\eta_\nu = \eta_2 > 0$ and $T_\nu = T_2$ on the other. Our basic assumption implies that $L_1 \equiv L_2$ and $\langle\epsilon\rangle_1 \equiv \langle\epsilon\rangle_2$. The latter relation allows us to use Eq. (20). Putting all together we derive

$$\frac{E_{\nu,2}}{E_{\nu,1}} = \left(\frac{T_2}{T_1}\right)^{-1+m+n} \frac{\mathcal{F}_{2+m+n}(\eta_2)/\mathcal{F}_3(\eta_2)}{\mathcal{F}_{2+m+n}(0)/\mathcal{F}_3(0)} . \tag{25}$$

Inserting representative numbers, $m = 1$, $n = 2$, $\eta_2 = 3$, we find this ratio being roughly 0.8. This means, not too astonishing, that due to the suppression of the high energy tail in case '2' the interaction of neutrino flow and stellar matter is reduced. The effect is drastical for very strong energy dependence of the cross sections, e.g. in case of inelastic neutrino-nucleus interactions (see e.g. Bruenn and Haxton 1991, Kolbe et al. 1992).

Let us state the question the other way round: Which consequences does the non-thermal spectral shape have for the conclusions drawn from a neutrino detection on the properties of the neutrino emitting source? Putting the question this way means that we now take a certain number of neutrino events $N_{\rm det}$ and a measured average energy $\langle\epsilon\rangle_{\rm det} = E_{\rm det}/N_{\rm det}$ of these recorded neutrinos as given. With a neutrino reaction cross section according to $\sigma(\epsilon) = \sigma_0\epsilon^n$ and the total energy emitted by the source in time Δt written as $E_{\rm em} = L \cdot \Delta t$, Eqs. (23), (24) yield

$$N_{\rm det} = N_{\rm T}\sigma_0 \frac{E_{\rm em}}{4\pi r^2} \frac{T_\nu^{n-1}}{\mathcal{F}_3(\eta_\nu)} \cdot \mathcal{I}_{2+n}(\eta_\nu) , \tag{26 a}$$

$$E_{\rm det} = N_{\rm T}\sigma_0 \frac{E_{\rm em}}{4\pi r^2} \frac{T_\nu^{n}}{\mathcal{F}_3(\eta_\nu)} \cdot \mathcal{I}_{3+n}(\eta_\nu) . \tag{26 b}$$

The integral $\mathcal{I}_k(y)$ is defined in analogy to Eq. (5):

$$\mathcal{I}_k(y) = \int_0^\infty {\rm d}x \, \frac{x^k \cdot \chi(x)}{1+\exp(x-y)} . \tag{27}$$

Deviding Eq. (26b) by Eq. (26a) one gets

$$\langle\epsilon\rangle_{\rm det} = T_\nu \cdot \frac{\mathcal{I}_{3+n}(\eta_\nu)}{\mathcal{I}_{2+n}(\eta_\nu)} . \tag{28}$$

Using Eq. (19) we can conclude from the average energy of the detected neutrino events $\langle\epsilon\rangle_{\rm det}$ on the average energy of neutrinos coming from the stellar source:

$$\langle\epsilon\rangle_{\rm em} = \langle\epsilon\rangle_{\rm det} \cdot \frac{\mathcal{F}_3(\eta_\nu)}{\mathcal{F}_2(\eta_\nu)} \frac{\mathcal{I}_{2+n}(\eta_\nu)}{\mathcal{I}_{3+n}(\eta_\nu)} . \tag{29}$$

Expressing T_ν in Eq. (26b) in terms of $\langle\epsilon\rangle_{\rm det}$ via Eq. (28), we can determine the energy emitted by the star in neutrinos, $E_{\rm em}$, from the measured quantities $E_{\rm det}$ and $\langle\epsilon\rangle_{\rm det}$ as

$$E_{\rm em} = \frac{1}{N_{\rm T}\sigma_0}\frac{4\pi r^2 E_{\rm det}}{\langle\epsilon\rangle_{\rm det}^n}\cdot\left(\frac{\mathcal{I}_{3+n}(\eta_\nu)}{\mathcal{I}_{2+n}(\eta_\nu)}\right)^n\frac{\mathcal{F}_3(\eta_\nu)}{\mathcal{I}_{3+n}(\eta_\nu)}\,. \qquad (30)$$

If we consider absorption of electron antineutrinos by protons and evaluate the expression of Eq. (29) with the IMB and Kamiokande detector efficiencies, we find that spectra with effective degeneracy parameters around $\eta_\nu \approx 3$–3.5 lead to 20–30% higher values for $\langle\epsilon\rangle_{\rm em}$ compared with the case $\eta_\nu = 0$ (see Janka and Hillebrandt 1989b). A *downward* correction of the same size is necessary in case of the estimated energy emission $E_{\rm em}$ of the neutron star according to Eq. (30). These corrections increase for high detector threshold energies and strong energy dependence of the neutrino-target interaction.

Finally one can try to obtain an approximate numerical value for the radius R of the neutrino emitting object. As we explained above, the neutrino emission and spectra are non-thermal, since neutrinos are in general not radiated close to thermal equilibrium from a well defined surface. Thus the spectral temperature T_ν introduced in Eq. (17) can deviate considerably from an 'effective temperature' to be used in the Stefan-Boltzmann radiation law for a black body. This means that when the neutrino energy emitted by the neutron star in a time interval Δt is written as

$$E_{\rm em} = L\cdot\Delta t = 4\pi R^2\,\Delta t\,|g_{tt}|\cdot\left(\frac{c}{4}\frac{4\pi}{(hc)^3}\cdot\beta\right)\cdot T_\nu^4\,\mathcal{F}_3(\eta_\nu)\,, \qquad (31\,a)$$

the parameter β has to be determined from detailed calculations of neutrino radiative transfer in neutron star atmospheres. β is found to be typically of the order $\beta \approx 0.08 \ldots 0.12$ for $\bar\nu_e$ (Janka and Hillebrandt 1989b, Janka 1990). This holds in supernova models early after core bounce as well as during protoneutron star cooling. (The coefficient g_{tt} in Eq. (31a) accounts for general relativistic redshift and time dilatation effects from the neutron star surface to an observer at infinity.) Replacing T_ν in Eq. (31a) by $\langle\epsilon\rangle_{\rm det}$ via Eq. (28) we arrive at

$$E_{\rm em} = 4\pi R^2\,\Delta t\,|g_{tt}|\cdot\left(\frac{c}{4}\frac{4\pi}{(hc)^3}\cdot\beta\right)\cdot\langle\epsilon\rangle_{\rm det}^4\left(\frac{\mathcal{I}_{n+2}(\eta_\nu)}{\mathcal{I}_{n+3}(\eta_\nu)}\right)^4\mathcal{F}_3(\eta_\nu)\,. \qquad (31\,b)$$

Combining Eqs. (31b) and (30) one ends up with an expression for R. Note, however, that an evaluation better than just an order of magnitude estimate requires knowledge of the parameter β.

3. Neutrino-driven supernova explosions

3.1 Neutrino heating and explosion energetics

In the context of Wilson's delayed mechanism neutrinos play the crucial role to drive and to power the type-II supernova explosion. During the phase of matter accretion, lasting for several hundred milliseconds after core bounce, material is falling through the standing accretion shock. Initially cooling processes dominate in this

material, which radiates away its gravitational binding energy by neutrinos, and settles onto the protoneutron star. As the neutron star becomes more and more compact and the accretion rate shrinks with the decreasing density of the infalling layers of the progenitor star, there is a moment, when net heating by neutrino energy deposition must win against neutrino cooling.

To see this, let us compare the most important neutrino processes in the hot, dissociated post shock material during the accretion phase, electron/positron absorption on protons/neutrons and the inverse reactions:

$$e^- + p \longleftrightarrow \nu_e + n\,, \qquad e^+ + n \longleftrightarrow \bar{\nu}_e + p\,. \tag{32a,b}$$

The cooling rate per baryon due to the emission of ν_e and $\bar{\nu}_e$, respectively, in these capture reactions can approximately be written as

$$Q^-_{\nu_e,\bar{\nu}_e} \cong 2.4 \cdot \left(\frac{T}{1\,\mathrm{MeV}}\right)^6 \cdot \begin{Bmatrix} Y_p \\ Y_n \end{Bmatrix} \left[\frac{\mathrm{MeV}}{\mathrm{s}\cdot\mathrm{nucleon}}\right], \tag{33}$$

the corresponding heating rates by the inverse processes are

$$Q^+_{\nu_e,\bar{\nu}_e} \cong 110 \cdot \frac{L_{52}}{r_7^2} \frac{\langle\epsilon^2\rangle}{(15\,\mathrm{MeV})^2} \cdot \begin{Bmatrix} Y_n \\ Y_p \end{Bmatrix} \left[\frac{\mathrm{MeV}}{\mathrm{s}\cdot\mathrm{nucleon}}\right]. \tag{34}$$

Here T denotes the gas temperature, Y_n and Y_p mean concentrations (i.e. numbers per baryon) of free neutrons and protons, respectively, L_{52} is the ν_e- or $\bar{\nu}_e$-luminosity in 10^{52} erg/s, r_7 gives the distance from the compact neutrino source in 10^7 cm, and $\langle\epsilon^2\rangle$ defines the average squared energy of the neutrinos. Assuming neutrino spectra according to Eq. (17) one gets

$$\langle\epsilon^2\rangle \equiv T_\nu^2 \cdot \frac{\mathcal{F}_5(\eta_\nu)}{\mathcal{F}_3(\eta_\nu)} \approx 20\,T_\nu^2\,, \tag{35}$$

where the numerical value is obtained by taking $\eta_\nu = 0$. These handy forms of the formulae are derived with a number of simplifications: Electrons are assumed to be non-degenerate (electron chemical potential $\mu_e \approx 0$), and Pauli blocking effects due to lepton degeneracy are completely ignored; moreover, electron rest masses are assumed to be small compared with typical neutrino energies, $m_e c^2 \ll \langle\epsilon\rangle$, and with the gas temperature, $m_e c^2 \lesssim T$. Recoil of nucleons is disregarded, nucleons are assumed to be non-relativistic, non-degenerate ideal gases, and the rest mass difference between neutron and proton is neglected. These approximations will be used in all given rate expressions below, too, yielding accuracies of order 10% for typical situations in the discussed context here. (We use $\alpha = 1.254$ for the axial vector correction factor (Boehm and Vogel 1987), $\sin^2\theta_W = 0.23$ for the Weinberg angle (Langacker 1988), and the standard weak interaction cross section $\sigma_0 = 1.761 \cdot 10^{-44}\,\mathrm{cm}^2$).

In a thin, hydrostatic, isothermal atmosphere of a neutron star of radius R and mass M with the pressure being dominated by a Boltzmann gas of baryons, $P = \mathcal{A}\rho T$, the density declines exponentially with height $h = r - R$:

$$\rho = \rho_0 \cdot \exp\left(-\frac{GM}{\mathcal{A}TR} \cdot \left[1 - \frac{R}{r}\right]\right) \approx \rho_0 \cdot \exp\left(-\frac{GM}{\mathcal{A}TR^2} \cdot h\right). \tag{36}$$

For the typical temperatures $T \gtrsim 1\,\mathrm{MeV}$ this immediately implies that at sufficiently small densities relativistic electrons, positrons, and photons will start to yield the main contribution to the pressure, i.e. $P \propto T^4$. Here our basic assumption breaks down: The matter in the gravity field of the neutron star must be stabilized by a temperature gradient instead of a density gradient. In case of an adiabatic atmosphere one has $\rho \propto T^3$, which requires a temperature decline $T \propto r^{-1}$. However, for neutrino heating being balanced by neutrino cooling, $Q^+ = Q^-$, Eqs. (33) and (34) imply $T \propto r^{-1/3}$. This means that net energy deposition in a region close to the newly formed neutron star is unavoidable in the described situation.

In addition to the processes of Eqs. (32a,b), which yield the main part to the neutrino heating with a rate given by Eq. (34), there are contributions on the 10% level by energy transfers in scattering events between neutrinos and free nucleons:

$$\nu + \left\{\begin{matrix} n \\ p \end{matrix}\right\} \longleftrightarrow \nu + \left\{\begin{matrix} n \\ p \end{matrix}\right\} . \tag{37}$$

Although the energy exchange per individual reaction is small due to the large rest mass of the nucleon, $\Delta\epsilon \propto (\epsilon - 6T) \cdot \epsilon/(m_\mathrm{N}c^2)$ (see Tubbs 1979), these reactions have cross sections comparable to those of reactions Eqs. (32a,b), and all neutrinos kinds participate. For low temperatures $T \ll \langle\epsilon\rangle$ the energy transfer rates per baryon are estimated to

$$Q_{\nu,n+p} \cong 1.0 \cdot (Y_n + Y_p) \cdot \frac{L_{52}}{r_7^2} \cdot \frac{\langle\epsilon^3\rangle}{(20\,\mathrm{MeV})^3} \left[\frac{\mathrm{MeV}}{\mathrm{s} \cdot \mathrm{nucleon}}\right] \tag{38}$$

with

$$\langle\epsilon^3\rangle \equiv T_\nu^3 \cdot \frac{\mathcal{F}_6(\eta_\nu)}{\mathcal{F}_3(\eta_\nu)} \approx 120 \cdot T_\nu^3 \tag{39}$$

(the numerical value again assumes $\eta_\nu = 0$). The total heating via reactions Eq. (37) is given as the sum of the rates according to Eq. (38) for neutrinos and antineutrinos of all three flavours.

Another source of energy transfer to the stellar gas around the protoneutron star is neutrino-electron/positron scattering

$$\nu + \left\{\begin{matrix} e^- \\ e^+ \end{matrix}\right\} \longleftrightarrow \nu + \left\{\begin{matrix} e^- \\ e^+ \end{matrix}\right\} . \tag{40}$$

For nondegenerate, relativistic leptons the rate per nucleon is calculated as (Tubbs and Schramm 1975; see also Janka 1990):

$$Q_{\nu,e^-+e^+} \cong 3.4 \cdot \left\{\begin{matrix} 3.12 \\ 0.67 \end{matrix}\right\} \cdot \frac{L_{52}}{r_7^2} \frac{\langle\epsilon\rangle}{15\,\mathrm{MeV}} \frac{1}{\rho_6} \left(\frac{T}{0.5\,\mathrm{MeV}}\right)^4 \left[\frac{\mathrm{MeV}}{\mathrm{s} \cdot \mathrm{nucleon}}\right] . \tag{41}$$

Here ρ_6 means the matter density in $10^6\,\mathrm{g/cm^3}$, and the average neutrino energy is defined as

$$\langle\epsilon\rangle = T_\nu \cdot \frac{\mathcal{F}_4(\eta_\nu)}{\mathcal{F}_3(\eta_\nu)} \approx 4 \cdot T_\nu , \tag{42}$$

the numerical value again computed with $\eta_\nu = 0$. The two cases in Eq. (41), distinguished by the factors 3.12 and 0.67, respectively, correspond to the different weak interactions of ν_e and $\bar{\nu}_e$ with electrons and positrons via charged and neutral currents on the one side, and of ν_x via neutral currents only on the other. Energy deposition by the processes of Eq. (40) becomes important when the density gets low, the gas temperature, however, stays around or above 0.5 MeV. As in the case of neutrino-nucleon scattering the total rate is obtained by summing up the contributions of ν_e, $\bar{\nu}_e$, ν_μ, $\bar{\nu}_\mu$, ν_τ, and $\bar{\nu}_\tau$.

Goodman et al. (1987) claimed the importance of neutrino pair annihilation,

$$\nu + \bar{\nu} \longrightarrow e^- + e^+ , \tag{43}$$

in the close vicinity of the young neutron star, just outside of the neutrino 'sphere'. The rate drops steeply with increasing distance from the protoneutron star, because the phase space for the reaction depends on the relative velocity of the colliding neutrinos. Assuming equal luminosities and spectra for neutrinos and antineutrinos, one finds for the heating rate

$$Q^+_{\nu\bar{\nu}} \cong 10^{-2} \cdot \begin{Bmatrix} 2.34 \\ 0.50 \end{Bmatrix} \cdot L^2_{52} \frac{\langle\epsilon\rangle}{15\,\mathrm{MeV}} \cdot \frac{R^4_6}{r^8_7} \cdot \frac{1}{\rho_6} \left[\frac{\mathrm{MeV}}{\mathrm{s \cdot nucleon}}\right] . \tag{44}$$

(For a derivation of the reaction rate see Cooperstein et al. (1987) and for a careful evaluation of the phase space effects see Janka (1990,1991)). The neutrino energy average $\langle\epsilon\rangle$ is given by Eq. (42), the two cases in Eq. (44) again account for the different interaction of electron neutrinos and heavy lepton neutrinos via charged and neutral currents on the one hand and neutral currents only on the other. The total energy transfer to the stellar gas is given as sum of the contributions for all flavours of neutrinos. A careful analysis of the heating using Monte Carlo results of neutrino transport in protoneutron stars (Janka 1991) could not confirm the very optimistic estimates by Goodman et al. (1987), so it is controversial whether reaction Eq. (43) really is relevant. The inverse reaction, electron-positron annihilation into neutrino/antineutrino pairs, however, certainly takes part in the cooling of the hot material near the neutron star surface. The rate due to production of neutrino pairs of all flavours is given by

$$Q^-_{\nu\bar{\nu}} \cong 16.2 \cdot \frac{1}{\rho_6} \left(\frac{T}{1\,\mathrm{MeV}}\right)^9 \left[\frac{\mathrm{MeV}}{\mathrm{s \cdot nucleon}}\right] . \tag{45}$$

Supposed the neutrino luminosities L_{ν_e}, $L_{\bar{\nu}_e}$ and average neutrino energies are sufficiently high, absorption of electron neutrinos and antineutrinos can deposit enough energy in the matter between protoneutron star and stalled shock (compare Eq. (34)) to slow down the infall of the post shock material and to drive the shock outwards. A 'hot bubble', a region of low density, but temperatures above and around 0.5 MeV, starts to form and expand (Bethe and Wilson 1985). The energy transferred to the stellar material in that bubble region during the subsequent evolution will decide about the final energy of the supernova explosion. One can obtain an order of magnitude estimate by integrating Eq. (34) for characteristic density profiles in the

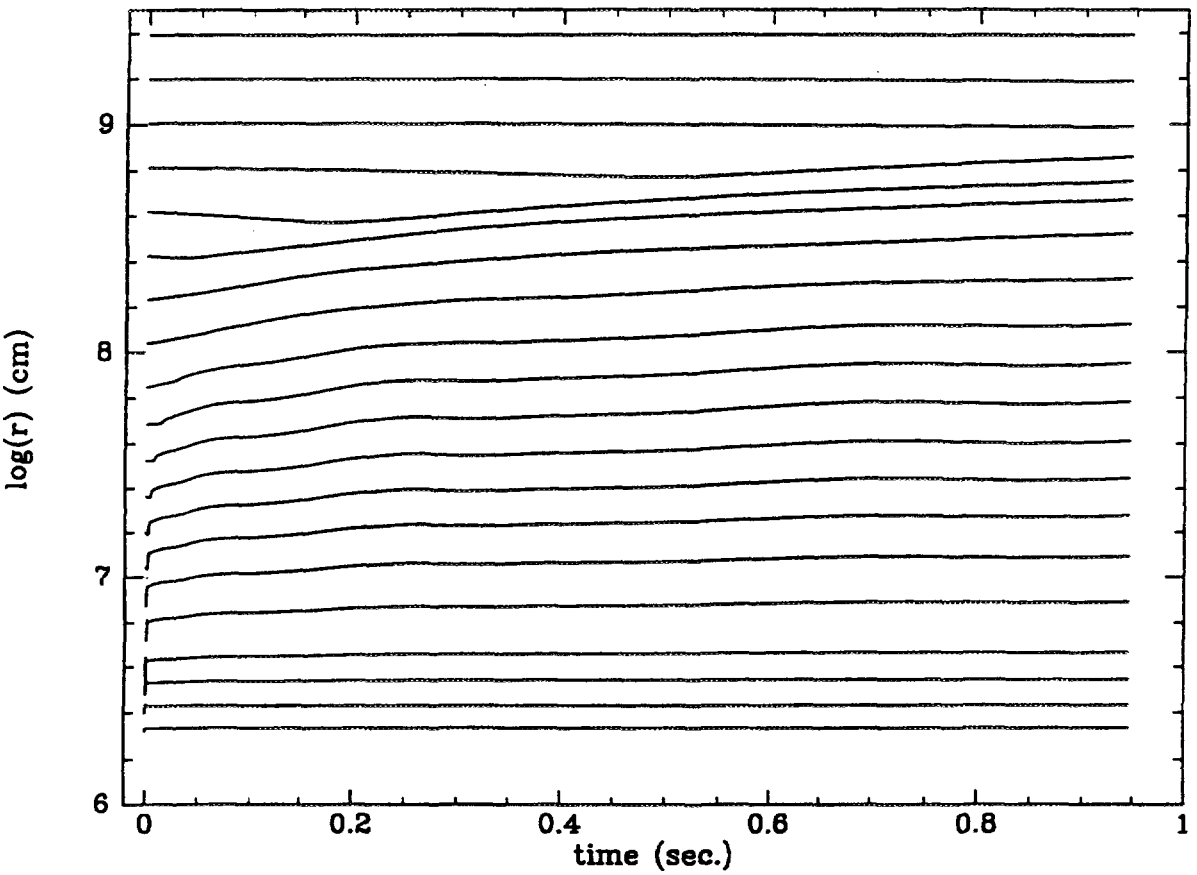

Figure 5a. Radial positions of selected mass shells as functions of time for a simulation run where neutrinos were completely ignored. Time is measured from the start of the computation. In the lower part of the figure the hydrostatic protoneutron star is sitting. The matter above is essentially in hydrostatic equilibrium, too.

region of net heating between an inner radius R_g ('gain radius', defined as the location where heating and cooling are equal) and an outer radius R_d, which is determined by the requirement that the matter must be completely dissociated into free nucleons inside this radius. Taking $Y_n + Y_p = 1$ and $\rho = \rho_g (R_g/r)^n$ with $n = 3$ and using $R_d \gg R_g$, one finds

$$\int_{R_g}^{R_d} \mathrm{d}r\, 4\pi r^2\, \rho(r) \mathcal{A} \cdot \left(Q^+_{\nu_e} + Q^+_{\bar{\nu}_e}\right) \approx 10^{50} \cdot L_{52}\, \frac{\langle \epsilon^2 \rangle}{(15\,\mathrm{MeV})^2} \cdot \rho_9\, \frac{R_g}{15\,\mathrm{km}} \left[\frac{\mathrm{erg}}{\mathrm{s}}\right] . \quad (46)$$

Equation (46) tells us that a fraction of about 1% of the energy emitted in ν_e and $\bar{\nu}_e$ will be deposited in the stellar gas. Integrating over the cooling time of the protoneutron star (several seconds) this result, together with contributions by the other heating reactions, in particular by neutrino-electron/positron scattering, suggests explosion energies of the order of several 10^{50} erg, quite close to typical energies of type-II supernova events of $1\text{–}2{\cdot}10^{51}$ erg as concluded from analyses of the early light curves (see e.g. Mair et al. 1992). Of course, our crude estimation neglects that the energy deposition might occur dynamically and that the neutrino spectra and luminosities change in time. Moreover, it does not tell anything about how much of the deposited energy will finally end up as kinetic energy of the explosion.

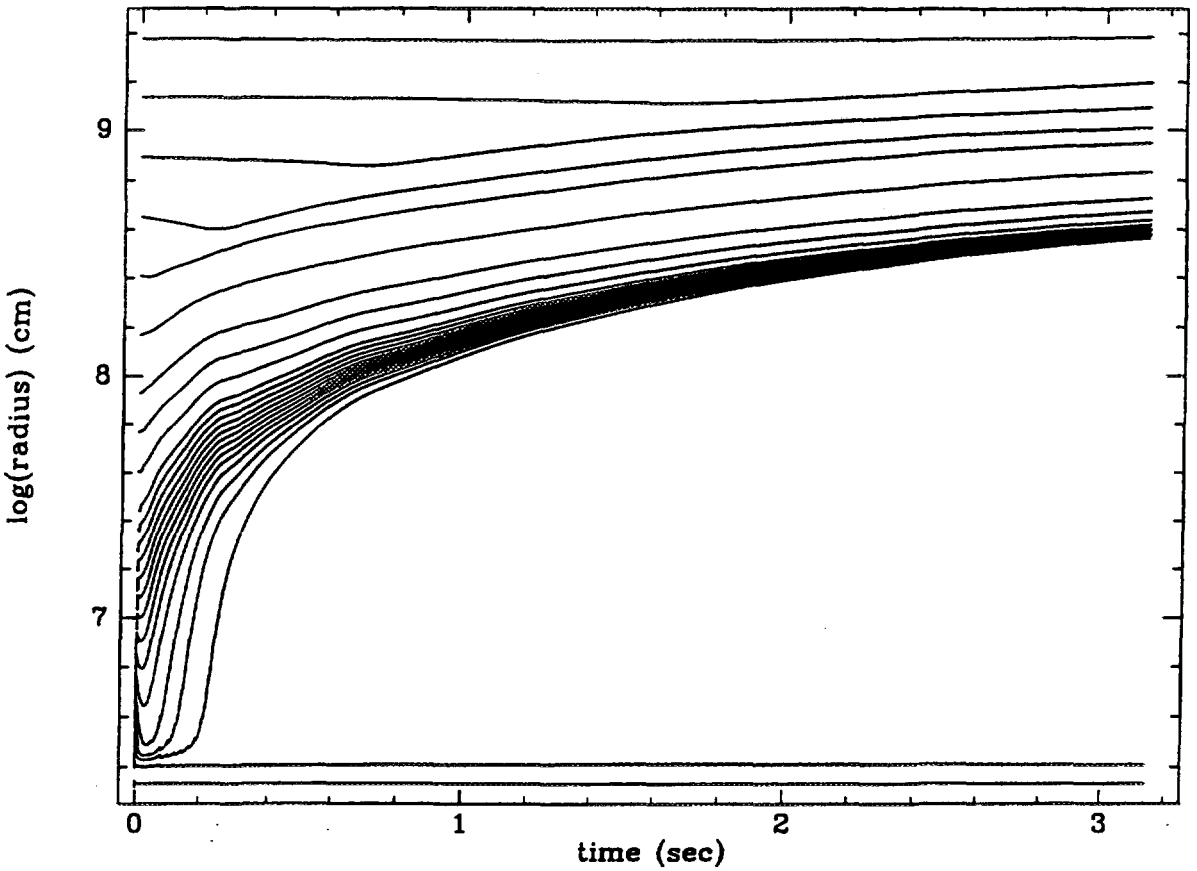

Figure 5b. Radial positions of selected mass shells as functions of time for the first three seconds of a simulation run where neutrino effects were included. Time is measured from the start of the computation. The matter external to the neutron star is heated by the neutrino flows from the neutron star and a huge expansion sets in.

In order to clearify this point and to work out the detailed requirements for powerful type-II supernova explosions via Wilson's delayed mechanism, we performed numerical studies (in one dimension) of the neutrino heating phase after core bounce (Janka and Müller 1992, Janka 1993). In particular, we followed the heating in the hot bubble region around a nascent neutron star for a period of more than 10 seconds, starting at about half a second after bounce. The computations were done for a model of a 25 $M_{\odot}$-star, evolved through core collapse and bounce by Wilson (1989). Figure 5a displays the result of a simulation run when neutrinos are completely ignored; Figure 5b gives a typical result of a computation with neutrinos included. The pictures show the radial positions of selected mass shells in the star as functions of time during the first second and the first three seconds, respectively, of the evolution. In the lower parts of the figures the protoneutron star is located. In case of Fig. 5b it is loosing its gravitational binding energy of $2.7 \cdot 10^{53}$ erg by radiating neutrinos with an exponentially decaying luminosity on a time scale of about 4.5 seconds. A part of this energy is deposited in the surrounding gas by the processes discussed above, driving a rapid expansion, which leads to a clear separation of the neutron star from the stellar mantle far out. In Table 1 results for a sample of model simulations with varied spectra and decay time scales of the neutrino emission from the neutron star

Table 1. Model data. $L_{\nu,0}$ is the neutrino luminosity of the neutron star at the start of the computation, $T_{\nu,0}$ and $T_{\nu,\infty}$ are initial and final spectral temperatures of neutrinos, respectively. Both $L_{\nu,0}$ and the neutrino temperatures are given for an observer at infinity. η_ν is the effective neutrino degeneracy parameter. $R_{\rm NS,0}$ and $R_{\rm NS,\infty}$ mean initial and final neutron star radii, $t_{\rm c}$ denotes the cooling time scale of the neutron star, and $E_{>0,\infty}$ the explosion energy of the model. In model BS an early burst of high-energetic neutrinos was added to the neutrino luminosity from the neutron star (see text).

M.	ν	$L_{\nu,0}$ [10^{51} erg/s]	$T_{\nu,0}$ [MeV]	$T_{\nu,\infty}$ [MeV]	η_ν	$t_{\rm c}$ [s]	$R_{\rm NS,0}$ [km]	$R_{\rm NS,\infty}$ [km]	$E_{>0,\infty}$ [10^{51} erg]
ST	ν_e	10.0	2.75	2.75	3.0	4.36	17.3	17.3	0.40
	$\bar{\nu}_e$	11.6	3.75	3.75	3.0				
	ν_x	10.0	6.00	6.00	3.0				
LF	ν_e	7.5	2.75	2.75	3.0	5.81	17.3	17.3	0.40
	$\bar{\nu}_e$	8.7	3.75	3.75	3.0				
	ν_x	7.5	6.00	6.00	3.0				
HT	ν_e	10.0	2.75	2.50	3.0	4.31	17.3	9.0	0.48
	$\bar{\nu}_e$	12.2	3.75	4.50	3.0				
	ν_x	10.0	6.00	5.00	3.0				
NS	ν_e	20.0	2.75	2.50	3.0	2.15	17.3	9.0	0.55
	$\bar{\nu}_e$	24.5	4.15	5.00	2.0				
	ν_x	20.0	6.75	5.25	2.0				
BS	ν_e	10.0	2.75	2.75	3.0	4.36	17.3	17.3	1.33
	$\bar{\nu}_e$	11.6	3.75	3.75	3.0				
	ν_x	10.0	6.00	6.00	3.0				

are collected (for more information see Janka and Müller 1992). Except for the last case the explosion energies — in agreement with our considerations above — stay fairly low. A closer look on the results reveals the reason: Although neutrinos deposit more than a factor of three more energy in the hot bubble region, most of this energy drives mass loss, i.e. is consumed to lift material in the gravity field of the neutron star.

The last case listed in Table 1 shows the result of a calculation, where in addition to the exponentially decaying neutrino fluxes from the protoneutron star a short 'burst' of high energetic neutrinos was included. On a time scale of about 100–200 ms (at a time 150 ms after the start of the computation) an energy of $1.5 \cdot 10^{52}$ erg is radiated away by neutrinos with typical energies of 20–30 MeV. This outburst of energy is small compared with the roughly $3 \cdot 10^{53}$ erg lost by the protoneutron star and cannot be discovered in the neutrino observations in connection with SN 1987A. The efficient heating due to these additional neutrinos leads to a significantly higher

explosion energy (Table 1): $1.33{\cdot}10^{51}$ erg agree well with expectations from theoretical models of SN 1987A (Mair et al. 1992). The main reason for the increase of the explosion energy is the short time scale of energy transfer to the matter. Different from the slow and quasistationary energy deposition by the exponentially decaying neutrino flows from the neutron star, the outburst heats the matter on dynamical time scales $t_{\rm dyn} \approx \Delta r/c_s = \mathcal{O}(100\,{\rm ms})$ (c_s is the sound speed) and powers a very fast expansion instead of driving mass loss. We therefore conclude that supernova explosions via the neutrino heating mechanism with explosion energies of the size expected for typical type-II supernova events require efficient neutrino heating on dynamical time scales. In the next section we shall address the question, which physical processes might lead to the production of sufficiently high luminosities of energetic neutrinos.

Let us add a remark on non-standard neutrino physics here. Matter-enhanced oscillations of light neutrinos according to the MSW-effect could lead to a considerable increase of the neutrino energy deposition outside the protoneutron star. Assume there would be resonant flavour conversion between the electron neutrino ν_e with a very small mass m_{ν_e} and a heavy lepton neutrino ν_x, most likely the tau neutrino ν_τ, with mass m_{ν_x}. Electron neutrinos of energy ϵ would transform into ν_x and vice versa at a density related to the squared mass difference and the lepton concentration in the star by the resonance condition (Fuller et al. 1987):

$$\frac{m_{\nu_x}^2 - m_{\nu_e}^2}{\rm eV^2} \approx \frac{m_{\nu_x}^2}{\rm eV^2} \approx 1.5 \cdot 10^3 \cdot \rho_{10}\,(Y_e + Y_\nu) \cdot \frac{\epsilon}{\rm MeV}\,, \qquad (47)$$

with ρ_{10} being the gas density in $10^{10}\,{\rm g/cm^3}$. The consequence of resonant neutrino oscillations on the supernova physics and on neutrino observations differs drastically with the considered mass m_{ν_x}. For typical neutrino energies $\epsilon \gtrsim 10\,{\rm MeV}$ masses $m_{\nu_x}^2 \gtrsim 10^5\,{\rm eV^2}$ lead to neutrino mixing at densities higher than about $10^{11}\,{\rm g/cm^3}$. This definitely has influence on the whole core collapse dynamics and, most likely, destructive consequences for the formation of the prompt shock (Fuller et al. 1987). For neutrino masses $m_{\nu_x}^2 \lesssim 10\,{\rm eV^2}$ neutrino transformations would occur in the mantle of the progenitor star far away from the central core region. Therefore they would affect the observations and, possibly, the neutrino nucleosynthesis in the star, however would be unimportant for the explosion mechanism and the explosion dynamics. Remarkably, neutrinos with masses in the cosmologically interesting range $10\,{\rm eV^2} \lesssim m_{\nu_x}^2 \lesssim 10^4\,{\rm eV^2}$ would undergo flavour mixing outside the neutrino sphere between the protoneutron star and the shock position (see Fuller et al. 1992). This would exchange 'cool' electron neutrinos with one species of 'hot' ν_x. While core collapse dynamics, formation of the prompt shock, and cooling of the protoneutron star would remain unaffected, this would help the delayed shock revival. One can easily obtain an estimate by using Eq. (46) together with the numbers given in Eqs. (10) and (13). Assuming symmetric matter, $Y_n = Y_p$, and distinguishing between contributions by ν_e and $\bar{\nu}_e$ in Eq. (46) we find for the ratio between heating with and without MSW flavour conversion:

$$\frac{\left(L\langle\epsilon^2\rangle\right)_{\rm MSW}}{\left(L\langle\epsilon^2\rangle\right)_{\rm Eq.\,(46)}} \approx \frac{\left[(0.8\,...\,1.0)\cdot(2^2\,...\,2.5^2)\right]_{\nu_x} + \left[1.2\cdot 1.5^2\right]_{\nu_e}}{\left[1.0\right]_{\nu_e} + \left[1.2\cdot 1.5^2\right]_{\bar{\nu}_e}} \approx 1.6\,...\,2.4\,. \qquad (48)$$

In a more careful evaluation, which takes into account the composition of the stellar gas and temporal changes of neutrino fluxes and spectra, Fuller et al. (1992) find a 60% increase of the neutrino heating. However, having in mind the discussion of our numerical results above, the final effect on the explosion can definitely be revealed only when neutrino flavour conversion is included in course of a hydrodynamical simulation.

3.2 Convective processes in supernovae

So far elaborate calculations of delayed type-II supernova explosions have been performed only in one dimension, i.e. with the assumption of spherical symmetry. However, it is well known (e.g. Burrows 1987, Burrows and Lattimer 1988, Bethe 1990) that convection may play an important role in the supernova and the newly formed neutron star. On the one hand the deleptonization after the supernova shock breaks through the neutrino sphere produces a negative lepton gradient in the collapsed stellar core. On the other hand regions of negative entropy gradients behind the weakened, finally stalling, prompt shock are a common feature of most supernova calculations (compare the collection of results in Burrows and Lattimer 1988; see also Bruenn 1992). Such situations are unstable against convection and large scale mixing seems unavoidable.

In fact, recent calculations (Burrows and Fryxell 1992, Janka and Müller 1992) confirm these considerations. The hot, neutronized material left behind by the propagating shock in a collapsed stellar iron core after bounce starts to develop a Rayleigh-Taylor-type instability on growth time scales of roughly 10 ms. After another 5–10 milliseconds the whole unstable region in the outer layer of the nascent neutron star is involved in the convective overturn. Figure 6 shows the entropy in a region between 20 km and roughly 220 km at four different times: 16, 21, 26 and 31 milliseconds after the start of the 2-d simulation. One can clearly see how first the inner layers become unstable and develop Rayleigh-Taylor fingers penetrating inward. A little later zones with negative entropy gradients farther out begin to break up, too, while the structures deeper inside merge to successively larger blobs. After another 10 milliseconds the inner region is completely mixed and homogenized. The convective velocities are near and even beyond the local speed of sound, therefore significant overshooting at the outer and inner boundaries of the initially unstable regions occurs.

These convective processes behind the supernova shock cannot prevent the failure of the prompt explosion mechansim, although the shock gets an additional boost, which helps to bring it out to larger radii (see Fig. 6). However, convection will have drastical consequences for the neutrino emission. Since the convective zone in the outer part of the nascent neutron star encompasses the neutrino sphere and the convective overturn transports leptons from opaque inner regions to neutrino transparent layers close to and above the neutrino sphere, the neutrino emission during this phase of the supernova evolution will be significantly enhanced. Comparing convective mixing time scales $t_{\rm mix}$ from our simulations with the neutrino diffusion time scale $t_{\rm diff}$ and the lepton loss time scale $t_{\rm L,loss}$ (see point (4) in Section 2.1) we can estimate the increase of the neutrino emission:

$$2 \approx \frac{t_{\rm diff}}{t_{\rm mix}} \lesssim \frac{L_\nu^{\rm conv}}{L_\nu^{\rm diff}} \lesssim \frac{t_{\rm L,loss}}{t_{\rm mix}} \approx 6 \ldots 10 \,. \qquad (49)$$

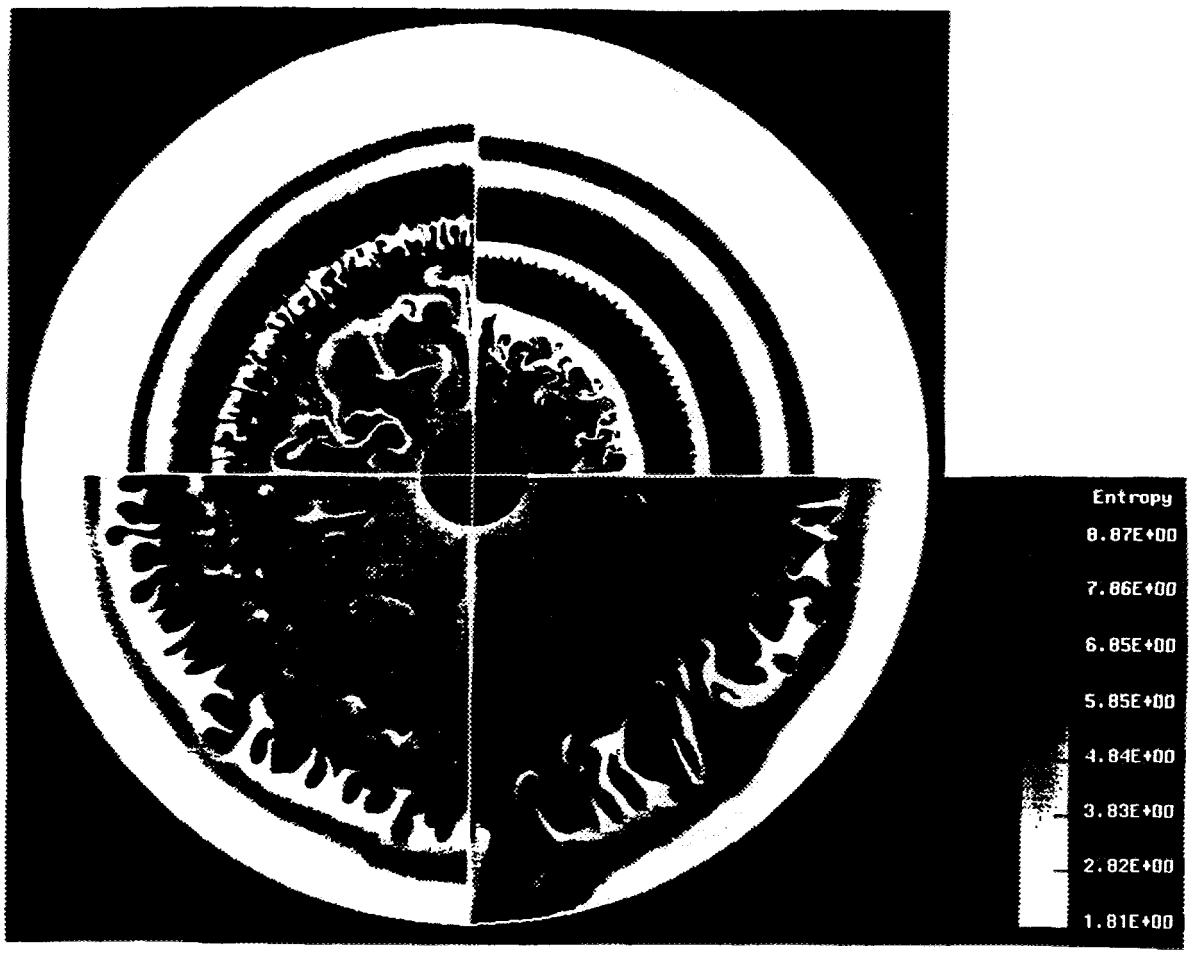

Figure 6. Convection in a protoneutron star some ten milliseconds after core bounce. The plot shows the time evolution of the entropy (in k_B per nucleon) in a region between 20 km and 218 km. The panels are arranged in counterclockwise order, starting from the right upper side, and show snapshots at 16 ms, 21 ms, 26 ms, and 31 ms after the start of the 2-d computation. The grey levels correspond to entropy values between 2 and 9 with a linear variation from bright to dark. The supernova shock is located at the interface between the grey inner region and the white zone outside. (The figure is taken from Janka and Müller (1992).)

So far our simulations are purely hydrodynamical, thus the neutrino emission must be further investigated by including neutrino transport in subsequent simulations. It will be interesting to see how this enhancement of the neutrino losses will influence the shock propagation on the one side and the neutron star formation on the other. Hopefully, it will help to settle the controversy on the question whether the neutrino luminosities are sufficiently high to revive the stalled shock or not.

At later stages, more than hundred milliseconds after core bounce, during the matter accretion phase, neutrino heating below the standing accretion shock may lead to thermally driven convection between protoneutron star and shock front. This is suggested by recent calculations by Herant et al. (1992), who, however, start from a completely artificial initial model and use a very crude description of the heating due to neutrinos. Nevertheless, their results are inspiring and destroy completely the

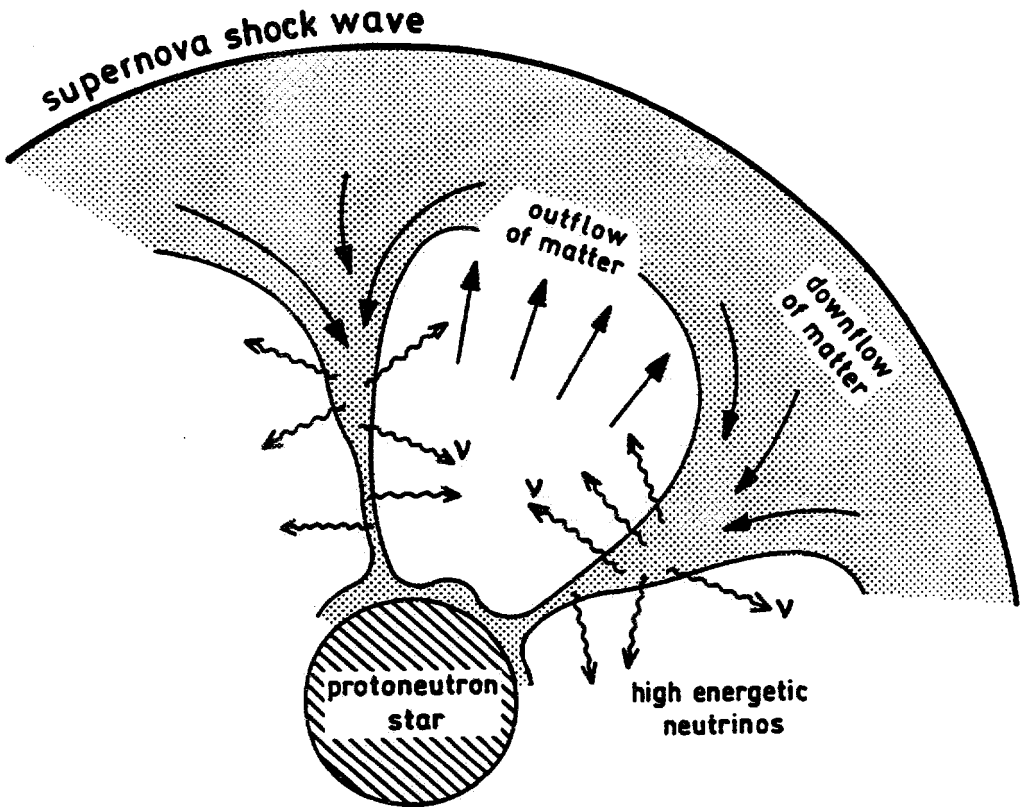

Figure 7. Imagined convective overturn in the region between protoneutron star and supernova shock during the matter accretion phase after core bounce. The matter is accreted onto the nascent neutron star in narrow flow tubes and emits high energetic neutrinos, which help to power the supernova explosion.

picture of a spherically symmetric, laminar spherical accretion flow onto the nascent neutron star. According to their results matter is falling down in long, narrow tubes, separated by expanding bubble regions (see Fig. 8). Since the calculations do not include neutrino radiative transfer, one can also in this case only imagine what might happen: The lepton rich matter flowing down must heat up and may be the source of high energetic neutrinos, which are emitted on a time scale of about the free fall time scale. We know from the one-dimensional simulations described above that this may well power an energetic type-II supernova explosion. The matter accretion, and thus further heating, will be shut down when the layers below the shock begin a rapid expansion and push the supernova shock outwards. Future investigations will have to show whether this scenario takes place and whether it leads to robust and powerful type-II supernova explosions.

4. Summary and conclusions

In this paper we described generic properties of the neutrino emission during stellar core collapse and the formation of a neutron star by reviewing results from numerous numerical simulations. Deriving simple analytical estimates we demonstrated that there are several phases with clearly distinct neutrino emission: The

core collapse, the phase of prompt shock propagation and shock breakout, the phase of matter accretion onto the nascent neutron star, and the Kelvin-Helmholtz-cooling of the protoneutron star. Most of the energy emitted in neutrinos is radiated away during the last phase, which is certainly responsible for the majority of the neutrino events detected in connection with SN 1987A. Details of the neutrino signal during the different emission phases may give evidence about the physics at high densities and temperatures in the supernova core and might also contain information about the sequence of events which finally lead to the explosive disruption of a massive star in a type-*II* supernova.

The neutrino spectra exhibit systematic and noticeable discrepancies from thermal distributions. These deviations are of minor importance for an interpretation of the few captured neutrinos from SN 1987A. However, they will have to be taken into account for an analyis of hopefully hundreds to thousands of neutrino events caused by a galactic supernova. We demonstated that a Fermi-Dirac function with non-vanishing degeneracy parameter is suitable to yield significantly improved fits to results of elaborate neutrino transport simulations and to account for most of the characteristics of the neutrino emission. The non-thermal spectral shape causes a reduced interaction of the neutrino flows in the stellar mantle and envelope and in experiments on earth. This reduction is of the order 20–40% for reactions with cross sections varying with the square of the neutrino energy, and becomes even more pronounced for stronger energy dependence and in the case of a small detector efficiency at low energies.

Despite of more than 25 years of theoretical and numerical work the mechanism driving the explosion of a massive star in a type-II supernova is not yet satisfactorily understood. However, currently there is 'convergence' on the point that neutrinos could play a crucial role. In Section 3 we gave arguments why there exists a region external to the newly formed neutron star where net energy deposition by the neutrino flows from the neutron star must occur. Numerical computations, which follow the neutrino heating over time scales of more than 10 seconds, indicate that this energy input is able to cause a delayed explosion. In agreement with crude analytical estimates the numerical results show, however, that the energy of the explosion stays low, of the order of several 10^{50} erg rather than more than 10^{51} erg as expected for a typical type-II supernova event. High explosion energies via the neutrino-driven mechanism require very efficient neutrino heating on dynamical time scales during the early phase of the explosion.

From these results one can conclude that essential physics is still missing in the described scenario. Since on the one hand all simulations so far have been performed in spherical symmetry, on the other hand the existence of convectively unstable regions in the collapsed stellar core is a generic feature of these computations, it may very well be that convection provides the way to robust and powerful type-II supernova explosions via the neutrino heating mechanism. Recent multi-dimensional hydrodynamical simulations support this expectation. They reveal large scale turbulent motions in the collapsed stellar core behind the supernova shock, and, at a later stage of the evolution, in the neutrino heated region outside the protoneutron star. The step that must be taken, and will be done now, is to couple neutrino transport into the multi-dimensional hydro-codes and to test our optimistic expectations.

Acknowledgements. The author wants to thank E. Müller for a careful reading of the manuscript and acknowledges grants of computer time on the Cray Y-MP 8/832 of the Höchstleistungsrechenzentrum (HLRZ) des Forschungszentrums Jülich.

References

Alexeyev, E.N., Alexeyeva, L.N., Krivosheina, I.V., Volchenko, V.I.: 1988, Phys. Lett. B 205, 209.

Aglietta, M., et al.: 1987, Europhys. Lett. 3, 1315.

Bahcall, J.N., Piran, T., Press, W.H., Spergel, D.N.: 1987, Nature 327, 682.

Bethe, H.A.: 1990, Rev. Mod. Phys. 62, 801.

Bethe, H.A., Wilson, J.R.: 1985, Astrophys. J. 295, 14.

Bionta, R.M., Blewitt, G., Bratton, C.B., Casper, D., Ciocio, A., Claus, R., Cortez, B., Crouch, M., Dye, S.T., Errede, S., Foster, G.W., Gajewsky, W., Ganezer, K.S., Goldhaber, M., Haines, T.J., Jones, T.W., Kielczewska, D., Kropp, W.R., Learned, J.G., LoSecco, J.M., Matthews, J., Miller, R., Mudan, M.S., Park, H.S., Price, L.R., Reines, F., Schultz, J., Seidel, S., Shumard, E., Sinclair, D., Sobel, H.W., Stone, J.L., Sulak, L.R., Svoboda, R., Thornton, G., van der Velde, J.C., Wuest, C.: 1987, Phys. Rev. Lett. 58, 1494.

Bludman, S.A., Schinder, P.J.: 1988, Astrophys. J. 326, 265.

Boehm, F., Vogel, P.: 1987, Physics of Massive Neutrinos, Cambridge Univ. Press, Cambridge, Great Britain.

Bruenn, S.W.: 1987, Phys. Rev. Lett. 59, 938.

Bruenn, S.W.: 1989a, Astrophys. J. 340, 955.

Bruenn, S.W.: 1989b, Astrophys. J. 341, 385.

Bruenn, S.W.: 1992, 'Numerical Simulations of Core Collapse Supernovae', in Proc. of First Symposium on Nuclear Physics in the Universe, Oak Ridge, Tennessee, Sept. 24-26, 1992.

Bruenn, S.W., Haxton, W.C.: 1991, Astrophys. J. 376, 678.

Burrows, A.: 1987, Astrophys. J. 318, L57.

Burrows, A.: 1988, Astrophys. J. 334, 891.

Burrows, A., Lattimer, J.M.: 1986, Astrophys. J. 307, 178.

Burrows, A., Lattimer, J.M.: 1988, Phys. Rep. 163, 51.

Burrows, A., Fryxell, B.A.: 1992, Science 258, 430.

Burrows, A., Klein, D., Gandhi, R.: 1992, Phys. Rev. D 45, 3361.

Cooperstein, J., van den Horn, L.J., Baron, E.A.: 1987, Astrophys. J. 321, L129.

Fuller, G.M., Mayle, R.W., Wilson, J.R., Schramm, D.N.: 1987, Astrophys. J. 322, 795.

Fuller, G.M., Mayle, R.W., Meyer, B.S., Wilson, J.R.: 1992, Astrophys. J. 389, 517.

Goodman, J., Dar, A., Nussinov, S.: 1987, Astrophys. J. 314, L7.

Hecht, Th.: 1989, Diploma Thesis, Technische Universität München.

Herant, M.. Benz, W., Colgate, S.: 1992, Astrophys. J. 395, 642.

Hillebrandt, W.: 1987, in High Energy Phenomena around Collapsed Stars, NATO-ASI C195, F. Pacini (ed.), Reidel, Dodrecht, p. 73.

Hillebrandt, W., Höflich, P.: 1989, Rep. Prog. Phys. 52, 1421.

Hirata, K., Kajita, T., Koshiba, M., Nakahata, M., Oyama, Y., Sato, N., Suzuki, A., Takita, M., Totsuka, Y., Kifune, T., Suda, T., Takahashi, K., Tanimori, T., Miyano, K., Yamada, M., Beier, E.W., Feldscher, L.R., Kim, S.B., Mann, A.K., Newcomer, F.M., Van Berg, R., Zhang, W., Cortez, B.G.: 1987, Phys. Rev. Lett. 58, 1490.

Kolbe, E., Langanke, K., Krewald, S., Thielemann, F.-K.: 1992, Nucl. Phys. A 540, 599.

Lamb, D.Q., Melia, F., Loredo, T.J.: 1988, in Supernova 1987A in the Large Magellanic Cloud, M. Kafatos and A. Michalitsianos (eds.), Cambridge Univ. Press, Cambridge, p. 204.

Langacker, P.: 1988, in Neutrinos, H.V. Klapdor (ed.), Springer, Berlin, p. 71.

Janka, H.-Th.: 1987, in Nuclear Astrophysics, W. Hillebrandt, R. Kuhfuß, E. Müller and J.W. Truran, Lecture Notes in Physics 287, Springer, Berlin, p. 319.

Janka, H.-Th.: 1990, Ph.D. Thesis, TU München, MPA-preprint 587 (1991), Max-Planck-Institut für Astrophysik, Garching.

Janka, H.-Th.: 1991, Astron. Astrophys. 244, 378.

Janka, H.-Th.: 1993, in preparation.

Janka, H.-Th., Hillebrandt, W.: 1989a, Astron. Astrophys. Suppl. 78, 375.

Janka, H.-Th., Hillebrandt, W.: 1989b, Astron. Astrophys. 224, 49.

Janka, H.-Th., Müller, E.: 1992, 'Neutrino-driven Type-II Supernovae: Neutrino heating and post bounce dynamics', in Frontiers of Neutrino Astrophysics, Univ. Academy Press, Tokyo, Japan; in press.

Mair, G., Hillebrandt, W., Höflich, P., Dorfi, A.: 1992, Astron. Astrophys. 266, 266.

Mayle, R.W.: 1985, Ph.D. Thesis, UC Berkeley, UCRL report no. 53713.

Mayle, R.W.: 1990, in Supernovae, A.G. Petschek (ed.), Springer, New York, p. 267.

Mayle, R.W., Wilson, J.R., Schramm, D.N.: 1987, Astrophys. J. 318, 288.

Myra, E.S., Bludman, S.A., Hoffman, Y., Lichtenstadt, I., Sack, N., Van Riper, K.A.: 1987, Astrophys. J. 318, 744.

Myra, E.S., Bludman, S.A.: 1989, Astrophys. J. 340, 384.

Myra, E.S., Burrows, A.: 1990, Astrophys. J. 364, 222.

Sato, K.: 1989, in Big Bang, Active Galactic Nuclei and Supernovae, S. Hayakawa and K. Sato (eds.), Univ. Academy Press, Tokyo, Japan, p. 463.

Sato, K., Suzuki, H.: 1987a, Phys. Rev. Lett. 58, 2722.

Sato, K., Suzuki, H.: 1987b, Phys. Lett. B 196, 267.

Schramm, D.N., Brown, L.E.: 1990, in Supernovae, J.C. Wheeler, T. Piran and S. Weinberg (eds.), World Scientific, Singapore, p. 261.

Suzuki, H.: 1989, Ph.D. Thesis, Univ. of Tokyo.

Suzuki, H., Sato, K.: 1987, Publ. Astron. Soc. Japan 39, 521.

Tubbs, D.L.: 1979, Astrophys. J. 231, 846.

Tubbs, D.L., Schramm, D.N.: 1975, Astrophys. J. 201, 467.

Wilson, J.R.: 1989, private communication.

Wilson, J.R.: 1985, in Numerical Astrophysics, J.M. Centrella, J.M. LeBlanc and R.L. Bowers (eds.), Jones and Bartlett, Boston, U.S.A., p. 422.

Wilson, J.R., Mayle, R.W., Woosley, S.E., Weaver, T.: 1986, Ann. N.Y. Acad. Sci. 470, 267.

Numerical models of protoneutron stars and type-II supernovae — recent developments

H.-Thomas Janka

Max-Planck-Institut für Astrophysik
Karl-Schwarzschild-Str. 1, D-85740 Garching, Germany
email: thj@mpa-garching.mpg.de

ABSTRACT

The results of recent multi-dimensional simulations of type-II supernovae are reviewed. They show that convective instabilities in the collapsed stellar core might play an important role already during the first second after the formation of the supernova shock. Convectively unstable situations occur below and near the neutrinosphere as well as in the neutrino-heated region between the nascent neutron star and the supernova shock after the latter has stalled at a radius of typically 100–200 km.

While convective overturn in the layer of neutrino energy deposition clearly helps the explosion to develop and potentially provides an explanation of strong mantle and envelope mixing, asphericities, and non-uniform ^{56}Ni distribution observed in supernova SN 1987A, its presence and importance depends on the strength of the neutrino heating and thus on the size of the neutrino fluxes from the neutron star. Convection in the hot-bubble region can only develop if the growth timescale of the instabilities and the heating timescale are both shorter than the accretion timescale of the matter advected through the stagnant shock. For too small neutrino luminosities this requirement is not fulfilled and convective activity cannot develop, leading to very weak explosions or even fizzling models, just as in the one-dimensional situation.

Convectively enhanced neutrino luminosities from the protoneutron star can therefore provide an essential condition for the explosion of the star. Very recent two-dimensional, self-consistent, general relativistic simulations of the cooling of a newly-formed neutron star demonstrate and confirm the possibility that Ledoux convection, driven by negative lepton number and entropy gradients, may encompass the whole protoneutron star within less than one second and can lead to an increase of the neutrino fluxes by up to a factor of two.

1. Introduction

Neutrinos play a crucial role in our understanding of type-II supernova explosions. According to the currently most widely accepted theory for the explosion of a massive star, the explosion energy is provided by the neutrinos that are abundantly emitted

from the nascent neutron star and interact at a probability between 1% and 10% with the material of the progenitor star. This energy deposition is not only supposed to power the propagation of the supernova shock into the stellar mantle and envelope regions and to cause the violent disruption of the star, but also drives a mass outflow from the surface of the protoneutron star that continues for more than 10 seconds and which might be a suitable site for r-process nucleosynthesis (Woosley & Hoffman 1992, Witti et al. 1994, Takahashi et al. 1994, Woosley et al. 1994). The emission of electron lepton number and energy via neutrinos determines the evolution of the hot, collapsed stellar core towards the cold deleptonized neutron star remnant. Moreover, the interactions of neutrinos with target nuclei and nucleons in the neutrino-driven wind and in the stellar mantle can have important implications for supernova nucleosynthesis. Last but not least, the ~ 20 neutrinos detected in the Baksan (Alexeyev 1988), Kamiokande (Hirata et al. 1987), and IMB laboratories (Bionta et al. 1987) in connection with SN 1987A were the first experimental confirmation of our theoretical picture of the events that precede the explosion of a massive star. Still they serve as a tool to constrain theories of neutrino properties and particle physics at the extreme conditions of nascent neutron stars.

As discussed in detail in Lecture 1, the neutrino emission from the newly born neutron star is characterized by the following properties. Electron neutrinos are emitted from the neutrinosphere with a typical energy of about 10 MeV, while electron antineutrinos have about 50% higher energies and muon and tau neutrinos are radiated with even higher mean energies. This can be easily be understood by the fact that ν_e and $\bar{\nu}_e$ experience charged-current interactions while ν_μ and ν_τ do not. In addition, due to the neutron-proton asymmetry of the medium the coupling of $\bar{\nu}_e$ to the medium via absorptions onto protons is less strong than ν_e absorptions onto the more abundant neutrons. Despite the different temperatures of their emission spectra, all kinds of neutrinos have roughly similar (say, within a factor of 2) luminosities during most of the Kelvin-Helmholtz cooling phase of the protoneutron star. Because the transport of ν_μ and ν_τ is strongly affected by isoenergetic scatterings off n and p, their characteristic spectral temperatures and effective temperatures are significantly different. The neutrino spectra are not thermal ("blackbody") spectra, but are pinched with a depletion in both the low-energy part and the high-energy tail. This depletion can be accounted for by using Fermi-Dirac distributions to describe the emission spectra at a certain time, and introducing an effective spectral degeneracy parameter of order unity (typically about 3–5 for ν_e, 2–3 for $\bar{\nu}_e$, and between 0 and 2 for $\nu_x \equiv \nu_\mu, \bar{\nu}_\mu, \nu_\tau, \bar{\nu}_\tau$).

About 99% of the total gravitational binding energy that is set free during the collapse of the stellar iron core and the formation of the neutron star is emitted in neutrinos, only about 1% ends up in the kinetic energy of the supernova explosion, and even less, only about 0.01% accounts for the spectacularly bright outburst of light that is seen as type-II supernova event on the sky. Despite the enormous amount of energy that is available from the gravitational collapse, it is not easy to channel the mentioned $\sim 1\%$ or about 10^{51} erg into kinetic energy. It is still an unresolved question how type-II manage to do this. It is generally accepted nowadays that for "reasonable" nuclear equations of state and core masses of the progenitor star the prompt or hydrodynamical mechanism does not work: The supernova shock formed at the moment of core bounce is too weak to overcome the huge energy losses due

to the disintegration of Fe group nuclei and additional neutrino losses. The shock stagnates before it reaches the surface of the stellar Fe core. During the following several hundred milliseconds of evolution, neutrinos deposit energy behind the shock. If this neutrino heating is strong enough, the shock can gain so much energy that it is "revived" and can indeed disrupt the star (see Lecture 1 and the references given there).

However, the neutrino-matter coupling is so weak that this "delayed" or neutrino-driven mechanism seems to be extremely sensitive to small changes of the physics inside the collapsed stellar core. In particular, if the neutrino fluxes do not surpass a certain threshold value, the explosion becomes too weak to be compatible with observations or even fizzles. Where are the uncertainties of our current knowledge of the physics inside stellar iron cores and what might be the missing link to a stable and robust explosion mechanism? What could help the neutrino-driven mechanism? Do current models underestimate the neutrino flux from the neutron star or do they treat the neutrino-matter coupling in the heating region incorrectly?

2. Different possibilities

There are different lines of exploration currently followed up by the supernova group at the MPI für Astrophysik in Garching and by other groups in Livermore, Los Alamos, and Oak Ridge. On the one hand, these activities focus on a closer investigation of the neutrino interactions and neutrino transport in the protoneutron star. On the other hand, they concentrate on the simulations of the hydrodynamical evolution of the collapsed star in more than one spatial dimension.

2.1 Lower neutrino opacities in the protoneutron star?

So far, the theoretical understanding of neutrino interactions with target nuclei and nucleons in a dense environment is incomplete and detailed calculations of the neutrino opacity of a nuclear medium including particle correlation and screening effects are not yet available. For that reason, partly also motivated and justified by the effort to simplify the numerical description, all current supernova codes employ neutrino reaction rates calculated for interactions with isolated target particles. At least, the rates are more or less reliably corrected for blocking effects in the fermion phase spaces. The real situation may be largely different and more complicated.

For example, Raffelt & Seckel (1991) considered auto-correlation effects for the nucleon spins which can lead to a dramatic reduction of the axial-vector neutral current (and possibly also charged current) cross sections. Rapid nucleon spin fluctuations of the scattering nucleons lead to a reduced effective spin "seen" by the neutrino as a reaction partner. In a parametric study, Keil et al. (1995) and Janka et al. (1996) have investigated the effects on the neutrino cooling of newly formed neutron stars and found a nearly linear decrease of the cooling time of the protoneutron star with the global reduction factor for the opacities. This is a non-trivial result because with reduced opacities also the deleptonisation of the star is accelerated. As a result of this, the star heats up faster and to higher peak temperatures. Since the opacities increase with the temperature (neutrino energy), the net effect on the cooling of the star is not obvious. Keil et al. (1995) also found that the emitted

neutrinos become more energetic when the opacity of the protoneutron star is lower and the neutrinosphere moves deeper into the star.

The combined effects, reduced cooling time and increased mean spectral neutrino energies, lead to a distortion of the predicted neutrino signal which can be compared with the neutrino burst observed in the Kamiokande II and IMB detectors in connection with SN 1987A. Keil et al. (1995) concluded that a reduction of the opacities by more than a factor of 2 seems quite unlikely unless the late and low-energy neutrino events in Kamiokande 2 and IMB are discarded as background or unless they can be explained by some non-standard neutrino emission process, e.g., associated with accretion or a spontaneous, first-order phase transition in the supranuclear matter that might occur after several seconds of Kelvin-Helmholtz cooling of the newly born neutron star. Despite a lot of vague speculations, there is no qualified and theoretically founded model for such events in or at the protoneutron star that can explain the involved energies, timescales, and structure of the neutrino signal. For a summary and discussion of some of the addressed aspects, see Janka (1995).

The derived lower bound for the reduction of the neutrino opacity which is still compatible with the SN 1987A neutrino signals sets interesting limits for the nucleon spin fluctuation rate in the supernova core (Janka et al. 1996). The theoretical background and formal justification for such a limit was discussed by Sigl (1996). Although an opacity reduction by a factor of about 2 is by far not as much as allowed from principle physical reasons, a corresponding doubling of the neutrino luminosities from the nascent neutron star would have a very large effect on the supernova explosion. In order to come to definite conclusions, however, more reliable calculations of the neutrino opacities in the dense medium of supernova cores are urgently called for.

2.2 Convection in the protoneutron star?

Alternatively, or in addition, convective processes in the hot and lepton-rich protoneutron star might raise the neutrino fluxes and could thus lead to more favorable conditions for neutrino heating outside the neutrinosphere and could help shock revival.

Epstein (1979) pointed out that not only entropy, S, inversions but also zones in the post-collapse core where the lepton fraction, Y_l, decreases with increasing radius tend to be unstable against Ledoux convection. Negative S and/or Y_l gradients in the neutrinospheric region and in the layers between the nascent neutron star and the weakening prompt shock front were realized in a variety of post-bounce supernova models by Burrows & Lattimer (1988), and after shock stagnation in computations by Hillebrandt (1987) and more recently by Bruenn (1993), Bruenn & Mezzacappa (1994), and Bruenn et al. (1995). Despite different equations of states (EOS), ν opacities, and ν transport methods, the development of negative Y_l and S gradients is common in these simulations and can also be found in protoneutron star cooling models of Burrows & Lattimer (1986), Keil & Janka (1995), and Sumiyoshi et al. (1995).

Convection above the neutrinosphere but below the neutrino-heated region can hardly be a direct help for the explosion (Bethe et al. 1987, Bruenn et al. 1995), whereas convectively enhanced lepton number and energy transport inside the neutrinosphere raise the ν luminosities and can definitely support neutrino-energized

supernova explosions (Bethe et al. 1987). In this context, Burrows (1987) and Burrows & Lattimer (1988) have discussed entropy-driven convection in the protoneutron star on the basis of 1D, general relativistic (GR) simulations of the first second of the evolution of a hot, $1.4\,M_\odot$ protoneutron star. Their calculations were done with a Henyey-like code using a mixing-length scheme for convective energy and lepton transport. Recent 2D models (Herant et al. 1994, Burrows et al. 1995, Janka & Müller 1996 and references therein) confirmed the possibility that convective processes can occur in the surface region of the protoneutron star immediately after shock stagnation ("prompt convection") for a period of at least several 10 ms. These models, however, have been evolved only over rather short times or with insufficient numerical resolution in the protoneutron star or with a spherically symmetrical description of the core of the protoneutron star that was in some cases even replaced by an inner boundary condition.

Mayle & Wilson (1988) and Wilson & Mayle (1988, 1993) demonstrated that convection in the nascent neutron star can be a crucial ingredient that leads to successful delayed explosions. With the high-density EOS and treatment of the ν transport used by the Livermore group, however, negative gradients of Y_l tend to be stabilized by positive S gradients (see, e.g., Wilson & Mayle 1989). Therefore they claim doubly diffusive neutron finger convection to be more important than Ledoux convection. Doubts about the presence of doubly diffusive instabilities, on the other hand, were recently raised by Bruenn & Dineva (1996). Bruenn & Mezzacappa (1994) and Bruenn et al. (1995) also come to a negative conclusion about the relevance of prompt convection in the neutrinospheric region. Although their post-bounce models show unstable S and Y_l stratifications, the mixing-length approach in their 1D simulations predicts convective activity inside and around the neutrinosphere to be present only for 10–30 ms after bounce and to have no significant impact on the ν fluxes and spectra when an elaborate multi-group flux-limited diffusion method is used for the ν transfer. Such conclusions seem to be supported by preliminary 2D simulations with the same input physics (Guidry 1996). These 2D models, however, still suffer from the use of an inner boundary condition at a fixed radius of 20–30 km.

From these differing and partly contradictory results it is evident that the question whether, where, when, and how long convection occurs below the neutrinosphere seems to be a matter of the EOS, of the core structure of the progenitor star, of the shock properties and propagation, and of the ν opacities and the ν transport description. In the work which will be reported in Sect. 3.1, we compare 1D simulations with the first self-consistent 2D models that follow the evolution of the newly formed neutron star for more than a second, taking into account the GR gravitational potential and making use of a flux-limited equilibrium diffusion scheme that describes the transport of ν_e, $\bar{\nu}_e$, and ν_x (sum of ν_μ, $\bar{\nu}_\mu$, ν_τ, and $\bar{\nu}_\tau$) and is very good at high optical depths but only approximative near the protoneutron star surface (Keil & Janka 1995). Our simulations demonstrate that Ledoux convection may continue in the protoneutron star for a long time and can involve the whole star after about one second.

2.3 Convective instabilities in the neutrino-heated region?

Observations of the light curve and spectra of SN 1987A strongly suggest that convective instabilities and aspherical processes might play an important role not only

inside the nascent neutron star, but also outside of it in its very close vicinity. This is the region where the radioactive elements, in particular ^{56}Ni, which power the supernova light curve, are synthesized during the explosion.

The occurrence of large-scale mixing and overturn processes which must reach deep into the exploding star was clearly indicated by SN 1987A. From the observations we learned that radioactive material had been mixed out with very high velocities from the layers of its formation near the nascent neutron star far into the hydrogen envelope of the progenitor star. This was supported by the early detection of X-rays (Dotani et al. 1987, Sunyaev et al. 1987, Wilson et al. 1988) and γ-emission (Matz et al. 1988, Mahoney et al. 1988, Cook et al. 1988, Sandie et al. 1988, Gehrels et al. 1988, Teegarden et al. 1989) and by the observation of strongly Doppler-shifted and -broadened infrared emission lines of iron group elements (Erickson et al. 1988, Rank et al. 1988, Barthelmy et al. 1989, Witteborn et al. 1989, Haas et al. 1990, Spyromilio et al. 1990, Tueller et al. 1990, Colgan et al. 1994) at a time when the photosphere of the supernova was still well inside the hydrogen envelope. Also, the expanding supernova ejecta developed a clumpy and inhomogeneous structure quite early during the explosion (Li et al. 1993).

Besides direct evidence from SN 1987A, theoretical modelling of the supernova light curve suggested the need for mixing of hydrogen with a large part of the stellar mantle (Arnett 1988, Woosley 1988, Shigeyama et al. 1988, Shigeyama & Nomoto 1990, Arnett et al. 1989). The smoothness of the light curve of SN 1987A provided indirect information about the existence and strength of the mixing process. Mixing of hydrogen towards the center helps to explain the smooth and broad light curve maximum by the time-spread of the liberation of recombination energy. Mixing of heavy elements into the hydrogen-rich envelope homogenizes the opacity and again smooths the light curve. Neither the required amount of mixing nor the observed high velocities of radioactive decay products could be accounted for merely by Rayleigh-Taylor instabilities at composition interfaces in the mantle and envelope of the progenitor star after shock passage (Arnett et al. 1989; Den et al. 1990; Yamada et al. 1990; Hachisu et al. 1990, 1991; Fryxell et al. 1991; Herant & Benz 1991, 1992). Moreover, fast moving, dense explosion fragments outside of the supernova shock front have recently been discovered in the Vela supernova remnant by ROSAT X-ray observations (Aschenbach et al. 1995), revealing a very clumpy and inhomogeneous structure of the Vela and other supernova remnants.

In addition, the increasing number of identified high-velocity pulsars (Harrison et al. 1993, Taylor et al. 1993, Lyne & Lorimer 1994, Frail & Kulkarni 1991, Stewart et al. 1993, Caraveo 1993) might also be interpreted as an aspect of the new picture that type-II supernova explosions are by no means spherically symmetrical events, but that violent processes with noticeable deviation from spherical symmetry take place in the deep interior of the star during the early moments of the explosion.

All this was taken as a serious motivation to extend the modelling of the onset of the explosion to more than one spatial dimension (Herant et al. 1992, 1994; Burrows & Fryxell 1992, 1993; Janka 1993; Janka & Müller 1993, 1994, 1995a, 1996; Müller 1993; Miller et al. 1993; Shimizu et al. 1993, 1994; Yamada et al. 1993; Müller & Janka 1994; Burrows et al. 1995). These numerical models could indeed show that convective overturn in the neutrino-heated region around the protoneutron star can be a crucial help for the explosion. However, it turned out (Janka & Müller 1995a,

Guidry 1996) that even with the helpful effects of convective energy transport from the heating region towards the supernova shock, the neutrino energy deposition and thus the neutrino luminosities from the neutron star have to be larger than some lower threshold. If the heating is not strong enough, hot-bubble convection does not have time to develop on the timescale of the accretion of matter from the shock onto the protoneutron star. In Sect. 3.2 we shall review some of the results of our simulations.

3. Multi-dimensional simulations of convective processes in type-II supernovae

Convection can be driven by a radial gradient of the entropy per nucleon S and/or by a gradient of the lepton number per baryon Y_l (Epstein 1979) where Y_l includes contributions from e^- and e^+ and from ν_e and $\bar{\nu}_e$ if the latter are in equilibrium with the matter. Convective instability in the Ledoux approximation sets in when

$$C_{\mathrm{L}}(r) \equiv \left(\frac{\partial\rho}{\partial S}\right)_{P,Y_l} \frac{\mathrm{d}S}{\mathrm{d}r} + \left(\frac{\partial\rho}{\partial Y_l}\right)_{P,S} \frac{\mathrm{d}Y_l}{\mathrm{d}r} > 0\,. \qquad (1)$$

There are different regions in the collapsed stellar core where this criterion is fulfilled during different phases of the evolution.

3.1 Two-dimensional simulations of protoneutron star cooling

Simulations of protoneutron star cooling in spherical symmetry were performed by Burrows & Lattimer (1986), Suzuki (1989), and more recently by Keil & Janka (1995) and Sumiyoshi et al. (1995). These models show the development of negative gradients of entropy and lepton fraction as the cooling and deleptonization of the nascent neutron star advances. Keil et al. (1996) therefore attempted to do the first two-dimensional cooling simulations for a period of more than one second after core bounce.

3.1.1 Numerical implementation

The simulations were performed with the explicit Eulerian hydrodynamics code *Prometheus* (Fryxell et al. 1989) that employs a Riemann-solver and is based on the Piecewise Parabolic Method (PPM) of Colella & Woodward (1984). A moving grid with 100 nonequidistant radial zones (initial outer radius $\sim 60\,\mathrm{km}$, final radius $\sim 20\,\mathrm{km}$) and with up to 60 angular zones was used, corresponding to a radial resolution of a few 100 m ($\lesssim 1\,\mathrm{km}$ near the center) and a maximum angular resolution of 1.5°. In the angular direction, periodic boundary conditions were imposed at ±45° above and below the equatorial plane. The stellar surface was treated as an open boundary where the velocity was calculated from the velocity in the outermost grid zone, the density profile was extrapolated according to a time-variable power law, and the corresponding pressure was determined from the condition of hydrostatic equilibrium. The *Prometheus* code was extended for the use of different time steps and angular resolutions in different regions of the star. Due to the extremely restrictive Courant-Friedrichs-Lewy (CFL) condition for the hydrodynamics, the implicit ν

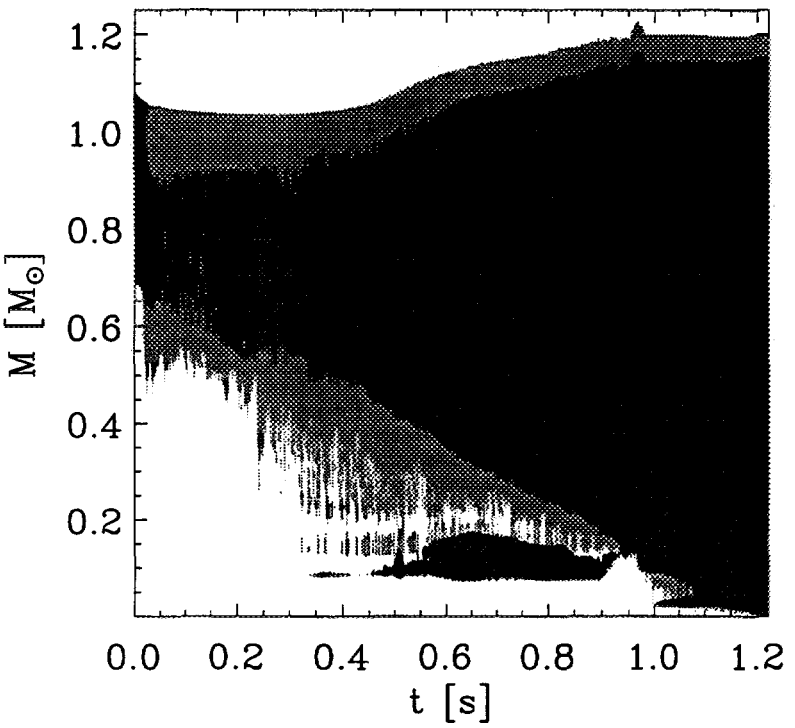

Fig. 1. Convective (baryon) mass region inside the protoneutron star versus time for the 2D simulation. Black indicates regions which are Ledoux unstable or only marginally stable, grey denotes over- and undershooting regions where the absolute value of the angular velocity is $|v_\theta| > 10^7$ cm/s.

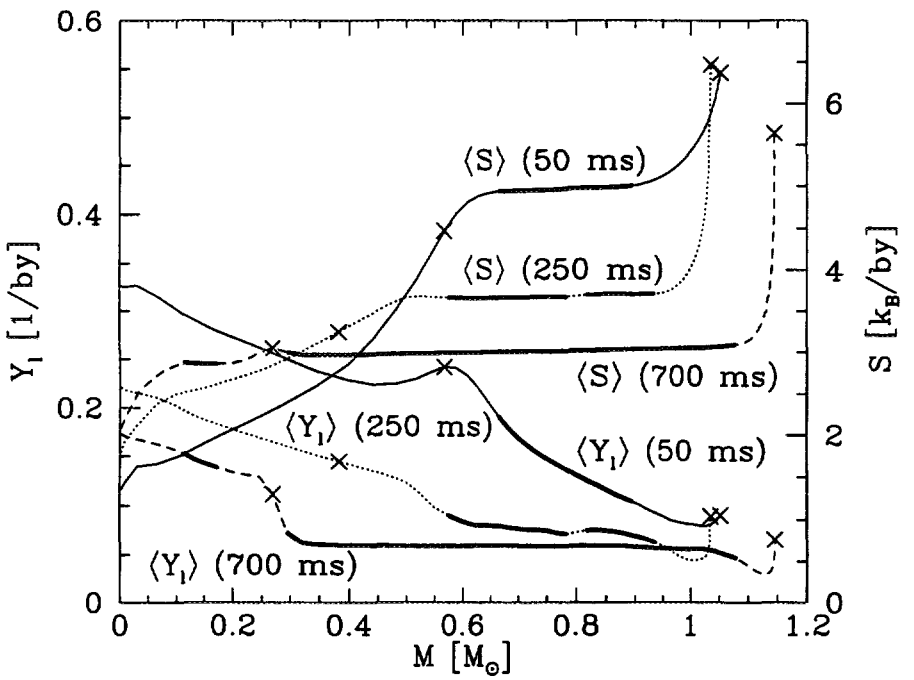

Fig. 2. Angle-averaged S and Y_l profiles in the protoneutron star. Thick solid lines indicate regions that are unstable or only marginally stable against Ledoux convection, crosses mark boundaries of over- and undershooting regions where the absolute value of the angular velocity is $|v_\theta| > 10^7$ cm/s.

transport was computed with typically 10 times larger time steps than the smallest hydrodynamics time step on the grid ($\sim 10^{-7}$ s) (Keil 1996).

Our simulations were started with the $\sim 1.1\,M_\odot$ (baryonic mass) central, dense part ($\rho \gtrsim 10^{11}$ g/cm^3) of the collapsed core of a $15\,M_\odot$ progenitor star (Woosley et al. 1988) that was computed to a time of about 25 ms after core bounce (i.e., a few ms after the stagnation of the prompt shock) by Bruenn (1993). Accretion was not considered but additional matter could be advected onto the grid through the open outer boundary. In the 2D run, Newtonian asphericity corrections were added to the spherically symmetrical GR gravitational potential: $\Phi_{2D} \equiv \Phi_{1D}^{GR} + (\Phi_{2D}^{N} - \Phi_{1D}^{N})$. This should be a sufficiently good approximation because convective motions produce only local and minor deviations of the mass distribution from spherical symmetry. Using the GR potential ensured that transients due to the mapping of Bruenn's (1993) relativistic 1D results to our code were very small. When starting our 2D simulation, the radial velocity (under conservation of the local specific total energy) was randomly perturbed in the whole protoneutron star with an amplitude of 0.1%. The thermodynamics of the neutron star medium was described by the EOS of Lattimer & Swesty (1991) which yields a physically reasonable description of nuclear matter below about twice nuclear density and is thus suitable to describe the interior of the considered low-mass neutron star ($M_{ns} \lesssim 1.2\,M_\odot$).

The ν transport was carried out in radial direction for every angular zone of the finest angular grid. Angular transport of neutrinos was neglected. This underestimates the ability of moving buoyant fluid elements to exchange lepton number and energy with their surroundings and is only correct if radial radiative and convective transport are faster. Moreover, ν shear viscosity was disregarded. Analytical estimates (see Keil et al. 1996) show that for typically chosen numerical resolution the neutrino viscosity is smaller than the numerical viscosity of the PPM code (which is very small compared to other hydrodynamics codes), but even the numerical viscosity is not large enough to damp out the growth and development of the convective instabilities in the protoneutron star.

3.1.2 Results

Shortly after core bounce, the criterion of Eq. (1) is fulfilled between $\sim 0.7\,M_\odot$ and $\sim 1.1\,M_\odot$ (black area in Fig. 1) and convective activity develops within ~ 10 ms after the start of the 2D simulation. About 30 ms later the outer layers become convectively stable which is in agreement with Bruenn & Mezzacappa (1994). In our 2D simulation, however, the convectively unstable region retreats to mass shells $\lesssim 0.9\,M_\odot$ and its inner edge moves deeper into the neutrino-opaque interior of the star, following a steeply negative lepton gradient that is advanced towards the stellar center by the convectively enhanced deleptonization of the outer layers (Figs. 1 and 2). Note that the black area in Fig. 1 and the thick solid lines in Fig. 2 mark not only those regions in the star which are convectively unstable but also those *which are only marginally stable* according to the Ledoux criterion of Eq. (1) for angle-averaged S and Y_l, i.e., regions where $\mathcal{C}_L(r) \geq a \cdot \max_r(|\mathcal{C}_L(r)|)$ with $a = 0.05$ holds. For $a \lesssim 0.1$ the accepted region varies only little with a and is always embedded by the grey-shaded area where the absolute value of the angular velocity is $|v_\theta| > 10^7$ cm/s. Yet, only sporadically and randomly appearing patches in the convective layer fulfill Eq. (1) rigorously. Figure 2 shows that the black region in Fig. 1 coincides with the

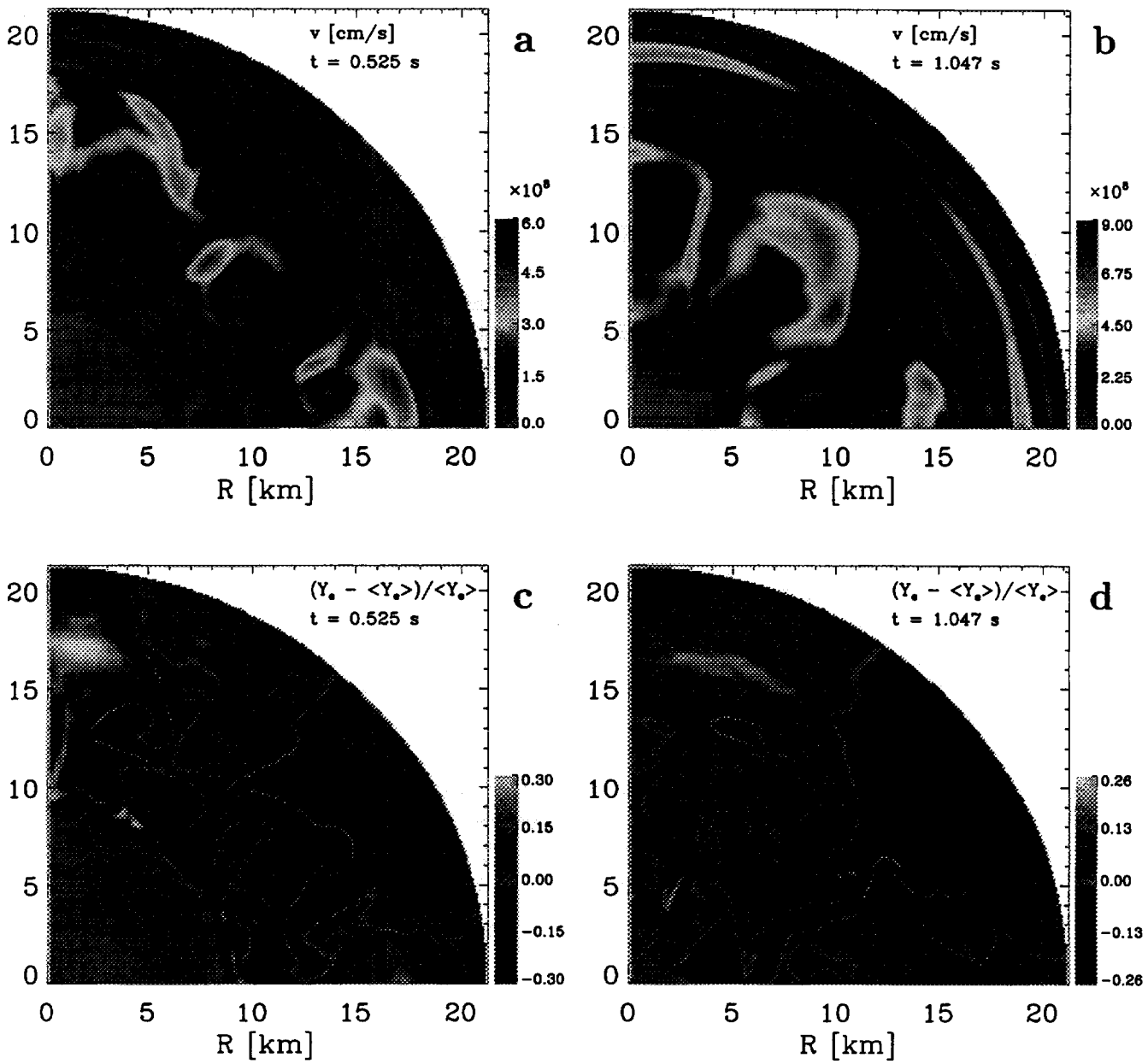

Fig. 3. Panels **a** and **b** show the absolute values of the velocity for the 2D simulation at times $t = 0.525$ s and $t = 1.047$ s, respectively, with the grey scale in units of 10^8 cm/s. Time is measured from the start of the simulation which is at about 25 ms after core bounce. The computation was performed in an angular wedge of 90° between +45° and −45° around the equatorial plane. The protoneutron star has contracted to a radius of about 21 km at the given times. Panels **c** and **d** display the relative deviations of the electron fraction Y_e from the angular means $\langle Y_e \rangle$ at each radius for the same two instants. The maximum deviations are of the order of 30%. Lepton-rich matter rises while deleptonized material sinks in. Comparison of both times shows that the inner edge of the convective layer moves inward from about 8.5 km at $t = 0.525$ s to less than 2 km at $t = 1.047$ s.

layers where convective mixing flattens the S and Y_l gradients.

The convective pattern is extremely non-stationary and has most activity on large scales with radial coherence lengths of several km up to $\sim 10\,\mathrm{km}$ and convective "cells" of 20°–30° angular diameter, at some times even 45° (Fig. 3). Significant over- and undershooting takes place (grey regions in Fig. 1) and the convective mass motions create pressure waves and perturbations in the convectively stable neutron star interior and in the surface layers. The maximum convective velocities are usually $\sim 4 \cdot 10^8\,\mathrm{cm/s}$, but peak values of $\sim 10^9\,\mathrm{cm/s}$ can be reached. These velocities are typically 5–10% of the average sound speed in the star. The kinetic energy of the convection is several $10^{49}\,\mathrm{erg}$ at $t \lesssim 1\,\mathrm{s}$ and climbs to $\sim 2 \cdot 10^{50}\,\mathrm{erg}$ when the protoneutron star is fully convective. Relative deviations of Y_l from the angular mean can be several 10% (even 100%) in rising or sinking buoyant elements, and for S can reach 5% or more. Rising flows always have larger Y_l *and* S than their surroundings. Corresponding temperature and density fluctuations are only $\sim$ 1–3%. Due to these properties and the problems in applying the Ledoux criterion with angle-averaged S and Y_l straightforwardly, we suspect that it is hardly possible to describe the convective activity with a mixing-length treatment in a 1D simulation.

Our 2D simulation shows that convection in the protoneutron star can encompass the whole star within $\sim 1\,\mathrm{s}$ and can continue for at least as long as the deleptonization takes place, possibly even longer. A deleptonization "wave" associated with the convectively enhanced transport moves towards the center of the protoneutron star. This reduces the timescale for the electron fraction Y_e to approach its minimum central value of about 0.1 from $\sim 10\,\mathrm{s}$ in the 1D case, where the lepton loss proceeds much more gradually and coherently, to only $\sim 1.2\,\mathrm{s}$ in 2D. With convection the entropy and temperature near the center rise correspondingly faster despite a similar contraction of the star in 1D and 2D (Fig. 4). Convection increases the total lepton number flux and the ν luminosities by up to a factor of 2 (Fig. 5) and therefore the emitted lepton number N_l and energy E_ν rise much more rapidly (Fig. 4). The convective energy (enthalpy plus kinetic energy) flux dominates the diffusive ν energy flux in the convective mantle after $t \gtrsim 250\,\mathrm{ms}$ and becomes more than twice as large later. Since convection takes place somewhat below the surface, ν's take over the energy transport exterior to $\sim 0.9\,M_\odot$. Thus the surface ν flux shows relative anisotropies of only 3–4%, in peaks up to $\sim$ 10%, on angular scales of 10°–40°. Averaged over all directions, the neutrinospheric temperatures and mean energies $\langle \epsilon_{\nu_i} \rangle$ of the emitted ν_e and $\bar{\nu}_e$ are higher by 10–20% (Fig. 5).

3.1.3 Consequences

Convectively increased neutrino emission from the protoneutron star does not only have influence on the supernova explosion mechanism. It is also of crucial importance to understand the nucleosynthesis in the neutrino-heated supernova ejecta and in the neutrino-driven wind whose degree of neutronization is determined by the interaction with the ν_e and $\bar{\nu}_e$ fluxes. Absorptions of ν_e onto free neutrons increase the free proton abundance while captures of $\bar{\nu}_e$ onto protons make the matter more n-rich.

As discussed above, convective neutrino transport in the nascent neutron star accelerates the deleptonization of the protoneutron star drastically. This means that during the first second or so the ν_e number flux $\mathcal{N}_{\nu_e}$ is increased relative to the $\bar{\nu}_e$ number flux $\mathcal{N}_{\bar{\nu}_e}$. If the protoneutron star atmosphere (where the neutrinospheres

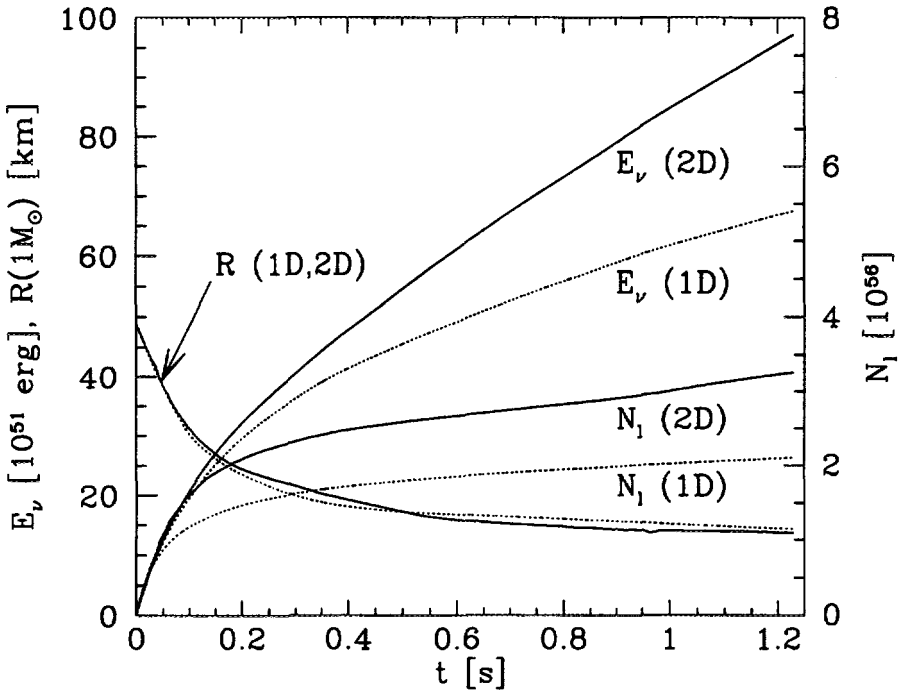

Fig. 4. Radius of the $M = 1\,M_\odot$ mass shell and total lepton number N_l and energy E_ν radiated away by neutrinos vs. time for the 2D (solid) and 1D (dotted) simulations.

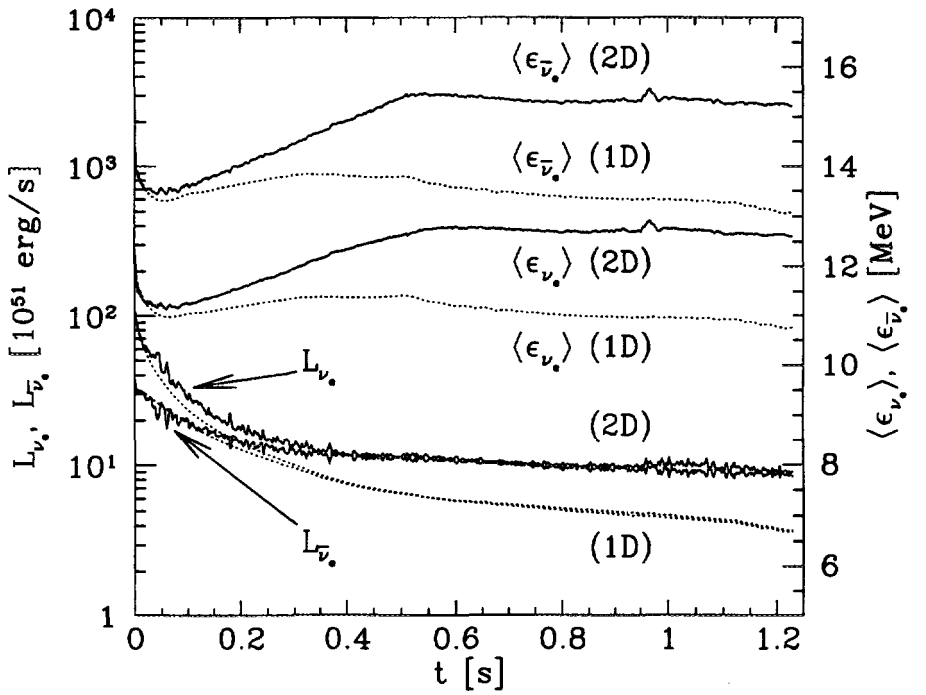

Fig. 5. ν_e and $\bar{\nu}_e$ luminosities and mean energies vs. time for the 2D simulation (solid) compared with the 1D run (dotted).

are located) is not convective but a radiative layer sitting on top of a convective region, then it can be shown (Keil et al. 1996) that the ratio of the average energies of $\bar{\nu}_e$ and ν_e, $\langle\epsilon^n_{\bar{\nu}_e}\rangle/\langle\epsilon^n_{\nu_e}\rangle$ (n is an arbitrary power), is not influenced very much by the convective activity deeper inside the star. In that case it is easy to see that the electron fraction in the ejecta, $Y_e^{\rm ej} \approx 1/\left[1+(\mathcal{N}_{\bar{\nu}_e}\langle\epsilon^2_{\bar{\nu}_e}\rangle)/(\mathcal{N}_{\nu_e}\langle\epsilon^2_{\nu_e}\rangle)\right]$ (Qian & Woosley 1996), will increase when the ratio $\mathcal{N}_{\bar{\nu}_e}/\mathcal{N}_{\nu_e}$ decreases. Keil et al. (1996) found that this is indeed the case before about 0.4 s after shock formation. This effect offers a solution of the overproduction problem of $N = 50$ nuclei in current supernova models (see Hoffman et al. 1996, McLaughlin et al. 1996).

Because the opacity of the protoneutron star increases for ν_e (which are absorbed on neutrons) but decreases for $\bar{\nu}_e$ (absorbed on protons) with progressing neutronization of the matter, the accelerated neutronization of the convective protoneutron star will lead to a more rapid increase of $\langle\epsilon_{\bar{\nu}_e}\rangle$ relative to $\langle\epsilon_{\nu_e}\rangle$ than in 1D models at times later than about 1 s. This will favor a faster drop of $Y_e^{\rm ej}$ and thus might help to produce the n-rich conditions required for a possible r-processing in the high-entropy neutrino-driven wind (for details, see Woosley et al. 1994, Takahashi et al. 1994).

Without any doubt, an increase of the neutrino luminosities by a factor of ~ 2 during the first second after core bounce may be decisive for a successful explosion via the neutrino-heating mechanism. This will have to be investigated in future multi-dimensional simulations where not only the evolution of the protoneutron star is followed but the whole collapsed star is included. Parametric 1D and 2D studies with varied neutrino luminosities carried out by Janka & Müller (1995a, 1996) have already demonstrated the sensitivity of the explosion to changes of the luminosity of the order of some 10%. In the next section these results will be addressed.

3.2 Two-dimensional simulations of convection in the neutrino-heated region

Herant et al. (1992) first demonstrated by a hydrodynamical simulation that strong, turbulent overturn occurs in the neutrino-heated layer outside of the protoneutron star and that this helps the stalled shock front to start re-expansion as a result of energy deposition by neutrinos. Although the existence and fast growth of these instabilities was confirmed by Janka & Müller (1994, 1995a, 1996) the results of their simulations in 1D and in 2D indicated a very strong sensitivity to the conditions at the protoneutron star and to the details of the description of neutrino interactions and neutrino transport. Since the knowledge about the high-density equation of state in the nascent neutron star and about the neutrino opacities of dense matter is incomplete (see Sect. 2.1), the influence of a contraction of the neutron star and of the size of the neutrino fluxes on the evolution of the explosion has been tested by systematic studies.

In the following we shortly report the main conclusions that can be drawn from our set of 1D and 2D models with different core-neutrino luminosities and with varied temporal contraction of the inner boundary (Janka & Müller 1996).

3.2.1 Numerical implementation

The inner boundary was placed somewhat inside the neutrinosphere and was used instead of simulating the evolution of the very dense inner core of the nascent neutron star. This gave us the freedom to set the neutrino fluxes to chosen values at the

inner boundary and also enabled us to follow the 2D simulations until about one second after core bounce with a reasonable number ($\mathcal{O}(10^5)$) of time steps and an "acceptable" computation time, i.e. several 100 h on one processor of a Cray-YMP with a grid of 400×90 zones and a highly efficient implementation of the microphysics. Note that doubling the angular resolution multiplies the computational load by a factor of about 4!

Our simulations started at ~ 25 ms after shock formation from an initial model evolved through core collapse and bounce by Bruenn (1993). Boundary motion, luminosities of all neutrino kinds, and non-thermal neutrino spectra were time-dependent and mimiced the behavior in Bruenn (1993) and in Newtonian computations by Bruenn et al. (1995). Except for Doppler-shift and gravitational redshift the neutrino fluxes were kept constant with radius and did not include accretion luminosity. Neutrinos interact with matter by scattering on $e^{\pm}$, n, p, α, and nuclei, by neutrino pair processes, and ν_e and $\bar{\nu}_e$ also by the β-reactions. The reaction rates were evaluated by using Monte Carlo calibrated variable Eddington factors that depended on the density gradient at the neutron star surface. Inside the neutrinosphere reactive equilibrium between neutrinos and matter can be established. Our EOS described $e^{\pm}$ as arbitrarily relativistic, ideal Fermi gases and n, p, α, and a representative nucleus as ideal Boltzmann gases in NSE (good at $\rho \lesssim 5 \times 10^{13}\,\mathrm{g/cm^3}$ for temperatures $T \gtrsim 0.5\,\mathrm{MeV}$). 2D computations were performed with the Eulerian *Prometheus* code (up to 1° resolution and 400×180 zones), 1D runs with a Lagrangian method (details in Janka & Müller 1996).

3.2.2 Results for spherically symmetric models

The evolution of the stalled, prompt shock in 1D models turned out to be extremely sensitive to the size of the neutrino luminosities and to the corresponding strength of neutrino heating exterior to the gain radius. In models with successively higher core neutrino fluxes the shock is driven further and further out to larger maximum radii during a phase of $\sim$ 100–150 ms of slow expansion. Nevertheless, it finally recedes again to become a standing accretion shock at a much smaller radius (Fig. 6, dotted lines; see also Fig. 8). For a sufficiently high threshold luminosity, however, neutrino heating is strong enough to cause a successful explosion (Fig. 6, solid lines). For even higher neutrino fluxes the explosion develops faster and gets more energetic. In case of our $15\,M_\odot$ star with $1.3\,M_\odot$ Fe-core (Woosley et al. 1988) we find that explosions occur for ν_e and $\bar{\nu}_e$ luminosities above 2.2×10^{52} erg/s in case of a contracting inner boundary (to mimic the shrinking protoneutron star), but of only 1.9×10^{52} erg/s when the radius of the inner boundary is fixed.

The transition from failure to explosion requires the neutrino luminosities to exceed some threshold value. Yet, this is not sufficient. High neutrino energy deposition has to be maintained for a longer period of time to ensure high pressure behind the shock. If the decay of the neutrino fluxes is too fast, e.g., if a significant fraction of the neutrino luminosity comes from neutrino emission by spherically accreted matter, being shut off when the shock starts to expand, then the outward shock propagation may break down again and the model fizzles. Continuous shock expansion needs a sufficiently strong push from the neutrino-heated matter until the material behind the shock has achieved escape velocity and does not need pressure support to make its way out.

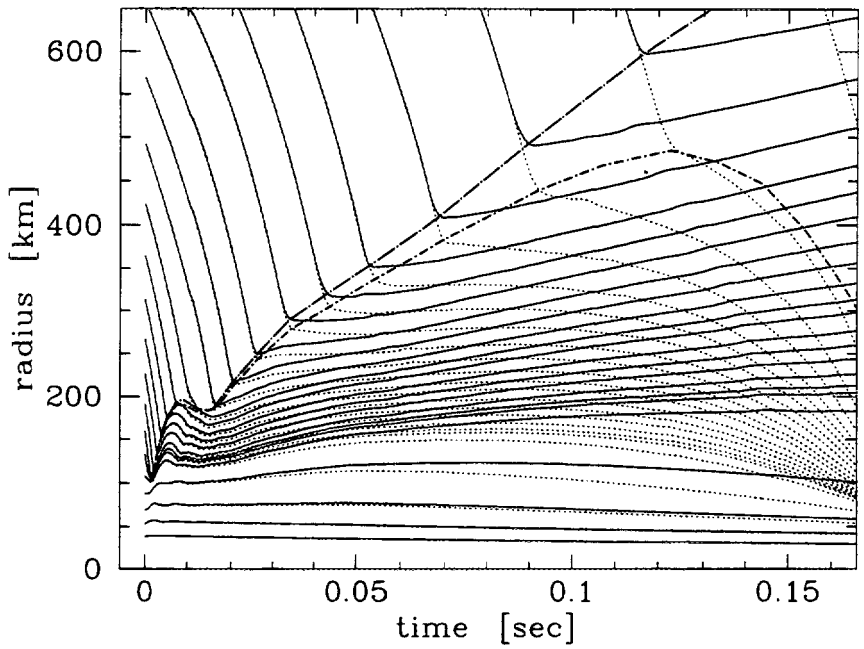

Fig. 6. Radial positions of mass shells of a marginally exploding model (solid lines) with initial neutrino luminosities from the lower boundary of $2.2 \cdot 10^{52}$ erg/s and of a still unsuccessful 1D model (dotted lines; initial boundary luminosities $2.1 \cdot 10^{52}$ erg/s) versus time after core bounce. The thick broken lines mark the shock positions.

This contradicts a recent suggestion by Burrows & Goshy (1993) that the explosion can be viewed at as a global instability of the star that, once excited, inevitably leads to an explosion. The analysis by Burrows & Goshy may allow one to estimate the radius of shock stagnation when stationarity applies. The start-up phase of the explosion, however, can hardly be described by steady-state assumptions, because the timescales of shock expansion, of neutrino cooling and heating, and of temperature and density changes between neutron star and shock are all of the same order, although long compared to the sound crossing time and (possibly) shorter than the characteristic times of luminosity changes and variations of the mass accretion rate into the shock. In particular, due to the high sound speed and rather slow shock expansion the shock propagation is very sensitive to changes of the conditions in the neutrino-heated layer. A contraction of the neutron star or enhanced cooling of the gas inside the gain radius accelerate the advection of matter through the gain radius and reduce the time the postshock material is heated. This is harmful to the outward motion of the shock just as a moderate decline of the neutrino fluxes can be.

3.2.3 Results for two-dimensional models

In spherical symmetry the expansion of the neutrino-heated matter and of the shock can occur only when also the overlying material is lifted in the gravitational field of the neutron star. In the multi-dimensional case this is different. Blobs and lumps of heated matter can rise by pushing colder material aside and cold material from the region behind the shock can get closer to the zone of strongest neutrino heating to readily absorb energy. Also, when buoyancy forces drive hot matter outward, the

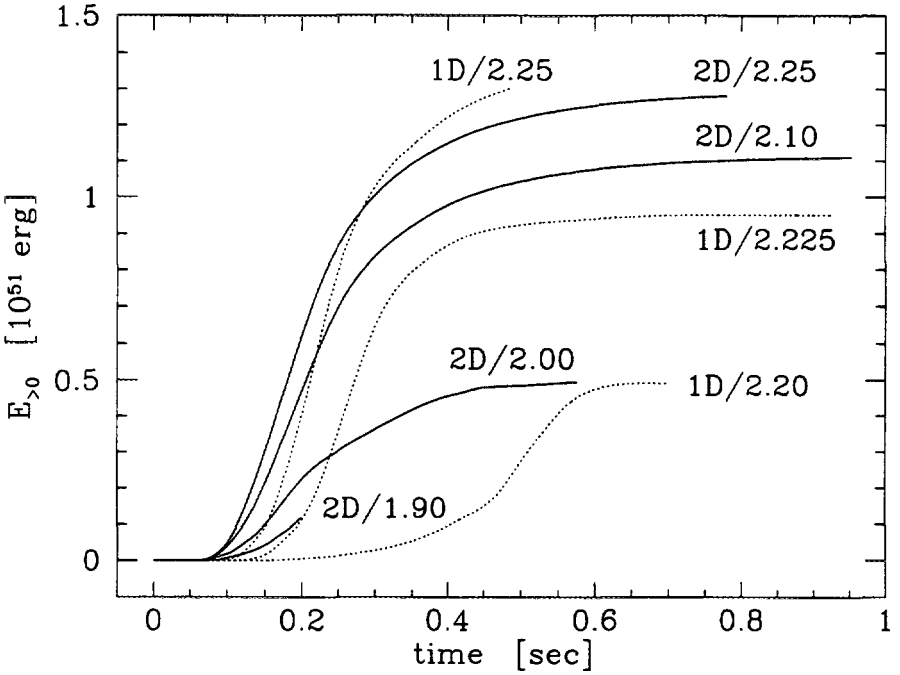

Fig. 7. Explosion energies vs. time after the start of the simulations ($\sim$ 25 ms after bounce) for exploding 1D (dotted) and 2D models (solid). The numbers denote the initial ν_e and $\bar{\nu}_e$ (approximately) luminosities in 10^{52} erg/s.

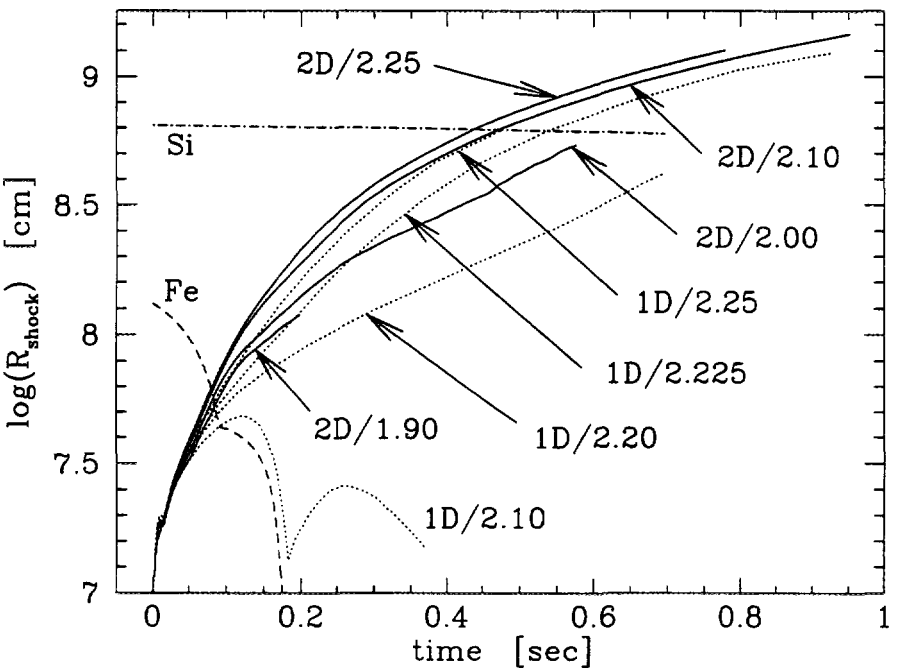

Fig. 8. Shock positions vs. time after core bounce for the exploding one-dimensional ("1D", dotted lines) and two-dimensional ("2D", solid lines) models of Fig. 7. The numbers indicate the size of the initial ν_e (and $\bar{\nu}_e$, approximately) luminosities in units of 10^{52} erg/s. In addition, the result for the unsuccessful 1D model with initial boundary luminosities of $2.1 \cdot 10^{52}$ erg/s is depicted. The dashed and dash-dotted curves mark the mass shells that correspond to the outer boundaries of Fe-core and Si-shell, respectively, for the latter model.

energy loss by re-emission of neutrinos is significantly reduced. Thus overturn of low-entropy and high-entropy gas increases the efficiency of neutrino energy deposition outside the radius of net energy gain and leads to explosions in 2D already for lower neutrino fluxes than in the spherically symmetrical case. Our models, however, do not show the existence of a "convective cycle" or "convective engine" (Herant et al. 1994) that transports energy from the heating region into the shock. The matter between protoneutron star and shock is subject to strong neutrino heating and cooling and our high-resolution calculations reveal a turbulent, unordered, and dynamically changing pattern of rising and sinking lumps of material with very different thermodynamical conditions and no clear indication of inflows of cool gas and outflows of hot gas at well-defined thermodynamical states.

2D models explode for core neutrino luminosities which cannot produce explosions in 1D. There is a window of neutrino fluxes with a width of $\sim$ 20% of the threshold luminosity for explosions in 1D, where convective overturn between gain radius and shock is a significant help for shock revival. For lower neutrino fluxes even convective overturn cannot ensure strong explosions but the explosion energy gets very low. We do not find a continuous "accumulation" (Herant et al. 1994) of energy in the convective shell until an explosion energy typical of a type-II supernova is reached. For neutrino fluxes that cause powerful explosions already in 1D, turbulent overturn occurs but is not crucial for the explosion. In fact, in this case the fast rise of bubbles of heated material leads to a less vigorous start of the explosion and to the saturation of the explosion energy at a somewhat lower level (Fig. 7). The explosion energy, defined as the *net energy of the expanding matter at infinity*, does not exceed 10^{50} erg earlier than after $\sim$ 100 ms of neutrino heating. This is the characteristic timescale of neutrinos to transfer an amount of energy to the material that is roughly equal to its gravitational binding energy and it is also the timescale that the convective overturn between gain radius and shock needs to develop to its full strength. It is not possible to determine or predict the final explosion energy of the star from a short period of only 100–200 ms after shock formation. Typically, the increase of the explosion energy with time levels off not before 400–500 ms after bounce, followed by only a very slow increase due to the much smaller contributions of the few $10^{-3}\,M_\odot$ of matter blown away from the protoneutron star in the neutrino wind (Fig. 7). Since the wind material is heated slowly and can expand as soon as the internal energy per nucleon roughly equals its gravitational binding energy, the matter does not have a large kinetic energy at infinity.

Although the global evolution of powerful explosions in 2D, i.e., the increase of the explosion energy with time (Fig. 7), the shock radius as a function of time (Fig. 8), or even the amount of ^{56}Ni produced by explosive nucleosynthesis, is not much different from energetic explosions of spherically symmetrical models, the structure of the shock and of the thick layer of expanding, dense matter behind the shock clearly bear the effects of the turbulent activity. The shock is deformed on large scales and its expansion velocity into different directions varies by $\sim$ 20–30%. The material behind the shock reveals large-scale inhomogeneities in density, temperature, entropy, and velocity, these quantities showing contrasts of up to a factor of 3. The typical angular scale of the largest structures is $\sim$ 30°–45°. We do not find that the turbulent pattern tries to gain power on the largest possible scales and to evolve into the lowest possible mode, $l = 1$ (Herant et al. 1992, 1994). Turbulent motions are still going

on in the extended, dense layer behind the shock when we stop our calculations at ~ 1 s after bounce. We consider them as possible origin of the anisotropies, inhomogeneities, and non-uniform distribution of radioactive elements which were observed in SN 1987A. The contrasts behind the shock are about an order of magnitude larger than the artificial perturbations that were used in hydrodynamical simulations to trigger the growth of Rayleigh-Taylor instabilities in the stellar mantle and envelope.

3.2.4 From core bounce to one second

Convective overturn in the neutrino-heated layer around the protoneutron star develops within $\sim$ 50–100 ms after shock formation. About 200–300 ms after bounce neutrinos have deposited a sizable amount of energy in the material below the shock front. The turbulent layer begins to move away from the region of strongest neutrino heating and to expand outward behind the accelerating shock (Fig. 9). At this time turbulent activity around and close to the protoneutron star comes to an end. An extended phase of convection and accretion outside the protoneutron star does not occur. Inflows of low-entropy, p-rich gas from the postshock region towards the neutrino-heated zone are not accreted onto the neutron star. Although the gas loses lepton number while falling in, it does not get as n-rich as the material inside the gain radius. In addition, neutrino heating and mixing with the surrounding, high-entropy gas increase the entropy in the downflows. Both high electron (proton) concentration and high entropy have a stabilizing effect and prevent the penetration of the gas through the gain radius into the cooler and more n-rich surface layer of the protoneutron star.

At $\sim$ 400–500 ms the protoneutron star has become quite compact and the density outside has dropped appreciably. This indicates the formation of the high-entropy, low-density "hot-bubble" region (Bethe & Wilson 1985) and the phase of small mass loss from the nascent neutron star in the neutrino-driven wind, accompanied by slowly increasing entropies. The wind accelerates because of the steepening density decline away from the shrinking neutron star. The faster expansion and push of the wind create a density inversion between the massive, slow, inert shell behind the shock and the evacuating hot-bubble region. Around the time the outgoing supernova shock passes the entropy and composition step of the Si-O interface at $\sim$ 5700 km (see Fig. 8), this density inversion steepens into a strong reverse shock that forms a sharp discontinuity in the neutrino wind, slowing down the wind expansion from $> 2 \times 10^9$ cm/s to a few times 10^8 cm/s. Since the velocities of the wind and of the layer behind the shock decrease with time, it is possible that this reverse shock will trigger fallback of a significant fraction of the matter that was blown out in the neutrino wind. Once the infall of the outer wind material is initiated and the pressure support for the gas further out vanishes, inward acceleration might even enforce the fallback of more slowly moving parts of the dense shell behind the supernova shock.

Fallback of a significant amount of matter, ~ 0.1 to $0.2\,M_\odot$, might be needed to solve two major problems in the current supernova models. On the one hand, due to the fast development of the explosion and the lack of an extended accretion phase, the protoneutron star formed at the center of the explosion has quite a small (initial) baryonic mass, only $\sim 1.2\,M_\odot$ in case of our $15\,M_\odot$ star with $1.3\,M_\odot$ Fe-core. On the other hand, the yields of Fe-peak elements by explosive nucleosynthesis are incompatible with observational constraints for type-II supernovae as deduced

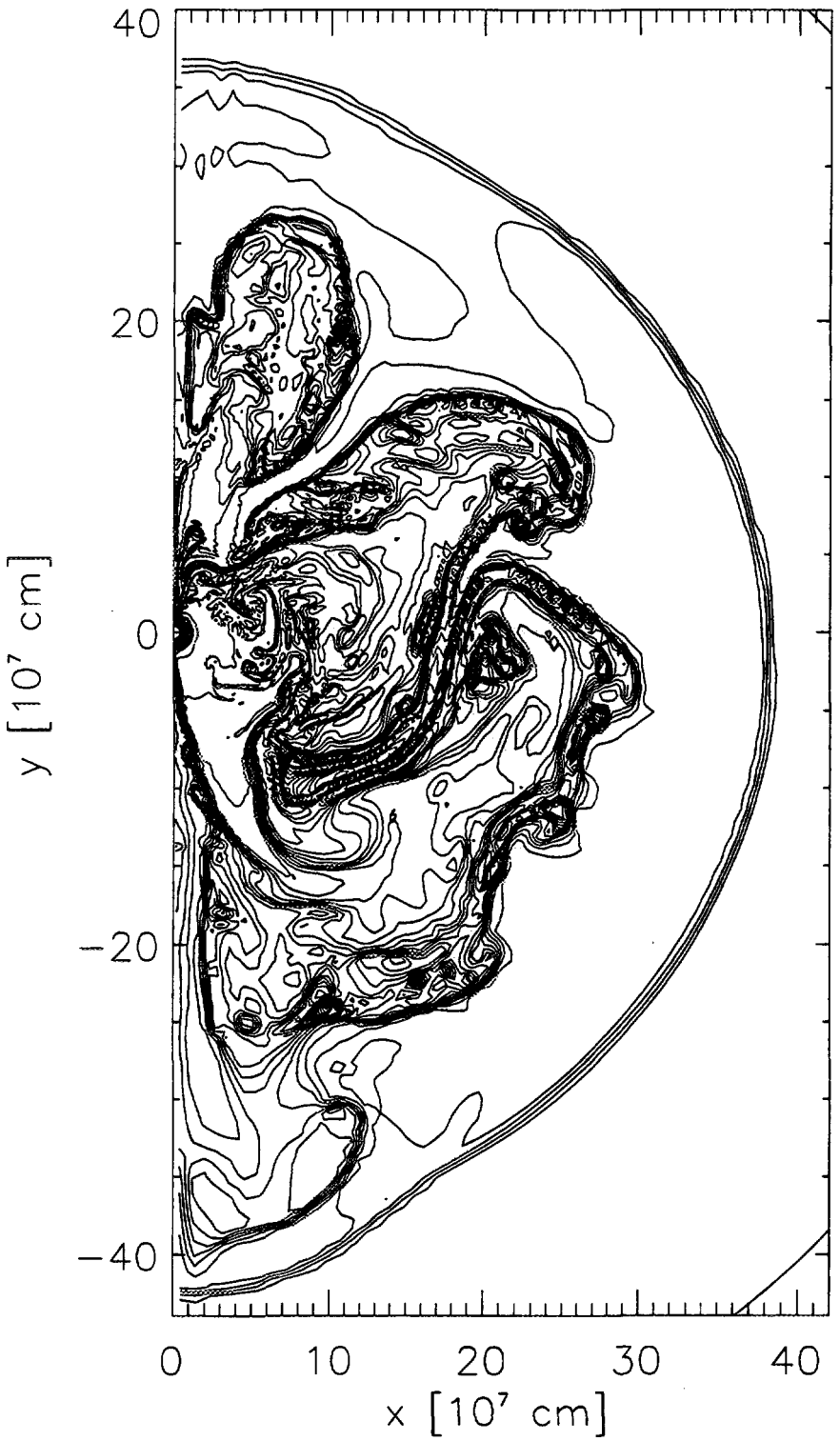

Fig. 9. A weakly exploding 2D model with an explosion energy of about $0.5 \cdot 10^{51}$ erg at a time $t = 377$ ms after bounce. The figure shows entropy contours, equidistantly spaced in steps of $0.5\,k_B$/nucleon between $5\,k_B$/nucleon and $16\,k_B$/nucleon and in steps of $1.0\,k_B$/nucleon between $16\,k_B$/nucleon and $23\,k_B$/nucleon. The shock is located at about 3800 km. Clumpy structures, inhomogeneities, and vortex patterns caused by Kelvin-Helmholtz instabilities are visible along the boundaries between downflows of cold gas from the postshock region and hot, rising gas from the neutrino-heated zone around the protoneutron star at the coordinate center.

from terrestrial abundances and galactic evolution arguments. In case of powerful explosions with energies of $1\text{–}1.3 \times 10^{51}$ erg material of $\sim 0.2\,M_\odot$ is heated to temperatures $T > 4.5 \times 10^9$ K and is ejected behind the shock during the early phase of the explosion. Only roughly half of this matter, 0.085–0.1 $M_\odot$, has an electron fraction $Y_e > 0.49$ and will end up with ^{56}Ni as the dominant nucleosynthesis product. In that respect the models seem to match the observations quite well. Yet, only some part ($\sim 0.05\,M_\odot$) of the matter that is shock-heated to $T > 4.5 \times 10^9$ K has $Y_e \gtrsim 0.495$ and will end up with relative abundance yields in acceptable agreement with solar-system values. The amount of ^{56}Ni produced in neutrino-driven explosions turns out to be correlated with the explosion energy. In case of more energetic explosions the shock is able to heat a larger mass to sufficiently high temperatures.

3.2.5 Consequences

Turbulent overturn between the zone of strongest neutrino heating and the supernova shock aids the re-expansion of the stalled shock and is able to cause powerful type-II supernova explosions in a certain, although rather narrow, window of core neutrino fluxes where 1D models do not explode. The turbulent activity outside and close to the protoneutron star is transient and between 300 and 500 ms after core bounce the (essentially) spherically symmetrical neutrino-wind phase starts and the turbulent shell moves outward behind the expanding supernova shock. Our 2D simulations do not show a long-lasting period of convection and accretion after core bounce. Only very little of the cool, low-entropy matter that flows down from the shock front to the zone of neutrino energy deposition is advected into the protoneutron star surface. Since the matter is p-rich and its entropy increases quickly due to neutrino heating, it stays in the heated region to gain more energy by neutrino interactions and to start rising again. The strong, large-scale inhomogeneities and anisotropies in the expanding layer behind the outward propagating shock front will probably help to explain the effects of macroscopic mixing seen in SN 1987A and can account for neutron star recoil velocities of a few 100 km/s (details in Janka & Müller 1994, 1995b).

Although the models develop energetic explosions for sufficiently high neutrino luminosities and produce an amount of ^{56}Ni that is in good agreement with observational constraints, the initial mass of the protoneutron star is clearly on the low side of the spectrum of measured neutron star masses. Moreover, the models eject ~ 0.1–$0.15\,M_\odot$ of material with $Y_e < 0.495$, which implies an overproduction of certain elements in the Fe-peak by an appreciable factor compared with the nucleosynthetic composition in the solar system. The fallback of a significant fraction of this matter to the neutron star at a later stage would ease these problems. It is possible that the reverse shock which develops in our models will trigger this fallback on a timescale of seconds. Due to the strong inhomogeneities in the dense layer behind the shock this fallback could happen with considerable anisotropy and impart an additional kick to the neutron star (Janka & Müller 1995b).

On the other hand, it is hard to see how fallback could achieve a clean disentanglement of desirable and undesirable ejecta, in particular if one has in mind the turbulent activity and the mixing of different conditions present in the neutrino-heated layer. Nevertheless, it may still be that the observed nucleosynthetic composition of the interstellar medium reflects the accidental result of a delicate separation of

"good" and "bad" products of explosive nucleosynthesis during the early phases of the explosion. Alternatively, as discussed in Sect. 3.1.3, the contamination of the supernova ejecta with overproduced $N = 50$ nuclei could be more naturally and plausibly avoided if the luminosities of ν_e and $\bar{\nu}_e$ and therefore the degree of neutronization in the neutrino-heated material were modified by convection in the nascent neutron star.

4. Summary and discussion

Recent multi-dimensional simulations of type-II supernova explosions (Herant et al. 1994, Burrows et al. 1995, Janka & Müller 1996) have shown that convective overturn in the neutrino-heating region helps the explosion and can be crucial for the success of the delayed explosion mechanism. The net efficiency of neutrino energy deposition is increased when cold (low-entropy) material from behind the shock can move inward to the region of strongest heating, while at the same time heated (high-entropy) gas can rise outward and expand, thus reducing the energy loss by reemission of neutrinos. The delicate balance of neutrino heating and cooling which is present in the spherically symmetric case is avoided, and the neutrino luminosity that is required for sufficiently strong heating to obtain an explosion is lowered.

However, there is still a competition between the neutrino heating timescale and the timescale for the growth of the convective instability on the one hand and the advection timescale of matter from the shock through the gain radius (interior of which neutrino heating is superseded by neutrino cooling) towards the protoneutron star on the other. For too low neutrino luminosities the heating in the postshock region is not strong enough to ensure short growth timescales of the convective overturn. In this case the matter is advected downward through the gain radius faster than it is driven outward by buoyancy forces. Inside the gain radius the absorbed neutrino energy is quickly radiated away again by neutrino emission. Therefore convective overturn in the neutrino-heated region is crucial for the explosion only in a rather narrow window of luminosities. For higher core neutrino fluxes also spherically symmetrical models yield energetic explosions, while for lower luminosities even with convection no strong explosions occur. In any case, the success of the delayed explosion mechanism requires sufficiently large neutrino luminosities from the nascent neutron star for a sufficiently long time.

Moreover, all current supernova models have severe problems concerning the nucleosynthetic composition of the neutrino-heated ejecta. These show huge overproduction factors (up to the order of 100) for elements around neutron number $N = 50$, indicating that the ejecta are too neutron-rich. Several suggestions have been made to solve this problem, e.g., fallback of some of the early ejecta towards the neutron star during a later phase of the explosion (Herant et al. 1994), a longer delay of the explosion than obtained in current models which would reduce the amount of neutron-rich material due to the density decrease in the region between supernova shock and protoneutron star (Burrows & Hayes 1995), or a slightly underestimated electron fraction Y_e in the ejecta because of still unsatisfactorily treated neutrino transport which affects the computed ν_e and $\bar{\nu}_e$ spectra and thus the neutrino-matter interactions in the hot bubble region (Hoffman et al. 1996). While the latter might certainly be true and has to be investigated carefully (see Sect. 2.1), all of these suggestions

rely on some fine-tuning and effects which might be very unstable and sensitive to minor changes.

Strong convection inside the newly formed neutron star during the first few hundred milliseconds after core bounce and shock formation offers a remedy of both problems (Keil et al. 1996). Faster cooling of the protoneutron star by convective energy transport increases the total neutrino luminosities and therefore helps the neutrino energy deposition in the postshock layers. The accompanying enhanced deleptonization raises the ν_e number flux relative to the $\bar{\nu}_e$ number flux. This leads to more frequent absorptions of ν_e onto neutrons in the neutrino-heated gas and thus can establish a higher electron fraction in the material that carries the supernova energy during the early moments of the explosion. The final confirmation of this picture has still to be waited for until multi-dimensional supernova simulations have been performed that follow the protoneutron star *and* the surrounding progenitor star for a sufficiently long time.

Acknowledgements. The author would like to thank the organizers, in particular M. Locher, for the great hospitality and the opportunity to attend the summer school in Zuoz. This work was supported by the Sonderforschungsbereich 375-95 for Astro-Particle Physics of the Deutsche Forschungsgemeinschaft. The computations were performed on the CRAY-YMP 4/64 of the Rechenzentrum Garching.

References

Alexeyev E.N., et al., 1988, Phys. Lett. B205, 209
Arnett W.D., 1988, ApJ 331, 337
Arnett W.D., Bahcall J.N., Kirshner R.P., Woosley S.E., 1989, ARA&A 27, 629
Arnett W.D., Fryxell B.A., Müller E., 1989, ApJ 341, L63
Aschenbach B., Egger R., Trümper J., 1995, Nat 373, 587
Barthelmy S., 1989, et al., IAU Circ. 4764
Bethe H.A., Wilson J.R., 1985, ApJ 295, 14
Bethe H.A., Brown G.E., Cooperstein J., 1987, ApJ 322, 201
Bionta R.M., et al., 1987, Phys. Rev. Lett. 58, 1494 (IMB collaboration)
Bruenn S.W., 1985, ApJS 58, 771
Bruenn S.W., 1993, in: Nuclear Physics in the Universe, eds. M.W. Guidry and M.R. Strayer, IOP, Bristol, p. 31
Bruenn S.W., Dineva T., 1996, ApJ 458, L71
Bruenn S.W., Mezzacappa A., 1994, ApJ 433, L45
Bruenn S.W., Mezzacappa A., Dineva T., 1995, Phys. Rep. 256, 69
Burrows A., 1987, ApJ 318, L57
Burrows A., Fryxell B.A., 1992, Sci 258, 430
Burrows A., Fryxell B.A., 1993, ApJ 418, L33
Burrows A., Goshy J., 1993, ApJ 416, L75
Burrows A., Hayes J., 1995, Ann. N.Y. Acad. Sci. 759, 375
Burrows A., Hayes J., Fryxell B.A., 1995, ApJ 450, 830
Burrows A., Lattimer J.M., 1986, ApJ 307, 178
Burrows A., Lattimer J.M., 1988, Phys. Rep. 163, 51
Caraveo P.A., 1993, ApJ 415, L111

Colella P., Woodward P.R., 1984, J. Comp. Phys. 54, 174

Colgan S.W.J., Haas M.R., Erickson E.F., Lord S.D., Hollenbach D.J., 1994, ApJ 427, 874

Colgate S.A., Herant M., Benz W., 1993, Phys. Rep. 227, 157

Colgate S.A., White R.H., 1966, ApJ 143, 626

Cook W.R., et al., 1988, ApJ 334, L87

Den M., Yoshida T., Yamada Y., 1990, Prog. Theor. Phys. 83, 723

Dotani T., et al., 1987, Nat 330, 230

Erickson E.F., et al., 1988, ApJ 330, L39

Epstein R.I., 1979, MNRAS 188, 305

Frail D.A., Kulkarni S.R., 1991, Nat 352, 785

Fryxell B.A., Müller E., Arnett W.D., 1989, MPA-Preprint 449, Max-Planck-Institut für Astrophysik, Garching

Fryxell B.A., Müller E., Arnett W.D., 1991, ApJ 367, 619

Gehrels N., Leventhal M., MacCallum C.J., 1988, in: Nuclear Spectroscopy of Astrophysical Sources, eds. N. Gehrels and G. Share, AIP, New York, p. 87

Guidry M.W., 1996, talk at the workshop of the 'European Centre for Theoretical Studies in Nuclear Physics' on Physics of Supernovae and Neutron Stars, Trento, Italy, June 3–14, 1996

Haas M.R., et al., 1990, ApJ 360, 257

Hachisu I., Matsuda T., Nomoto K., Shigeyama T., 1990, ApJ 358, L57

Hachisu I., Matsuda T., Nomoto K., Shigeyama T., 1991, ApJ 368, L27

Harrison P.A., Lyne A.G., Anderson B., 1993, MNRAS 261, 113

Herant M., Benz W., 1991, ApJ 345, L412

Herant M., Benz W., 1992, ApJ 387, 294

Herant M., Benz W., Colgate S.A., 1992, ApJ 395, 642

Herant M., Benz W., Hix W.R., Fryer C.L., Colgate S.A., 1994, ApJ 435, 339

Hillebrandt W., 1987, in: High Energy Phenomena Around Collapsed Stars, NATO ASI C195, ed. F. Pacini, Reidel, Dodrecht, p. 73

Hirata K., et al., 1987, Phys. Rev. Lett. 58, 1490 (Kamiokande II collaboration)

Hoffman R.D., Woosley S.E., Fuller G.M., Meyer B.S., 1996, ApJ 460, 478

Janka H.-Th., 1993, in: Frontier Objects in Astrophysics and Particle Physics, eds. F. Giovannelli and G. Mannocchi, Società Italiana di Fisica, Bologna, p. 345

Janka H.-Th., 1995, in: Proc. of the Workshop on Astro-Particle Physics of the Sonderforschungsbereich 375, Ringberg Castle, Tegernsee, March 6–10, 1995, eds. A. Weiss, G. Raffelt, W. Hillebrandt, F. von Feilitzsch, Technische Universität München, p. 154

Janka H.-Th., Müller E., 1993, in: Frontiers of Neutrino Astrophysics, eds. Y. Suzuki and K. Nakamura, Universal Academy Press, Tokyo, p. 203

Janka H.-Th., Müller E., 1994, A&A 290, 496

Janka H.-Th., Müller E., 1995a, ApJ 448, L109

Janka H.-Th., Müller E., 1995b, Ann. N.Y. Acad. Sci. 759, 269

Janka H.-Th., Müller E., 1996, A&A 306, 167

Janka H.-Th., Keil W., Raffelt G., Seckel D., 1996, Phys. Rev. Lett. 76, 2621

Keil W., 1996, Ph.D. Thesis, TU München (in preparation)

Keil W., Janka H.-Th., 1995, A&A 296, 145

Keil W., Janka H.-Th., Müller E., 1996, MPA-preprint 971, ApJL, in press

Keil W., Janka H.-Th., Raffelt G., 1995, Phys. Rev. D 51, 6635

Lattimer J.M., Swesty F.D., 1991, Nucl. Phys. A535, 331

Li H., McCray R., Sunyayev R.A., 1993, ApJ 419, 824

Lyne A.G., Lorimer D.R., 1994, Nat 369, 127

Mahoney W.A., et al., 1988, ApJ 334, L81

Matz S.M., et al., 1988, Nat 331, 416

Mayle R.W., Wilson J.R., 1988, ApJ 334, 909

McLaughlin G.C., Fuller G.M., Wilson J.R., 1996, ApJ, in press

Miller D.S., Wilson J.R., Mayle R.W., 1993, ApJ 415, 278

Müller E., 1993, in: Proc. of the 7th Workshop on Nuclear Astrophysics (Ringberg Castle, March 22-27, 1993), eds. W. Hillebrandt and E. Müller, Report MPA/P7, Max-Planck-Institut für Astrophysik, Garching, p. 27

Müller E., Fryxell B.A., Arnett W.D., 1991, in: ESO/EIPC Workshop on SN 1987A and other Supernovae, ESO Workshop and Conference Proceedings No. 37, eds. I.J. Danziger and K. Kjär, ESO, Garching, p. 99

Müller E., Janka H.-Th., 1994, in: Reviews in Modern Astronomy 7, Proceedings of the International Scientific Conference of the AG (Bochum, Germany, 1993), ed. G. Klare, Astronomische Gesellschaft, Hamburg, p. 103

Qian Y.-Z., Woosley S.E., 1996, ApJ, in press

Raffelt G., Seckel D., 1991, Phys. Rev. Lett. 67, 2605

Rank D.M., 1988, et al., Nat 331, 505

Sandie W.G., et al., 1988, ApJ 334, L91

Shigeyama T., Nomoto K., 1990, ApJ 360, 242

Shigeyama T., Nomoto K., Hashimoto M., 1988, A&A 196, 141

Shimizu T., Yamada S., Sato K., 1993, PASJ 45, L53

Shimizu T., Yamada S., Sato K., 1994, ApJ 432, L119

Sigl G., 1996, Phys. Rev. Lett. 76, 2625

Spyromilio J., Meikle W.P.S., Allen D.A., 1990, MNRAS 242, 669

Stewart R.T., Caswell J.L., Haynes R.F., Nelson G.J., 1993, MNRAS 261, 593

Sumiyoshi K., Suzuki H., Toki H., 1995, A&A 303, 475

Sunyaev R.A., et al., 1987, Nat 330, 227

Suzuki H., 1989, Ph.D. Thesis, Univ. of Tokyo

Takahashi K., Witti J., Janka H.-Th., 1994, A&A 286, 857

Taylor J.H., Manchester R.N., Lyne A.G., 1993, ApJS 88, 529

Teegarden B.J., et al., 1989, Nat 339, 122

Tueller J., et al., 1990, ApJ 351, L41

Wilson J.R., Mayle R.W., 1988, Phys. Rep. 163, 63

Wilson J.R., Mayle R.W., 1989, in: The Nuclear Equation of State, Part A, eds. W. Greiner and H. Stöcker, Plenum Press, New York, p. 731

Wilson J.R., R.W. Mayle, 1993, Phys. Rep. 227, 97

Wilson R.B., et al., 1988, in: Nuclear Spectroscopy of Astrophysical Sources, eds. N. Gehrels and G. Share, AIP, New York, p. 66

Witteborn F., et al., 1989, ApJ 338, L9

Witti J., Janka H.-Th., Takahashi K., 1994, A&A 286, 841

Woosley S.E., 1988, ApJ 330, 218

Woosley S.E., Hoffman R.D., 1992, ApJ 395, 202

Woosley S.E., Pinto P.A., Ensman L., 1988, ApJ 324, 466

Woosley S.E., Wilson J.R., Mathews G.J., Hoffman R.D., Meyer B.S., 1994, ApJ 433, 229

Yamada Y., Nakamura T., Oohara K., 1990, Prog. Theor. Phys. 84, 436

Yamada S., Shimizu T., Sato K., 1993, Prog. Theor. Phys. 89, 1175

Zürich University ZU-TH 21/96

NEUTRINOS AND DARK MATTER IN GALACTIC HALOS [1]

Philippe Jetzer

Paul Scherrer Institute, Laboratory for Astrophysics, CH-5232 Villigen PSI, and
Institute of Theoretical Physics, University of Zürich, Winterthurerstrasse 190,
CH-8057 Zürich, Switzerland

Abstract

One of the most important problems in astrophysics concerns the nature of the dark matter in galactic halos, whose presence is implied mainly by the observed flat rotation curves in spiral galaxies. Due to the Pauli exclusion principle it can be shown that neutrinos cannot be a major constituent of the halo dark matter. As far as cold dark matter is concerned there might be a discrepancy between the results of the N-body simulations and the measured rotation curves for dwarf galaxies. A fact this, if confirmed, which would exclude cold dark matter as a viable candidate for the halo dark matter.

In the framework of a baryonic scenario the most plausible candidates are brown or white dwarfs and cold molecular clouds (mainly of H_2). The former can be detected with the ongoing microlensing experiments. In fact, the French collaboration EROS and the American-Australian collaboration MACHO have reported the observation of altogether $\sim$ 10 microlensing events by monitoring during several years the brightness of millions of stars in the Large Magellanic Cloud. In particular, the MACHO team announced the discovery of 8 microlensing candidates by analysing their first 2 years of observations. This would imply that the halo dark matter fraction in form of MACHOs (Massive Astrophysical Compact Halo Objects) is of the order of 45-50% assuming a standard spherical halo model. The most accurate way to get information on the mass of the MACHOs is to use the method of mass moments, which leads to an average mass of $0.27 M_{\odot}$.

[1] Invited lecture to appear in the proceedings of the Zuoz Summer School on Physics with neutrinos (Zuoz, 4-10 August 1996)

1 Introduction

One of the most important problems in astrophysics concerns the nature of the dark matter in galactic halos, whose presence is implied by the observed flat rotation curves in spiral galaxies [1, 2], the X-ray diffuse emission in elliptical galaxies as well as by the dynamics of galaxy clusters. Primordial nucleosynthesis entails that most of the baryonic matter in the Universe is nonluminous, and such an amount of dark matter falls suspiciously close to that required by the rotation curves. Surely, the standard model of elementary particle forces can hardly be viewed as the ultimate theory and all the attempts in that direction invariably call for new particles. Hence, the idea of nonbaryonic dark matter naturally enters the realm of cosmolgy and may help in the understanding of the process of galaxy formation and clustering of galaxies.

The problem of dark matter started already with the pioneering work of Oort [3] in 1932 and Zwicky [4] in 1933 and its mistery is still not solved. Actually, there are several dark matter problems on different scales ranging from the solar neighbourhood, galactic halos, cluster of galaxies to cosmological scales. Dark matter is also needed to understand the formation of large scale structures in the universe.

Many candidates have been proposed, either baryonic or not, to explain dark matter. It is beyond the scope of this lecture to go through all of these candidates. Here, we restrict ourself to the dark matter in galactic halos, and in particular in the halo of our own Galaxy. First, we review the evidence for dark matter near the Sun and in the halo of spiral galaxies. In Section 3 we discuss the constraint due to the Pauli exclusion principle on neutrinos as a candidate for halo dark matter. Based on that argument neutrinos can practically be excluded as a major constituent of the dark galactic halos. In Section 4 we present the baryonic candidates and in Section 5 we elaborate in some detail on the detection of MACHOs (Massive Astrophysical Compact Halo Objects) through microlensing as well as on the most recent observations. Section 6 is devoted to a scenario in which part of the dark matter is in the form of cold molecular clouds (mainly of H_2).

2 Evidence for dark matter

In this Section we briefly outline the evidence for dark matter in the solar neighbourhood and in the halos of spiral galaxies. Moreover, we discuss also the total mass of our Galaxy, which can be inferred from studies of the proper motion of the satellites of the Milky Way.

2.1 Dark matter near the Sun

The local mass density [5] in main sequence and giant stars, stellar remnants (directly observed or inferred from models of galactic and stellar evolution), gas and dust yields a lower limit to the total density of $\rho \simeq 0.114\ M_\odot\ \mathrm{pc}^{-3}$. Correspondingly, one finds a mass-to-light ratio of

$$\Upsilon \simeq 1.7 \Upsilon_\odot \tag{1}$$

($\Upsilon_\odot = M_\odot/L_\odot$, where $M_\odot$ is the mass and $L_\odot$ the luminosity of the Sun, respectively). The local mass density is determined from carefully selected star samples by analyzing the

velocity dispersion and density profile in the direction normal to the galactic plane. This yields a total density $\rho = 0.18 \pm 0.03\ M_\odot\ \mathrm{pc}^{-3}$ for the local matter, or equivalently

$$\Upsilon \simeq 2.7 \Upsilon_\odot\ . \tag{2}$$

Therefore, at least $0.03\ M_\odot\ \mathrm{pc}^{-3}$ is the contribution from dark matter. The presence of disk dark matter has long been suspected [3] and it is most likely baryonic.

Recently, at least 8 brown dwarfs have been detected within a distance of about 100 light years from the Sun. One of these brown dwarfs is about 70 million years old and has an estimated mass of $0.065\ M_\odot$. Moreover, some brown dwarfs have been found orbiting brighter compagnons, and other as free flying in the Pleiades cluster. It is still premature to infer on their contribution to the local dark matter, although it is plausible that they may make up an important fraction, if not all.

2.2 Rotation curves of spiral galaxies

The best evidence for dark matter in galaxies comes from the rotation curves of spirals. Measurements of the rotation velocity v_{rot} of stars up to the visible edge of the spiral galaxies and of HI gas in the disk beyond the optical radius (by measuring the Doppler shift in the 21-cm line) imply that $v_{rot} \approx$ constant out to very large distances, rather than to show a Keplerian falloff. These observations started around 1970 [6], thanks to the improved sensitivity in both optical and 21-cm bands. By now there are observations for over thousand spiral galaxies with reliable rotation curves out to large radii [7]. In almost all of them the rotation curve is flat or slowly rising out to the last measured point. Very few galaxies show falling rotation curves and those that do either fall less rapidly than Keplerian have nearby companions that may perturb the velocity field or have large spheroids that may increase the rotation velocity near the centre.

One of the best exemple for the measurement of the rotation velocity is the spiral galaxy NGC 3198 [8] (see Fig. 1). Its halo density can be fitted by the following formula

$$\rho(r) = \frac{\rho_0}{1 + (r/a)^\gamma}\ , \tag{3}$$

where $\rho_0 = 0.013 h_0^2\ M_\odot\ \mathrm{pc}^{-3}$ (h_0 being the Hubble constant in units of $H_0 = 100 h_0$ km s^{-1} kpc^{-1}, and $0.4 \leq h_0 \leq 1$), $a = 6.4 h_0^{-1}$ kpc, and $\gamma = 2.1$. The total mass inside the last measured point of the rotation curve is $1.1 \times 10^{11} h_0^{-1} M_\odot$, which yields a total mass-to-light-ratio $\Upsilon = 28 h_0 \Upsilon_\odot$. This has to be considered as a lower limit, since there is certainly still a lot of dark matter beyond the last measured point on the rotation curve. The dark halo is at least four times as massive as the disk. Such a value for the mass-to-light-ratio is typical for spiral galaxies. Similar conclusions hold also for elliptical galaxies, although one cannot measure rotation velocities.

2.3 Mass of the Milky Way

There are also measurements of the rotation velocity for our Galaxy. However, these observations turn out to be rather difficult, and the rotation curve has been measured only up to a distance of about 20 kpc. Without any doubt our own galaxy has a typical flat

rotation curve. A fact this which imply that it is possible to search directly for dark matter characteristic of spiral galaxies in our own Milky Way.

In oder to infer the total mass one can also study the proper motion of the Magellanic Clouds and of other satellites of our Galaxy. Recent studies [9, 10, 11] do not yet allow an accurate determination of $v_{rot}(LMC)/v_0$ ($v_0 = 210 \pm 10$ km/s being the local rotational velocity). Lin et al. [10] analyzed the proper motion observations and concluded that within 100 kpc the Galactic halo has a mass $\sim 5.5 \pm 1 \times 10^{11} M_\odot$ and a substantial fraction $\sim 50\%$ of this mass is distributed beyond the present distance of the Magellanic Clouds of about 50 kpc. Beyond 100 kpc the mass may continue to increase to $\sim 10^{12} M_\odot$ within its tidal radius of about 300 kpc. This value for the total mass of the Galaxy is in agreement with the results of Zaritsky et al. [9], who found a total mass in the range 9.3 to 12.5 $\times 10^{11} M_\odot$, the former value by assuming radial satellite orbits whereas the latter by assuming isotropic satellite orbits.

The results of Lin et al. [10] suggest that the mass of the halo dark matter up to the Large Magellanic Cloud (LMC) is roughly half of the value one gets for the standard halo model (with flat rotation curve up to the LMC and spherical shape), implying thus the same reduction for the number of expected microlensing events. Kochanek [11] analysed the global mass distribution of the Galaxy adopting a Jaffe model, whose parameters are determined using the observations on the proper motion of the satellites of the Galaxy, the Local Group timing constraint and the ellipticity of the M31 orbit. With these observations Kochanek [11] concludes that the mass inside 50 kpc is $5.4 \pm 1.3 \times 10^{11} M_\odot$. This value becomes, however, slightly smaller when using only the satellite observations and the disk rotation constraint, in this case the median mass interior to 50 kpc is in the interval 3.3 to 6.1 (4.2 to 6.8) without (with) Leo I satellite in units of $10^{11} M_\odot$. The lower bound without Leo I is 65% of the mass expected assuming a flat rotation curve up to the LMC.

3 Neutrinos as halo dark matter

For stable neutrinos (with mass < 1 MeV) one gets the following cosmological upper bound on the sum of their masses [12, 13]

$$\sum_\nu m_\nu < 200 h_0^2 \; eV \; . \tag{4}$$

If neutrinos make up the dark matter in the galactic halos, we may decribe them as forming a bound system which resembles in the central regions to an isothermal gas sphere. The core radius of such an isothermal sphere is

$$r_c = \left(\frac{9\sigma^2}{4\pi G \rho_0} \right)^{1/2} \; , \tag{5}$$

where σ is the one-dimensional velocity dispersion and ρ_0 is the central density. The velocity distribution of the neutrinos is Maxwellian and the maximum phase-space density is

$$n_c = \frac{4.5}{(2\pi)^5 G \; r_c^2 \; \sigma \; m_\nu^4} \; . \tag{6}$$

The requirement that the maximum phase-space density does not violate the Pauli exclusion principle ($n_c < g_\nu/h^3$, where g_ν is the number of helicity states and h Planck's constant) leads then to the following lower limit for the neutrino mass [14] [2]

$$m_\nu > 120\ eV \left(\frac{100\ km\ s^{-1}}{\sigma}\right)^{1/4} \left(\frac{1\ kpc}{r_c}\right)^{1/2} g_\nu^{-1/4}\ . \tag{7}$$

Typical values for spiral galaxies are $\sigma \simeq 150$ km s^{-1} and $r_c \simeq 20$ kpc. This way we get a lower bound $m_\nu > 25 - 30$ eV [14, 15], which is still consistent with the cosmological bound eq.(4). See also refs. [16, 17] for a discussion of more precise bounds for spirals and ellipticals by considering different visible and dark matter distributions as well as the case where the neutrinos are not fully degenerate. However, when considering dwarf galaxies for which $r_c < 2$ kpc and $\sigma \sim 10 - 30$ km s^{-1} one gets $m_\nu > 100 - 500$ eV [18], which is clearly in contraddiction with the cosmological bound, excluding thus neutrinos as dark matter candidate for the halo of dwarf galaxies and in turn of spiral galaxies.

This latter point follows also from considering the dwarf galaxies Draco and Ursa Minor, which are both satellites of our Galaxy [19] and, therefore, are located in its halo. In fact, if their dark matter halo consist of neutrinos with mass ~ 30 eV, then $r_c \sim 10$ kpc and the total mass would be $\sim 4 \times 10^{11}\ M_\odot$. However, such a high value for the total mass can be excluded by the requirement that the dynamical friction time for such a satellite galaxy moving in the halo of our Galaxy has to be longer than the age of Galaxy $\sim 10^{10}$ yr. The upper value for the total mass one infers this way is of the order of $10^{10}\ M_\odot$. Therefore, one gets a lower limit of ~ 80 eV for the neutrino mass.

4 Baryonic dark matter

Before discussing the baryonic dark matter we would like to mention that another class of candidates which is seriously taken into consideration is the so-called cold dark matter, which consists for instance of axions or supersymmetric particles like neutralinos [20]. Here, we will not discuss cold dark matter in detail. However, recent studies seem to point out that there is a discrepancy between the calculated (through N-body simulations) rotation curve for dwarf galaxies assuming an halo of cold dark matter and the measured curves [21, 22]. If this fact is confirmed, this would exclude cold dark matter as a major constituent of the halo of dwarf galaxies and possibly also of spiral galaxies.

From the Big Bang nucleosynthesis model [23, 24] and from the observed abundances of primordial elements one infers: $0.010 \leq h_0^2 \Omega_B \leq 0.016$ or with $h_0 \simeq 0.4 - 1$ one gets $0.01 \leq \Omega_B \leq 0.10$ (where $\Omega_B = \rho_B/\rho_{crit}$, and $\rho_{crit} = 3H_0^2/8\pi G$). Since for the amount of luminous baryons one finds $\Omega_{lum} \ll \Omega_B$, it follows that an important fraction of the baryons are dark. In fact the dark baryons may well make up the entire dark halo matter.

The halo dark matter cannot be in the form of hot ionized hydrogen gas otherwise there would be a large X-ray flux, for which there are stringent upper limits. The abundance of neutral hydrogen gas is inferred from the 21-cm measurements, which show that its contribution is small. Another possibility is that the hydrogen gas is in molecular form clumped

[2] One gets a slightly higher bound, by a factor $2^{1/4}$, using the fact that neutrinos behaves practically as collisionless particles and thus by applying Liouville's theorem [14].

into cold clouds, as we will discuss in some detail in Section 6. Baryons could otherwise have been processed in stellar remnants (for a detailed discussion see [25]). If their mass is below $\sim 0.08\ M_\odot$ they are too light to ignite hydrogen burning reactions. The possible origin of such brown dwarfs or Jupiter like bodies (called also MACHOs), by fragmentation or by some other mechanism, is at present not understood. It has also been pointed out that the mass distribution of the MACHOs, normalized to the dark halo mass density, could be a smooth continuation of the known initial mass function of ordinary stars [26]. The ambient radiation, or their own body heat, would make sufficiently small objects of H and He evaporate rapidly. The condition that the rate of evaporation of such a hydrogenoid sphere be insufficient to halve its mass in a billion years leads to the following lower limit on their mass [26]: $M > 10^{-7} M_\odot (T_S/30\ K)^{3/2} (1\ g\ cm^{-3}/\rho)^{1/2}$ (T_S being their surface temperature and ρ their average density, which we expect to be of the order $\sim 1\ g\ cm^{-3}$).

Otherwise, MACHOs might be either M-dwarfs or else white dwarfs. As a matter of fact, a deeper analysis shows that the M-dwarf option look problematic. The null result of several searches for low-mass stars both in the disk and in the halo of our galaxy suggest that the halo cannot be mostly in the form of hydrogen burning main sequence M-dwarfs. Optical imaging of high-latitude fields taken with the Wide Field Camera of the Hubble Space Telescope indicates that less than $\sim 6\%$ of the halo can be in this form [27]. Also a substantial component of neutron stars and black holes with mass higher than $\sim 1\ M_\odot$ is excluded, for otherwise they would lead to an overproduction of heavy elements relative to the observed abundances. A scenario with white dwarfs as a major constituent of the galactic halo dark matter has been explored [28]. However, it requires a rather ad hoc initial mass function sharply peaked around 2 - 6 $M_\odot$. Future Hubble deep field exposures could either find the white dwarfs or put constraints on their fraction in the halo [29].

5 Detection of MACHOs through microlensing

It has been pointed out by Paczyński [30] that microlensing allows the detection of MACHOs located in the galactic halo in the mass range [26] $10^{-7} < M/M_\odot < 1$. In September 1993 the French collaboration EROS [31] announced the discovery of 2 microlensing candidates and the American–Australian collaboration MACHO of one candidate [32]. In the meantime the MACHO team reported the observation of altogether 8 events (one of which is a binary lensing event) analyzing 2 years of their data by monitoring about 8.5 million of stars in the LMC [33]. Their analysis leads to an optical depth of $\tau = 2.9^{+1.4}_{-0.9} \times 10^{-7}$ and correspondingly to a halo MACHO fraction of the order of 45-50% and an average mass $0.5^{+0.3}_{-0.2} M_\odot$, under the assumption of a standard spherical halo model. It may well be that there is also a contribution of events due to MACHOs located in the LMC itself or in a thich disk of our galaxy, the corresponding optical depth is estimated to be $\tau = 5.4 \times 10^{-8}$ [33]. EROS has also searched for very-low mass MACHOs by looking for microlensing events with time scales ranging from 30 minutes to 7 days [34]. The lack of candidates in this range places significant constraints on any model for the halo that relies on objects in the range $5 \times 10^{-8} < M/M_\odot < 5 \times 10^{-4}$. Similar conclusions have been reached also by the MACHO team [33]. Moreover, the Polish-American team OGLE [35], the MACHO [36] and the French DUO [37] collaborations found altogether more than ~ 100 microlensing events by monitoring stars

located in the galactic bulge. The inferred optical depth for the bulge turns out to be higher than previously thought. These results are very important in order to study the structure of our Galaxy.

In the following we present the main features of microlensing, in particular its probability and the rate of events [38]. An important issue is the determination from the observations of the mass of the MACHOs that acted as gravitational lenses as well as the fraction of halo dark matter they make up. The most appropriate way to compute the average mass and other important information is to use the method of mass moments developed by De Rújula et al. [39], which will be briefly discussed in Section 5.4.

5.1 Microlensing probability

When a MACHO of mass M is sufficiently close to the line of sight between us and a more distant star, the light from the source suffers a gravitational deflection (see Fig. 2). The deflection angle is usually so small that we do not see two images but rather a magnification of the original star brightness. This magnification, at its maximum, is given by

$$A_{max} = \frac{u^2+2}{u(u^2+4)^{1/2}} \ . \tag{8}$$

Here $u = d/R_E$ (d is the distance of the MACHO from the line of sight) and the Einstein radius R_E is defined as

$$R_E^2 = \frac{4GMD}{c^2} x(1-x) \tag{9}$$

with $x = s/D$, and where D and s are the distance between the source, respectively the MACHO and the observer.

An important quantity is the optical depth τ_{opt} to gravitational microlensing defined as

$$\tau_{opt} = \int_0^1 dx \frac{4\pi G}{c^2} \rho(x) D^2 x(1-x) \tag{10}$$

with $\rho(x)$ the mass density of microlensing matter at distance $s = xD$ from us along the line of sight. The quantity τ_{opt} is the probability that a source is found within a radius R_E of some MACHO and thus has a magnification that is larger than $A = 1.34$ ($d \leq R_E$).

We calculate τ_{opt} for a galactic mass distribution of the form

$$\rho(\vec{r}) = \frac{\rho_0(a^2+R_{GC}^2)}{a^2+\vec{r}^2} \ , \tag{11}$$

$\mid \vec{r} \mid$ being the distance from the Earth. Here, a is the core radius, ρ_0 the local dark mass density in the solar system and R_{GC} the distance between the observer and the Galactic centre. Standard values for the parameters are $\rho_0 = 0.3\ GeV/cm^3 = 7.9\ 10^{-3} M_\odot/pc^3$, $a = 5.6\ kpc$ and $R_{GC} = 8.5\ kpc$. With these values we get, for a spherical halo, $\tau_{opt} = 0.7 \times 10^{-6}$ for the LMC and $\tau_{opt} = 10^{-6}$ for the SMC [40].

The magnification of the brightness of a star by a MACHO is a time-dependent effect. For a source that can be considered as pointlike (this is the case if the projected star radius at

the MACHO distance is much less than R_E) the light curve as a function of time is obtained by inserting

$$u(t) = \frac{(d^2 + v_T^2 t^2)^{1/2}}{R_E} \tag{12}$$

into eq.(8), where v_T is the transverse velocity of the MACHO, which can be inferred from the measured rotation curve ($v_T \approx 200\ km/s$). The achromaticity, symmetry and uniqueness of the signal are distinctive features that allow to discriminate a microlensing event from background events such as variable stars.

The behaviour of the magnification with time, $A(t)$, determines two observables namely, the magnification at the peak $A(0)$ - denoted by A_{max} - and the width of the signal T (defined as being $T = R_E/v_T$).

5.2 Microlensing rates

The microlensing rate depends on the mass and velocity distribution of MACHOs. The mass density at a distance $s = xD$ from the observer is given by eq.(11). The isothermal spherical halo model does not determine the MACHO number density as a function of mass. A simplifying assumption is to let the mass distribution be independent of the position in the galactic halo, i.e., we assume the following factorized form for the number density per unit mass dn/dM,

$$\frac{dn}{dM} dM = \frac{dn_0}{d\mu} \frac{a^2 + R_{GC}^2}{a^2 + R_{GC}^2 + D^2 x^2 - 2DR_{GC} x cos\alpha}\, d\mu = \frac{dn_0}{d\mu} H(x) d\mu\ , \tag{13}$$

with $\mu = M/M_\odot$ (α is the angle of the line of sight with the direction of the galactic centre), n_0 not depending on x and is subject to the normalization $\int d\mu \frac{dn_0}{d\mu} M = \rho_0$. Nothing a priori is known on the distribution dn_0/dM.

A different situation arises for the velocity distribution in the isothermal spherical halo model, its projection in the plane perpendicular to the line of sight leads to the following distribution in the transverse velocity v_T

$$f(v_T) = \frac{2}{v_H^2} v_T e^{-v_T^2/v_H^2}. \tag{14}$$

($v_H \approx 210\ km/s$ is the observed velocity dispersion in the halo).

In order to find the rate at which a single star is microlensed with magnification $A \geq A_{min}$, we consider MACHOs with masses between M and $M + \delta M$, located at a distance from the observer between s and $s + \delta s$ and with transverse velocity between v_T and $v_T + \delta v_T$. The collision time can be calculated using the well-known fact that the inverse of the collision time is the product of the MACHO number density, the microlensing cross-section and the velocity. The rate $d\Gamma$, taken also as a differential with respect to the variable u, at which a single star is microlensed in the interval $d\mu du dv_T dx$ is given by [39, 41]

$$d\Gamma = 2v_T f(v_T) D r_E [\mu x(1-x)]^{1/2} H(x) \frac{dn_0}{d\mu} d\mu du dv_T dx, \tag{15}$$

with

$$r_E^2 = \frac{4GM_\odot D}{c^2} \sim (3.2 \times 10^9 km)^2. \tag{16}$$

One has to integrate the differential number of microlensing events, $dN_{ev} = N_\star t_{obs} d\Gamma$, over an appropriate range for μ, x, u and v_T, in order to obtain the total number of microlensing events which can be compared with an experiment monitoring $N_\star$ stars during an observation time t_{obs} and which is able to detect a magnification such that $A_{max} \geq A_{TH}$. The limits of the u integration are determined by the experimental threshold in magnitude shift, Δm_{TH}: we have $0 \leq u \leq u_{TH}$.

The range of integration for μ is where the mass distribution $dn_0/d\mu$ is not vanishing and that for x is $0 \leq x \leq D_h/D$ where D_h is the extent of the galactic halo along the line of sight (in the case of the LMC, the star is inside the galactic halo and thus $D_h/D = 1$.) The galactic velocity distribution is cut at the escape velocity $v_e \approx 640\ km/s$ and therefore v_T ranges over $0 \leq v_T \leq v_e$. In order to simplify the integration we integrate v_T over all the positive axis, due to the exponential factor in $f(v_T)$ the so committed error is negligible.

However, the integration range of $d\mu du dv_T dx$ does not span all the interval we have just described. Indeed, each experiment has time thresholds T_{min} and T_{max} and only detects events with: $T_{min} \leq T \leq T_{max}$, and thus the integration range has to be such that T lies in this interval. The total number of micro-lensing events is then given by

$$N_{ev} = \int dN_{ev}\ \Theta(T - T_{min})\Theta(T_{max} - T), \tag{17}$$

where the integration is over the full range of $d\mu du dv_T dx$. T is related in a complicated way to the integration variables, because of this, no direct analytical integration in eq.(17) can be performed.

To evaluate eq.(17) we define an efficiency function $\epsilon_0(\mu)$ which measures the fraction of the total number of microlensing events that meet the condition on T at a fixed MACHO mass $M = \bar{\mu} M_\odot$. A more detailed analysis [39] shows that $\epsilon_0(\mu)$ is in very good approximation equal to unity for possible MACHO objects in the mass range of interest here. We now can write the total number of events in eq.(17) as

$$N_{ev} = \int dN_{ev}\ \epsilon_0(\mu). \tag{18}$$

Due to the fact that ϵ_0 is a function of μ alone, the integration in $d\mu du dv_T dx$ factorizes into four integrals with independent integration limits.

In order to quantify the expected number of events it is convenient to take as an example a delta function distribution for the mass. The rate of microlensing events with $A \geq A_{min}$ (or $u \leq u_{max}$), is then

$$\Gamma(A_{min}) = \tilde{\Gamma} u_{max} = D r_E u_{max} \sqrt{\pi}\ v_H \frac{\rho_0}{M_\odot} \frac{1}{\sqrt{\bar{\mu}}} \int_0^1 dx [x(1-x)]^{1/2} H(x)\ . \tag{19}$$

Inserting the numerical values for the LMC (D=50 kpc and $\alpha = 82^0$) we get

$$\tilde{\Gamma} = 4 \times 10^{-13}\ \frac{1}{s} \left(\frac{v_H}{210\ km/s}\right) \left(\frac{1}{\sqrt{D/kpc}}\right) \left(\frac{\rho_0}{0.3\ GeV/cm^3}\right) \frac{1}{\sqrt{M/M_\odot}}\ . \tag{20}$$

For an experiment monitoring $N_\star$ stars during an observation time t_{obs} the total number of events with a magnification $A \geq A_{min}$ is: $N_{ev}(A_{min}) = N_\star t_{obs} \Gamma(A_{min})$. In the following Table

1 we show some values of N_{ev} for the LMC, taking $t_{obs} = 10^7$ s ($\sim$ 4 Months), $N_\star = 10^6$ stars and $A_{min} = 1.34$ (or $\Delta m_{min} = 0.32$).

Table 1

MACHO mass in units of $M_\odot$	Mean R_E in km	Mean microlensing time	N_{ev}
10^{-1}	0.3×10^9	1 month	1.5
10^{-2}	10^8	9 days	5
10^{-4}	10^7	1 day	55
10^{-6}	10^6	2 hours	554

Gravitational microlensing could also be useful for detecting MACHOs in the halo of nearby galaxies [42, 43] such as M31 or M33, for which experiments are under way. In fact, it turns out that the massive dark halo of M31 has an optical depth to microlensing which is of about the same order of magnitude as that of our own galaxy $\sim 10^{-6}$ [42, 44]. Moreover, an experiment monitoring stars in M31 would be sensitive to both MACHOs in our halo and in the one of M31. One can also compute the microlensing rate [44] for MACHOs in the halo of M31, for which we get

$$\tilde{\Gamma} = 1.8 \times 10^{-12} \frac{1}{s} \left(\frac{v_H}{210\ km/s} \right) \left(\frac{1}{\sqrt{D/kpc}} \right) \left(\frac{\rho(0)}{1\ Gev/cm^3} \right) \frac{1}{\sqrt{M/M_\odot}} \ . \qquad (21)$$

($\rho(0)$ is the central density of dark matter.) In the following Table 2 we show some values of N^a_{ev} due to MACHOs in the halo of M31 with $t_{obs} = 10^7$ s and $N_\star = 10^6$ stars. In the last column we give the corresponding number of events, N_{ev}, due to MACHOs in our own halo. The mean microlensing time is about the same for both types of events.

Table 2

MHO mass in units of $M_\odot$	Mean R_E in km	Mean microlensing time	N^a_{ev}	N_{ev}
10^{-1}	7×10^8	38 days	2	1
10^{-2}	2×10^8	12 days	7	4
10^{-4}	2×10^7	30 hours	70	43
10^{-6}	2×10^6	3 hours	700	430

Of course these numbers should be taken as an estimate, since they depend on the details of the model one adopts for the distribution of the dark matter in the halo.

5.3 Most probable mass for a single event

The probability P that a microlensing event of duration T and maximum amplification A_{max} be produced by a MACHO of mass μ (in units of $M_\odot$) is given by [45]

$$P(\mu, T) \propto \frac{\mu^2}{T^4} \int_0^1 dx (x(1-x))^2 H(x) exp\left(-\frac{r_E^2 \mu x(1-x)}{v_H^2 T^2} \right) \ , \qquad (22)$$

which does not dependent on A_{max} and $P(\mu, T) = P(\mu/T^2)$. The measured values for T are listed in Table 3, where μ_{MP} is the most probable value. We find that the maximum corresponds to $\mu r_E^2/v_H^2 T^2 = 13.0$ [45, 46]. The 50% confidence interval embraces for the mass μ approximately the range $1/3\mu_{MP}$ up to $3\mu_{MP}$. Similarly one can compute $P(\mu, T)$ also for the bulge events (see [46]).

Table 3: Values of μ_{MP} (in $M_\odot$) for eight microlensing events detected in the LMC (A_i = American-Australian collaboration events (i = 1,..,6); F_1 and F_2 French collaboration events). For the LMC: $v_H = 210$ km s^{-1} and $r_E = 3.17 \times 10^9$ km.

	A_1	A_2	A_3	A_4	A_5	A_6	F_1	F_2
T (days)	17.3	23	31	41	43.5	57.5	27	30
$\tau(\equiv \frac{v_H}{r_E}T)$	0.099	0.132	0.177	0.235	0.249	0.329	0.155	0.172
μ_{MP}	0.13	0.23	0.41	0.72	0.81	1.41	0.31	0.38

5.4 Mass moment method

A more systematic way to extract information on the masses is to use the method of mass moments [39]. The mass moments $< \mu^m >$ are defined as

$$< \mu^m >= \int d\mu \; \epsilon_n(\mu) \; \frac{dn_0}{d\mu} \mu^m \; . \tag{23}$$

$< \mu^m >$ is related to $< \tau^n >= \sum_{events} \tau^n$, with $\tau \equiv (v_H/r_E)T$, as constructed from the observations and which can also be computed as follows

$$< \tau^n >= \int dN_{ev} \; \epsilon_n(\mu) \; \tau^n = V u_{TH} \Gamma(2-m) \widehat{H}(m) < \mu^m > \; , \tag{24}$$

with $m \equiv (n+1)/2$ and

$$V \equiv 2 N_\star t_{obs} \; D \; r_E \; v_H = 2.4 \times 10^3 \; pc^3 \; \frac{N_\star \; t_{obs}}{10^6 \; \text{star} - \text{years}} \; , \tag{25}$$

$$\Gamma(2-m) \equiv \int_0^\infty \left(\frac{v_T}{v_H}\right)^{1-n} f(v_T) dv_T \; , \tag{26}$$

$$\widehat{H}(m) \equiv \int_0^1 (x(1-x))^m H(x) dx \; . \tag{27}$$

The efficiency $\epsilon_n(\mu)$ is determined as follows (see [39])

$$\epsilon_n(\mu) \equiv \frac{\int dN^\star_{ev}(\bar{\mu}) \; \epsilon(T) \; \tau^n}{\int dN^\star_{ev}(\bar{\mu}) \; \tau^n} \; , \tag{28}$$

where $dN^\star_{ev}(\bar{\mu})$ is defined as dN_{ev} in eq.(17) with the MACHO mass distribution concentrated at a fixed mass $\bar{\mu}$: $dn_0/d\mu = n_0 \; \delta(\mu - \bar{\mu})/\mu$. $\epsilon(T)$ is the experimental detection efficiency. For a more detailed discussion on the efficiency see ref. [47].

A mass moment $< \mu^m >$ is thus related to $< \tau^n >$ as given from the measured values of T in a microlensing experiment by

$$< \mu^m >= \frac{< \tau^n >}{V u_{TH} \Gamma(2-m) \hat{H}(m)} \ . \tag{29}$$

The mean local density of MACHOs (number per cubic parsec) is $< \mu^0 >$. The average local mass density in MACHOs is $< \mu^1 >$ solar masses per cubic parsec. In the following we consider only 6 (see Table 3) out of the 8 events observed by the MACHO group, in fact the two events we neglect are a binary lensing event and an event which is rated as marginal. The mean mass, which we get from the six events detected by the MACHO team, is

$$\frac{< \mu^1 >}{< \mu^0 >} = 0.27 \ M_\odot \ . \tag{30}$$

(To obtain this result we used the values of τ as reported in Table 3, whereas $\Gamma(1)\widehat{H}(1) = 0.0362$ and $\Gamma(2)\widehat{H}(0) = 0.280$ as plotted in Fig. 6 of ref. [39]). If we include also the two EROS events we get a value of 0.26 $M_\odot$ for the mean mass. The resulting mass depends on the parameters used to describe the standard halo model. In order to check this dependence we varied the parameters within their allowed range and found that the average mass changes at most by $\pm$ 30%, which shows that the result is rather robust. Although the value for the average mass we find with the mass moment method is marginally consistent with the result of the MACHO team, it definitely favours a lower average MACHO mass.

One can also consider other models with more general luminous and dark matter distributions, e.g. ones with a flattened halo or with anisotropy in velocity space [48], in which case the resulting value for the average mass would decrease significantly. If the above value will be confirmed, then MACHOs cannot be brown dwarfs nor ordinary hydrogen burning stars, since for the latter there are observational limits from counts of faint red stars. Then white dwarfs are the most likely explanation. As mentioned in Section 4 such a scenario has been explored recently [28]. However, it has some problems, since it requires that the initial mass function must be sharply peaked around $2 - 6 \ M_\odot$. Given these facts, we feel that the brown dwarf option can still provide a sensible explanation of the observed microlensing events [49].

Another important quantity to be determined is the fraction f of the local dark mass density (the latter one given by ρ_0) detected in the form of MACHOs, which is given by $f \equiv M_\odot/\rho_0 \sim 126 \ \mathrm{pc}^3 < \mu^1 >$. Using the values given by the MACHO collaboration for their two years data [33] (in particular $u_{TH} = 0.661$ corresponding to $A > 1.75$ and an effective exposure $N_\star t_{obs}$ of $\sim 5 \times 10^6$ star-years for the observed range of the event duration T between $\sim$ 20 - 50 days) we find $f \sim 0.54$, which compares quite well with the corresponding value ($f \sim 0.45$ based on the six events we consider) calculated by the MACHO group in a different way. The value for f is obtained again by assuming a standard spherical halo model.

Table 4: Values of μ_{MP} (in $M_\odot$) as obtained by the corresponding $P(\mu, T)$ for eleven microlensing events detected by OGLE in the galactic bulge [47]. ($v_H = 30$ km s^{-1} and $r_E = 1.25 \times 10^9$ km.) (T is in days as above.)

	1	2	3	4	5	6	7	8	9	10	11
T	25.9	45	10.7	14	12.4	8.4	49.5	18.7	61.6	12	20.9
τ	0.054	0.093	0.022	0.029	0.026	0.017	0.103	0.039	0.128	0.025	0.043
μ_{MP}	0.61	1.85	0.105	0.18	0.14	0.065	2.24	0.32	3.48	0.13	0.40

Similarly, one can also get information from the events detected so far towards the galactic bulge. The mean MACHO mass, which one gets when considering the first eleven events detected by OGLE in the galactic bulge (see Table 4), is $\sim 0.29 M_\odot$ [46]. From the 40 events discovered during the first year of operation by the MACHO team [36] (we considered only the events used by the MACHO team to infer the optical depth without the double lens event) we get an average value of $0.16 M_\odot$. The lower value inferred from the MACHO data is due to the fact that the efficiency for the short duration events ($\sim$ some days) is substantially higher for the MACHO experiment than for the OGLE one. These values for the average mass suggest that the lens are faint disk stars.

Once several moments $< \mu^m >$ are known one can get information on the mass distribution $dn_0/d\mu$. Since at present only few events towards the LMC are at disposal the different moments (especially the higher ones) can be determined only approximately. Nevertheless, the results obtained so far are already of interest and it is clear that in a few years, due also to the new experiments under way (such as EROS II and OGLE II), it will be possible to draw more firm conclusions.

6 Dark clusters of MACHOs and cold molecular clouds

A major problem which arises is to explain the formation of MACHOs, as well as the nature of the remaining amount of dark matter in the galactic halo. We feel it hard to conceive a formation mechanism which transforms with 100% efficiency hydrogen and helium gas into MACHOs. Therefore, we expect that also cold clouds (mainly of H_2) should be present in the galactic halo. Recently, we have proposed a scenario [50, 51] in which dark clusters of MACHOs and cold molecular coulds naturally form in the halo at galactocentric distances larger than 10-20 kpc, where the relative abundance depends on the distance (similar ideas have also been developed in refs. [52, 53]). Our scenario can be summarized as follows.

After its initial collapse, the proto galaxy (PG) is expected to be shock heated to its virial temperature $\sim 10^6$ K. Since overdense regions cool more rapidly than average (by hydrogen recombination), proto globular cluster (PGC) clouds form in pressure equilibrium with diffuse gas. At this stage, the PGC cloud temperature is $\sim 10^4$ K, its mass and size are $\sim 10^6 (R/kpc)^{1/2} M_\odot$ and $\sim 10\ (R/kpc)^{1/2}$ pc, respectively. The subsequent evolution of the PGC clouds will be different in the inner and outer part of the galaxy, depending on the decreasing collision rate and ultraviolet (UV) fluxes as the galactocentric distance increases. Below 10^4 K, the main coolants are H_2 molecules and any heavy element produced in a first chaotic galactic phase. In the central region of the galaxy an Active Galactic Nucleus and/or a first population of massive stars are expected to exist, which act as strong sources

of UV radiation that dissociates the H_2 molecules present in the inner part of the halo. As a consequence, cooling is heavily suppressed and so inner PGC clouds remain for a long time at temperature $\sim 10^4$ K, resulting in the imprinting of a characteristic mass $\sim 10^6 M_\odot$. Later on, the cloud temperature suddenly drops below 10^4 K and the subsequent evolution leads to the formation of stars and ultimately to stellar globular clusters. In the outer regions of the halo the UV-flux is suppressed, so that no substantial H_2 depletion actually happens. This fact has three distinct implications: (*i*) no imprinting of a characteristic PGC cloud mass shows up, (*ii*) the Jeans mass can now be lower than $10^{-1} M_\odot$, (*iii*) the cooling time is much shorter than the collision time. PGC clouds subsequently fragment into smaller clouds that remain optically thin until the minimum value of the Jeans mass is attained, thus leading to MACHO formation in dark clusters. Moreover, because the conversion efficiency of the constituent gas in MACHOs could scarcely have been 100%, we expect the remaining fraction of the gas to form self-gravitating molecular clouds, since, in the absence of strong stellar winds, the surviving gas remains bound in the dark cluster, but not in diffuse form as in this case the gas would be observable in the radio band.

6.1 Observational Tests

Let us now address the possible signatures of the above scenario, in addition to the single MACHO detection via microlensing.

We proceed to estimate the γ-ray flux produced in molecular clouds through the interaction with high-energy cosmic-ray protons. Cosmic rays scatter on protons in the molecules producing π^0's, which subsequently decay into γ's. An essential ingredient is the knowledge of the cosmic ray flux in the halo. Unfortunately, this quantity is experimentally unknown and the only available information comes from theoretical estimates. More precisely, from the mass-loss rate of a typical galaxy we infer a total cosmic ray flux in the halo $F \simeq 1.1 \times 10^{-4}$ erg cm^{-2} s^{-1}. We also need the energy distribution of the cosmic rays, for which we assume the same energy dependence as measured on the Earth. We then scale the overall density in such a way that the integrated energy flux agrees with the above value. Moreover, we assume that the cosmic ray density scales as R^{-2} for large galactocentric distance R. Accordingly, we obtain [50, 51]

$$\Phi_{CR}(E,R) \simeq 1.9 \times 10^{-3}\, \Phi_{CR}^{\oplus}(E)\, \frac{a^2 + R_{GC}^2}{a^2 + R^2}\ , \tag{31}$$

where $\Phi_{CR}^{\oplus}(E)$ is the measured primary cosmic ray flux on the Earth, $a \sim 5$ kpc is the halo core radius and $R_{GC} \sim 8.5$ kpc is our distance from the galactic center. The source function $q_\gamma(r)$, which gives the photon number density at distance r from the Earth, is

$$q_\gamma(r) = \frac{4\pi}{m_p} \rho_{H_2}(r) \int dE_p\ \Phi_{CR}(E_p, R(r))\ \sigma_{in}(p_{lab}) < n_\gamma(E_p) >\ . \tag{32}$$

Actually, the cosmic ray protons in the halo which originate from the galactic disk are mainly directed outwards. This circumstance implies that the induced photons will predominantly leave the galaxy. However, the presence of magnetic fields in the halo might give rise to a temporary confinement of the cosmic ray protons similarly to what happens in the disk. In addition, there could also be sources of cosmic ray protons located in the halo itself, as for instance isolated or binary pulsars in globular clusters. As we are unable to give

a quantitative estimate of the above effects, we take them into account by introducing an efficiency factor ϵ, which could be rather small. In this way, the γ-ray photon flux reaching the Earth is obtained by multiplying $q_\gamma(r)$ by $\epsilon/4\pi r^2$ and integrating the resulting quantity over the cloud volume along the line of sight.

The best chance to detect the γ-rays in question is provided by observations at high galactic latitude. Therefore we find

$$\Phi_\gamma(90^0) \simeq \epsilon f \; 3.5 \times 10^{-6} \; \frac{\text{photons}}{\text{cm}^2 \text{ s sr}} \; . \tag{33}$$

The inferred upper bound for γ-rays in the 0.8 - 6 GeV range at high galactic latitude is 3×10^{-7} photons cm^{-2} s^{-1} sr^{-1} [54]. Hence, we see from eq. (33) that the presence of halo molecular clouds does not lead nowadays to any contradiction with such an upper limit, provided $\epsilon f < 10^{-1}$.

Molecular clouds can be detected via the anisotropy they would introduce in the Cosmic Background Radiation (CBR), even if the ratio of the temperature excess of the clouds to the CBR temperature is less than $\sim 10^{-3}$. Consider molecular clouds in M31. Because we expect they have typical rotational speeds of $50 - 100$ km s^{-1}, the Doppler shift effect will show up as an anisotropy in the CBR. The corresponding anisotropy is then [55]

$$\frac{\Delta T}{T_r} = \pm \frac{v}{c} \; S \; f \; \tau_\nu \; , \tag{34}$$

where S is the spatial filling factor and T_r is the CBR temperature. If the clouds are optically thick only at some frequencies, one can use the average optical depth over the frequency range of the detector $\bar{\tau}$. We estimate the expected CBR anisotropy between two fields of view (on opposite sides of M31) separated by $\sim 4^0$ and with angular resolution of $\sim 1^0$. Supposing that the halo of M31 consists of $\sim 10^6$ dark clusters and that all of them lie between 25 kpc and 35 kpc, we would be able to detect $10^3 - 10^4$ dark clusters per degree square. Scanning an annulus of 1^0 width and internal angular diameter 4^0, centered at M31, in 180 steps of 1^0, we would find anisotropies of $\sim 2 \times 10^{-5} \; f \; \bar{\tau}$ in $\Delta T/T_r$ (as now $S = 1/25$). In conclusion, the theory does not permit to establish whether the expected anisotropy lies above or below current detectability ($\sim 10^{-6}$), and so only observations can resolve this issue.

An attractive strategy to discover the halo molecular clouds clumped into dark clusters relies upon the absorption lines they would introduce in the spectrum of a LMC star [56].

Let us now turn to the possibility of detecting MACHOs in M31 via their infrared emission. For simplicity, we assume all MACHOs have equal mass $\sim 0.08 \; M_\odot$ (which is the upper mass limit for brown dwarfs) and make up the fraction f of the dark matter in M31. In addition, we suppose that all MACHOs have the same age $t \sim 10^{10}$ yr [57]. As a consequence, MACHOs emit most of their radiation at the wavelength $\lambda_{max} \sim 2.6$ μm. The infrared surface brightness $I_\nu(b)$ of the M31 dark halo as a function of the projected separation b (impact parameter) is given by

$$I_\nu(b) \sim 5 \times 10^5 \frac{x^3}{e^x - 1} \frac{a^2 \; f}{D\sqrt{a^2 + b^2}} \arctan \sqrt{\frac{L^2 - b^2}{a^2 + b^2}} \;\; \text{Jy sr}^{-1}, \tag{35}$$

where the M31 dark halo radius is taken to be $L \sim 50$ kpc. Some numerical values of $I_{\nu_{max}}(b)$ with $b = 20$ and 40 kpc are $\sim 1.6 \times 10^3 \; f$ Jy sr^{-1} and $\sim 0.4 \times 10^3 \; f$ Jy sr^{-1}, respectively.

The planned SIRTF Satellite contains an array camera with expected sensitivity of $\sim 1.7 \times 10^3$ Jy sr^{-1} per spatial resolution element in the wavelength range 2-6 μm. Therefore, the MACHOs in the halo of M31 can, hopefully, be detected in the near future.

7 Conclusions

The mistery of the dark matter is still unsolved, however, thanks to the ongoing microlensing experiments there is hope that progress on its nature in the galactic halo can be achieved within the next few years. It is well plausible that only a fraction of the halo dark matter is in form of MACHOs, either brown dwarfs or white dwarfs, in which case there is the problem of explaining the nature of the remaining dark matter and the formation of the MACHOs. Before invoking the need for new particles as galactic dark matter candidates for the remaining fraction, one should seriously consider the possibility that it is in the form of cold molecular clouds. A scenario this, for which several observational tests have been proposed, thanks to which it should be feasible in the near future to either detect or to put stringent limits on these clouds.

I would like to thank F. De Paolis for carefully reading the manuscript.

References

[1] S.M. Faber and J.S. Gallagher, Ann. Rev. Astron. Astrophys. **17** (1979) 135

[2] V. Trimble, Ann. Rev. Astron. Astrophys. **25** (1987) 425

[3] J.H. Oort, Bull. Astron. Inst. Netherlands **6** (1932) 249

[4] F. Zwicky, Helv. Phys. Acta **6** (1933) 110

[5] J.J. Binney and S.T. Tremaine, Galactic Dynamics (Princeton University Press) 1987

[6] V.C. Rubin and W.K. Ford, Astrophys. J. **159** (1970) 379

[7] M. Persic, P. Salucci and F. Stel, Mont. Not. R. Astr. Soc. **281** (1996) 27

[8] T.S. van Albada, J.N. Bahcall, K. Begeman and R. Sancisi, Astrophys. J. **295** (1985) 305

[9] D. Zaritsky et al., Astrophys. J. **345** (1989) 759

[10] D.N. Lin, B.F. Jones and A.R. Klemola, Astrophys. J. **439** (1995) 652

[11] C.S. Kochanek, Astrophys. J. **457** (1996) 228

[12] S.S. Gerstein and Y.B. Zeldovich, Zh. Exsp. Teor. Fiz. Pis'ma Lett. **4** (1966) 174

[13] R. Cowsik and J. McClelland, Phys. Rev. Lett. **29** (1972) 669

[14] S. Tremaine and J.E. Gunn, Phys. Rev. Lett. **42** (1979) 407

[15] R. Paganini, N. Straumann and D. Wyler, Astron. and Astrophys. **177** (1987) 84

[16] G. Ingrosso, M. Merafina, R. Ruffini and F. Strafella, Astron. and Astrophys. **258** (1992) 223

[17] F. De Paolis, G. Ingrosso and F. Strafella, Astrophys. J. **438** (1995) 83

[18] S.M. Faber and D.C. Lin, Astrophys. J. **266** (1983) L21

[19] O. Gerhard and D. Spergel, Astrophys. J. **389** (1992) L9

[20] G. Jungman, M. Kamionkowski and K. Griest, Phys. Rept. **267** (1996) 195

[21] B. Moore, Nature **370** (1994) 629

[22] J.F. Navarro, C.S. Frenk and S.D. White, astro-ph 9508025

[23] C.J. Copi, D.N. Schramm and M.S. Turner, Science **267** (1995) 192

[24] Particle Data Group, Phys. Rev. **D54** (1996) 109-111

[25] B. Carr, Annu. Rev. Astron. Astrophys. **32** (1994) 531

[26] A. De Rújula, Ph. Jetzer and E. Massó, Astron. and Astrophys. **254** (1992) 99

[27] J. Bahcall, C. Flynn, A. Gould and S. Kirhakos, Astrophys. J. **435** (1994) L51

[28] C.M. Tamanaha, J. Silk, M.A. Wood and D.E. Winget, Astrophys. J. **358** (1990) 164

[29] S.D. Kawaler, astro-ph 9606094

[30] B. Paczyński, Astrophys. J. **304** (1986) 1

[31] E. Aubourg et al., Nature **365** (1993) 623

[32] C. Alcock et al., Nature **365** (1993) 621; Astrophys. J. **445**, (1995) 133

[33] C. Alcock et al., astro-ph 9606165

[34] E. Aubourg et al., astro-ph 9503211

[35] A. Udalski et al., Acta Astron. **43** (1993) 289; **44** (1994) 165 and 227

[36] C. Alcock et al., astro-ph 9512146

[37] C. Alard et al., ESO Messenger **80** (1995) 31

[38] E. Roulet and S. Mollerach, astro-ph 9603119 to appear in Phys. Rept.

[39] A. De Rújula, Ph. Jetzer and E. Massó, Mont. Not. R. Astr. Soc. **250** (1991) 348

[40] Ph. Jetzer, Atti del Colloquio di Matematica (CERFIM) **7** (1991) 259

[41] K. Griest, Astrophys. J. **366** (1991) 412

[42] A.P. Crotts, Astrophys. J. **399** (1992) L43

[43] P. Baillon, A. Bouquet, Y. Giraud-Héraud and J. Kaplan, Astron. and Astrophys. **277** (1933) 1; R. Ansari et al., astro-ph 9607040

[44] Ph. Jetzer, Astron. and Astrophys. **286** (1994) 426

[45] Ph. Jetzer and E. Massó, Phys. Lett. **B 323** (1994) 347

[46] Ph. Jetzer, Astrophys. J. **432** (1994) L43

[47] Ph. Jetzer and E. Massó, to appear in the proceedings of the second workshop: "The dark side of the Universe: experimental efforts and theoretical frameworks" (Rome, 1995)

[48] F. De Paolis, G. Ingrosso and Ph. Jetzer, to appear in Astrophys. J. (1996)

[49] F. De Paolis, G. Ingrosso, Ph. Jetzer and M. Roncadelli, ZU-TH 8/1996

[50] F. De Paolis, G. Ingrosso, Ph. Jetzer and M. Roncadelli, Phys. Rev. Lett. **74** (1995) 14; Astron. and Astrophys. **295** (1995) 567; Comments on Astrophys. **18** (1995) 87;

[51] F. De Paolis, G. Ingrosso, Ph. Jetzer and M. Roncadelli, Int. J. Mod. Phys. **D5** (1996) 151

[52] D. Pfenniger, F. Combes and L. Martinet, Astron. and Astrophys. **285** (1994) 79

[53] O.E. Gerhard and J. Silk, astro-ph 9509149

[54] A. Bouquet, P. Salati and J. Silk, Phys. Rev. **D40** (1989) 3168

[55] F. De Paolis, G. Ingrosso, Ph. Jetzer, A. Qadir and M. Roncadelli, Astron. and Astrophys. **299** (1995) 647

[56] F. De Paolis, G. Ingrosso, Ph. Jetzer and M. Roncadelli, Astrophys. and Space Science **235** (1996) 329

[57] F.C. Adams and T.P. Walker, Astrophys. J. **359** (1990) 57

Figure Captions

Fig. 1: Rotation curve for NGC 3198 according to van Albada et al. [8]. The dotted line with error bars refers to the optical and 21 cm hydrogen data, while the solid lines are theoretical fits.

Fig. 2: Definition of various quantities describing a microlensing event. The observer is O, the source is S and M is the MACHO.

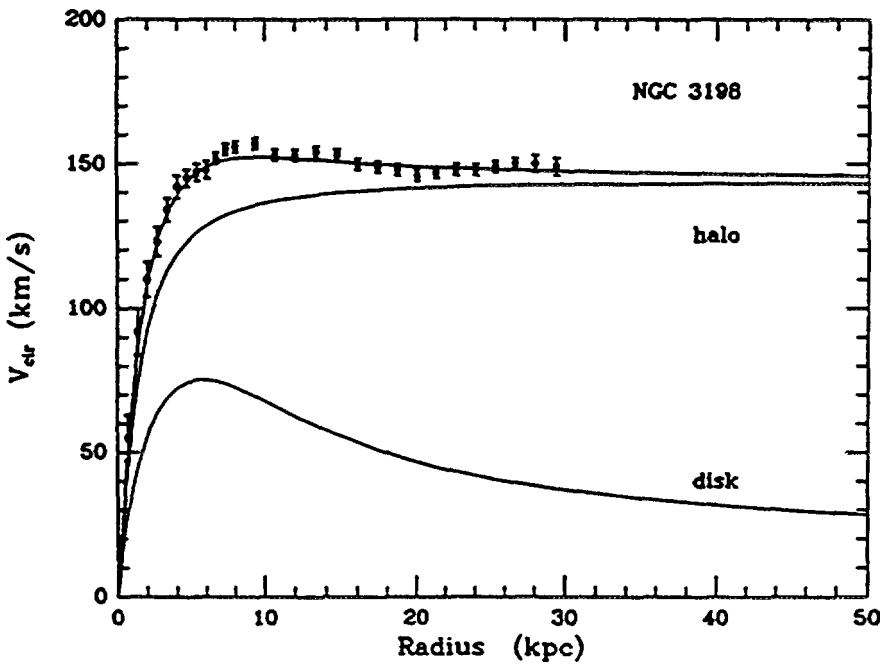
NGC 3198
halo
disk
V_{cir} (km/s)
Radius (kpc)
0
50
100
150
200
0
10
20
30
40
50

Fig. 1

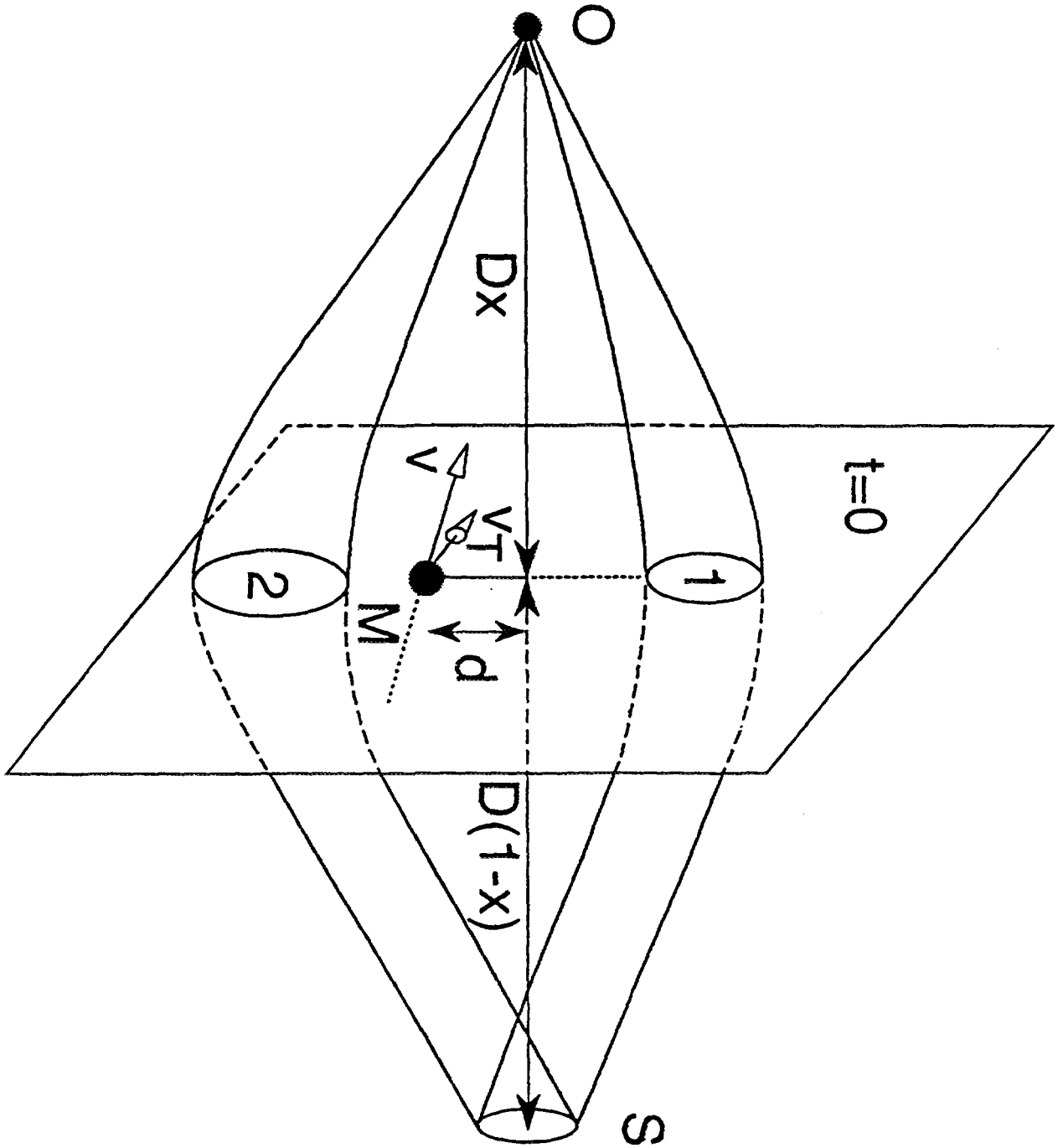

Fig. 2

Early History of Gauge Theories and Weak Interactions[1]

By Norbert Straumann

Institut für Theoretische Physik der Universität Zürich–Irchel,
Winterthurerstrasse 190, CH–8057 Zürich, Switzerland

1 Introduction

It took decades until physicists understood that all known fundamental interactions can be described in terms of gauge theories. My historical account begins with Einstein's general theory of relativity (GR), which is a non-Abelian gauge theory of a special type (see Secs. 3,4). The other gauge theories emerged in a slow and complicated process gradually from GR, and their common geometrical structure — best expressed in terms of connections of fiber bundles — is now widely recognized. Thus, also in this respect, H. Weyl was right when he wrote in the preface to the first edition of Space – Time – Matter (RZM) early in 1918: "Wider expanses and greater depths are now exposed to the searching eye of knowledge, regions of which we had not even a presentiment. It has brought us much nearer to grasping the plan that underlies all physical happening" [1].

It was Weyl himself who made in 1918 the first attempt to extend GR in order to describe gravitation and electromagnetism within a unifying geometrical framework [2]. This brilliant proposal contains all mathematical aspects of a non-Abelian gauge theory, as I will make clear in §2. The words gauge (Eich–) transformation and gauge invariance appear the first time in this paper, but in the everyday meaning of change of length or change of calibration.

Einstein admired Weyl's theory as "a coup of genius of the first rate . . . ", but immediately realized that it was physically untenable: "Although your idea is so beautiful, I have to declare frankly that, in my opinion, it is impossible that the theory corresponds to nature." This led to an intense exchange of letters between Einstein (in Berlin) and Weyl (at the ETH

[1]Invited talk at the PSI Summer School on Physics with Neutrinos, Zuoz, Switzerland, August 4-10, 1996.

in Zürich), which will hopefully soon be published in *The Collected Papers* of Einstein. (In my article [3] I gave an account of this correspondence which is preserved in the Archives of the ETH.) No agreement was reached, but Einstein's intuition proved to be right.

Although Weyl's attempt was a failure as a physical theory it paved the way for the correct understanding of gauge invariance. Weyl himself re-interpreted his original theory after the advent of quantum theory in a seminal paper [4] which I will discuss at length in §3. Parallel developments by other workers and interconnections are indicated in Fig.1.

At the time Weyl's contributions to theoretical physics were not appreciated very much, since they did not really add new physics. The attitude of the leading theoreticians is expressed in familiar distinctness in a letter by Pauli to Weyl from July 1, 1929, after he had seen a preliminary account of Weyl's work:

> *Before me lies the April edition of the Proc.Nat.Acad. (US). Not only does it contain an article from you under "Physics" but shows that you are now in a 'Physical Laboratory': from what I hear you have even been given a chair in 'Physics' in America. I admire your courage; since the conclusion is inevitable that you wish to be judged, not for success in pure mathematics, but for your true but unhappy love for physics [5].*

Weyl's reinterpretation of his earlier speculative proposal had actually been suggested before by London, but it was Weyl who emphasized the role of gauge invariance as a *symmetry principle* from which electromagnetism can be *derived.* It took several decades until the importance of this symmetry principle — in its generalized form to non-Abelian gauge groups developed by Yang, Mills, and others — became also fruitful for a description of the weak and strong interactions. The mathematics of the non-Abelian generalization of Weyl's 1929 paper would have been an easy task for a mathematician of his rank, but at the time there was no motivation for this from the physics side. The known properties of the weak and strong nuclear interactions, in particular their short range, did not point to a gauge theoretical description. We all know that the gauge symmetries of the Standard Model are very hidden and it is, therefore, not astonishing that progress was very slow indeed.

Today, the younger generation, who learned the Standard Model from polished textbook presentations, complains with good reasons about many of its imperfections. It is one of the aims of this talk to make it obvious that it was extremely difficult to reach our present understanding of the fundamental interactions. The Standard Model, with all its success, is a great achievement, and one should not be too discouraged when major further progress is not coming rapidly.

Because of limitations of time and personal knowledge, I will discuss in the rest of my talk mainly the two important papers by Weyl from 1918 and 1929. The latter contains also his two-component theory of massless spin 1/2 fermions. In this context I will make in §5 a few remarks about the developments which led in 1958 to the phenomenological $V - A$ current-current Lagrangian for the weak interactions. My historical account of the non-Abelian generalizations by Klein, Pauli and others, culminating in the paper by Yang

and Mills, will also be much abbreviated. This is not too bad, since there will soon be a book by Lochlain O'Raifeartaigh that is devoted entirely to the early history of gauge theories [6]. Those who do not know German will find there also English translations of the most important papers of the first period (1918–1929). The book contains in addition the astonishing paper by Klein (1938) [7], Pauli's letters to Pais on non-Abelian Kaluza-Klein reductions [8], parts of Shaw's dissertation, in which he develops a non-Abelian $SU(2)$ gauge theory [9], and Utiyama's generalization of Yang-Mills theory to arbitrary gauge groups [10]. These works are behind the diagram in Fig.1.

This talk covers mostly material contained in the papers [3], [11], and [12], which I have published some time ago in German, partly because all early publications and letters related to our subject are written in this language.

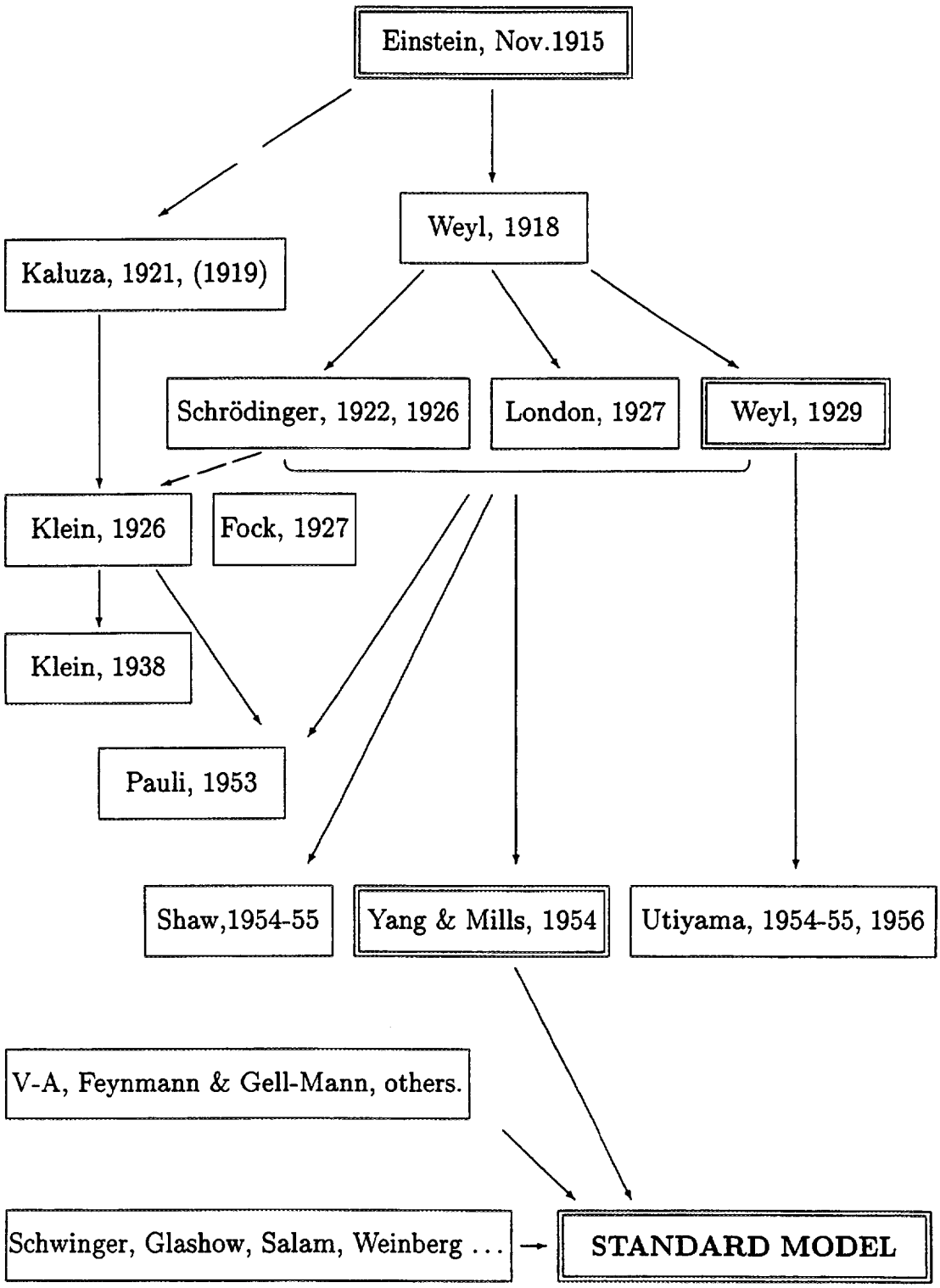

Figure 1: Key papers in the development of gauge theories.

2 Weyl's attempt to unify gravitation and electromagnetism

On the 1st of March 1918 Weyl writes in a letter to Einstein: "These days I succeeded, as I believe, to derive electricity and gravitation from a common source ...". Einstein's prompt reaction by postcard indicates already a physical objection which he explained in detail shortly afterwards. Before I come to this I have to describe Weyl's theory of 1918.

2.1 Weyl's generalization of Riemannian geometry

Weyl's starting point was purely mathematical. He felt a certain uneasiness about Riemannian geometry, as is clearly expressed by the following sentences early in his paper[2]:

> *But in Riemannian geometry described above there is contained a last element of geometry "at a distance" (ferngeometrisches Element) — with no good reason, as far as I can see; it is due only to the accidental development of Riemannian geometry from Euclidean geometry. The metric allows the two magnitudes of two vectors to be compared, not only at the same point, but at any arbitrarily separated points. A true infinitesimal geometry should, however, recognize only a principle for transferring the magnitude of a vector to an infinitesimally close point and then, on transfer to an arbitrary distant point, the integrability of the magnitude of a vector is no more to be expected that the integrability of its direction.*

After these remarks Weyl turns to physical speculation and continues as follows:

> *On the removal of this inconsistency there appears a geometry that, surprisingly, when applied to the world, explains not only the gravitational phenomena but also the electrical. According to the resultant theory both spring from the same source, indeed in general one cannot separate gravitation and electromagnetism in a unique manner. In this theory all physical quantities have a world geometrical meaning; the action appears from the beginning as a pure number. It leads to an essentially unique universal law; it even allows us to understand in a certain sense why the world is four-dimensional.*

In brief, Weyl's geometry can be described as follows. First, the spacetime manifold M is equipped with a conformal structure, i.e., with a class $[g]$ of conformally equivalent Lorentz metrics g (and not a definite metric as in GR). This corresponds to the requirement that it should only be possible to compare lengths at one and the same world point. Second, it is

[2] I am using here and at other places the English translation of L. O'Raifeartaigh [6].

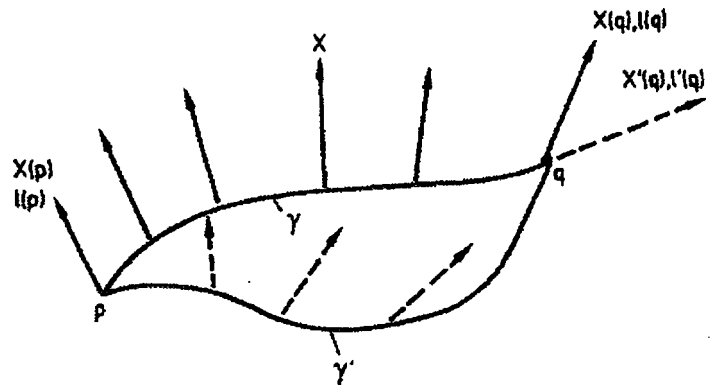

Figure 2: Path dependence of parallel displacement and transport of length in Weyl space.

assumed, as in Riemannian geometry, that there is an affine (linear) torsion-free connection which defines a covariant derivative ∇, and respects the conformal structure. Differentially this means that for any $g \in [g]$ the covariant derivative ∇g should be proportional to g:

$$\nabla g = -2A \otimes g \qquad (\nabla_\lambda g_{\mu\nu} = -2A_\lambda g_{\mu\nu}), \tag{2.1}$$

where $A = A_\mu dx^\mu$ is a differential 1-form.

Consider now a curve $\gamma : [0,1] \to M$ and a parallel-transported vector field X along γ. If l is the length of X, measured with a representative $g \in [g]$, we obtain from (2.1) the following relation between $l(p)$ for the initial point $p = \gamma(0)$ and $l(q)$ for the end point $q = \gamma(1)$:

$$l(q) = \exp\left(-\int_\gamma A\right)\ l(p). \tag{2.2}$$

Thus, the ratio of lengths in q and p (measured with $g \in [g]$) *depends in general on the connecting path* γ (see Fig.2). The length is only independent of γ if the curl of A,

$$F = dA \qquad (F_{\mu\nu} = \partial_\mu A_\nu - \partial_\nu A_\mu), \tag{2.3}$$

vanishes.

The compatibility requirement (2.1) leads to the following expression for the Christoffel symbols in Weyl's geometry:

$$\Gamma^\mu_{\nu\lambda} = \frac{1}{2} g^{\mu\sigma}(g_{\lambda\sigma,\nu} + g_{\sigma\nu,\lambda} - g_{\nu\lambda,\sigma}) + g^{\mu\sigma}(g_{\lambda\sigma}A_\nu + g_{\sigma\nu}A_\lambda - g_{\nu\lambda}A_\sigma). \tag{2.4}$$

The second A-dependent term is a characteristic new piece in Weyl's geometry which has to be added to the Christoffel symbols of Riemannian geometry.

Until now we have chosen a fixed, but arbitrary metric in the conformal class $[g]$. This corresponds to a choice of calibration (or gauge). Passing to another calibration with metric $\bar{g}$, related to g by

$$\bar{g} = e^{2\lambda} g, \tag{2.5}$$

the potential A in (2.1) will also change to $\bar{A}$, say. Since the covariant derivative has an absolute meaning, $\bar{A}$ can easily be worked out: On the one hand we have by definition

$$\nabla \bar{g} = -2\bar{A} \otimes \bar{g}, \tag{2.6}$$

and on the other hand we find for the left side with (2.1)

$$\nabla \bar{g} = \nabla(e^{2\lambda} g) = 2d\lambda \otimes \bar{g} + e^{2\lambda} \nabla g = 2d\lambda \otimes \bar{g} - 2A \otimes \bar{g}. \tag{2.7}$$

Thus

$$\bar{A} = A - d\lambda \qquad (\bar{A}_\mu = A_\mu - \partial_\mu \lambda). \tag{2.8}$$

This shows that a change of calibration of the metric induces a *"gauge transformation"* for A:

$$g \to e^{2\lambda} g, \qquad A \to A - d\lambda. \tag{2.9}$$

Only gauge classes have an absolute meaning. (The Weyl connection is, however, gauge-invariant.)

2.2 Electromagnetism and Gravitation

Turning to physics, Weyl assumes that his "purely infinitesimal geometry" describes the structure of spacetime and consequently he requires that physical laws should satisfy a double-invariance: 1. They must be invariant with respect to arbitrary smooth coordinate transformations. 2. They must be *gauge invariant*, i.e., invariant with respect to substitutions (2.9) for an arbitrary smooth function λ.

Nothing is more natural to Weyl, than identifying A_μ with the vector potential and $F_{\mu\nu}$ in eq.(2.3) with the field strength of electromagnetism. In the absence of electromagnetic fields ($F_{\mu\nu} = 0$) the scale factor $\exp(-\int_\gamma A)$ in (2.2) for length transport becomes path independent (integrable) and one can find a gauge such that A_μ vanishes. In this special case one is in the same situation as in GR.

Weyl proceeds to find an action which is generally invariant as well as gauge invariant and which would give the coupled field equations for g and A. I do not want to enter into this, except for the following remark. In his first paper [2] Weyl proposes what we call nowadays the Yang-Mills action

$$S(g, A) = -\frac{1}{4} \int Tr(\Omega \wedge *\Omega). \tag{2.10}$$

Here Ω denotes the curvature form and $*\Omega$ its Hodge dual[3]. Note that the latter is gauge invariant, i.e., independent of the choice of $g \in [g]$. In Weyl's geometry the curvature form splits as $\Omega = \hat{\Omega} + F$, where $\hat{\Omega}$ is the metric piece [13]. Correspondingly, the action also splits,

$$Tr(\Omega \wedge *\Omega) = Tr(\hat{\Omega} \wedge *\hat{\Omega}) + F \wedge *F. \tag{2.11}$$

[3]The integrand in (2.10) is in local coordinates indeed just the expression $R_{\alpha\beta\gamma\delta} R^{\alpha\beta\gamma\delta} \sqrt{-g} dx^0 \wedge \ldots \wedge dx^3$ which is used by Weyl ($R_{\alpha\beta\gamma\delta}$ = curvature tensor of the Weyl connection).

The second term is just the Maxwell action. Weyl's theory thus contains formally all aspects of a non-Abelian gauge theory.

Weyl emphasizes, of course, that the Einstein-Hilbert action is not gauge invariant. Later work by Pauli [14] and by Weyl himself [1, 2] led soon to the conclusion that the action (2.10) could not be the correct one, and other possibilities were investigated (see the later editions of RZM).

Independent of the precise form of the action Weyl shows that in his theory gauge invariance implies the *conservation of electric charge* in much the same way as general coordinate invariance leads to the conservation of energy and momentum[4]. This beautiful connection pleased him particularly: "... [it] seems to me to be the strongest general argument in favour of the present theory — insofar as it is permissible to talk of justification in the context of pure speculation." The invariance principles imply five 'Bianchi type' identities. Correspondingly, the five conservation laws follow in two independent ways from the coupled field equations and may be "termed the eliminants" of the latter. These structural connections hold also in modern gauge theories.

2.3 Einstein's objection and reactions of other physicists

After this sketch of Weyl's theory I come to Einstein's striking counterargument which he first communicated to Weyl by postcard (see Fig.3). The problem is that if the idea of a nonintegrable length connection (scale factor) is correct, then the behavior of clocks would depend on their history. Consider two identical atomic clocks in adjacent world points and bring them along different world trajectories which meet again in adjacent world points. According to (2.2) their frequencies would then generally differ. This is in clear contradiction with empirical evidence, in particular with the existence of stable atomic spectra. Einstein therefore concludes (see [3]):

> *... (if) one drops the connection of the ds to the measurement of distance and time, then relativity looses all its empirical basis.*

Nernst shared Einstein's objection and demanded on behalf of the Berlin Academy that it should be printed in a short amendment to Weyl's article, and Weyl had to cope with it. I have described the intense and instructive subsequent correspondence between Weyl and Einstein elsewhere [3]. As an example, let me quote from one of the last letters of Weyl to Einstein:

> *This [insistence] irritates me of course, because experience has proven that one can rely on your intuition; so little convincing your counterarguments seem to me, as I have to admit ...*

[4] I adopt here the somewhat naive interpretation of energy-momentum conservation for generally invariant theories of the older literature.

By the way, you should not believe that I was driven to introduce the linear differential form in addition to the quadratic one by physical reasons. I wanted, just to the contrary, to get rid of this 'methodological inconsistency (Inkonsequenz)' which has been a stone of contention to me already much earlier. And then, to my surprise, I realized that it looks as if it might explain electricity. You clap your hands above your head and shout: But physics is not made this way ! (Weyl to Einstein 10.12.1918).

Weyl's reply to Einstein's criticism was, generally speaking, this: The real behavior of measuring rods and clocks (atoms and atomic systems) in arbitrary electromagnetic and gravitational fields can be deduced only from a dynamical theory of matter.

Not all leading physicists reacted negatively. Einstein transmitted a very positive first reaction by Planck, and Sommerfeld wrote enthusiastically to Weyl that there was "... hardly doubt, that you are on the correct path and not on the wrong one."

In his encyclopedia article on relativity [15] Pauli gave a lucid and precise presentation of Weyl's theory, but commented Weyl's point of view very critically. At the end he states:

... Resuming one may say that Weyl's theory has not yet contributed to get closer to the solution of the problem of matter.

Also Eddington's reaction was first very positive but he changed his mind soon and denied the physical relevance of Weyl's geometry.

The situation was later appropriately summarized by F.London in his 1927 paper [16] as follows:

In the face of such elementary experimental evidence, it must have been an unusually strong metaphysical conviction that prevented Weyl from abandoning the idea that Nature would have to make use of the beautiful geometrical possibility that was offered. He stuck to his conviction and evaded discussion of the above-mentioned contradictions through a rather unclear re-interpretation of the concept of "real state", which, however, robbed his theory of its immediate physical meaning and attraction.

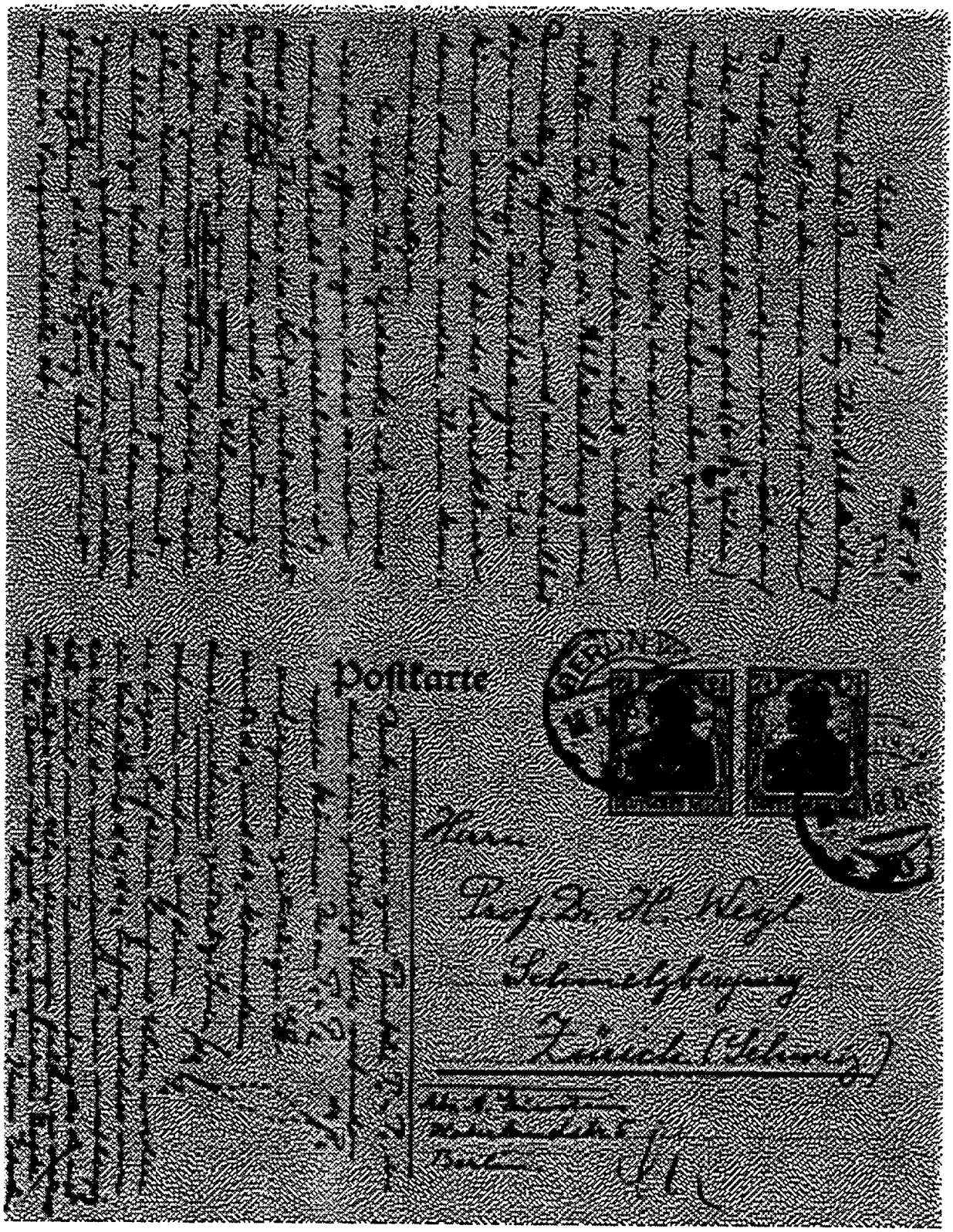

Figure 3: Postcard of Einstein to Weyl 15.4.1918 (Archives of ETH).

3 Weyl's 1929 Classic: "Electron and Gravitation"

Shortly before his death late in 1955, Weyl wrote for his *Selecta* [17] a postscript to his early attempt in 1918 to construct a 'unified field theory'. There he expressed his deep attachment to the gauge idea and adds (p.192):

> *Later the quantum-theory introduced the Schrödinger-Dirac potential ψ of the electron-positron field; it carried with it an experimentally-based principle of gauge-invariance which guaranteed the conservation of charge, and connected the ψ with the electromagnetic potentials ϕ_i in the same way that my speculative theory had connected the gravitational potentials g_{ik} with the ϕ_i, and measured the ϕ_i in known atomic, rather than unknown cosmological units. I have no doubt but that the correct context for the principle of gauge-invariance is here and not, as I believed in 1918, in the intertwining of electromagnetism and gravity.*

This re-interpretation was developed by Weyl in one of the great papers of this century [4]. Weyl's classic does not only give a very clear formulation of the gauge principle, but contains, in addition, several other important concepts and results — in particular his two-component theory. The richness of the paper is clearly visible from the following table of contents:

> *Introduction. Relationship of General Relativity to the quantum-theoretical field equations of the spinning electron: mass, gauge-invariance, distant-parallelism. Expected modifications of the Dirac theory. -I. Two-component theory: the wave function ψ has only two components. -§1. Connection between the transformation of the ψ and the transformation of a normal tetrad in four-dimensional space. Asymmetry of past and future, of left and right. -§2. In General Relativity the metric at a given point is determined by a normal tetrad. Components of vectors relative to the tetrad and coordinates. Covariant differentiation of ψ. -§3. Generally invariant form of the Dirac action, characteristic for the wave-field of matter. -§4. The differential conservation law of energy and momentum and the symmetry of the energy-momentum tensor as a consequence of the double-invariance (1) with respect to coordinate transformations (2) with respect to rotation of the tetrad. Momentum and moment of momentum for matter. -§5. Einstein's classical theory of gravitation in the new analytic formulation. Gravitational energy. -§6. The electromagnetic field. From the arbitrariness of the gauge-factor in ψ appears the necessity of introducing the electromagnetic potential. Gauge invariance and charge conservation. The space-integral of charge. The introduction of mass. Discussion and rejection of another possibility in which electromagnetism appears, not as an accompanying phenomenon of matter, but of gravitation.*

The modern version of the gauge principle is already spelled out in the introduction:

The Dirac field-equations for ψ together with the Maxwell equations for the four potentials f_p of the electromagnetic field have an invariance property which is formally similar to the one which I called gauge-invariance in my 1918 theory of gravitation and electromagnetism; the equations remain invariant when one makes the simultaneous substitutions

$$\psi \quad \text{by} \quad e^{i\lambda}\psi \quad \text{and} \quad f_p \quad \text{by} \quad f_p - \frac{\partial \lambda}{\partial x^p},$$

where λ is understood to be an arbitrary function of position in four-space. Here the factor $\frac{e}{ch}$, where $-e$ is the charge of the electron, c is the speed of light, and $\frac{h}{2\pi}$ is the quantum of action, has been absorbed in f_p. The connection of this "gauge invariance" to the conservation of electric charge remains untouched. But a fundamental difference, which is important to obtain agreement with observation, is that the exponent of the factor multiplying ψ is not real but pure imaginary. ψ now plays the role that Einstein's ds played before. It seems to me that this new principle of gauge-invariance, which follows not from speculation but from experiment, tells us that the electromagnetic field is a necessary accompanying phenomenon, not of gravitation, but of the material wave-field represented by ψ. Since gauge-invariance involves an arbitrary function λ it has the character of "general" relativity and can naturally only be understood in that context.

We shall soon enter into Weyl's justification which is, not surprisingly, strongly associated with general relativity. Before this I have to describe his incorporation of the Dirac theory into GR which he achieved with the help of the tetrad formalism.

One of the reasons for adapting the Dirac theory of the spinning electron to gravitation had to do with Einstein's recent unified theory which invoked a distant parallelism with torsion. E.Wigner [18] and others had noticed a connection of this theory and the spin theory of the electron. Weyl did not like this and wanted to dispense with teleparallelism. In the introduction he says:

I prefer not to believe in distant parallelism for a number of reasons. First my mathematical intuition objects to accepting such an artificial geometry; I find it difficult to understand the force that would keep the local tetrads at different points and in rotated positions in a rigid relationship. There are, I believe, two important physical reasons as well. The loosening of the rigid relationship between the tetrads at different points converts the gauge-factor $e^{i\lambda}$, which remains arbitrary with respect to ψ, from a constant to an arbitrary function of space-time. In other words, only through the loosening the rigidity does the established gauge-invariance become understandable.

This thought is carried out in detail after Weyl has set up his two-component theory in special relativity, including a discussion of P and T invariance. He emphasizes thereby that the two-component theory excludes a linear implementation of parity and remarks: "It

is only the fact that the left-right symmetry actually appears in Nature that forces us to introduce a second pair of ψ-components." To Weyl the mass-problem is thus not relevant for this. Indeed he says: "Mass, however, is a gravitational effect; thus there is hope of finding a substitute in the theory of gravitation that would produce the required corrections."

We shall return to the two-component theory in §5 in connection with parity violation and the $V-A$ interaction.

3.1 Tetrad formalism

The method of Weyl for incorporating his two-component spinors into general relativity makes use of local tetrads (Vierbeins).

In the tetrad formalism the metric is described by an arbitrary basis of orthonormal vector fields $\{e_\alpha(x); \alpha = 0,1,2,3\}$. If $\{e^\alpha(x)\}$ denotes the dual basis of 1-forms, the metric is given by

$$g = \eta_{\mu\nu} e^\nu(x) \otimes e^\nu(x), \qquad (\eta_{\mu\nu}) = diag(1,-1,-1,-1). \tag{3.1}$$

Weyl emphasizes, of course, that only a class of such local tetrads is determined by the metric: the metric is not changed if the tetrad fields are subject to spacetime-dependent Lorentz transformations:

$$e^\alpha(x) \to \Lambda^\alpha{}_\beta(x) e^\beta(x). \tag{3.2}$$

With respect to a tetrad, the connection forms[5] $\omega = (\omega^\alpha{}_\beta)$ have values in the Lie algebra of the homogeneous Lorentz group:

$$\omega_{\alpha\beta} + \omega_{\beta\alpha} = 0. \tag{3.3}$$

(Indices are raised and lowered with $\eta^{\alpha\beta}$ and $\eta_{\alpha\beta}$, respectively.) They are determined (in terms of the tetrad) by the first structure equation of Cartan:

$$de^\alpha + \omega^\alpha{}_\beta \wedge e^\beta = 0. \tag{3.4}$$

Under local Lorentz transformations (3.2) the connection forms transform in the same way as the gauge potential of a non-Abelian gauge theory:

$$\omega(x) \to \Lambda(x)\omega(x)\Lambda^{-1}(x) - d\Lambda(x)\Lambda^{-1}(x). \tag{3.5}$$

The curvature forms $\Omega = (\Omega^\mu{}_\nu)$ are obtained from ω in exactly the same way as the Yang-Mills field strength from the gauge potential:

$$\Omega = d\omega + \omega \wedge \omega \tag{3.6}$$

(second structure equation).

For a vector field V, with components V^α relative to $\{e_\alpha\}$, the covariant derivative DV is given by

$$DV^\alpha = dV^\alpha + \omega^\alpha{}_\beta V^\beta. \tag{3.7}$$

[5] I am using more modern notations; for details see [18].

Weyl generalizes this in a unique manner to spinor fields ψ:

$$D\psi = d\psi + \frac{1}{4}\omega_{\alpha\beta}\sigma^{\alpha\beta}\psi. \tag{3.8}$$

Here, the $\sigma^{\alpha\beta}$ describe infinitesimal Lorentz transformations (in the representation of ψ). For a Dirac field these are the familiar matrices

$$\sigma^{\alpha\beta} = \frac{1}{2}[\gamma^{\alpha}, \gamma^{\beta}]. \tag{3.9}$$

(For 2-component Weyl fields one has similar expressions in terms of the Pauli matrices.)

With these tools the action principle for the coupled Einstein-Dirac system can be set up. In the massless case the Lagrangian is

$$\mathcal{L} = \frac{1}{16\pi G}R - i\bar{\psi}\gamma^{\mu}D_{\mu}\psi, \tag{3.10}$$

where the first term is just the Einstein-Hilbert Lagrangian (which is linear in Ω). Weyl discusses, of course, immediately the consequences of the following two symmetries:

(i) local Lorentz invariance,

(ii) general coordinate invariance.

3.2 The new form of the gauge-principle

All this is kind of a preparation for the final section of Weyl's paper, which has the title "electric field". Weyl says:

> *We come now to the critical part of the theory. In my opinion the origin and necessity for the electromagnetic field is in the following. The components ψ_1 ψ_2 are, in fact, not uniquely determined by the tetrad but only to the extent that they can still be multiplied by an arbitrary "gauge-factor" $e^{i\lambda}$. The transformation of the ψ induced by a rotation of the tetrad is determined only up to such a factor. In special relativity one must regard this gauge-factor as a constant because here we have only a single point-independent tetrad. Not so in general relativity; every point has its own tetrad and hence its own arbitrary gauge-factor; because by the removal of the rigid connection between tetrads at different points the gauge-factor necessarily becomes an arbitrary function of position.*

In this manner Weyl arrives at the gauge-principle in its modern form and emphasizes: "From the arbitrariness of the gauge-factor in ψ appears the necessity of introducing the electromagnetic potential." The first term $d\psi$ in (3.8) has now to be replaced by the covariant

gauge derivative $(d - ieA)\psi$ and the nonintegrable scale factor (2.1) of the old theory is now replaced by a phase factor:

$$\exp\left(-\int_\gamma A\right) \to \exp\left(-i\int_\gamma A\right),$$

which corresponds to the replacement of the original gauge group $\mathbf{R}$ by the compact group $U(1)$. Accordingly, the original Gedankenexperiment of Einstein translates now to the Aharonov-Bohm effect. The close connection between gauge invariance and conservation of charge is again uncovered. The current conservation follows, as in the original theory, in two independent ways: On the one hand it is a consequence of the field equations for matter plus gauge invariance, at the same time, however, also of the field equations for the electromagnetic field plus gauge invariance. This corresponds to an identity in the coupled system of field equations which has to exist as a result of gauge invariance. All this is nowadays familiar to students of physics and needs not to be explained in more detail.

Much of Weyl's paper penetrated also into his classic book "The Theory of Groups and Quantum Mechanics" [19]. There he mentions also the transformation of his early gauge-theoretic ideas: "This principle of gauge invariance is quite analogous to that previously set up by the author, on speculative grounds, in order to arrive at a unified theory of gravitation and electricity. But I now believe that this gauge invariance does not tie together electricity and gravitation, but rather electricity and matter."

When Pauli saw the full version of Weyl's paper he became more friendly and wrote [20]:

> *In contrast to the nasty things I said, the essential part of my last letter has since been overtaken, particularly by your paper in Z. f. Physik. For this reason I have afterward even regretted that I wrote to you. After studying your paper I believe that I have really understood what you wanted to do (this was not the case in respect of the little note in the Proc.Nat.Acad.). First let me emphasize that side of the matter concerning which I am in full agreement with you: your incorporation of spinor theory into gravitational theory. I am as dissatisfied as you are with distant parallelism and your proposal to let the tetrads rotate independently at different space-points is a true solution.*

In brackets Pauli adds:

> *Here I must admit your ability in Physics. Your earlier theory with $g'_{ik} = \lambda g_{ik}$ was pure mathematics and unphysical. Einstein was justified in criticizing and scolding. Now the hour of your revenge has arrived.*

Then he remarks in connection with the mass-problem:

> *Your method is valid even for the massive* [Dirac] *case. I thereby come to the other side of the matter, namely the unsolved difficulties of the Dirac theory*

(two signs of m_0) and the question of the 2-component theory. In my opinion these problems will not be solved by gravitation ... the gravitational effects will always be much too small.

Many years later, Weyl summarized this early tortuous history of gauge theory in an instructive letter to the Swiss writer and Einstein biographer C.Seelig, which I reproduce in the German original [21].

Aus dem Jahre 1918 datiert der von mir unternommene erste Versuch, eine einheitliche Feldtheorie von Gravitation und Elektromagnetismus zu entwickeln, und zwar auf Grund des Prinzips der Eichinvarianz, das ich neben dasjenige der Koordinaten-Invarianz stellte. Ich habe diese Theorie selber längst aufgegeben, nachdem ihr richtiger Kern: die Eichinvarianz, in die Quantentheorie herübergerettet ist als ein Prinzip, das nicht die Gravitation, sondern das Wellenfeld des Elektrons mit dem elektromagnetischen verknüpft. — Einstein war von Anfang dagegen, und das gab zu mancher Diskussion Anlass. Seinen konkreten Einwänden glaubte ich begegnen zu könen. Schliesslich sagte er dann: "Na, Weyl, lassen wir das! So — das heisst auf so spekulative Weise, ohne ein leitendes, anschauliches physikalisches Prinzip — macht man keine Physik!" Heute haben wir in dieser Hinsicht unsere Standpunkte wohl vertauscht. Einstein glaubt, dass auf diesem Gebiet die Kluft zwischen Idee und Erfahrung so gross ist, dass nur der Weg der mathematischen Spekulation, deren Konsequenzen natürlich entwichelt und mit den Tatsachen konfrontiert werden müssen, Aussicht auf Erfolg hat, während mein Vertrauen in die reine Spekulation gesunken ist und mir ein engerer Anschluss an die quanten-physikalischen Erfahrungen geboten scheint, zumal es nach meiner Ansicht nicht genug ist, Gravitation und Elektromagnetismus zu einer Einheit zu verschmelzen. Die Wellenfelder des Elektrons und was es sonst noch an unreduzierbaren Elementarteilchen geben mag, müssen mit eigeschlossen werden.

4 Yang-Mills Theory

In his Hermann Weyl Centenary Lecture at the ETH [22], C.N. Yang commented on Weyl's remark "The principle of gauge-invariance has the character of general relativity since it contains an arbitrary function λ, and can certainly only be understood in terms of it" [23] as follows:

The quote above from Weyl's paper also contains something which is very revealing, namely, his strong association of gauge invariance with general relativity. That was, of course, natural since the idea had originated in the first place with Weyl's attempt in 1918 to unify electromagnetism with gravity. Twenty years later, when Mills and I worked on non-Abelian gauge fields, our motivation

was completely divorced from general relativity and we did not appreciate that gauge fields and general relativity are somehow related. Only in the late 1960's did I recognize the structural similarity mathematically of non-Abelian gauge fields with general relativity and understand that they both were connections mathematically.

Later, in connection with Weyl's strong emphasis of the relation between gauge invariance and conservation of electric charge, Yang continues with the following instructive remarks:

Weyl's reason, it turns out, was also one of the melodies of gauge theory that had very much appealed to me when as a graduate student I studied field theory by reading Pauli's articles. I made a number of unsuccessful attempts to generalize gauge theory beyond electromagnetism, leading finally in 1954 to a collaboration with Mills in which we developed a non-Abelian gauge theory. In [...] we stated our motivation as follows:

The conservation of isotopic spin points to the existence of a fundamental invariance law similar to the conservation of electric charge. In the latter case, the electric charge serves as a source of electromagnetic field; an important concept in this case is gauge invariance which is closely connected with (1) the equation of motion of the electro-magnetic field, (2) the existence of a current density, and (3) the possible interactions between a charged field and the electromagnetic field. We have tried to generalize this concept of gauge invariance to apply to isotopic spin conservation. It turns out that a very natural generalization is possible.

Item (2) is the melody referred to above. The other two melodies, (1) and (3), where what had become pressing in the early 1950's when so many new particles had been discovered and physicists had to understand now they interact which each other.

I had met Weyl in 1949 when I went to the Institute for Advanced Study in Princeton as a young "member". I saw him from time to time in the next years, 1949–1955. He was very approachable, but I don't remember having discussed physics or mathematics with him at any time. His continued interest in the idea of gauge fields was not known among the physicists. Neither Oppenheimer nor Pauli ever mentioned it. I suspect they also did not tell Weyl of the 1954 papers of Mills' and mine. Had they done that, or had Weyl somehow came across our paper, I imagine he would have been pleased and excited, for we had put together two things that were very close to his heart: gauge invariance and non-Abelian Lie groups.

It is indeed astonishing that during those late years Pauli never talked with Weyl on non-Abelian generalizations of gauge-invariance, since he himself had worked on this — even before the work of Yang and Mills. During a discussion following a talk by Pais at the 1953 Lorentz Conference [24] in Leiden, Pauli said:

... I would like to ask in this connection whether the transformation group [isospin] with constant phases can be amplified in a way analogous to the gauge

group for electromagnetic potentials in such a way that the meson-nucleon interaction is connected with the amplified group ...

Stimulated by this discussion, Pauli worked on this problem and drafted a manuscript to Pais that begins with [8]:

Written down July 22-25, 1953, in order to see how it looks. Meson-Nucleon Interaction and Differential Geometry.

Unaware of Klein's earlier contribution [7], Pauli generalizes in this manuscript the Kaluza-Klein theory to a sixdimensional space, and arrives through dimensional reduction at the essentials of an $SU(2)$ gauge theory. The extra-dimensions are two-spheres with spacetime dependent metrics on which $SU(2)$ operates in a spacetime dependent manner. Pauli develops first in "local language" the geometry of what we now call a fiber bundle with a homogeneous space as typical fiber (in his case $S^2 \cong SU(2)/U(1)$). Studying the curvature of the higher dimensional space, Pauli automatically finds for the first time the correct expression for the non-Abelian field strengths. Afterwards, Pauli sets up the 6-dimensional Dirac equation and writes it out in an explicit manner which is adapted to the fibration. Later, in December 1953, he sends a "Mathematical Appendix" to Pais and determines — among other things — the mass spectrum implied by this equation. The final sentence reads: "So this leads to some rather unphysical 'shadow particles'." Pauli did not write down a Lagrangian for the gauge fields, but as we shall see shortly, it was clear to him that the gauge bosons had to be massless. This, beside the curious fermion spectrum, must have been the reason why he did not publish anything.

With this background, the following story of spring 1954 becomes more understandable. In late February, Yang was invited by Oppenheimer to return to Princeton for a few days and to give a seminar on his joint work with Mills. Here, Yang's report [25]:

Pauli was spending the year in Princeton, and was deeply interested in symmetries and interactions. (He had written in German a rough outline of some thoughts, which he had sent to A. Pais. Years later F.J. Dyson translated this outline into English. It started with the remark, "Written down July 22-25, 1953, in order to see how it looks," and had the title "Meson-Nucleon Interaction and Differential Geometry.") Soon after my seminar began, when I had written down on the blackboard,

$$(\partial_\mu - i\epsilon B_\mu)\psi,$$

Pauli asked, "What is the mass of this field B_μ?" I said we did not know. Then I resumed my presentation, but soon Pauli asked the same question again. I said something to the effect that that was a very complicated problem, we had worked on it and had come to no definite conclusions. I still remember his repartee: "That is not sufficient excuse." I was so taken aback that I decided, after a few moments' hesitation to sit down. There was general embarrassment.

Finally Oppenheimer said, "We should let Frank proceed." I then resumed, and Pauli did not ask any more questions during the seminar.

I don't remember what happened at the end of the seminar. But the next day I found the following message:

February 24, Dear Yang, I regret that you made it almost impossible for me to talk with you after the seminar. All good wishes. Sincerely yours, W.Pauli.

I went to talk to Pauli. He said I should look up a paper by E. Schrödinger, in which there were similar mathematics[6]*. After I went back to Brookhaven, I looked for the paper and finally obtained a copy. It was a discussion of space-time-dependent representations of the γ_μ matrices for a Dirac electron in a gravitational field. Equations in it were, on the one hand, related to equations in Riemannian geometry and, on the other, similar to the equations that Mills and I were working on. But it was many years later when I understood that these were all different cases of the mathematical theory of connections on fiber bundles.*

Later Yang adds:

I often wondered what he [Pauli] would say about the subject if he had lived into the sixties and seventies.

At another occasion [22] he remarked:

I venture to say that if Weyl were to come back today, he would find that amidst the very exciting, complicated and detailed developments in both physics and mathematics, there are fundamental things that he would feel very much at home with. He had helped to create them.

Having quoted earlier letters from Pauli to Weyl, I add what Weyl said about Pauli in 1946 [26]:

The mathematicians feel near to Pauli since he is distinguished among physicists by his highly developed organ for mathematics. Even so, he is a physicist; for he has to a high degree what makes the physicist; the genuine interest in the experimental facts in all their puzzling complexity. His accurate, instructive estimate of the relative weight of relevant experimental facts has been an unfailing guide for him in his theoretical investigations. Pauli combines in an exemplary way physical insight and mathematical skill.

To conclude this section, let me emphasize the main differences of GR and Yang-Mills theories. Mathematically, the $so(1,3)$-valued connection forms ω in §3.1 and the Liealgebra-valued gauge potential A are on the same footing; they are both representatives of connections in (principle) fiber bundles over the spacetime manifold. Eq.(3.6) translates into the

[6] E. Schrödinger, Sitzungsberichte der Preussischen (Akademie der Wissenschaften, 1932), p. 105.

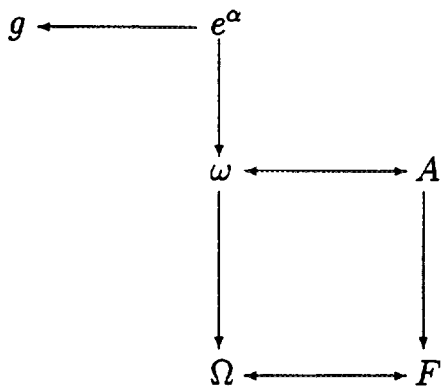

Figure 4: General Relativity versus Yang-Mills theory.

formula for the Yang-Mills field strength F,

$$F = dA + A \wedge A. \tag{4.1}$$

In GR one has, however, additional geometrical structure, since the connection derives from a metric, or the tetrad fields $e^\alpha(x)$, through the first structure equation (3.4). Schematically, we have:

(In bundle theoretical language one can express this as follows: The principle bundle of GR, i.e., the orthonormal frame bundle, is constructed from the base manifold and its metric, and has therefore additional structure, implying in particular the existence of a canonical 1-form (soldering form), whose local representative are the tetrad fields; see, e.g. [38].)

Another important difference is that the gravitational Lagrangian $*R = \frac{1}{2}\Omega_{\alpha\beta} \wedge *(e^\alpha \wedge e^\beta)$ is linear in the field strengths, whereas the Yang-Mills Lagrangian $F \wedge *F$ is quadratic.

5 Parity Violation and 2-Component Neutrino

The two-component spinor theory was only briefly mentioned in my discussion of Weyl's great 1929 paper. Since this massless spin 1/2 equation became very important after the discovery of parity violation I would now like to add a few remarks.

Due to the fact that there exist two inequivalent irreducible (projective) representations of the one-component of the homogeneous Lorentz group, $L_+^\uparrow$ (with $SL(2,C)$ as universal covering group), there are two types of fundamental Weyl spinors, ϕ_α and $\chi\dot{\beta}$, for which the free Weyl equations read as follows:

$$\hat{\sigma}^\mu \partial_\mu \phi = 0, \quad \sigma^\mu \partial_\mu \chi = 0. \tag{5.1}$$

Here, $(\sigma^\mu) = (1\!\!1, -\vec{\sigma})$, $(\hat{\sigma}^\mu) = (1\!\!1, \vec{\sigma})$ ($\vec{\sigma}$: Pauli matrices). In spinor calculus these equations

become

$$\partial^{\alpha\dot{\beta}}\phi_\alpha = 0, \quad \partial_{\alpha\dot{\beta}}\chi^{\dot{\beta}} = 0. \tag{5.2}$$

In his "New Testament" from 1933 [27], Pauli rejected these equations: "Indessen sind diese Wellengleichungen, wie ja aus ihrer Herleitung hervorgeht, nicht invariant gegenüber Spiegelungen (Vertauschlung von links und recht) und infolgedessen sind sie auf die physikalische Wirklichkeit nicht anwendbar."

However, as long as no interactions are taken into account, this statement is not correct. To make this evident one only has to note that both equations in (5.1) are equivalent to the Majorana formulation: Consider, for instance, the ϕ-field and set

$$\psi = \begin{pmatrix} \phi \\ \varepsilon\phi^* \end{pmatrix}, \qquad \varepsilon = \begin{pmatrix} 0 & 1 \\ -1 & 0 \end{pmatrix}, \tag{5.3}$$

then the first equation in (5.1) is equivalent to the massless Dirac equation,

$$\gamma^\mu \partial_\mu \psi = 0. \tag{5.4}$$

Furthermore, ψ is self-conjugate: A general Dirac spinor $\begin{pmatrix} \phi_\alpha \\ \chi^{\dot{\beta}} \end{pmatrix}$ transforms under charge conjugation C according to

$$C : \begin{pmatrix} \phi \\ \chi \end{pmatrix} \to \begin{pmatrix} -\varepsilon\chi^* \\ \varepsilon\phi^* \end{pmatrix} \tag{5.5}$$

and, for (5.3), this reduces to the Majorana condition $C : \psi \to \psi$. Nobody would say that the Majorana theory is not reflection invariant.

Note in this connection also the following: A Dirac field transforms under P as

$$P : \psi \to \psi'(x) = \gamma^0 \psi(Px). \tag{5.6}$$

For the Majorana field (5.3) this translates into an antilinear transformation for ϕ,

$$P : \phi \to \phi'(x) = \varepsilon\phi^*(Px), \tag{5.7}$$

which leaves the Weyl equation invariant. Usually this operation is interpreted as CP, but without interactions this is a matter of semantics.

Before I will return to history, let me also remind you of the formulation of Lee and Yang [28]. These authors introduce in the Weyl representation of the γ-matrices the Dirac spinor $\psi = \begin{pmatrix} \phi \\ 0 \end{pmatrix}$, whence $(1-\gamma^5)\psi = 0$. The first Weyl equation in (5.1) is then again equivalent to the massless Dirac equation (5.4). In the Lee-Yang formulation one thus has

$$\gamma^\mu \partial_\mu \psi = 0, \qquad (1-\gamma^5)\psi = 0. \tag{5.8}$$

These equations are, of course, independent of the representation of the γ-algebra.

Thus, the three formulations of Weyl, Majorana, and Lee-Yang are entirely equivalent. This was noticed by several authors [28] shortly after the discovery of parity violation, but had been worked out by J.Serpe [29] already in 1952. Today, because of the chiral nature of the fundamental fermions, the use of Weyl spinors has become common practice.

The discovery of parity violation early in 1957 in several experiments suggested by Lee and Yang [30] was one of the most exciting events in the fifties. Its impact was enormous, as is illustrated by the following letter from Pauli to Weisskopf [31]:

Dear Weisskopf,

Now the first shock is over and I begin to collect myself again (as one says in Munich).

Yes, it was very dramatic. On Monday 21st at 8:15 p.m. I was supposed to give a talk about "past and recent history of the neutrino". At 5 p.m. the mail brought me three experimental papers: C.S. Wu, Lederman and Telegdi; the latter was so kind to send them to me. The same morning I received two theoretical papers, one by Yang, Lee and Oehme, the second by Yang and Lee about the two-component spinor theory. The latter was essentially identical with the paper by Salam, which I received as a preprint already six to eight weeks ago and to which I referred in my last short letter to you. (Was this paper known in the USA?) (At the same time came a letter from Geneva by Villars with the New York Times article.)

Now, where shall I start? It is good that I did not make a bet. I would have resulted in a heavy loss of money (which I cannot afford); I did make a fool of myself, however (which I think I can afford to do)— incidentally, only in letters or orally and not in anything that was printed. But the others now have the right to laugh at me.

What shocks me is not the fact that "God is just left-handed" but the fact that in spite of this He exhibits Himself as left/right symmetric when He expresses Himself strongly. In short, the real problem now is why the strong interaction are left/right symmetric. How can the strength of an interaction produce or create symmetry groups, invariances or conservation laws? This question prompted me to my premature and wrong prognosis. I don't know any good answer to that question but one should consider that already there exists a precedent: the rotation group in isotopic spin-space, which is not valid for the electromagnetic field. One does not understand why it is valid at all. It seems that there is a certain analogy here!

In my lecture I described how Bohr (Faraday lecture, 1932, Solvay Conference, 1932), as my main opponent in regard to the neutrino, considered plausible the violation of the energy law in the beta-decay (what one calls today "weak interaction"), how his opposition then became weaker and how he said in a more general way (1933) that one must be "prepared for surprises" not anywhere but specifically with the beta-decay. Then I said spontaneously (on the spur of the moment) that at the end of my talk I would come back to the surprises which Professor Bohr had foreseen here ...

Many questions, no answers !

Let me say a bit more about the paper of Salam which is mentioned in Pauli's letter. In September 1956 Salam had heard Yang's talk at the Seattle Conference on his and Lee's famous solution of the $\vartheta - \tau$ puzzle by abandoning left/right symmetry in weak interactions. In his Nobel Price lecture Salam recollects [32]:

> *I remember travelling back to London on an American Air Force (MATS) transport flight. Although I had been granted, for that night, the status of a Brigadier or a Field Marshal — I don't quite remember which — the plane was very uncomfortable, full of crying servicemen's children — that is, the children were crying, not the servicemen. I could not sleep. I kept reflecting on why Nature should violate left/right symmetry in weak interactions. Now the hallmark of most weak interactions was the involvement in radioactivity phenomena of Pauli's neutrino. While crossing over the Atlantic came back to me a deeply perceptive question about the neutrino which Professor Rudolf Peierls had asked when he was examining me for a Ph.D. a few years before. Peierls' question was: "The photon mass is zero because of Maxwell's principle of a gauge symmetry for electromagnetism; tell me, why is the neutrino mass zero?"*

During that comfortless night he realized that Weyl's two-component equation for the neutrino would account for both parity violation and the masslessness of the neutrino. Soon afterwards he presented the idea to Peierls, who replied: "I do not believe left/right symmetry is violated in weak forces at all." After that, Salam was hoping to find more resonance at CERN. There he communicated the idea to Pauli, through Villars, who "returned the next day with a message of the Oracle: Give my regards to my friend Salam and tell him to think of something better."

Meanwhile parity violation was discovered and Salam got a kind, apologetic letter from Pauli. But this changed again soon afterwards. I quote:

> *Thinking that Pauli's spirit should by now be suitably crushed, I sent him two short notes (Salam, 1957b) I had written in the meantime. These contained suggestions to extend chiral symmetry to electrons and muons, assuming that their masses were a consequence of what has come to be known as dynamical spontaneous symmetry breaking. With chiral symmetry for electrons, muons, and neutrinos, the only mesons that could mediate weak decays of the muons would have to carry spin one. Reviving thus the notion of charged intermediate spin-one bosons, one could then postulate for these a type of gauge invariance which I called the "neutrino gauge". Pauli's reaction was swift and terrible. He wrote on 30 January 1957, then on 18 February and later on 11, 12 and 13 March: "I am reading (along the shores of Lake Zurich) in bright sunshine quietly your paper ..." "I am very much startled on the title of your paper 'Universal Fermi Interaction' ... For quite a while I have for myself the rule if a theoretician says*

universal it just means pure nonsense. This holds particularly in connection with the Fermi interaction, but otherwise too, and now you too, Brutus, my son, come with this word ... " *Earlier, on 30 January, he had written: "There is a similarity between this type of gauge invariance and that which was published by Yang and Mills... In the latter, of course, no* γ_5 *was used in the exponent,*" *and he gave me the full reference of Yang and Mills' paper [18]. I quote from this letter: "However, there are dark points in your paper regarding the vector field* B_μ*. If the rest mass is infinite (or very large), how can this be compatible with the gauge transformation* $B_\mu \rightarrow B_\mu - \partial_\mu \Lambda$ *?*" *and he concludes his letter with the remark: "Every reader will realize that you deliberately conceal here something and will ask you the same questions.*

6 Chiral Invariance and Universal $V-A$ Interaction

These recollections bring me to the last subject of my lecture. The two-component model of the neutrino paved also the way for a successful phenomenological description of weak interaction processes at low energies. In his masterly written review article "On the earlier and more recent history of the Neutrino" [33], Pauli remarks:

> *For some time I faced this particular model with a certain skepticism [42], since it seemed to me that the special role of the neutrino was emphasized too strongly. It turned out, however, that by further developing the ideas of Stech and Jensen (see §3 above) the model allowed an interesting generalization for the form of the interaction energy for all weak interactions.*

After an inventory of the experimental situation, mentioning in particular the new recoil experiments on ^{6}He, Pauli continues with:

> *Based on the Stech-Jensen transformation and the two-component model of the neutrino the following postulate suggests itself for the theoretical interpretation: The Hamiltonian of each weak 4-fermion interaction shall "universally" contain either only R or only L components of the involved fermions. Equivalent to this postulate is the formulation that in the transformation* $\psi' = \gamma_5 \psi$ *the density of the interaction energy for each particle separately should "universally" remain unchanged or change its sign.*

At this point the classical papers [34] are quoted, followed by the statement:

> *The Stech-Jensen transformation referred to a pair of the particles simultaneously while the two-component model of the neutrino is equivalent to the validity of the result of the transformation for the neutrino alone. The postulate of the extended Stech-Jensen transformation now under discussion is therefore a generalization of the two-component model of the neutrino.*

As we all know this postulate leads uniquely to the universal $V-A$ interaction. At the time it was disturbing that the V and A interaction strengths for nucleons in beta decay are empirically not equal. Today we know that the equality does hold on the level of the quark fields.

It is, unfortunately, not generally known that W. Theis proposed independently the parity violating V-A interaction in a paper submitted on 20 December 1957 to the *Zeitschrift für Physik* [35]. Theis emphasized that in the spinor calculus a Dirac spinor can be expressed in terms of a single two-component Weyl spinor

$$\psi = \begin{pmatrix} \phi_\alpha \\ \frac{i}{m}\partial^{\alpha\dot{\beta}}\phi_\alpha \end{pmatrix}, \tag{6.1}$$

and that the Dirac equation is then equivalent to the Klein-Gordon equation for ϕ_α. Since in this representation ψ contains derivatives, the author finds Fermi's requirement of a derivative-free coupling not so convincing and requires instead a derivative-free four-Fermi interaction for the Weyl spinors. This allows for only one possibility, namely

$$p_\alpha^* n_{\dot{\beta}} e^{*\alpha} \nu^{\dot{\beta}} + \text{h.c.}, \tag{6.2}$$

which is just the $V-A$ coupling.

This formal argument is similar to the one in the classic paper by Feynman and Gell-Mann [34]. The latter goes, however, beyond the $V-A$ interaction and advocates a current-current interaction Lagrangian, containing also hypothetical self-terms. These imply processes like neutrino-electron scattering or the annihilation process $e^- + e^+ \to \nu + \bar{\nu}$, which was soon recognized to be very important in the later evolutionary stages of massive stars [36]. (We have heard a lot about this during the school.)

It may also not be known to the young generation that various experiments[7] were in conflict with chiral invariance at the time when Feynman and Gell-Mann wrote their paper. They had the courage to question the correctness of these experiments:

> *These theoretical arguments seem to the authors to be strong enough to suggest that the disagreement with the ^6He recoil experiment and with some other less accurate experiments indicates that these experiments are wrong. The $\pi \to e + \bar{\nu}$ problem may have a more subtle solution.*

The later verification of the prediction for the ratio $\Gamma(\pi \to e\nu)/\Gamma(\pi \to \mu\nu)$ was one of the triumphs of the universal $V-A$ interaction.

We will certainly hear more from J. Steinberger about the experimental side of the story.

[7] For a description of the classic experiments, I refer to an excellent paper by Telegdi [37].

7 Epilogue

The developments after 1958 consisted in the gradual recognition that — contrary to phenomenological appearances — Yang-Mills gauge theory can describe weak and strong interactions. This important step was again very difficult, with many hurdles to overcome.

One of them was the mass problem which was solved, perhaps in a preliminary way, through spontaneous symmetry breaking. Of critical significance was the recognition that spontaneously broken gauge theories are renormalizable. On the experimental side the discovery and intensive investigation of the neutral current was, of course, extremely crucial. For the gauge description of the strong interactions, the discovery of asymptotic freedom was decisive . That the $SU(3)$ color group should be gauged was also not at all obvious. And then there was the confinement idea which explains why quarks and gluons do not exist as free particles. All this is described in numerous modern text books and does not have to be repeated.

The next step of creating a more unified theory of the basic interactions will probably be much more difficult. All major theoretical developments of the last twenty years, such as grand unification, supergravity and supersymmetric string theory are almost completely separated from experience. There is a great danger that theoreticians get lost in pure speculations. Like in the first unification proposal of Hermann Weyl they may create beautiful and highly relevant mathematics which does, however, not describe nature. Remember what Weyl wrote to C. Seelig in his late years:

> *Einstein glaubt, dass auf diesem Gebiet die Kluft zwischen Idee und Erfahrung so gross ist, dass nur der Weg der mathematischen Spekulation (...) Aussicht auf Erfolg hat, während mein Vertrauen in die reine Spekulation gesunken ist ...*

References

[1] H. Weyl, *Space · Time · Matter.* Translated from the 4th German Edition. London: Methmen 1922. *Raum · Zeit · Materie*, 8. Auflage, Springer-Verlag (1993).

[2] H. Weyl, *Gravitation und Elektrizität.* Sitzungsberichte Akademie der Wissenschaften Berlin, 465-480 (1918). Siehe auch die *Gesammelten Abhandlungen.* 6 Vols. Ed. K. Chadrasekharan, Springer-Verlag.

[3] N. Straumann, *Zum Ursprung der Eichtheorien bei Hermann Weyl.* Physikalische Blätter **43** (11), 414-421 (1987).

[4] H. Weyl, *Elektron und Gravitation. I.* Z. Phys. **56**, 330 (1929).

[5] W.Pauli, *Wissenschaftlicher Briefwechsel*, Vol. I: 1919-1929. p. 505. Springer-Verlag 1979. (Translation of the letter by L. O'Raifeartaigh.)

[6] L. O'Raifertaigh, *The Dawning of Gauge Theory.* Princeton University Press, to appear.

[7] O. Klein, *On the Theory of charged Fields.* 1938 Conference on New Theories in Physics held at Kazimierz, Poland 1938.

[8] W. Pauli, *Meson-Nucleon Interaction and Differential Geometry.* Letter to Pais, to appear in [6].

[9] R. Shaw, Thesis, Cambridge University 1955.

[10] R. Utiyama, *Butsurigaku wa dokumade susunkada* (How far has Physics progressed). Iwanami Shoten, Tokyo 1983.

[11] N. Straumann. *Ursprünge der Eichtheorien.* DMV-Seminar Geschichte der Mathematik (H. Weyls "Raum-Zeit-Materie"), to appear in Springer-Verlag (1996).

[12] N. Straumann *Von der Stech-Jensen-Transformation zur universellen V-A Wechselwirkung.* Archive for History of Exact Sciences, **44**, 365 (1992).

[13] J. Audretsch, F.Gähler and N. Straumann, *Comm.Math.Phys.* **95**, 41 (1984).

[14] W. Pauli, *Zur Theorie der Gravitation und der Elektrizität von H. Weyl.* Physikalische Zeitschrift **20**, 457-467 (1919).

[15] W. Pauli, *Relativitätstheorie.* Encyklopädie der Mathematischen Wissenschaften 5.2, Leipzig: Teubner, 539-775 (1921).

[16] F. London, *Quantenmechanische Deutung der Theorie von Weyl.* Z. Phys. **42**, 375 (1927).

[17] H. Weyl, *Selecta.* Birkhäuser-Verlag 1956.

[18] N. Straumann, *General Relativity and Relativistic Astrophysics.* Texts and Monographs in Physics, Springer-Verlag (1984).

[19] H. Weyl, *Gruppentheorie und Quantenmechanik.* Wissenschaftliche Buchgesellschaft, Darmstadt 1981 (Nachdruck der 2. Aufl., Leipzig 1931). Engl. translation: "Group Theory and Quantum Mechanics", Dover, New York, 1950.

[20] Ref.[5], p. 518.

[21] In Carl Seelig: *Albert Einstein.* Europa Verlag Zürich 1960, p. 274.

[22] C.N. Yang, *Hermann Weyl's Contribution to Physics.* In: *Hermann Weyl*, Edited by K. Chandrasekharan, Springer-Verlag 1980.

[23] H. Weyl, *Gesammelte Abhandlungen*, Vol.I to IV. Springer-Verlag 1968. Edited by K. Chandrasekharan. (Vol.III, p.229).

[24] Conference in Honour of H.A. Lorentz, Leiden 1953. *Proceedings in Physica*, **19** (1953). A.Pais, p. 869.

[25] C.N. Yang, *Selected Papers 1945-1980 with Commentary.* Freeman and Co. 1983, p.525.

[26] H. Weyl. *Memorabilia.* Ref. [22], p. 85.

[27] W. Pauli, *Die allgemeinen Prinzipien der Wellenmechanik.* Handbuch der Physik, Geiger und Scheel, 2. Auff., Vol.24, Teil 1 (1933).

Von N. Straumann neu herausgegeben und mit historischen Anmerkungen versehen, Springer-Verlag (1990). English translation: *General Principles of Quantum Mechanics.* Springer-Verlag 1980.

[28] T.D. Lee, C.N. Yang, *Phys.Rev.* **105**, 1671 (1957);

L.D. Landau, *Nucl.Phys.* **3**, 127 (1957);

A. Salam, *Nuovo Cimento* **5**, 299 (1957);

K.M. Case, *Phys.Rev.* **107**, 307 (1957);

J.A. McLennan, Jr. *Phys.Rev.* **106**, 821 (1957).

[29] J. Serpe, *Physica* **18**, 295 (1952).

[30] T.D. Lee and C.N. Yang, *Phys.Rev.* **104**, 254 (1956).

[31] In Ref.[5]. Translation by V.F. Weisskopf.

[32] A. Salam, *Gauge Unification and fundamental Forces, Rev.Mod.Phys.* **52**, 525 (1980).

[33] W. Pauli, *Zur älteren und neueren Geschichte des Neutrinos,* in W. Pauli: Aufsätze und Vorträge über Physik und Erkenntnistherorie. Vieweg, Braunschweig 1961. English translation in: *Neutrino Physics,* Ed.: K. Winter, Cambridge University Press 1991, p.1.

[34] E.C.G. Sudarshan and R.E. Marshak, *Phys.Rev.* **19**, 1860 (1958);

J.J. Sakurai, *Nuovo Cimento* **7**, 649 (1958);

R.P. Feynman and M. Gell-Mann, *Phys.Rev.* **109**, 193 (1958).

[35] W.R. Theis, *Z.Physik* **150**, 590 (1958).

[36] H.Y. Chiu, P. Morrison, *Phys.Rev.Lett.* **5**, 573 (1960).

[37] V.L.Telegdi, *The early experiments leading to V-A interaction.* In: *"Pions to Quarks: particle physics in the 1950's"*, Ed: L.M. Brown, M. Dresden, Cambridge University Press 1989.

[38] D. Bleecker, *Gauge Theory and Variational Principles*, Addison-Wesley 1981.

Experiments on Double Beta Decay

J. Busto

Institut de Physique, Université de Neuchâtel, CH-2000 Neuchâtel, Suisse

1. Introduction

From a very general point of view, Double Beta Decay (DBD) can be defined as an isobaric second order process from which a (A, Z) nucleus decays directly to a $(A, Z \pm 2)$. There are four of them:

$$\beta^-, \beta^- : (A, Z) \rightarrow (A, Z+2) + 2e^- + 2\bar{\nu}_e$$
$$\beta^+, \beta^+ : (A, Z) \rightarrow (A, Z-2) + 2e^+ + 2\nu_e$$
$$\beta^+, E.C. : (A, Z) \rightarrow (A, Z+2) + e^+ + 2\nu_e$$
$$E.C., E.C. : (A, Z) \rightarrow (A, Z+2) + 2\nu_e$$

First two reaction, producing two $e^{\pm}$, have the best signature from *direct* experimental point of view and would be obviously called Double Beta Decay. In this lecture we only consider $\beta\beta$ process, in particular $\beta\beta^-$.($\beta\beta^+$ is generally disadvantaged because of the Coulomb barrier and the small space phase).

The candidates for DBD are even-even nuclei, particularly those for which the single beta decay is forbidden. There are around forty natural isotopes with $Q_{\beta\beta}$ values between a few keV and 4.7 MeV that are good $\beta\beta$ candidates.

According to light particles produced with two electrons, DBD can be classified into various decay modes.

The first mode, called two neutrino DBD ($(\beta\beta)_{2\nu}$), was proposed by Goeppert-Mayer in 1935 as second order extension of Fermi's theory of beta decay[1].

$$(A, Z) \rightarrow (A, Z+2) + 2e^- + 2\bar{\nu}_e$$

This rare, but allowed process, was directly observed by Moe et al.[2] in 1987.

The classical papers of Majorana [3] and Racah [4] have motivated Furry in 1939 [5] to consider a 'new' DBD mode from which it will be possible to study the neutrino character (Dirac or Majorana). This mode called neutrinoless DBD ($(\beta\beta)_{0\nu}$) is characterized by leptonic number non-conservation ($\Delta L = 2$), and would be forbidden in the Standard Model.

$$(A, Z) \rightarrow (A, Z+2) + 2e^-$$

Here, a virtual neutrino is expected to be exchanged between single β^- and $(\beta^-)^{-1}$ processes according to the Racah sequence:

$$\left\{ \begin{array}{l} n \rightarrow p + e^- + \nu_1 \\ \nu_2 + n \rightarrow p + e^- \end{array} \right\} \nu_1 \rightarrow \nu_2 \qquad (1)$$

According to the leptonic number consevation, and the Left handed coupling of the charged currents one has : $\nu_1 = \bar{\nu}_{RH}$ and $\nu_2 = \nu_{LH}$ (where RH and LH represent respectively Right and Left handed helicities) . Therefore, the existence of Racah sequence requires:

$$\left\{ \begin{array}{ll} -Mayorana\ neutrino\ character & (\Longrightarrow \bar{\nu} \equiv \nu) \\ -Non-zero\ neutrino\ mass & (\Longrightarrow \nu_{RH} \rightarrow \nu_{LH}) \end{array} \right. \qquad (2)$$

The presence of Right Handed Currents would also solve the problem of spin-flip arrangement, even if their existence is not *sine qua non* condition.

Requirements for neutrinoless DBD are in contradiction with the Standard Model, where neutrinos are Dirac massless particles, charged currents are pure Left Handed, and the leptonic number is conserved. However they would be observed in several GUT or Super Symmetric theories, proving that neutrinoless DBD is an excellent test of new physics beyond the SM. [6]

Other DBD modes have been studied recently, for example the DBD with emission of Majoron:

$$(A, Z) \rightarrow (A, Z+2) + 2e^- + \chi$$

In this process, proposed by Gelmini et al. in 1981 [7], two electrons are emitted with a hypothetically massless and weak interacting particle called Majoron, from which the B-L symmetry present in some GUT theories is broken leading to leptonic number non-conservation and massive Majorana neutrinos. This idea was abandoned in 1989 beacause the "classical" Majoron was expected to contribute to the Z^0 width. However, recently, a new Majoron mode has been proposed in a more general theory, where the LEP results do not influence [8].

2. Experimental characteristics

From experimental point of view, the main characteristic of DBD is its decay period $T_{1/2}$. This period can be calculated from second order perturbation theory. For different DBD modes, the decay periods are listed below :

$$[T^{2\nu}_{1/2}]^{-1} \sim G^{2\nu} \mid M^{2\nu} \mid^2$$
$$[T^{0\nu}_{1/2}]^{-1} \sim G^{0\nu} \mid M^{0\nu} \mid^2 < m_\nu >^2$$
$$[T^{\chi}_{1/2}]^{-1} \sim G^{\chi} \mid M^{0\nu} \mid^2 < g_{\nu\chi} >^2$$

The $G^{2\nu,0\nu,\chi}$ parameter represents space phase integrals which include kinematics of the problem. Th $M^{2\nu,0\nu,\chi}$ are nuclear matrix elements containing nuclear structure of initial, final and intermediate nucleus in the decay. This parameter is not very well known, although an important progress has been made in the last decade, especially for the two neutrino process. Anyway, a correct estimation of nuclear matrix element plays a very important role in the precision of DBD experiments.

The period of $(\beta\beta)_{0\nu}$ decay is also proportional to the effective neutrino mass, defined as:

$$< m_\nu >= \sum_i \mid U_{ei} \mid^2 m_{\nu i} \phi_{ci} \tag{3}$$

This parameter represents the mean neutrino mass weighted by mixing parameter $\mid U_{ei} \mid$ and CP phase ϕ_{ci} ($\phi_{ci} = +1$ *or* -1). Therefore, $(\beta\beta)_{0\nu}$ experiments are only qualitative for the neutrino mass estimation. However, a positive result would be a clear indication that at least one neutrino is massive Majorana particle.

Finally, the $< g_{\nu\chi} >$ parameter corresponds to the effective $\nu - \chi$ coupling in the Majoron mode.

The period of the DBD can, on the other hand, be written as :

$$T_{1/2} \sim \varepsilon \frac{a}{A} \sqrt{\frac{M.t}{\sigma.B}} \tag{4}$$

The parameters of equation (4) are experimetally determined : ε is efficiency for $2e^-$ detection, a the sample enrichement, A the atomic mass number, M the sample mass, t the runnig time, σ the energy resolution, and B the background (c/keV.y.kg). The adjustement of these parameters can increase the sensitivity of *direct experiments*. In particular, the use of enriched samples has been the main reason of a very important improvement of sensitivity in the last decade.

The spectra of different decay modes are shown in figure. 1 The $((\beta\beta)_{0\nu})$ characterized by a narrow line would be the best signed mode.

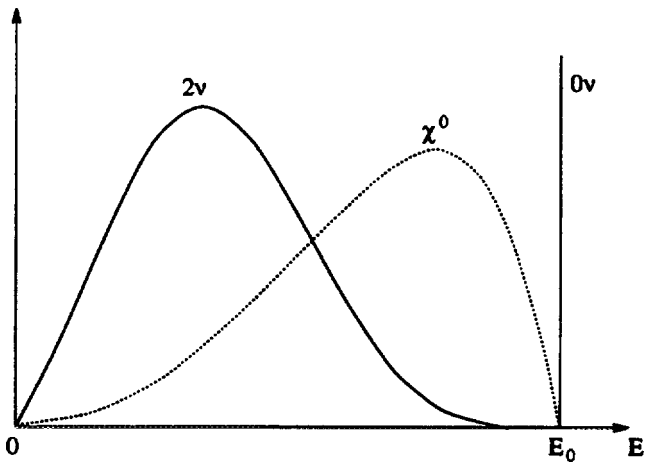

Fig. 1. Two electron spectrum for $(\beta\beta)_{2\nu}$, $(\beta\beta)_{0\nu}$, and $(\beta\beta)_{\chi}$ modes.

3. Experimental techniques for $\beta\beta$ detection

Since 1948, a large number of different techniques has been used in the study of $\beta\beta$ decay [9]. It is however possible to divide them in two kinds, depending which characteristic of the process is considered : daugther nucleus $(A, Z+2)$, or two electrons.

Indirect experiments.

In this case, the daugther nucleus are sought in samples rich in $\beta\beta$ candidates. If the sample is an old mineral, the experiment is called geochemical and the $(A, Z+2)$ isotopes are extracted using mass spectroscopy technique. Here, the decay time is very long ($\sim 10^9$ y). Therefore, a large amount of daugther nucleus is produced , but also some not very well establish background.

A better background estimation can be done using an artificial sample. The control of background during the decay time is now possible, but this time will be much shorter ($\sim$ 10 y) . This experiments are called radiochemical and are principaly used for high Z elements with daugther nucleus as α emitters.

Although the first evidence of $\beta\beta$ decay was obtained in 1968 using geochemical technique [10], its main disadvantage is the difficulty to distinguish allowed and forbidden modes.

Direct experiments.

In direct experiments we are looking for emission of the two electrons 'on line'. This reduces the ambiguity, $(\beta\beta)_{2\nu}$ or $(\beta\beta)_{0\nu}$, of indirect technique.

In spite of a huge number of techniques used, the direct experiments can be, in a good approximation, divided in two philosophies :

- **Foil detectors :** $\beta\beta$ source is a thin foil placed between two electron detection regions. In this configuration, simultanity and common origin of the process are particulary well defined. The possibility of studing different $\beta\beta$ candidates is another important advantage of this technique.

- **Block detectors:** the source is distributed in the volume of the detector. Here generally, the

detector and the source are identical and the detection is principaly calorimetric. (In gaseous detectors the tracking of two electrons is also possible.)

Around forty experiments are running now. Here we will consider only four of them like small, but representative sample of the experimentation in $\beta\beta$ decay.

Experiments with Ge.

The ^{76}Ge isotope is a good candidate for $\beta\beta$ decay with natural abundance of 7.8% and 2038 keV of $Q_{\beta\beta}$. Moreover, the very good energy resolution (typically $\sim 0.1\%$) is an important tool for extraction of the narrow line of $(\beta\beta)_{0\nu}$ from continuous background. This technique was proposed for the first time in 1967 and has been used with natural enrichement, up to 1990 [11]. Since this date, the possibility of using enriched Ge cristals was considered.

At the present, two important experiments are running, using enriched Ge detectors, the International Germanium Experiment (IGEX) and the Heidelberg-Moscou collaboration. This two experiments are very similar in desing and here we will describe only the Heidelberg-Moscou experiment [12].

The experimental set-up is rather simple. The Ge crystal is placed in a cryostat and surrounded with passive shielding. Five enriched crystals (enriched at 85.6 to 88.3 %) are used, weighting between 0.9 to 2.9 kg. Four of crystals are placed in the same shielding, made out of 10 cm of low activity lead, inside, and 20 cm of Boliden Pb, outside. An additional neutron and Radon shielding surrounds the whole set-up. (Detector number "4" is closed in another shielding where the lead is replaced by copper.). Finally, the experiment is placed in the Gran Sasso Underground Laboratory (Italy) with 3500 m.w.e. The total energy resolution is $3.37 \pm 0.32 keV$ at $Q_{\beta\beta}$, and the total background between 2000 - 2100 keV 0.203 ± 0.014 count/keV.y.kg. Further reduction of background can be obtained using Pulse Shape Discrimination analysis. The results after 17.2 kg.y of exposure are given in table 1.

Table 1: Heidelberg-Moscou results. All limits are at 90% C.L.

$(\beta\beta)_{0\nu}$	$T_{1/2} \geq 9.6 \cdot 10^{24} y$	$\Rightarrow$	$\langle m_\nu \rangle \leq 0.5 eV$ [19]
$(\beta\beta)_{\chi}$	$T_{1/2} \geq 7.8 \cdot 10^{21} y$	$\Rightarrow$	$\langle g_{\nu\chi} \rangle \leq 10^{-4}$
$(\beta\beta)_{2\nu}$	$T_{1/2} = (1.77 \pm 0.1\,(stat) \pm 0.12\,(sys))10^{21}\ y$		

The Gotthard experiment.[13]

The Gotthard collaboration (Neuchatel-P.S.I.-Caltech) is studing the $\beta\beta$ decay of ^{136}Xe to ^{136}Ba characterized with $Q_{\beta\beta} = 2.480 keV$. The detector is a copper Time Projection Chamber of 180 l of fiducial volume (ϕ = 60 cm, h = 70 cm), 5 cm wall thickness, filled with 62.5 % ^{136}Xe at 5 bars. It is surrounded by 15-20 cm of Pb, 5 cm of B_4C (neutron shielding), and a plastic bag, protecting the detector against the external radon (figure 2). The experiment is running in the Gotthard tunnel (Switzerland) since 1990. The active volume is limited at one side by a cathode plane and at the other side by a Grid-Anode plane behind which, a foil containing strips in X and Y directions is placed (XY-plane). In this configuration, the ionisation electrons produced in the gas by primary charge particles, drift towards the anode plane where they give a signal proportional to the energy, and induce a pulse in the XY plane. The third coordinate cames from time evolution of ionisation electrons arriving to the anode.

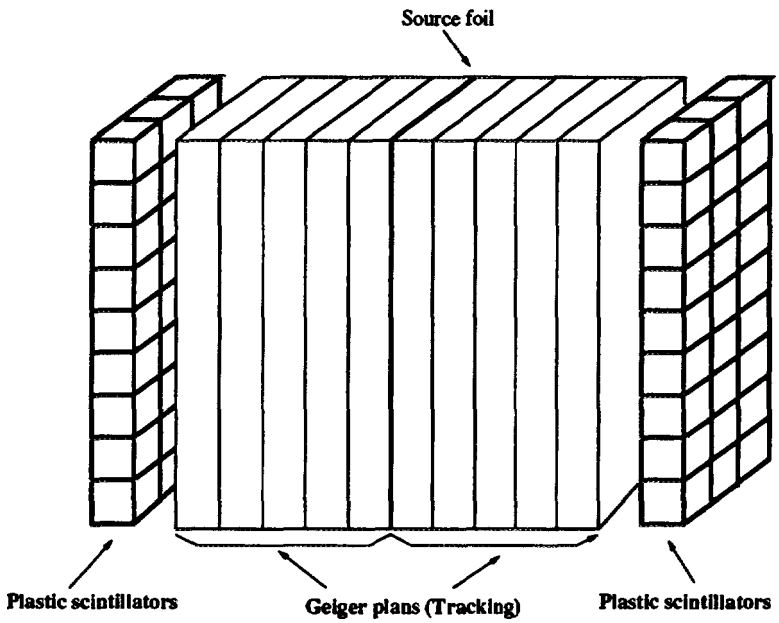

Fig. 3. Simplify sketch of NEMO-II detector.

measurements are listed in the table 3.

The total efficiency for the $(\beta\beta)_{0\nu}$ is around 5% and therefore the sensitivity for the forbidden decay is very low. The NEMO-II detector is consider by NEMO–collaboration as a 'test detector' for future experiments. The future for NEMO–collaboration is the NEMO-III detector already in construction. The detector (based on the same general concept as NEMO-II), will have cylindrical structure. The source is a $20m^2$ foil containing up to 10 kg of enriched isotopes. The energy measurement will be done with 1940 P.M.T. surrounding the tracking region. Here, the efficiency grows up to around 30%, and the sensitivity would be about 10^{25} y. It is forseen to start runnig the detector in 1999 and measure several $\beta\beta$ candidates (Mo, Se,...)[15].

Table 3: NEMO-II results. (All limits are at 90% C.L.)

	^{100}Mo	^{116}Cd
$(\beta\beta)_{0\nu}$	$T_{\frac{1}{2}} \geq 6.4 \cdot 10^{21} y \Rightarrow \langle m_\nu \rangle \leq 13\, eV$	$T_{\frac{1}{2}} \geq 6.1 \cdot 10^{21} y$
$(\beta\beta)_{\chi}$	$T_{\frac{1}{2}} \geq 5.0 \cdot 10^{20} y \Rightarrow \langle g \rangle \leq 2.4 \cdot 10^{-4}$	$T_{\frac{1}{2}} \geq 1.2 \cdot 10^{21} y$
$(\beta\beta)_{2\nu} T_{1/2}$	$= (0.95 \pm 0.04\,(stat) \pm 0.09\,(sys))10^{19}\, y$	$T_{1/2} = (3.6 \pm 0.3\,(stat) \pm 0.3\,(sys))10^{19}\, y$

Thermal experiments.

Most of the energy released by particles in matter is transformed in phonons. At the usual bolometer working temperature ($\sim$ 10 mK), the energy released gives a detectable increase of temperature on an adequate sensor. We have:

$$\Delta T = E/C_{th}$$

C_{th} is the heat capacity given by Debye law : $C_{th} \propto (T/T_{Debye})^3$ and E is the energy released by the particle. Moreover, the theoretical energy resolution can be rather high ($\sigma \sim$ 10 eV @ 2 MeV for 1 kg), much better than for Germanium detectors.

The use of thermal detectors to search for $(\beta\beta)_{0\nu}$ in calorimetric ("block detectors") approach has been suggested in 1984 [16]. The use of large crystals with low heat capacity and working at low

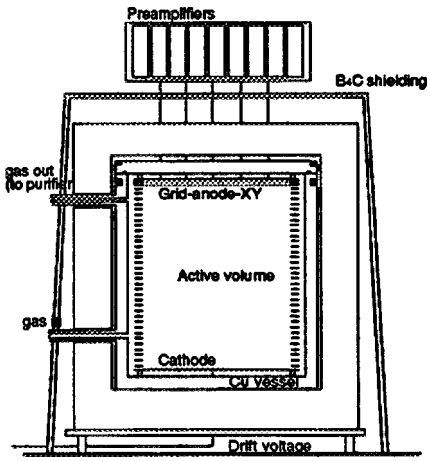

Fig. 2. Gotthard $\beta\beta$ Xe detector.

Table 2 sumarizes the results after 12750 h for total statistics and 5925 h in low background configuration.

The main performances of the set-up are : Δ E = 7% at 2.5 MeV; Δ X,Y = 3.5 mm.; Δ Z = 2.0 mm. (FWHM)

Table 2: Results for the first (before upgrade) and second period (after upgrade) of data taking for $\beta\beta$ analysis. (Limits are at 90% C.L.)

	First period	Second period
$(\beta\beta)_{0\nu}$	$T_{\frac{1}{2}} \geq 3.7 \cdot 10^{23} y \Rightarrow \langle m_\nu \rangle \leq \begin{cases} 2.8eV \\ 2.4eV \end{cases}$	$T_{\frac{1}{2}} \geq 4.2 \cdot 10^{23} y \Rightarrow \langle m_\nu \rangle [18] \leq \begin{cases} 2.7eV \\ 2.3eV \end{cases}$
$(\beta\beta)_\chi$	$T_{\frac{1}{2}} \geq 5.0 \cdot 10^{21} y \Rightarrow \langle g \rangle \leq 2.4 \cdot 10^{-4}$	$T_{\frac{1}{2}} \geq 1.4 \cdot 10^{22} y \Rightarrow \langle g \rangle \leq 1.5 \cdot 10^{-4}$
$(\beta\beta)_{2\nu}$	$T_{\frac{1}{2}} \geq 2.0 \cdot 10^{20} y$	$T_{\frac{1}{2}} \geq 5.5 \cdot 10^{20} y$

The results of the experiment can be divided in two periods. The first ones from 1991 to 1994 and the second ones from 1994 to 1996. This second period is characterized by the use of a new readout system, as well as the addition of the neutron shielding. With those improvements, the original background was reduced by a factor of 4 in region of interest for the single electrons events.

The NEMO collaboration.

The NEMO collaboration includes, principally, laboratories from France and Russia, searching for the $\beta\beta$ decay of several isotopes using a typical 'foil technique'. In the NEMO-II detector, described here, the source is a $1m^2$ foil, thick about 50 μm, placed in the middle of a wire chamber, from which it is possible to extract the trajectory of electrons produced in the foil. The wire chamber is made out of ten modules each one containing 32 horizontal cells and 32 vertical cells working in Geiger mode in 1 bar helium gas . Tracking precision is $\Delta_{Long} = 5mm, \Delta_{Trans} = 0.5mm$ (FWHM) [14].

The energy and time information in the experiment is given by two scintillator walls, placed at the ends of tracking region. Each wall contains 24 plastic scintillators coupled to low background P.M.T.

Finally, the whole detector is protected with 10 cm of iron and 15 cm of lead, and is running in the Frejus tunnnel (France) (figure 3).

Up to now, the NEMO collaboration has measured two different isotopes. The results of this

temperatures are the main conditions of this technique. The technique opens as well the possibility to study, with high energy resolution, other DBD candidates than ^{76}Ge.

One of the experiments using this technique is made by Milano group. In this experiment, TeO_2 monocrystals are used as DBD source (^{130}Te is an interesting candidate to DBD with $Q_{\beta\beta} = 2528$ keV and 33.9 % of natural abundance).

Table 4: Milano group results

	All limits are at 90% C.L.
$(\beta\beta)_{0\nu}$	$T_{1/2} \geq 3.25 \cdot 10^{22} y$
$(\beta\beta)_{2\nu}$	$T_{1/2} \geq 1.8 \cdot 10^{22}\ y$

Several crystals of around 330 g have been made and installed in different set-up's. In particular, four crystals were mounted in the same cryostat. The energy resolution for three of them was 12 keV at 2.6 MeV, and the background in the region of interest $\sim$ 4 counts/kg.keV.yr. The results are summarized in table 4.

The Milano group is now preparing a new and more competitive set-up containing 20 crystals in the same cryostat, from which they expect to increase the limits up to 10^{25} y.

4. Experiment - Theory comparison

Comparison between theory and experimental results is presented in table 5 for some $\beta\beta$ candidates. As we can see, the calculation using nuclear matrix elements from references [17] and [19] are in quite good agreement with $(\beta\beta)_{2\nu}$ experimental observation. However the extrapolation of nuclear matrix calculations to $(\beta\beta)_{0\nu}$ mode is not obvious and important incertitudes in the estimation of the limits for effective neutrino mass remain.

Table 5: Experimental and theoretical comparison

Isotope	$(\beta\beta)_{2\nu}$		$(\beta\beta)_{0\nu}$	
	$T_{1/2}^{Exp.}$	$T_{1/2}^{Theo.}$	$T_{1/2}^{Exp.}$	$\langle m_\nu \rangle$
^{76}Ge	$1.80 \cdot 10^{21}$	$(2.2 - 3.6) \cdot 10^{21}$[19] $1.3 \cdot 10^{21}$[17] $7.0 \cdot 10^{19} - 3.0 \cdot 10^{21}$[18]	$\leq 9.6 \cdot 10^{24} y$	$1.35eV$[19] $1.14 - 1.30eV$[17] $0.5eV$ [18]
^{82}Se	$1.08 \cdot 10^{20}$	$(4.9 - 8.0) \cdot 10^{19}$[19] $1.2 \cdot 10^{20}$[17] $2.9 \cdot 10^{18} - 5.9 \cdot 10^{21}$[18]	$\leq 1.7 \cdot 10^{22} y$	$12.6eV$[19] $7.4eV$[17] $6.1eV$ [18]
^{136}Xe	$\geq 5.5 \cdot 10^{20}$	$(2.0 - 1.6) \cdot 10^{21}$[19] $8.2 \cdot 10^{20}$[17] $1.5 \cdot 10^{19} - 2.1 \cdot 10^{21}$[18]	$\leq 4.2 \cdot 10^{23} y$	$5.3eV$[19] $(2.3 - 2.8)eV$[17] $2.3eV$ [18]

5. How far can we go in $\beta\beta$ experiments

Before concluding, it would be interesting to try to see how far it would be possible to go, reasonably, in $\beta\beta$ decay experiments, if the signal is not observed before.

In this purpose we consider an ideal case with zero background. Here, the effective neutrino mass can be expressed as:

$$< m_\nu > \sim C^{theo.} \cdot (M \times T)^{-1}$$

where C^{theo} contains the nuclear matrix elements, M is the mass and T the running time.

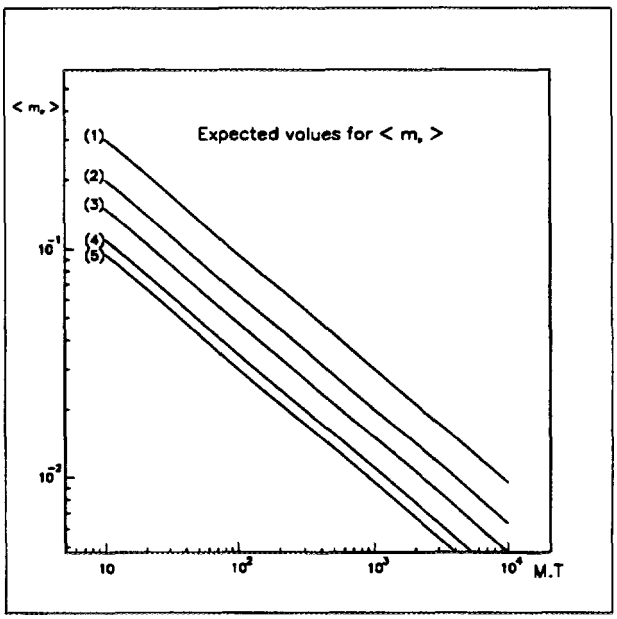

Fig. 4. Expectation values for $< m_\nu >$ versus *mass* × *time* product according to Heidelberg nuclear matrix elements. Numbers (1) to (5) represent respectively :^{136}Xe, ^{76}Ge, ^{100}Mo, ^{130}Te, and ^{82}Se

Figure 4 shows the values of $< m_\nu >$ as a function of $M \times T$ product according to, as an exemple, the Heidelberg calculation (other origins of nuclear matrix elements give the same conclusions). As we can see, because of the dependence in $\sqrt{M \times T}$, the improvement of the sensitivity to $< m_\nu >$ becomes very difficult to achive. In particular, any future experiment with sensitivity to 10^{-2} eV would need several ton of enriched material !.

Another important remark comes from the background induced by allowed $\beta\beta$ mode in the region where $(\beta\beta)_{0\nu}$ is expected. This background, always present, would have a huge importance in future experiments with very high $T_{1/2}$ ($> 10^{25}$ y). As an exemple, an one ton experiment with a sensitivity of 10^{-2} eV, and $T^{2\nu}_{1/2} \sim 10^{19}$ y, would have a background in a 6% energy window center at $Q_{\beta\beta}$ of around 400 events/y due to $(\beta\beta)_{2\nu}$ spectrum (to be compared with around 1evt/y from the signal) [20]. Therefore, a good energy resolution becomes necessary.

In spite of those another difficulties for future $\beta\beta$ experiments, several new ideas have already been proposed [21].

6. Conclusion

The Double Beta Decay, and especialy $(\beta\beta)_{0\nu}$ mode, is an excelent test of Standard Model as well as of neutrino physics.

From experimental point of view, a very large number of different techniques are or have been used increasing the sensitivity of this experiments quite a lot (the factor of 10^4 in the last 20 years).

In future, in spite of several difficulties, the sensitivity would be increased further, keeping the

interest of this very important process.

7. References

1. M. Goeppert-Mayer *Phys. Rev.* **48** (1932) 512
2. Elliot et al. *Phys. Rev. Lett.* **59** (1987) 2020-23
3. E. Majorana Nuovo Cimento **14** (1937) 171
4. G. Racah Nuovo Cimento **14** (1937) 322
5. W.H. Furry *Phys. Rev.* **56** (1939) 1184
6. M.Hirsch et al. *Phys. Rev.* **D53** (1996) 1329
7. Gelmini et al.*Phys. Lett.* **B99** (1981) 411-15
   Georgi et al. *Nucl. Phys.* **B193** (1981) 297-316
8. C.P. Burgess and J.M. Cline: *Phys. Lett.***298B** (1993) 141;
   Phys. Rev. **D49** (1994) 5925.
9. M. Moe and P. Vogel: *Annu. Rev. Nucl. Part. Sci. 1994* (1994) 247–283.
   M.Moe *J. Mod Phys* **E2** (1993) 507-46
   W.C. Haxton, G.J. Stephenson *Prog. Part. Nucl. Phys. 12* (1984) 409-479
10. T. Kirsten et al.*Phys. Rev. Lett.* **20** (1968) 1300
11. Fiorini et al.*Phys. Lett.* **B25** (1967) 602
    D.O. Caldwell *J. Phys. G : Nucl. Part. Phys.* **17** (1991) s137-S144
    Reusser et al. *Phys. Rev.* **D45** (1992) 2548-51
12. A. Balysh et al. *Phys. Lett.* **B356** (1995) 450
13. J.C. Vuilleumier et al. *Phys. Rev.***D48** (1993) 1009-20.
14. Arnold et al. *Nucl. Phys.***B35** (Proc. Suppl) (1994) 369-71.
    Dassie et al. *Phys. Rev.* **D51** (1995) 2090
15. NEMO3 *propossal LAL 94-29* (1994)
16. Fiorini et al. *Nucl. Inst. and Meth.* **224** (1984), 83
17. J. Engel, P. Vogel and MR. Zirnbauer *Phys. Rev.* **C37** (1988) 731–46.
18. A. Staudt, K. Muto and HV Klapdor-Kleingrothaus *Europhys. Lett.* **13** (1990) 31–36.
19. Caurier et al. *Phys. Rev. Lett.* **77** (1996) 1954
20. M.K. Moe *Phys. Rev.* **C44** (1988) r931
21. MUNU *Proposal IPH-Univ. Neuchâtel* (1992)

CH9700124

Electromagnetic Properties of Neutrinos

F. Ould-Saada [1]
Physics Institute, University of Zurich

Abstract

Electromagnetic properties of neutrinos and their implications are discussed, and the experimental situation summarised. Spin precession in solar magnetic fields presents a solution of the solar neutrino problem. A magnetic moment, μ_ν, of the order of $10^{-11}\mu_B$ would be needed. In the simplest extension of the standard model, with non-vanishing neutrino masses, dipole moment interactions are allowed through higher order processes. A neutrino mass of $\sim 10\ eV$ would give $\mu_\nu \sim 10^{-18}\mu_B$, much smaller than the present experimental upper limit of $2 \times 10^{-10}\mu_B$. Although model-dependent, upper bounds on dipole moments from astrophysics and cosmology are 10 to 100 times more stringent. Any values of μ_ν, larger than the SM predictions, would then signal the onset of new physics. Among the processes sensitive to the magnetic moment, νe^- scattering presents two advantages: it is a pure weak, theoretically well understood process, and the recoil electron can be easily measured. A hypothetical electromagnetic contribution to the cross-section would dominate at low energies. A low background detector, MUNU, being built at the Bugey nuclear reactor is presented. It is based on a gas TPC, surrounded by a liquid scintillator. The threshold on the electron recoil energy can be set very low, around 500 keV, giving the experiment a good sensitivity to the magnetic moment of the $\overline{\nu_e}$, extending down to $2 \times 10^{-11}\mu_B$.

1 Introduction and Motivations

1.1 What do we know about neutrinos?

The neutrino, a neutral particle of spin one half, was proposed in 1930 by W. Pauli "...as a desperate remedy to save the principle of energy conservation in β-Decay...". The electron antineutrino, $\overline{\nu}_e$, was discovered a quarter of a century later by Reines and his collaborators[1, 2] at a nuclear reactor. The neutrino helicity was measured to be negative 1957[3]. The proof for the existence of a second Neutrino related to the muon was obtained in 1962[4] using high energy neutrinos produced by an accelerator. The existence of a third neutrino, ν_τ, related to the tau-lepton was inferred in 1975[5].

What do we know about neutrinos today? Neutrinos are weakly interacting, spin $\frac{1}{2}$ particles. There are 3 kinds of light neutrinos ν_e, ν_μ and ν_τ corresponding to the three known leptons e^-, μ^- and τ^- ($m_{\nu_4} > 45\ GeV/c^2$ from LEP data). Neutrinos are described in the framework of the standard model of electroweak interactions based on the group $SU(2)_L \times U(1)$. In the standard model neutrinos are massless and of Dirac type. Only ν_L and $\overline{\nu}_R$ have the weak interaction. ν_R and $\overline{\nu}_L$ are sterile. Up to now neutrinos are massless with the upper limits $m_{\nu_e} < 4.35\ eV/c^2$[6], $m_{\nu_\mu} < 170\ keV/c^2$[7], and $m_{\nu_\tau} < 24\ MeV/c^2$[8].

What needs to be learned about neutrinos today? Do they have a mass? If yes, why are they so much lighter than other leptons and quarks? (see-saw mechanism?) Do they oscillate in vacuum? in matter? What is the origin of the 'solar neutrino problem'? What is the origin of the 'atmospheric neutrino problem'? Are neutrinos heavy enough to explain dark matter? Are neutrinos Majorana (neutrinoless double β decay?) or Dirac particles? Do neutrinos interact electromagnetically? Do they acquire any dipole moment (magnetic or electric)? Do they have any structure (charge radius)?

1.2 Electromagnetic properties of neutrinos

Although neutrinos are neutral[9] ($Q_\nu < 2 \times 10^{-15}$), they can couple to the electromagnetic field through higher order weak interactions. The EM ν-Vertex (Fig.1) has the form

$$F_R(q^2, r_\nu^2)\gamma^\alpha - \left(\mu_{ll'} + d_{ll'}\gamma^5\right)\sigma^{\alpha\beta}q^\beta$$

The formfactor $F_R(q^2, r_\nu^2)$ is related to the charge radius r_ν: $F_R(q^2, r_\nu^2) \sim \frac{1}{6}q^2 r_\nu^2$. $\mu_{ll'}$ and $d_{ll'}$ are the magnetic and electric dipole moments, respectively.

For $l = l'$ one has a diagonal dipole moment ($\nu_{eL} \to \nu_{eR}$). In case $l \neq l'$ ($\nu_{eL} \to \nu_{\mu R}$), the neutrino is said to have a transition moment. For diagonal moments ($l = l'$) the dipole

[1] E-Mail: Farid.Ould-Saada@cern.ch

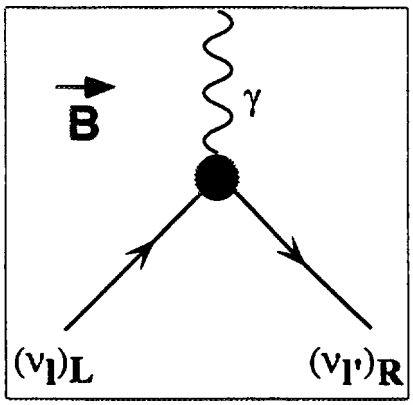

Figure 1: *Spin Precession in a magnetic field B.*

interaction energy has the known form: $\mu_\nu\langle\vec{s}\cdot\vec{B}\rangle$; $d_\nu\langle\vec{s}\cdot\vec{E}\rangle$. For highly relativitic neutrinos it is not possible to distinguish between the electric and magnetic dipole moments. What is measured experimentally is the recoil e^-, for example, not the neutrino. One thus defines an effective dipole moment (magnetic moment) ν_l as

$$\mu_{\nu_l} = \sqrt{\sum_{l'=e,\mu,\tau} \mid \mu_{ll'} - d_{ll'} \mid^2}$$

There exist two possible ways to describe neutrinos. A massive Dirac neutrino ν^D, for which $\nu \neq \overline{\nu}$, has four distinct states, whereas a Majorana neutrino ν^M[10], ($\nu = \overline{\nu}$) has 2 distinct states:

$$\nu^D = \begin{pmatrix} \nu_L \\ \overline{\nu}_L \\ \nu_R \\ \overline{\nu}_R \end{pmatrix} \; ; \; \nu^M = \begin{pmatrix} \nu_L \\ \nu_R \end{pmatrix}$$

If the neutrino is massless there is no way to distinguish between ν^D and ν^M. Dirac neutrinos may have a magnetic dipole moment, and if CP is not conserved, an electric dipole moment. For a Majorana neutrino the diagonal terms must vanish, as a consequence of CPT [12, 11].

In the standard model, including right handed (massive) neutrinos, Dirac neutrinos acquire a magnetic moment proportional to mass m_ν: $\mu_\nu \sim 3.2 \cdot 10^{-19}\frac{m_\nu}{eV} \cdot \mu_B$, where $\mu_B = e/2m_e$ is the Bohr Magneton. For a neutrino mass corresponding to the actual measured upper limit, $m_{\nu_e} \simeq 10\ eV$ one expects $\mu_\nu^{SM} \sim 3 \cdot 10^{-18}\mu_B$, whereas the laboratory limits are $\sim 10^{-10}\mu_B$. Therefore, a measurement of the magnetic moment of the neutrino probes new physics beyond the standard model.

1.3 The Solar Neutrino Problem

The comparison of the detected solar neutrino flux to the predictions of the solar models shows a clear deficit (Tab.1 and Fig.2), known as the Solar Neutrino Problem (SNP). Furthermore

Experiment	Process	E_ν^{thresh} [keV]	Sensitivity	data [SNU]	B-P [SNU]	T-C-L [SNU]
Homestake	$e - {}^{37}Cl \rightarrow \nu_e {}^{37}Ar$	0.814	${}^8B, Be$	$2.54 \pm 0.14 \pm 0.14$	8.0 ± 3.0	6.4
Kamiokande	$\nu e - \rightarrow \nu_e e -$	7.500	${}^8B$	$2.80^{\pm}0.19 \pm 0.33$	5.7 ± 2.4	4.4
Gallex	$e - {}^{71}Ga \rightarrow \nu_e {}^{71}Ge$	0.233	pp, Be, B	$69.7 \pm 6.7^{+3.9}_{-4.5}$	131.5^{+21}_{-17}	122.5
Sage	$e - {}^{71}Ga \rightarrow \nu_e {}^{71}Ge$	0.233	pp, Be, B	72^{+12+5}_{-10-7}	131.5^{+21}_{-17}	122.5

Table 1: *Solar neutrinos: Data vs Standard Solar Model expectations. B-P: Bahcall and Pinsonneault[13] T-C-L: Turck-Chièze and Lopes[14]. Data are from Homestake[15], Gallex[16] Sage[17], and Kamiokande[18]. 1 SNU is defined to be one neutrino reaction per second in* 10^{36} *target atoms.*

the solar ν-flux observed by the ${}^{37}Cl$ experiment seemed[19] to show an anticorrelation with

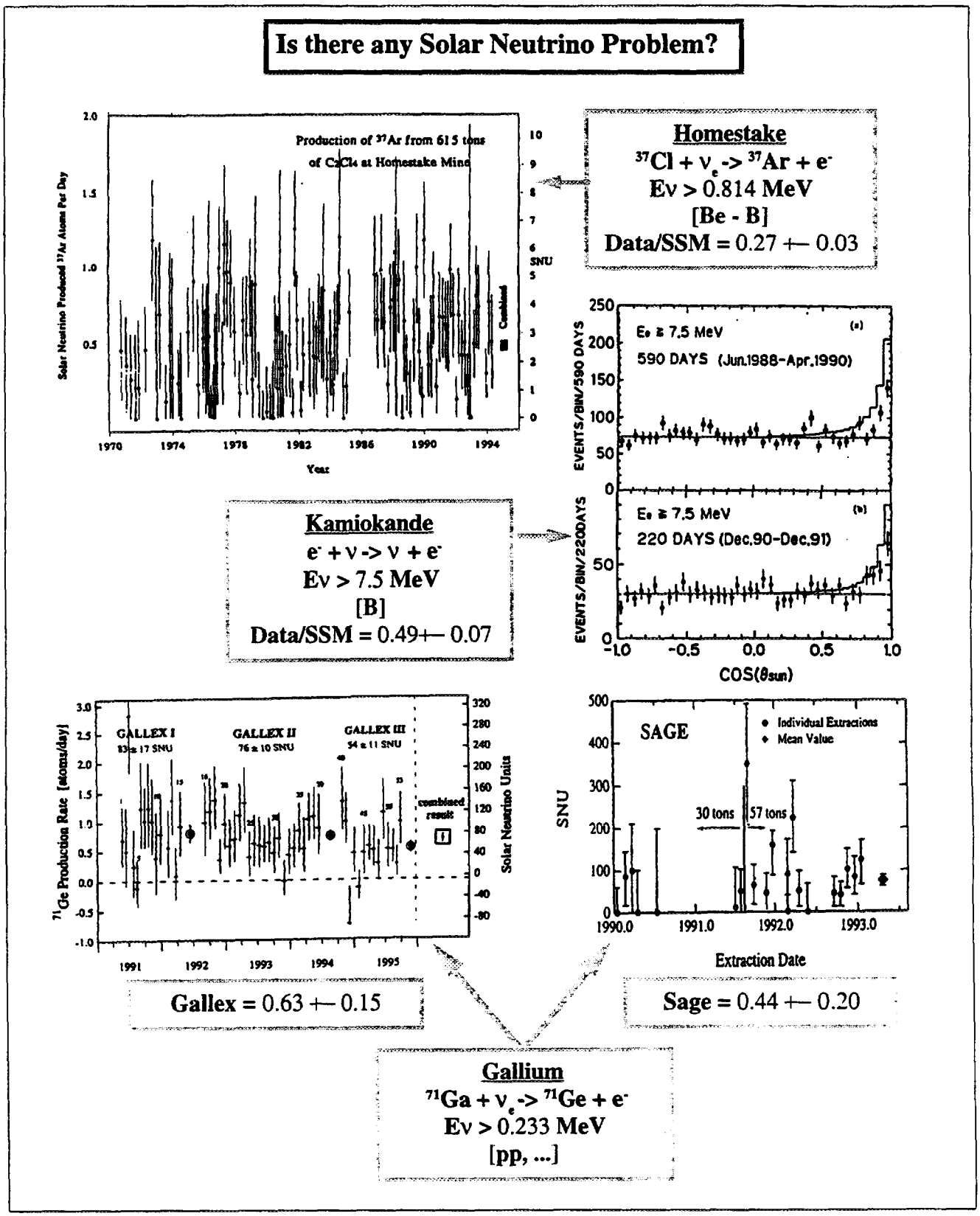

Figure 2: *Solar neutrino fluxes detected by various experiments and the Solar Neutrino Problem.*

the number of sunspots (Fig.3), which follows the 11 year period of the solar magnetic activity cycle. The convective zone of the sun contains currents responsible for toroidal magnetic fields, $B_\odot$. If the neutrino has a magnetic dipole moment, it undergoes spin precession in $B_\odot$ (see next chapter). Lefthanded neutrinos, which take part in the weak interaction, flip into righthanded, sterile, neutrinos. At high solar activity, i.e. maximum number of sunspots, the probability for spin flip is large, and hence less neutrinos would be detected on earth. At low solar activity, less neutrinos become sterile, and one would detect more neutrinos. The Kamiokande II water Cherenkov experiment does not see any anticorrelation (Fig.3), and in fact, even for Homestake the effect might be only a statistical fluctuation (at most 10% probability). The authors of Ref.[21] pointed out that the ^8B neutrinos should be modulated with a half-year period by the combined effect of the 7° inclination of the plane of the ecliptic to the solar equator and the weakening of the toroidal magnetic field near the equator. The toroidal field has opposite signs on different sides of the equator. The transition gap in the magnetic field, $\sim 7 \times 10^9\ cm$ shades the ^8B and ^8Be neutrinos produced in a small region near the center ($\sim 0.05 R_\odot \sim 3 \times 10^9\ cm$). The pp neutrinos are produced in a much more extended region $\sim 0.10 R_\odot$ up to $\sim 1.7 \times 10^{10}\ cm$. Results from Kamiokande and Gallex are discussed by W. Hampel[22]. Superkamiokande is a good candidate to follow these studies and look for such effects.

More recently, other indicators for the solar magnetic activity have been considered. McNutt[26] showed that there is an anticorrelation between the solar neutrino rates and the solar wind flux as measured near Earth by the MIT plasma experiment on the IMP 8 satellite. The surface magnetic flux[25, 27] has an advantage over sunspots in that it spans the whole solar disk. Oakley et al.[25] found, for the 2 solar cycles between 1970 and 1991, a "highly significant" anticorrelation between the Homestake data and the magnetograph-measured surface magnetic flux from the latitude zones centered on the solar disk, in the vicinity of the neutrino flight path. Fig.3 from reference[27],shows data from all 4 neutrino experiments plotted against the delayed magnetic flux. Interior fields travel to the solar surface in $\sim 0.3 - 1.4$ years. The question whether these anticorrelations might be only statistical fluctuations, requires data that span several solar cycles to answer.

If one beleives the experimental measurements, the question to ask is: is the Solar Neutrino Problem caused by unknown properties of neutrinos or by a lack of underdstanding of the interior of the sun? Is the deficit due to new physics or to faulty astrophysics? Here we assume the solar models[20] correct[2] and concentrate on the possibility for new physics. Solutions to the solar neutrino problem through neutrino oscillations (in vacuum or in matter) are addressed by S. Petcov[24] and W. Hampel[22]. Here we further consider neutrinos having electromagnetic properties.

2 Magnetic Moment and Spin Precession

2.1 Spin precession in vacuum

The evolution equation of a system with lefthanded ν_L and righthanded ν_R Dirac neutrinos in a magnetic field B is described by the Schrödinger-like equation

$$
\begin{aligned}
i\frac{d}{dx}\begin{pmatrix}\nu_L\\ \nu_R\end{pmatrix} &= \left[\begin{pmatrix}E_L & \mu B\\ \mu B & E_R\end{pmatrix}\right]\begin{pmatrix}\nu_L\\ \nu_R\end{pmatrix}\\
&= \left[p\begin{pmatrix}1 & 0\\ 0 & 1\end{pmatrix}+\begin{pmatrix}\frac{m_L^2}{2p} & \mu B\\ \mu B & \frac{m_R^2}{2p}\end{pmatrix}\right]\begin{pmatrix}\nu_L\\ \nu_R\end{pmatrix}\\
&= \left[\begin{pmatrix}\frac{\Delta_{LR}}{4E} & \mu B\\ \mu B & -\frac{\Delta_{LR}}{4E}\end{pmatrix}+\left(p+\frac{m_L^2+m_R^2}{4p}\right)\begin{pmatrix}1 & 0\\ 0 & 1\end{pmatrix}\right]\begin{pmatrix}\nu_L\\ \nu_R\end{pmatrix}
\end{aligned}
$$

where μ is the magnetic moment of the neutrino, $E = p\sqrt{1+\frac{m^2}{p^2}} \sim p\left(1+\frac{m^2}{2p^2}\right)$ its energy and $\Delta_{LR} = m_L^2 - m_R^2$. If we omit the terms proportional to the unit matrix, which are not responsible

[2] Dar and Shaviv claim that their model (see A. Dar in[23]) does reproduce the solar neutrino data. For Homestake, for example, they expect 0.2 *SNU* (*pep*), 0.9 *SNU* (^7Be), 2.7 *SNU* (^8B) and 0.3 *SNU* (*CNO*) (in total 4.1 *SNU*), whereas Bahcall and Pinsonneault[13] find 0.2, 1.2, 6.2 and 0.4 SNU, respectively (in total 8.0 *SNU*). The SNP problem is thus reduced to a "^8B neutrino problem". The situation is more complicated if gallium data are taken into account. One talks about a "^7Be neutrino problem", which cannot (yet?) be solved by non-standard solar models (see Ref.[22]).

for the spin precession, we obtain:

$$i\frac{d}{dx}\begin{pmatrix}\nu_L\\ \nu_R\end{pmatrix} = \left[\frac{\Delta_{LR}}{4E}\begin{pmatrix}1 & 0\\ 0 & -1\end{pmatrix}+\mu B\begin{pmatrix}0 & 1\\ 1 & 0\end{pmatrix}\right]\begin{pmatrix}\nu_L\\ \nu_R\end{pmatrix}$$
$$= \left(\frac{\Delta_{LR}}{4E}\sigma_3+\mu B\sigma_1\right)\begin{pmatrix}\nu_L\\ \nu_R\end{pmatrix}$$

The solution of the differential equation in the case of a uniform magnetic field B is

$$\begin{pmatrix}\nu_L(x)\\ \nu_R(x)\end{pmatrix} = \exp\left[-i\left(\frac{\Delta_{LR}}{4E}\sigma_3+\mu B\sigma_1\right)x\right]\cdot\begin{pmatrix}\nu_L(0)\\ \nu_R(0)\end{pmatrix}$$
$$= \left[\cos\Omega x-\frac{i}{\Omega}\left(\frac{\Delta_{LR}}{4E}\sigma_3+\mu B\sigma_1\right)\sin\Omega x\right]\cdot\begin{pmatrix}\nu_L(0)\\ \nu_R(0)\end{pmatrix}$$

where $\Omega^2 \equiv (\mu B)^2 + (\frac{\Delta_{LR}}{4E_\nu})^2$.

If at $x = 0$ there were only lefthanded Neutrinos ($\nu_R(0) = 0$), than after a distance x the probabilities to find a lefthanded neutrino or a righthanded neutrino are:

$$P_{\nu_L\nu_L}(x) = |<\nu_L(x)|\nu_L(0)>|^2 = |\cos\Omega x-\frac{i}{\Omega}\frac{\Delta_{LR}}{4E_\nu}\sin\Omega x|^2 = cos^2\Omega x + cos^2\beta\ sin^2\Omega x$$

$$P_{\nu_L\nu_R}(x) = |<\nu_R(x)|\nu_L(0)>|^2 = 1 - P_{\nu_L\nu_L}(x) = sin^2\beta\ sin^2\Omega x$$

where $\tan\beta \equiv \frac{\mu B}{\Delta_{LR}/4E_\nu}$.

Efficient spin precession can be obtained[21] for $\beta \simeq 1$, giving $\Delta_{LR} \simeq 4E_\nu\ \mu\ B$. In the sun, where neutrinos are produced with an energy $E_\nu \sim 10\ MeV$ and assuming a magnetic field of $B \sim 10^3 - 10^4\ Gauss$, this leads to $|\ \Delta_{LR}\ | \simeq 10^{-7}\ eV^2$, for $\mu_\nu < 10^{-10}\mu_B$. This condition can be relaxed when matter effects are taken into account. From $\Omega x \sim \mu B x \sim 1$ and for $x \sim 2\times 10^{10}\ cm$ (solar convective zone) and $B \sim 10^3 - 10^4\ Gauss$, one would need $\mu \sim (0.1 - 1.0)\times 10^{-10}\mu_B$, in order to explain the solar neutrino deficit.

2.2 Spin precession in matter

In matter the neutrino gets an effective energy à la MSW[28, 29], due to its interaction with e^-, p and n (Fig.4)

$$H_\nu = H_{vac} + H_{int}$$

$$H_{int} = \sqrt{2}G_F\sum_f (I_3^f - 2Q_f\sin^2\theta_W)$$

	$I_3 - 2Q\sin^2\theta_W$	Effective energy $[V_\nu]$
Neutral Currents		
$\nu(e,p)\to\nu(e,p)$	cancel	0
$\nu n\to\nu n$	$-\frac{1}{2}$	$-\frac{G_F}{\sqrt{2}}n_n$
Charged Currents		
$\nu_e e^-\to\nu_e e^-$	$\frac{1}{2}+2\sin^2\theta_W$	$\sqrt{2}G_F n_e$

$$V_{\nu_e} = \sqrt{2}G_F(n_e - \frac{1}{2}n_n)\ ;\ V_{\nu_\mu} = -\frac{G_F}{\sqrt{2}}n_n$$

Only the lefthanded neutrino acquires an effective mass, the righthanded neutrino being sterile

$$\tilde{m}_L^2 = m_L^2 + 2\sqrt{2}G_F E_\nu\left(n_e - \tfrac{1}{2}n_n\right)\ ;\ \tilde{m}_R^2 = m_R^2$$

The condition for an efficient spin precession reads now

$$2\sqrt{2}G_F E_\nu\left(n_e - \frac{1}{2}n_n\right) \simeq 4E\mu B$$

$$\left(\left(n_e - \tfrac{1}{2}n_n\right) \le 10^{22} cm^{-3}\right) \Longrightarrow Solar\ Convective\ Zone!$$

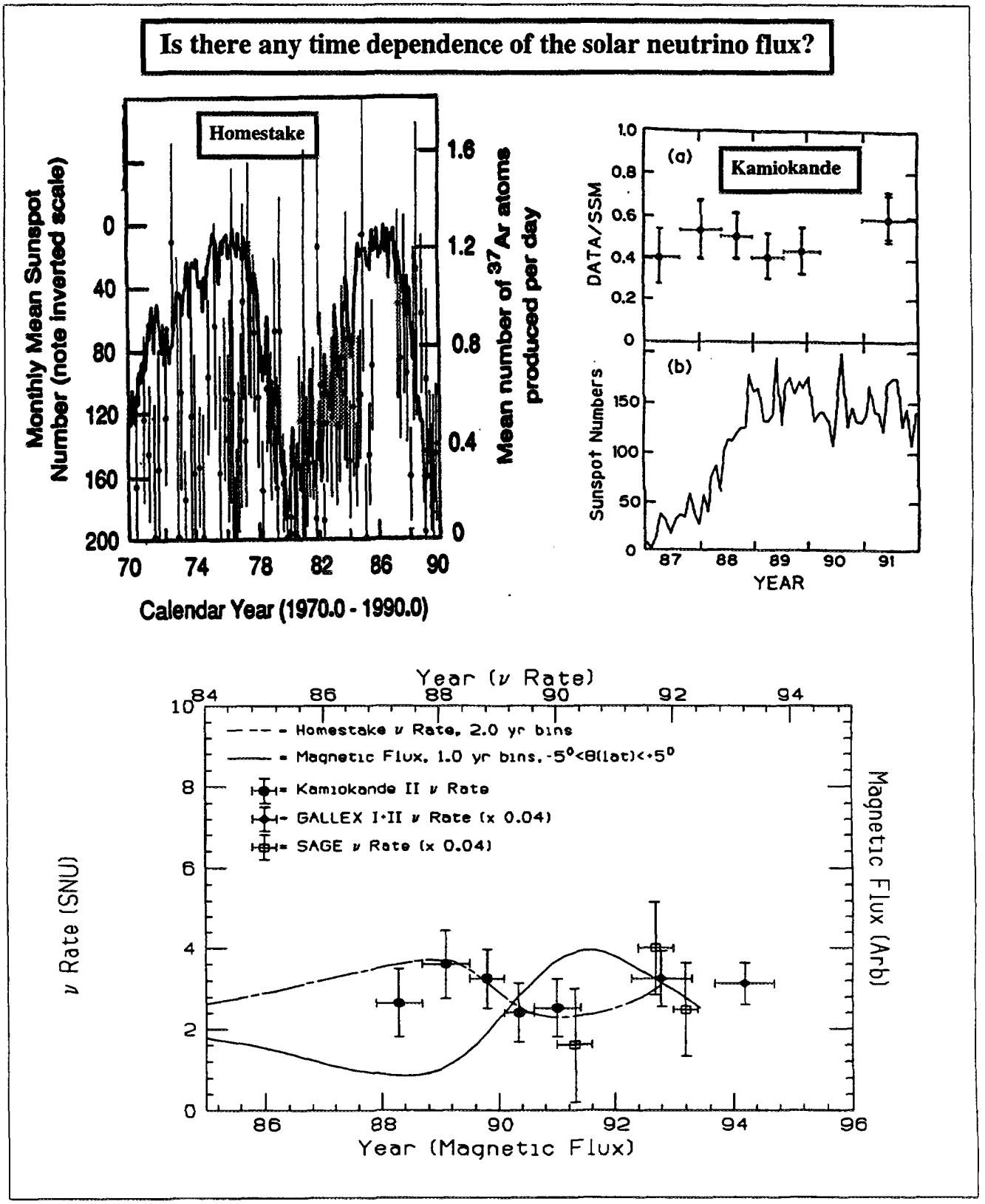

Figure 3: *Time evolution of the solar neutrino flux detected by various experiments compared to the number of sun spots (top) and to the solar magnetic flux. The magnetic scale is shifted by 1 year in order to plot a 1984 neutrino with a 1984 interior fiels, proxied by a 1985 surface field.*

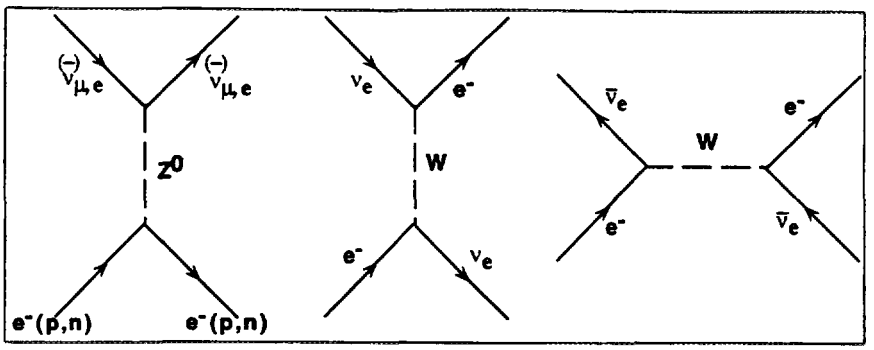

Figure 4: *Neutrino scattering off* e^-, p, n.

2.3 Resonant Spin-Flavour Precession

The effect [31, 33, 34] can be easily seen if two neutrino flavours are taken[41, 42].

The evolution equation in the case of 2 Dirac neutrinos and their antiparticles is

$$i\frac{d}{dx}\begin{pmatrix}\nu_{eL}\\ \nu_{\mu L}\\ \nu_{eR}\\ \nu_{\mu R}\end{pmatrix} = H\begin{pmatrix}\nu_{eL}\\ \nu_{\mu L}\\ \nu_{eR}\\ \nu_{\mu R}\end{pmatrix}$$

with

$$H = \begin{bmatrix} -\frac{\Delta m^2}{4E_\nu}\cos 2\theta + V_{\nu_e} & \frac{\Delta m^2}{4E_\nu}\sin 2\theta & \mu_{ee}B & \mu_{e\mu}B \\ \frac{\Delta m^2}{4E_\nu}\sin 2\theta & \frac{\Delta m^2}{4E_\nu}\cos 2\theta + V_{\nu_\mu} & \mu_{e\mu}B & \mu_{\mu\mu}B \\ \mu^*_{ee}B & \mu^*_{\mu e}B & -\frac{\Delta m^2}{4E_\nu} & 0 \\ \mu^*_{e\mu}B & \mu^*_{\mu\mu}B & 0 & +\frac{\Delta m^2}{4E_\nu} \end{bmatrix}$$

where

$$\Delta m^2 = m^2_{\nu_\mu} - m^2_{\nu_e}$$

In this case both diagonal (μ_{ll}) and transition moments ($\mu_{ll'}$) are possible. The right-handed neutrino is sterile, and hence no $\nu_{eR} - \nu_{\mu R}$ oscillations accur (no mixing). The crossing of diagonal elements are the regions where resonances occur:

- The SFP $\nu_{eL} - \nu_{\mu R}$ Resonance ($H_{11} = H_{44}$):

$$V_{\nu_e} = \frac{\Delta m^2}{4E}(1+\cos 2\theta) \Longrightarrow \left(n_e - \frac{1}{2}n_n\right)_R = \frac{\Delta m^2 \cos^2\theta}{2\sqrt{2}G_F E_\nu}$$

- The MSW $\nu_{eL} - \nu_{\mu L}$ Resonance ($H_{11} = H_{22}$):

$$(n_e)_R = \frac{\Delta m^2 \cos 2\theta}{2\sqrt{2}G_F E_\nu}$$

The condition for efficient precession with flavour mixing becomes: $\mid \Delta m^2 \mid \simeq 10^{-4}\ eV^2$.

The evolution equation in the case of 2 Majorana neutrinos and their antiparticles is

$$i\frac{d}{dx}\begin{pmatrix}\nu_{eL}\\ \nu_{\mu L}\\ \overline{\nu}_{eR}\\ \overline{\nu}_{\mu R}\end{pmatrix} = H\begin{pmatrix}\nu_{eL}\\ \nu_{\mu L}\\ \overline{\nu}_{eR}\\ \overline{\nu}_{\mu R}\end{pmatrix}$$

$$H = \begin{bmatrix} -\frac{\Delta m^2}{4E}\cos 2\theta + V_{\nu_e} & \frac{\Delta m^2}{4E_\nu}\sin 2\theta & 0 & \mu_{e\mu}B \\ \frac{\Delta m^2}{4E_\nu}\sin 2\theta & \frac{\Delta m^2}{4E_\nu}\cos 2\theta + V_{\nu_\mu} & -\mu_{e\mu}B & 0 \\ 0 & -\mu^*_{\mu e}B & -\frac{\Delta m^2}{4E_\nu}\cos 2\theta - V_{\nu_e} & \frac{\Delta m^2}{4E_\nu}\sin 2\theta \\ \mu^*_{e\mu}B & 0 & \frac{\Delta m^2}{4E_\nu}\sin 2\theta & \frac{\Delta m^2}{4E_\nu}\cos 2\theta - V_{\nu_\mu} \end{bmatrix}$$

In this case only transition moments ($\mu_{ll'}$) are possible; diagonal moments (μ_{ll}) must vanish. The right-handed neutrino ($\overline{\nu}_R = \nu_R$) interacts, and hence $\nu_{eR} - \nu_{\mu R}$ oscillations can accur.

It has been shown[35] that the three solar neutrino experiments could be reconciled for certain field configurations in the sun. A numerical integration of the evolution equation of the system $(\nu_e, \overline{\nu}_\mu)$ leads to the solution [$\Delta m^2 \sim 10^{-8}\ eV^2$; $\mu_\nu \sim 10^{-11}\ \mu_B$; $B_0 \sim 40kG$]. A better experimental measurement of μ_ν could therefore give more information about the magnetic field in the sun. Pulido[36] and Lim-Nunokawa[39] found a common solution to all solar neutrino experiments for a simple field configuration in the sun by taking into account the energy dependence of the survival probability $P_{\nu_e\nu_e}(x)$. Akhmedov[38] and Nunokawa-Minakata[37] treated the combined effect of the resonant spin-flavour precession and neutrino oscillations in matter.

The interest in measuring the dipole moment of the neutrino was triggered by the solar neutrino problem, especially the possible anticorrelation with the solar magnetic activity. Whether these are true is certainly questionable. It is nevertheless important to study a possible electromagnetic interaction of the neutrino, as part of its intrinsic properties. A non zero (Dirac) neutrino magnetic moment was postulated by Pauli[40] in the same letter in which the neutrino hypothesis was formulated.

Among the processes sensitive to the electromagnetic properties of the neutrino, we discuss νe^- scattering which presents two advantages: it is a pure weak, theoretically well understood process, and the recoil electron can be easily measured.

3 νe^- scattering

3.1 νe^- elastic scattering

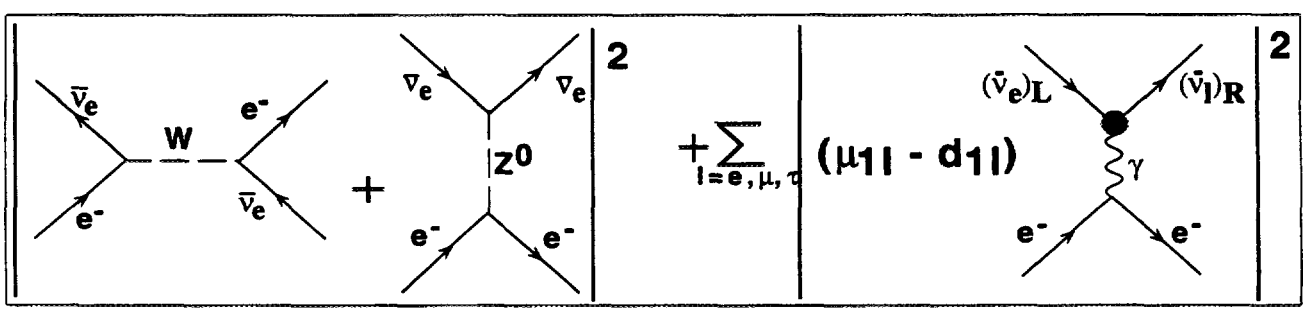

Figure 5: *Feynman diagrams contributing to $\overline{\nu}e^-$-Scattering.*

The differential cross-section for the elastic process $\nu e^- \to \nu e^-$ (Fig.5) gets two contributions: one from the weak interaction and one from a possible electromagnetic interaction of the neutrino[43, 44, 45]:

$$\frac{d\sigma}{dT} = \frac{d\sigma^W}{dT} + \frac{d\sigma^M}{dT}$$

$$\frac{d\sigma^W}{dT} = \frac{2G_F^2 m_e}{\pi}\left[g_L^2 + g_R^2(1 - \frac{T}{E_\nu})^2 - g_L g_R \frac{m_e T}{E_\nu^2}\right] \ ; \ \frac{d\sigma^M}{dT} = \frac{\pi\alpha^2}{m_e^2}\left(\frac{\mu_\nu}{\mu_B}\right)^2 \frac{1 - T/E_\nu}{T} \ ,$$

where $g_L = \frac{1}{2}[g'_V + g_A] = \frac{1}{2}[(g_V + x) + g_A]$ and $g_R = \frac{1}{2}[g'_V - g_A] = \frac{1}{2}[(g_V + x) - g_A]$.

$$g_V = \left\{ \begin{array}{l} 2\sin^2\theta_W + 1/2 \\ 2\sin^2\theta_W - 1/2 \end{array} \right\} \ , \ g_A = \left\{ \begin{array}{l} +1/2 \\ -1/2 \end{array} \right\} \ for \left(\begin{array}{l} \nu_e e^- \\ \nu_\mu e^- \ ; \ \nu_\tau e^- \end{array} \right)$$

$$\left\{ \begin{array}{l} g_L \leftrightarrow g_R \\ g_A \rightarrow -g_A \end{array} \right\} \; for \; \overline{\nu} e^-$$

The other parameters are T : kinetic energy of the recoil electron, E_ν : energy of the incoming neutrino, G_F : Fermi constant, α : QED coupling constant, and θ_W : Weinberg weak mixing angle ($\sin^2\theta_W \sim 0.23$). An intrinsic neutrino charge radius, indicating an internal structure of the neutrino would manifest itself as a shift, x, of the weak neutral current vector coupling, g_V

$$x = \frac{\sqrt{2}\pi\alpha}{3G_F}\langle r^2\rangle = \frac{2M_W^2}{3}\sin^2\theta_W\langle r^2\rangle \sim 2.38\times 10^{30} cm^{-2}\langle r^2\rangle.$$

Other shifts due to radiative corrections within the standard model are predicted to be small[49], of the order of -0.004. Note that high neutrino energies are better suited to set limits on this quantity.

The one-photon exchange mechanism leads to a spin-flip of the outgoing leptons, therefore the electromagnetic and weak contributions to the toal cross section do not interfere, and the neutrino magnetic moment leads to an increase of the event rate. Notice that the constant electromagnetic term, $\frac{\pi\alpha^2}{m_e^2} \sim 2.5\times 10^{-25}$, is much larger than the weak cross section. A measurement of μ_ν consists in looking for deviations from purely weak processes.

The weak νe and $\overline{\nu} e$ elastic cross sections increase linearly with the neutrino energy: $\sigma \sim (0.14 - 0.9)\times 10^{-44}[E_\nu/MeV]\ cm^2$. As a comparison the νN cross-sections are proportional to E^2: $\sigma(\overline{\nu}_e p \rightarrow e^+ n) \sim \sigma(\nu_e n \rightarrow e^- p) \simeq 9.75\times 10^{-44}[E_\nu/MeV]^2\ cm^2$ for $E_\nu \ll m_N$.

The electromagnetic cross section, on the other hand, rises only logarithmically with the neutrino energy E_ν $\sigma^M \sim \ln E_\nu$. Therefore, it is advantageous to perform experiments searching for a magnetic moment of the neutrino at low energies. Reactors, with an antineutrino energy spectrum peaking around 1 MeV, are more suitable than accelerators.

The quantities to be measured experimentally are the recoil kinetic energy T_e and the scattering angle θ_e of the electron. These are related by

$$\cos\theta_e = \frac{E_\nu + m_e}{E_\nu}\sqrt{\frac{T_e}{T_e + 2m_e}} \;\; ; \;\; T_e = m_e \frac{E_\nu^2\cos^2\theta_e}{E_\nu + m_e/2 + (E_\nu^2\sin^2\theta_e)/2m_e}$$

The maximal recoil (Compton edge) is for electrons emitted in the forward direction ($\theta_e = 0°$)

$$T_e^{max} = \frac{2E_\nu^2}{2E_\nu + m_e}$$

The differential cross-section for $\overline{\nu}_e e \rightarrow \overline{\nu}_e e$, averaged over the antineutrino spectrum[45], as function of the recoil electron energy T_e, is

$$\langle\frac{d\sigma}{dT_e}\rangle = \int_{E_\nu^{min}(T_e)}^{\infty} \frac{dN_\nu}{dE_\nu}\frac{d\sigma}{dT_e}dE_\nu$$

The ratio of the total and weak integrated cross sections are depicted in Fig.6 for different values of μ_ν. $\sin^2\theta_W = 0.226$ was used. One can see why it is important to go to lower energies to probe the magnetic moment of the neutrino. Furthermore, the electromagnetic cross section is more strongly peaked in the forward direction than the weak cross section The goal of a precision experiment is, therefore, to measure both the energy and the angular distribution of the recoil electron.

3.2 Dynamical zero in $\overline{\nu} e^-$ elastic scattering

The weak contribution to the differential cross-section for the elastic process $\overline{\nu}_e e^- \rightarrow \overline{\nu}_e e^-$ is given by

$$\frac{d\sigma^W}{dT_e} = \frac{2G_F^2 m_e}{\pi}\left[g_R^2 + g_L^2(1 - \frac{T_e}{E_\nu})^2 - g_L g_R \frac{m_e T_e}{E_\nu^2}\right]$$

For forward electrons with a maximal recoil T_e^{max} one obtains

$$\frac{d\sigma^W}{dT_e} = \frac{2G_F^2 m_e}{\pi}\left[g_R - g_l\frac{m_e}{2E_\nu + m_e}\right]^2$$

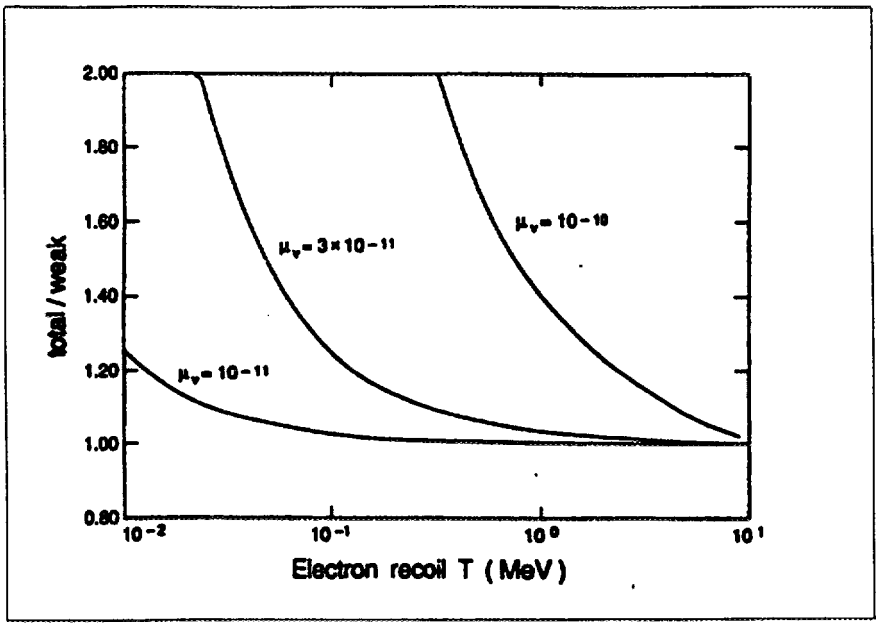

Figure 6: *Ratio of total to weak cross-sections for $\overline{\nu}_e e^- \to \overline{\nu}_e e^-$, averaged over the antineutrino spectrum, as a function of the electron recoil energy. Different value of μ_ν are considered*

which can vanish if the following condition is fulfilled

$$\left(\frac{d\sigma^W}{dT_e}\right)_{forward} = 0 \Longrightarrow g_R = g_l \frac{m_e}{2E_\nu + m_e} \Longrightarrow E_\nu = \frac{g_L - g_R}{2g_R} m_e$$

With $g_L = 2\sin^2\Theta_W + 1$ and $g_R = 2\sin^2\Theta_W$, the condition for dynamical zero reads $E_\nu = \frac{m_e}{4\sin^2\Theta_W} \sim 500\ keV$. It is interesting to see that these $\overline{\nu}$-energies are provided by reactors. The corresponding maximal recoil energies, $T_e^{max} \sim 350\ keV$, could be measured by the MUNU detector, as we will see later on. As the electromagnetic contribution to the cross-section is not affected by the dynamical zero, the study of forward electrons is sensitive to a hypothetical magnetic moment of the neutrino. Such an experiment requires high rates and good energy and angular resolutions. Notice that for all other types of neutrinos ($\nu_{e,\mu,\tau}, \overline{\nu}_{\mu,\tau}$) there is no cancellation. As a consequence oscillations $\overline{\nu}_e \leftrightarrow \overline{\nu}_\mu$ can be performed. The authors of Ref.[46, 47] showed results that could be obtained with a detector (of type MUNU) sitting 20 meters from the core of a reactor. The bounds could be comparable to that obtained for $\nu_e \leftrightarrow \nu_\mu$ oscillations by atmospheric neutrino detectors.

3.3 $\overline{\nu}e^-$ inelastic scattering

In the case of elastic scattering $\overline{\nu}_e e^- \to \overline{\nu}_e e^-$ the sensitivity to the magnetic moment is limited by the threshold T_e^{min} ($\sim 300 - 500\ keV$ for MUNU): $Q^2 = 2m_e T_e \geq 2m_e T_e^{min}$. In the inelastic case (Fig.7) $\overline{\nu}_e e^- \to \overline{\nu}_e e^- \gamma$, there is no Q^2 limitation. The normalised quantity

$$x = \frac{Q^2}{2m_e(T_e + T_\gamma)}$$

can take values between 0 and 1. This enhances the sensitivity to μ_ν. Experimentally, however, it is necessary to measure the photon energy, and the rates are suppressed by a factor α.

The authors of reference [48, 47]) computed the ratio of the magnetic and weak differential cross sections as function of x and $\nu = T_e + E_\gamma$ for $\mu_\nu = 10^{-10}\mu_B$, by taking into account the reactor spectrum. The threshold energies assumed are $T_e^{min} = 100\ keV$ and $E_\gamma^{min} = 100\ keV$. For $\nu \leq 0.5\ MeV$ and $x \leq 0.5$, the electromagnetic cross section is $\sigma_M = 2.7 \times 10^{-47} cm^2$, and is 4.4 times larger than the weak cross section σ_W.

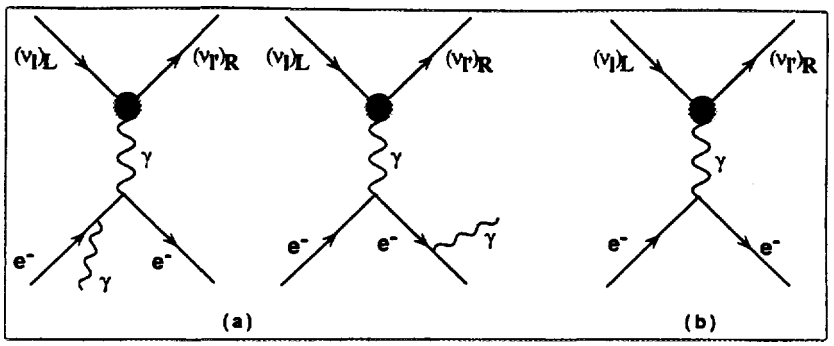

Figure 7: *Electromagnetic interaction Feynman diagrams contributing to νe^- inelastic (a) and elastic (b) scattering.*

4 Experimental Limits

4.1 Laboratory limits

4.1.1 Reactor experiments

The neutrino (in fact $\overline{\nu}_e$) was experimentally discovered in 1956 at the Savannah River nuclear reactor[2], by observing the reaction $\overline{\nu}p \rightarrow ne^+$ The reactor power was 1800 MW corresponding to a neutrino flux of $1.9 \times 10^{13} \frac{\overline{\nu}}{cm^2 \cdot s}$. The detector consisted of a large liquid scintillator, of high hydrogen content and loaded with a cadmium compound. Positrons lead to prompt scintillations while photons from the absorbtion of neutrons in cadmium give delayed pulses with predictable energy and time delay spectra.

Savannah River Reactor

The reaction $\overline{\nu}_e e^- \rightarrow \overline{\nu}_e e^-$ was first observed at the Savannah River nuclear plant[54]. The experiment used a segmented 15.9 kg plastic scintillator (CH_2), surrounded by an anti-Compton, NaI counter to suppress the γ background, a lead shield and a liquid scintillator to veto cosmics. A Signal event was defined by a single count in one of the elements of the plastic scintillator with nothing in coincidence. Annihilation γ rays and neutrons from reaction $\overline{\nu_e}p \rightarrow e^+n$ (200 events/day in the plastic scintillator) were detected or identified by the delayed neutron capture signal in the plastic scintillator or in NaI. Assuming a vanishing magnetic moment, the experiment lead to a measurement of the Weinberg weak angle $\sin^2\theta_W = 0.29 \pm 0.05$. With today's improved knowledge on both the Weinberg angle and the reactor spectrum Vogel and Engel[45] obtained a magnetic moment $\mu_{\nu_e} \sim 3 \times 10^{-10}\mu_B$, with a significance of about 3σ! The main limitation of the experiment was the short running time (2 months) and the high electron detection threshold (1 MeV).

	$\bar{\nu}_e$ events/day			
Reactor	T[MeV]	Reactor on	Reactor off	on-off
Savannah		(64.6 days)	(60.7 days)	
($P = 1800\ MW$				
$1.9 \times 10^{13}\overline{\nu}/cm^2 \cdot s$	$1.5 - 3.0$	45.1 ± 1.0	39.2 ± 0.9	5.9 ± 1.4
$11.2\ m$ from core)	$3.0 - 4.5$	2.4 ± 0.19	1.2 ± 0.14	1.2 ± 0.25
Kurchatov		(254 days)	(78 days)	
$P = 2000\ MW$				
$2.7 \times 10^{12}\overline{\nu}/cm^2 \cdot s$	$3.15 - 5.17$	8.27 ± 0.18	7.49 ± 0.31	0.78 ± 0.36
Rovno		(29.6 days)	(16.7 days)	
$(2 \times 10^{13}\overline{\nu}/cm^2 \cdot s$	$0.6 - 2.0$	4962 ± 12	4921 ± 16	41 ± 20
$15\ m$ from core)	$1.3 - 2.0$	508.5 ± 4.0	503.3 ± 5.6	5.2 ± 6.8

Table 2: *Event Rates in the Savannah River, Kurchatov and Rovno reactor experiments[54, 55, 56].*

Kurchatov Reactor

A more recent experiment at the Kurchatov Institute in Moscow[55] used seven cells filled with a C_6F_6 based liquid scintillator (103 kg) as active target material, containing 3×10^{28} electrons. The number of hydrogen atoms in the scintillator is 1.6×10^{25}. The detector is surrounded by various shielding layers, to suppress background from local activities, and by a plastic scintillator

on the top to veto cosmic rays. The reactor power and the neutrino flux are 2000 MW and $3.4 \times 10^{12} \frac{\overline{\nu}}{cm^2 \cdot s}$, respectively. The signal to noise ratio is $S/N \sim 1/10$ in the energy domain $3.15 \leq T_e \leq 5.175$ (it was $\sim 1/50$ at the beginning of the experiment.). The measured $\overline{\nu}e^-$ total cross section is: $\sigma_{\overline{\nu}e} = (4.5 \pm 2.4) \times 10^{-46} cm^2$/fission, giving, in the framework of the standard model, a value for the Weinberg-angle of: $\sin^2 \theta_W = 0.22^{+0.7}_{-0.8}$. The upper limit for the magnetic moment obtained so far ($\sin^2 \theta_W = 0.23$ as input) is

$$\mu_{\nu_e} < 2.4 \times 10^{-10} \mu_B \ , \quad CL = 90\%$$

limited by background and the low reactor flux. The experiment gives an upper limit on the neutrino charge radius of

$$|r_{\nu_e}| < 2.7 \times 10^{-16} cm \ , \quad CL = 90\%$$

Rovno Reactor

Derbin et al.[56] used a 75 kg silicon multidetector which consisted of 600 Si(Li) modules, 30 mm

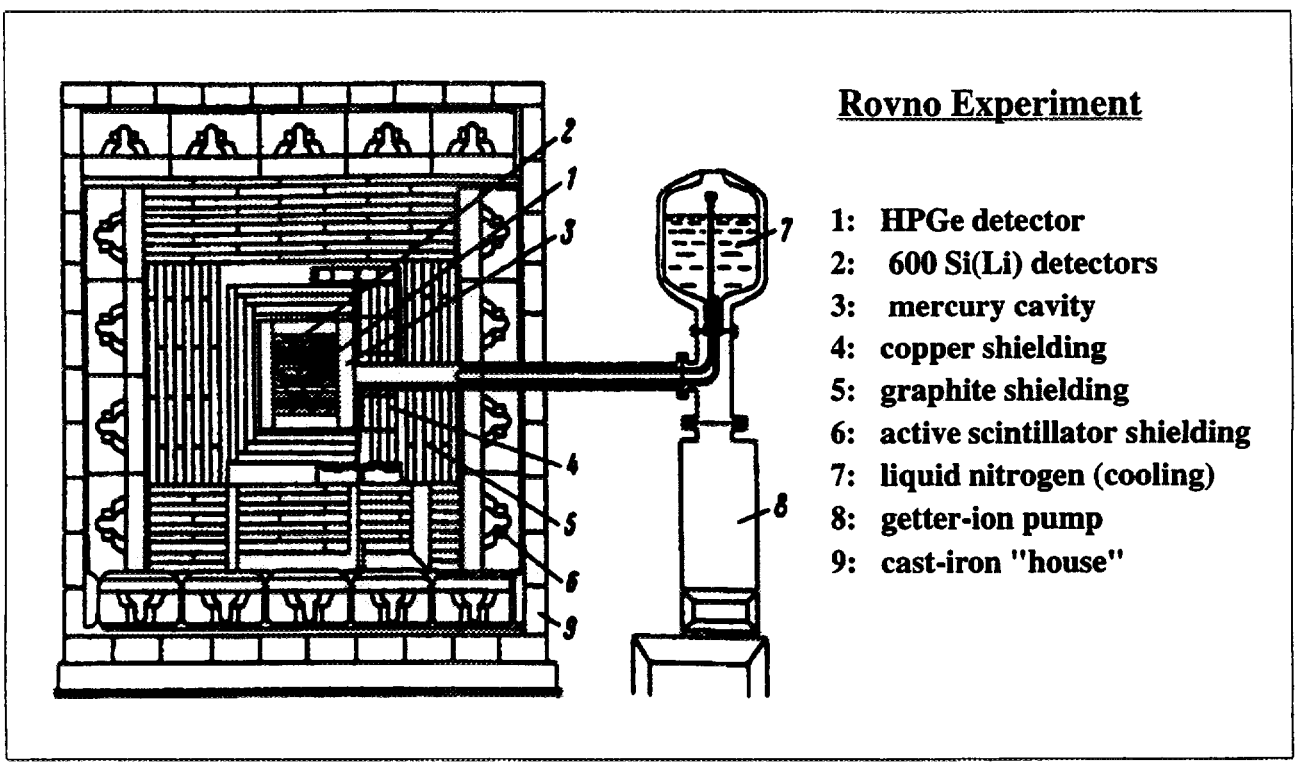

Figure 8: *Experimental setup at the Rovno nuclear power plant.*

in diameter and 125 mm long each. The multidetector (Fig.8) is surrounded by an active shielding (120 plastic scintillators $2.5 \times 2.5 \times 2.0\ m^3$) and by various passive shielding layers (80 mm mercury, 150 mm copper, 500 mm graphite, a cadmium absorber and 150 mm iron). The neutrino flux of the reactor (VVR-100) is $2 \times 10^{13} \frac{\overline{\nu}}{cm^2 \cdot s}$ and the detector is 15 m away from the core. The count rates obtained with 37.5 kg detector[3] during 29.6 days (reactor ON) and 16.7 days (reactor OFF) are summarised in Tab.3 for various energy intervals. Notice the very low signal to noise ratio. The cross section measured in the interval $0.6 - 2.0\ MeV$ is: $\sigma_{\overline{\nu}e} = (1.26 \pm 0.62) \times 10^{-44} cm^2$/fission, corresponding to $\sigma_{\overline{\nu}e} = (1.28 \pm 0.63) \times \sigma_{weak}$ ($\sin^2 \theta_W = 0.22$ assumed). Allowing for a magnetic interaction, the following upper limit was obtained

$$\mu_{\nu_e} < 1.8 \times 10^{-10} \mu_B \ , \quad CL = 90\%$$

[3] By studying the distribution of the count rate as a function of the lower threshold, it was found that the dispersion exceeded that expected statistically up to 0.6 MeV. Half of the detectors were thus removed.

	events/day				
T[MeV]	Reactor on	Reactor off	on-off	$\mu_\nu = 0$	$\mu_\nu = 2 \times 10^{-10}$
0.2-2.0	15327 ± 92	14878 ± 90	449 ± 130	62	178
0.3-2.0	11193 ± 70	10908 ± 70	285 ± 98	53	128
0.6-2.0	4962 ± 12	4921 ± 16	41 ± 20	32	54
1.3-2.0	508.5 ± 4.0	503.3 ± 5.6	5.2 ± 6.8	8.9	10

Table 3: *Count rates measured by the Rovno experiment with 37.5 kg detectors [56].*

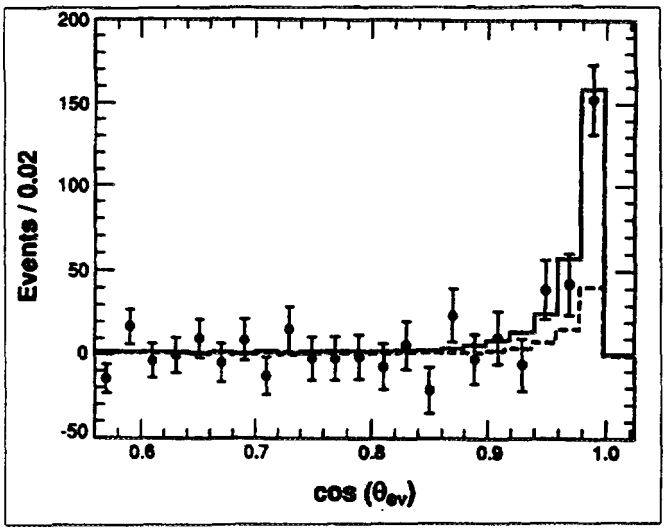

Figure 9: *Angular distribution of the νe elastic scattering signal measured by E225. The solid line is the result of the best fit,* 295 ± 35 *events. The dotted line is the background contribution from the* 59.2 $(\nu_\mu + \overline{\nu}_\mu)e^-$ *scattering events.*

4.1.2 Accelerator experiments

Beam dump experiments at accelerators produce intermediate and high energy neutrinos through the decay of pions: $\pi^+ \to \mu^+\nu_\mu$, $\mu^- \to e^-\overline{\nu}_e\nu_\mu$. The fact that the ν_e are accompanied by ν_μ and $\overline{\nu}_\mu$ complicates the interpretation of the data.

Los Alamos Meson Physics Facility (LAMPF)

Neutrinos are emitted isotropically by pion decay at rest ($\pi^+ \to \mu^+\nu_\mu$), followed by muon decay at rest ($\mu^+ \to e^+\overline{\nu}_\mu\nu_e$), in the 800 MeV proton beam stop. The muon neutrinos are produced with an energy of 29.8 MeV, whereas ν_e and $\overline{\nu}_\mu$ have a maximum energy of 52 MeV. For the beam exposure of 1.12×10^{23} protons, the time integrated neutrino flux for each of the 3 neutrino types was $(9.16 \pm 0.67) \times 10^{14}/cm^2$ at the average detector distance from the beam stop of ~ 9 m.

The E225 experiment aimed to measure the NC-CC interference, I, in $\nu_e e^-$-scattering. The central detector consisted of 40 plastic scintillation planes containing $(4.94 \pm 0.05) \times 10^{30}$ target electrons (energy loss measurement), interleaved by flash chamber modules to measure the position and direction of the particles. It is surrounded by massive shielding and high-efficiency cosmic-ray anticoincidence counters. The other sources of background are neutron capture and $\nu_e C$ reactions. 295 ± 35 $\nu_e e^-$ events are observed with a contribution of 59 events due to $(\nu_\mu + \overline{\nu}_\mu)e^-$ scattering (Fig.9). A neutrino flux-weighted cross section of $\sigma(\nu_e e^-) = (3.18 \pm 0.48 \pm 0.29) \times 10^{-43} cm^2$ is obtained. This is equivalent to $\sigma(\nu_e e^-)/E_\nu = (10.0 \pm 1.5 \pm 0.9) \times 10^{-45} cm^2/MeV$ at a mean neutrino energy $< E_\nu >= 31.7$ MeV. The interfernce term is obtained after subtracting the NC and CC contributions $I = -1.07 \pm 0.17 \pm 0.11$, in good agreement with the standard model prediction (assuming $\sin^2\theta_W = 0.233$) of $I = 4g_L = -2 + 4\sin^2\theta_W = -1.07$. A magnetic moment contribution has been tested for both ν_e and ν_μ. The angular distribution consisted of 274 ± 37 νe events, 626 $\nu^{12}C$ events, 136 other ν-nuclear interactions, and 442 ± 75 remaining neutron induced background events. An energy threshold of 10 MeV was used. Comparing the SM rate, $R_{SM} = 285$ asuming $\sin^2\theta_W = 0.227$, to the observed rate of 274 ± 37, there are fewer than 68 events ($CL = 90\%$) due to magnetic scattering. These are interpreted as the following limits on

μ_ν[57, 53]

$$\begin{array}{lll} \mu_{\nu_e} < 1.08 \times 10^{-9}\mu_B\ , & CL = 90\% & (\mu_{\nu_\mu} = 0) \\ \mu_{\nu_\mu} < 7.4 \times 10^{-10}\mu_B\ , & CL = 90\% & (\mu_{\nu_e} = 0) \\ \mu_\nu < 6.1 \times 10^{-10}\mu_B\ , & CL = 90\% & (\mu_\nu = \mu_{\nu_e} = \mu_{\nu_\mu}) \end{array}$$

The experiment gives an upper limit on the neutrino charge radius of

$$-3.56 \times 10^{-32}cm^2 < |r_\nu|^2 < 5.44 \times 10^{-32}cm^2\ ;\ |r_\nu| < 2.3 \times 10^{-16}cm\ \ (CL = 90\%)$$

Alternating Gradient Synchrotron (AGS at BNL)

The wide band neutrino (antineutrino) beam is produced with a mean energy of 1.3 GeV by 28.3 GeV protons. The E734 experiment at Brookhaven National Laboratory accumulated $159 \pm 17.3 \pm 3.7$ $\nu_\mu e^-$ and $96.7 \pm 13.2 \pm 4.7$ $\overline{\nu}_\mu e^-$ events between 1981 and 1986. The 170 ton-detector consisted of a target calorimeter (112 planes of liquid scintillator and 2 planes of proportional drift tubes) followed by a gamma catcher and a muon spectrometer. The following results have been obtained[52]

$$\mu_{\nu_\mu} < 8.5 \times 10^{-10}\mu_B\ \ (CL = 90\%)\ ;\ -2.11 \times 10^{-32}cm^2 < |r_\nu|^2 < 0.24 \times 10^{-32}cm^2$$

or $\sin^2\theta_W = 0.195 \pm 0.018 \pm 0.013$.

Super Proton Sychrotron (SPS at CERN)

The CHARM II experiment at the CERN-SPS wide band beam (450 GeV protons) produced neutrinos with energies ranging from 0 to 120 GeV ($< E_\nu > \sim 25\ GeV$). The detector consisted of a 600 ton target calorimeter (420 glass plates, 5 cm thick, interspaced by planes of limited streamer tubes), preceded by a veto system with iron plates and scintillator hodoscope, and followed by a muon spectrometer. Between 1987 and 1991, more than 5000 $(\nu_\mu + \overline{\nu}_\mu)e^-$ events were accumulated. The quantities μ_ν and $< r_\nu^2 >$ were obtained from a fit of modelled differential distributions in E_e and $E_e\theta_e^2$ to the data ($E_e > 3\ GeV$). The fit yields[58] $\mu_{\nu_\mu} = \left[1.5^{+0.4}_{-0.6}(stat.)^{+0.8}_{-1.3}(syst.)\right] \times 10^{-9}\mu_B$. Adding statistical and systematical errors in quadrature, the result is compatible with zero with the upper limit

$$\mu_{\nu_\mu} < 3 \times 10^{-9}\mu_B\ ,\ \ CL = 90\%$$

The electroweak mixing angle was found to be $\sin^2\theta_W = 0.2324 \pm 0.0062 \pm 0.0059$. A comparison to the value measured at LEP, $\sin^2\theta_W^{eff} = 0.2324 \pm 0.0005$, leads to a value of the anomalous charge radius of the muon neutrino of $|r_\nu|^2 = (0.4 \pm 3.7) \times 10^{-33}cm^2$, corresponding to the upper bounds

$$|r_\nu|^2 < 0.6 \times 10^{-32}cm^2\ \ ;\ \ |r_\nu| < 0.77 \times 10^{-16}cm\ \ (CL = 90\%)$$

The best upper limits on the magnetic moment of the tau-neutrino are obtained by Cooper et al.[60] in a reanalysis of the data taken in 1982 by the WA66 experiment at Cern/SPS, using the Big European Bubble Chamber (BEBC)[61], to look for $\nu_\tau e^- \to \nu_\tau e^-$. A beam of 400 GeV protons from SPS was dumped onto a high density target (copper block, 404 m upstream of BEBC) which absorbed most of the long-lived secondaries (π, K) thus suppressing the conventional flux of decay neutrinos. The neutrino beam was hence enriched in neutrinos from decays of short-lived hadrons, $D^\pm$, D^0, $\overline{D}^0$, Λ_c, and D_s: $D_s \to \tau\nu_\tau$; $\tau \to \nu_\tau X$. Three events were found (visible momentum above 0.5 GeV), 2 with an e^+ and 1 with an e^-, with no observed hadrons in the final state. The 2 e^+ events are consistent with background from $\overline{\nu_e}p \to e^+n$. The e^- has a momentum of 3.7 GeV/c and is emitted in the forward direction (20 ± 15 $mrad$), consistent with $\nu e^- \to \nu e^-$. With one event observed and 0.5 ± 0.1 predicted by the standard model with $\sin^2\theta_W = 0.23$, a 90% CL upper limit of 3.5 events could be attributed to any other production processes. Recent measurements of charm production and charmed meson decay branching ratios were taken into account in order to estimate the ν_τ-flux: The following ingredients were used as inputs: $\sigma(pp \to D\overline{D} + X) = 13\ \mu b$,

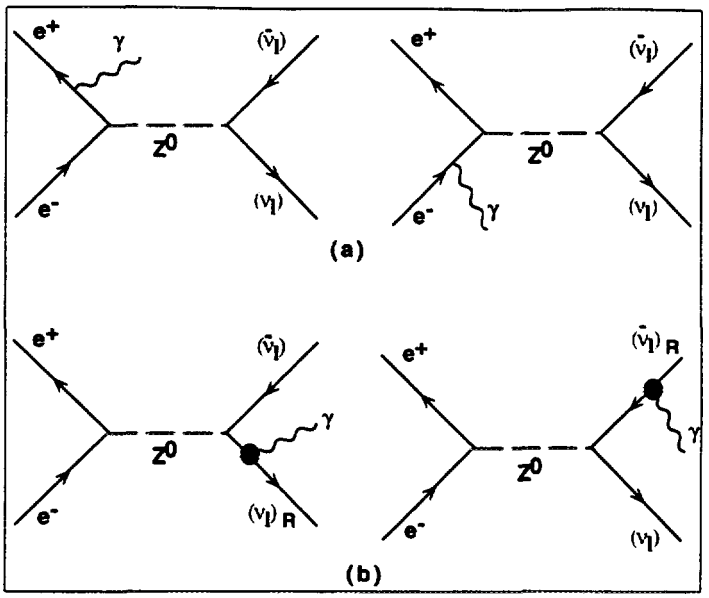

Figure 10: *Feynman diagrams contributing to $e^+e^- \to \nu\overline{\nu}\gamma$: (a) in the standard model (initial state photon radiation); (b) with a contribution from a magnetic interaction of the neutrino (final state radiation).*

$\sigma(pp \to \Lambda_c\overline{D} + X) = 5\ \mu b$, $\sigma(D_s\overline{D}_s)/\sigma(D\overline{D}) = 0.1$, $BR(D_s \to \tau\nu_\tau) = 4.83^{+0.38}_{-0.31}\%$ (obtained by scaling from $\pi \to \mu\nu_\mu$ using the D_s lifetime $\tau_{D_s} = 4.45^{+0.35}_{-0.29} \times 10^{-13}s$). Assuming $\mu_\nu = 10^{-6}\mu_B$, $14.8^{+1.5}_{-1.2}$ events were expected ($E_\nu > 1\ GeV$).The 90% CL upper limit translates to

$$\mu_{\nu_\tau} < 5.4 \times 10^{-7}\mu_B\ ,\quad CL = 90\%$$

which, however, requires assumptions on the D_s production cross section and its branching ratio into $\tau\nu_\tau$, which are not yet measured.

e^+e^--colliders (PEP, PETRA, LEP)

The process $e^+e^- \to \nu\overline{\nu}\gamma$, in which the only final-state particle detected is a photon, proceeds through the exchange of a Z^0 boson. In the standard model the single photon is emitted by the $e^\pm$ (Fig.10(a)). Near the Z resonance, the energy carried by a photon from initial-state radiation tends to be a few GeV at most. A magnetic interaction of the neutrino would manifest itself through a photon emission by the final-state $\nu\overline{\nu}$ (Fig.10(b)). These photons would carry a sizable fraction of the beam energy.

The best limit comes from single photon searches at PEP and PETRA. Data from ASP, MAC, CELLO and MARKJ experiments have been used to obtain the bounds [62]

$$\mu_{\nu_\tau} < 4 \times 10^{-6}\mu_B\ ,\quad CL = 90\%$$

A similar work using data taken in 1990 an 1991 by the ALEPH and L3 experiments [63] resulted in $\mu_{\nu_\tau} < 5.5 \times 10^{-6}\mu_B\ , CL = 90\%$.

The L3 collaboration reported recently on a search for energetic single-photon events ($E_\gamma > 15\ GeV$) in the data collected at LEP in 1991-1993. Fig.11 shows the energy distribution of the single photons. The data are compared to the standard model only (solid histogram) and to the SM with a possible magnetic contribution $\nu_\tau = 5 \times 10^{-6}\mu_B$ (dashed histogram). Requiring the photon energy to be greater than one half the beam energy, L3 obtains the limit[64] $\mu_{\nu_\tau} < 4.1 \times 10^{-6}\mu_B$ ($CL = 90\%$).

The experimental upper limits in reactor and accelerator experiments are summarised in Tab.5, together with the astrophysical bounds, we will discuss in the next chapter. To be complete, upper limits on the charge radius squared of the neutrino are given in Tab.4.

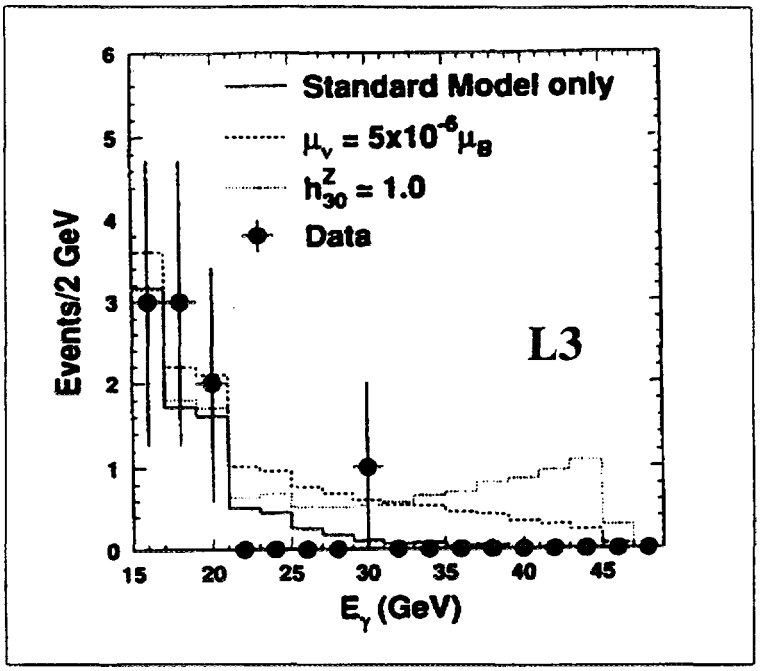

Figure 11: *Energy spectrum of single photon event search from L3 at LEP[64]. The data are compared to the standard model only (solid histogram), SM with a contribution from* $\nu_\tau = 5 \times 10^{-6}\mu_B$ *(dashed histogram), SM extention including an anomalous* $ZZ\gamma$ *coupling (dotted histogram))*

$\nu_\mu e^- \to \nu_\mu e^-$ [50]	$\langle r^2_{\nu_\mu}\rangle < 0.81 \times 10^{-32} cm^2 \quad (\langle r^2_{\nu_\mu}\rangle > 0)$
	$\langle r^2_{\nu_\mu}\rangle > -7.3 \times 10^{-32} cm^2 \quad (\langle r^2_{\nu_\mu}\rangle < 0)$
$\nu_\mu e^- \to \nu_\mu e^-$ [51]	$\langle r^2_{\nu_\mu}\rangle = (-0.3 \pm 1.5) \times 10^{-32} cm^2$
$\nu_\mu e^- \to \nu_\mu e^-$ [52]	$\langle r^2_{\nu_\mu}\rangle = (-1.1 \pm 1.0) \times 10^{-32} cm^2$
$\nu_e e^- \to \nu_e e^-$ [53]	$\langle r^2_{\nu_e}\rangle = (0.9 \pm 2.7) \times 10^{-32} cm^2$
$\overline{\nu}_e e^- \to \overline{\nu}_e e^-$ (Reactor)[55]	$\langle r^2_{\overline{\nu}_e}\rangle < 7.3 \times 10^{-32} cm^2$

Table 4: *Limits on the neutrino charge radius squared obtained by accelerator and reactor experiments.*

Accelerator experiments		
$\mu_{\nu_e} < 1.08 \times 10^{-9}$	[57, 53]	$\nu_e e \to \nu_e e$
$\mu_{\nu_\mu} < 7.4 \times 10^{-10}$	[57, 53]	$\nu_\mu e \to \nu_\mu e$
$\mu_{\nu\tau} < 5.4 \times 10^{-7}$	[60]	$\nu_\tau e^- \to \nu_\tau e^-$
$\mu_{\nu\tau} < 4 \times 10^{-6}$	[62, 64]	$e^+e^- \to \nu\bar{\nu}\gamma$
Reactor experiments		
$\mu_{\nu_e} < 1.8 \times 10^{-10}$	[56]	$\bar{\nu}_e e \to \bar{\nu}_e e$
$\mu_{\nu_e} < 2.4 \times 10^{-10}$	[55]	$\bar{\nu}_e e \to \bar{\nu}_e e$
$\mu_{\nu_e} < 3 \times 10^{-10}$	[54, 45]	$\bar{\nu}_e e \to \bar{\nu}_e e$
Astrophysical Limits		
$\mu_\nu < (2\text{-}3) \times 10^{-12}$	[69, 70, 71, 74]	Luminosity of red giants
$\mu_\nu < 1 \times 10^{-11}$	[75, 76]	Cooling of helium stars
$\mu_\nu < (2\text{-}8) \times 10^{-12}$	[77]	Supernova 1987A
$\mu_\nu < (0.3\text{-}0.05) \times 10^{-12}$	[78]	Supernova 1987A
Cosmological Limits		
$\mu_\nu < (1\text{-}2) \times 10^{-11}$	[66]	^{4}He synthesis in the Big Bang
$d_\nu < 2.5 \times 10^{-22}$ e cm	[67]	^{4}He synthesis in the Big Bang

Table 5: *Upper bounds on dipole moments of the neutrino.*

4.2 Astrophysical Limits

4.2.1 Stellar Cooling

The existence of neutrino dipole moments could influence the rate of generation and emission of energy from a stellar plasma. In dense stars, an off-shell photon, plasmon, can couple to a dipole moment through $\gamma^* \to \nu_{m'}\bar{\nu}_m$. The produced neutrinos would escape with some energy E_ν, leading to a cooling of the core of the star. As the star in the main sequence burns hydrogen, the He^4 core increases, and so does the luminosity. When the core reaches a critical density the $3\alpha \to^{12} C + 7.27\ MeV$ ignites and the core size expands rapidly while the overall luminosity drops suddenly (helium flash). The dip is associated with neutrino losses. A large neutrino magnetic moment would delay helium ignition due to cooling from the reaction $\gamma^* \to \nu\bar{\nu}$ and the larger radius leads to a more efficient helium burning. The enhanced plasmon decay rate would lead to an increased core mass of $\frac{\Delta M_c}{M_\odot} = 0.013\frac{\mu_{\nu_e}}{10^{-12}\mu_B}$. The enhanced neutrino losses could accelerate the cooling rate of white dwarfs (WD). It was found that the "neutrino" dip at the bright side of the luminosity function was too deep unless $\mu_\nu < 10^{-11}\mu_B$. A comparison of luminosities of red giants in 26 globular clusters before and after helium flash sets the even smaller upper limit[69, 70, 71, 74]

$$\mu_\nu < (2-3) \times 10^{-12}\mu_B\ ,\quad CL = 90\%$$

These limits apply to both Majorana and Dirac neutrinos.

4.2.2 Supernova (SN1987A)

In the core of a collapsing star, neutrinos have an energy of $E_\nu \sim 100\ MeV$. The spin-flip reactions $\nu_L e^- \to \nu_R e^-$ and $\nu_L p \to \nu_R p$, induced by a hypothetical neutrino dipole moment, could produce sterile neutrinos (right handed Dirac neutrinos) that could escape freely, cooling the supernova and modifying the corresponding time scale. In addition, due to the the residual magnetic field of the interstellar medium, reflipping is possible, $\nu_R \to \nu_L$, and the lefthanded neutrinos could be detected on the earth by the Kamiokande and IMB detectors. The abscence of neutrinos with energies greater than 50 MeV in SN1987A and the study of the duration of the neutrino pulse lead to an upper limit of[77]

$$\mu_\nu < 10^{-12} - 10^{-13}\mu_B\ ,\quad CL = 90\%$$

The SN1987A bounds have recently been reexamined by Goyal et al.[78] by assuming the presence of a large number of pions and/or a very different composition of the core, consisting of degenerate quarks and leptons. They calculated the energy loss due to helicity flip scattering processes: $\pi^- p \to n + \nu_R\bar{\nu}_R(\nu_L\bar{\nu}_L)$, $\pi^-\nu_L(\bar{\nu}_R) \to \pi^-\nu_R(\bar{\nu}_L)$ and $q\nu_L(\bar{\nu}_R) \to q\nu_R(\bar{\nu}_L)$. They obtained the

limits

$$\mu_\nu < (0.3 - 0.05) \times 10^{-12} \mu_B \ , \quad CL = 90\%$$

by imposing bounds on the ν_R luminosity for the observed neutrino flux at Kamiokande II and IMB. The SN arguments however only apply to Dirac neutrinos, since for Majorana neutrinos $\nu_R = \overline{\nu}_R$ is not sterile.

4.2.3 ^4He-Nucleosynthesis

Using cosmological arguments, an upper limit to a possible magnetic moment of $\mu_\nu < (1-2) \times 10^{-11} \mu_B$ is obtained[66] by requiring that nucleosynthesis of ^{4}He in the Big Bang not be disrupted by the excitation of additional neutrino helicity states, through reactions like $e^\pm + \nu_R \leftrightarrow e^\pm + \nu_L$, $e^+e^- \rightarrow \nu_L \overline{\nu}_R, \nu_R \overline{\nu}_L$. The neutrino component would contribute with its full spin statistical weight of 2, rather than 1, as assumed in standard models of the Big Bang. The escaping sterile ν_R would then lead to a quicker cooling and hence to more He^4, of the order of 15%. The same arguments were used[67] to derive the only existing upper limit on neutrino electric dipole moments of

$$d_\nu < 2.5 \times 10^{-22} e \ cm \ , \quad CL = 90\%$$

Globular cluster limits quoted by Raffelt are $d_\nu < 2 \times 10^{-14} e \ cm$.

4.2.4 Radiative neutrino decays

Radiative decays of neutrinos $\nu_i \rightarrow \nu_j$ can proceed through transition dipole moments. The absence of a γ-burst in association with the SN1987A neutrino burst allows the lifetime of the neutrino to be constrained: $\frac{\tau_\nu}{m_\nu} \geq 2 \times 10^{15} s/eV$. The data stem from gamma ray observations by the Solar Maximum Mission Satellite[79]. Recently, new results are obtained by the COMPTEL instrument[72]. The results on τ_ν from SMMS can be expressed in terms of transition dipole moments

$$\frac{\mu_\nu}{\mu_B} \leq \left\{ \begin{array}{ll} 1 \times 10^{-8} \left(\frac{1eV}{m_\nu}\right) , & m_\nu \leq 20 \ eV \\ 5 \times 10^{-10} \left(\frac{1eV}{m_\nu}\right) , & m_\nu \geq 100 \ eV \end{array} \right\}$$

The stellar cooling arguments are valid up to neutrino masses of $\sim 10 \ keV$, whereas reactor experiments can go beyond. Upper limits from SN1987A are only valid for Dirac neutrinos, and those resulting from radiative neutrino decays depend on assumptions about the non-radiative decay modes. It is very unlikely that the upper bounds derived from astrophysics and cosmology can be improved by a factor of more than two[73]. Experiments, on the other hand, go by improvement steps of typically one order of magnitude. So it is very important to perform further laboratory measurements.

Before describing the MUNU project, we now address the question whether it is theoretically possible to generate large dipole moments with very small neutrino masses.

5 Are large μ_ν theoretically possible?

In the standard model, when right handed neutrinos are included, neutrinos can couple to the photon through higher order weak interactions Dirac neutrinos with mass m_ν acquire a magnetic moment[80],

$$\mu_\nu = \frac{3eG_F}{8\sqrt{2}\pi^2} m_\nu = 3.2 \times 10^{-19} \frac{m_\nu}{eV} \cdot \mu_B$$

where G_F is the Fermi coupling constant and $\mu_B = e/2m_e$ the Bohr Magneton.

$$m_{\nu_e} \simeq 10 \ eV \implies \mu_\nu^{SM} \simeq 3 \times 10^{-18} \mu_B$$

The simplest extension of the standard model is achieved by extending its gauge group structure. In the Left-Right symmetric models the group is $SU(2)_L \times SU(2)_R \times U(1)$ and new gauge

bosons, $W_R^{\pm}$ and Z_R are required. The mass of the neutrino in the SM expression above is replaced by a lepton mass times a certain mixing angle between the left- and right-handed gauge bosons:

$$\mu_\nu \simeq 3.2 \cdot 10^{-19} \frac{m_l \sin 2\theta}{eV} \cdot \mu_B$$

Relatively larger magnetic moments $\mu_\nu^{LR} \simeq 10^{-14}\mu_B$ could be reached[81].

Beyond Standard Model, Voloshin introduced a new ν-isospin symmetry based on the group $SU(2)_\nu$. The left-handed neutrino ν_L and the left-handed antineutrino $(\nu^c)_L$, defined as the antiparticle of the right-handed neutrino, form a doublet[82]

$$\begin{pmatrix} \nu \\ \nu_L^c \end{pmatrix} \; ; \; \begin{pmatrix} \eta_1^+ \\ \eta_2^+ \end{pmatrix} \; ; \; \tau^-$$

the τ (for illustration) is a singlet of ν-isospin. It happens that the $SU(2)_\nu$ symmetry permits magnetic moments while prohibiting masses, as discussed in Ref.[86]. A Dirac neutrino mass term, of the form $\frac{M_D}{2}\left(\nu^{cT}C\nu + \nu^T C\nu^c\right)$ has the ν-spin structure $(\downarrow\uparrow + \uparrow\downarrow)$. It is a component of a ν-spin triplet that is not invariant under rotations in ν-spin space, and consequently is forbidden. The same arguments hold for a Majorana mass term. The dipole moment interaction $\mu_\nu \overline{\nu}\sigma_{\alpha\beta}\nu F^{\alpha\beta}$, which can be written as $\frac{\mu_\nu}{2}\left(\nu^{cT}C\sigma_{\alpha\beta}\nu - \nu^T C\sigma_{\alpha\beta}\nu^c F^{\alpha\beta}\right)$, has the ν-spin structure $(\downarrow\uparrow - \uparrow\downarrow)$, which is a singlet invariant under ν-spin rotations, and consequently is allowed.

In addition to the $SU(2)_L$ symmetry of the standard model, a new symmetry is introduced[84], the horizontal symmetry $SU(2)_H$, which connects the usual e- and μ-generations

$$\begin{pmatrix} \nu_e & \nu^\mu \\ e & \mu \end{pmatrix}_L \; ; \; \begin{pmatrix} \nu_\tau \\ \tau \end{pmatrix}_L \; ; \; \begin{pmatrix} \eta_1^+ & \eta_2^+ \end{pmatrix}_L$$

A horizontal doublet of Higgs scalars is required and neutrinos are Majorana particles. This model predicts relatively large magnetic moments while masses are kept small. It has been shown ([83]) that a bound on the Higgs mass of $M_H < 100\ GeV$ can be obtained for $m_\nu < 10\ MeV$ and $\mu_\nu \sim 10^{-11}\mu_B$. Other models incorporating large dipole moments are described in references [94, 87].

6 The MUNU Detector at the Bugey Reactor

Antineutrino electron scattering at very low energies will be measured by the MUNU collaboration to probe μ_ν[88, 89, 90, 91, 92].

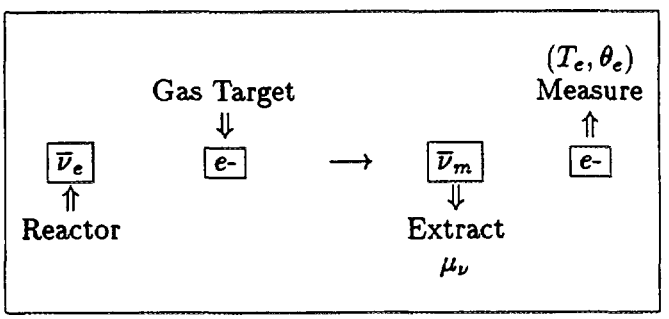

The Requirements are

- (High Flux + Low Energy) $\overline{\nu}_e$	$\Longrightarrow$	⋆ REACTOR
- Measure Track (Energy + Angle)	$\Longrightarrow$	⋆ TPC
- Minimise $\overline{\nu_e}p \to e^+n$	$\Longrightarrow$	⋆ no Hydrogen
- Very low Background	$\Longrightarrow$	⋆ radiochemically clean materials
		⋆ Anti-Compton
		⋆ Shielding

MUNU chose the Bugey nuclear reactor, a Time Projection Chamber filled with CF_4-Gas, a mineral oil based liquid scintillator as anti-compton, readout with photomultipliers, and lead and polyethylene as shielding.

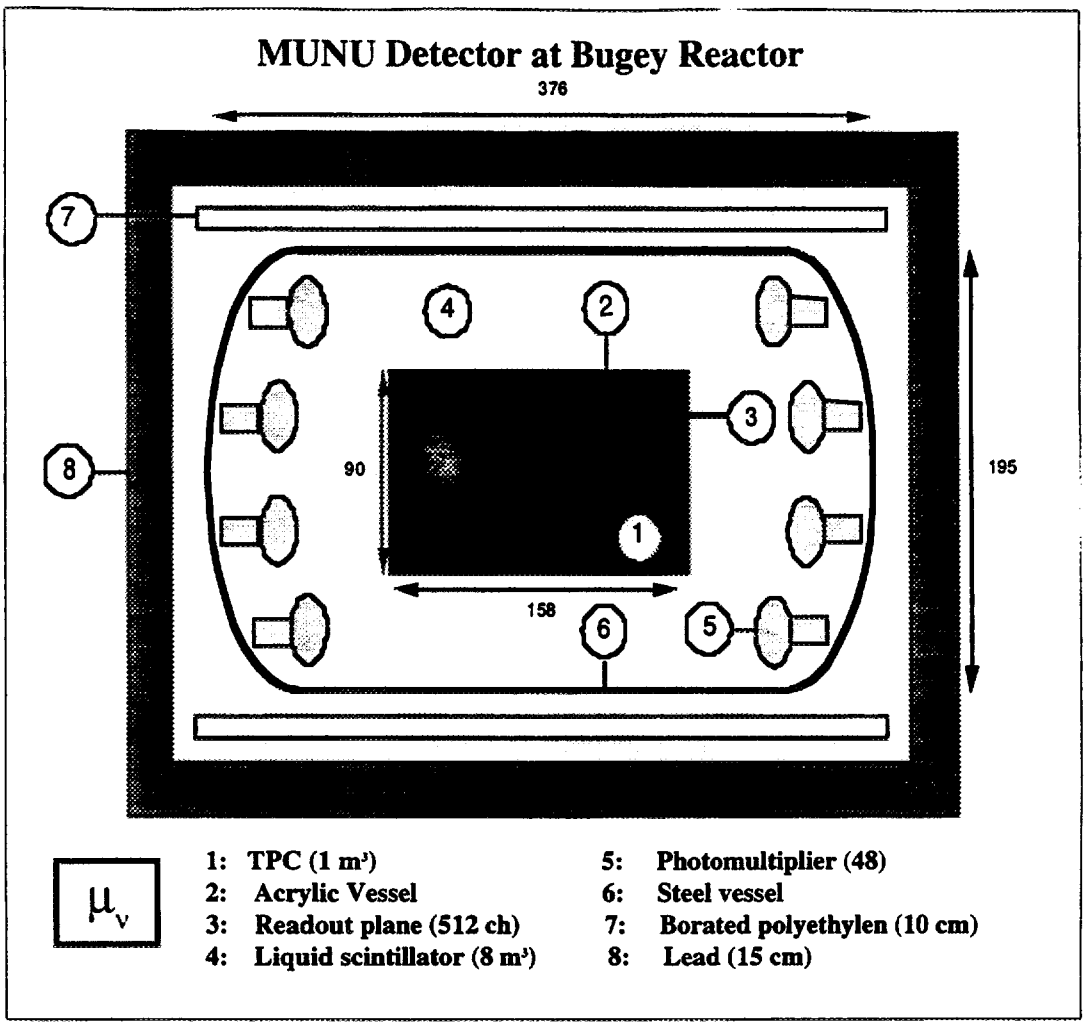

Figure 12: *The MUNU detector at Bugey reactor.*

The Bugey 5 reactor has a power of 2800 $MWth$ and produces $5 \times 10^{20}\ \overline{\nu}_e/s$ in 4π. It is located about 40 km east of Lyon and 150 km from Geneva. The detector will be installed 18.6 m from the core (20 m water equivalent), where the antineutrino flux is $\sim 10^{13}\overline{\nu}_e/s \cdot cm^2$. The cosmic muon flux is $\sim 32/s \cdot m^2$.

A schematic view of the detector is shown in Fig.12.

The Time Projection Chamber (TPC)

The container is a cylindrical acrylic vessel of length 158 cm and diameter 90 cm. The CF_4 gas is chosen as target and detector because of the following properties:

- It has a low Z (C=6, F=9), which minimises multiple scattering,
- a high electron density of 3.68 g/l, corresponding to 6 10^{27} e/m^3 at 5 bar, and
- a high drift velocity of 4 cm/μ for 600 V/cm at 5 bar.
- CF_4 is not toxic, not flammable and relatively cheap (2 CHF/l).
- It is a pure electron target (no free Hydrogen), which suppresses the reaction $\overline{\nu_e}p \rightarrow e^+n$.

Details of the TPC (no magnetic field!) are given in Fig.13. The cathode (negative high voltage) is on the top and the readout plane on the bottom. The anode wires are connected together to provide a total energy trigger signal. A threshold of 500 keV is forseen at the beginning. Two planes of 256 perpendicular strips (3.3 mm pitch) pick up induced signals and define the x, y coordinates. The z coordinate is obtained through the time evolution of the signal. The anode and strip signals are sampled by a 25 MHz- flash ADC system. The spatial resolution is $\sigma_{x,y,z} \sim 1\ mm$. From the first 2 cm of the track it is possible to determine the angle of the recoil

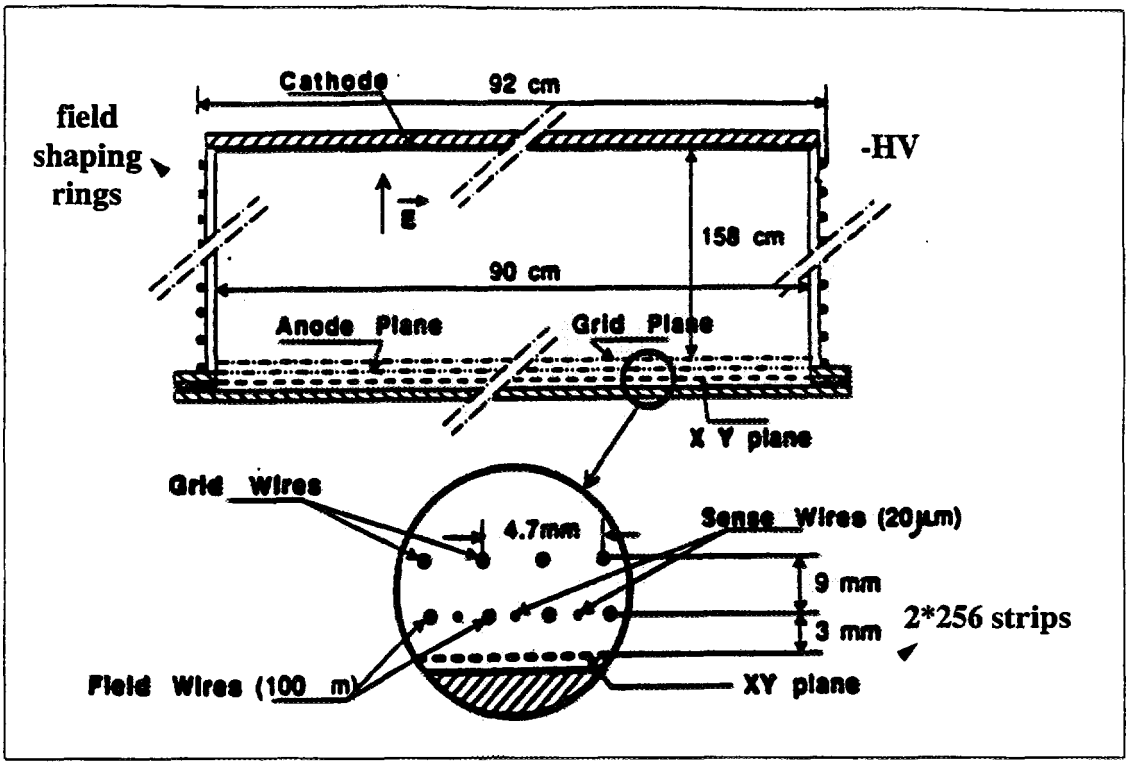

Figure 13: *MUNU Time Projection Chamber*

electron, θ_e, with an accuracy of $\sigma_\theta \sim 15°$. This is mainly due to multiple scattering. The core size of the reactor contributes to $\pm 6°$.

Tests with a prototype mini TPC ($\Phi = 10\ cm, L = 30\ cm$) have been concluded, and electron and muon tracks are seen (Fig.14). Preliminary results have also been obtained with a full scale ($1\ m^3$) TPC. Fig.15 shows a muon event. The signal to noise ratio is about 10 to 1.

The Liquid Scintillator and the shielding

Eight m^3 mineral oil based liquid scintillator (NE235, attenuation length $\lambda_{att} \sim 6.5\ m$ at $420\ nm$) are contained in a stainless steel vessel supporting 5 bar ($L = 376\ cm$, $\Phi = 195\ cm$). It acts as an anti-Compton shield and allows detection of low energy photons and vetos cosmic muons. It is readout by 48 photomultipliers (EMI9351 8", B53 glass with 0.2 Bq; 100 keV threshold; 180 photoelectrons/MeV; FADC readout). The passive shielding is based on 15 cm low activity lead to reduce local activity and 10 cm borated polyethylene (CH_2+B_4C) to reduce the neutron flux created in lead by cosmic muons.

Background Studies and sensitivity

Background, defined to be γ and β rays giving one single electron in the chamber, depositing less than 100 keV in the Anti-Compton shield and at least 500 keV in the TPC, comes from three sources.

Natural activities : (Th, U, K, ^{60}Co, etc...)
All materials must be radiochemically clean, especially the ones present in large quantities. For example, mineral oil and acrylic are produced with concentrations of Th and U of $< 10^{-12}$g/g. One expects 1.5 evts/day.

Muons:
Muons can be captured either in the TPC: $\mu + {}^{12}C({}^{19}F) \rightarrow {}^{12}B({}^{19}O) + \nu$, followed by the decay of ${}^{12}B({}^{19}O)$ with neutron emission (0.5 evts/day), or can interact in the shielding (0.6 evt/day).

Neutrons:
Slow neutrons from the reactor lead to a negligible background. Those induced by muons contribute to 0.15 evt/day, and those from $\overline{\nu_e}p \rightarrow e^+n$ in the scintillator to 0.15 evt/day.

From measurements, simulations and the experience gained with the Xe-TPC at Gotthard, $\sim$ 3 background events are expected per day[88]. The trigger is based on 3 levels, corresponding to the following photon energy levels

- $E > 100\ keV \Longrightarrow \gamma$ rejection (100 Hz, 40 μs)

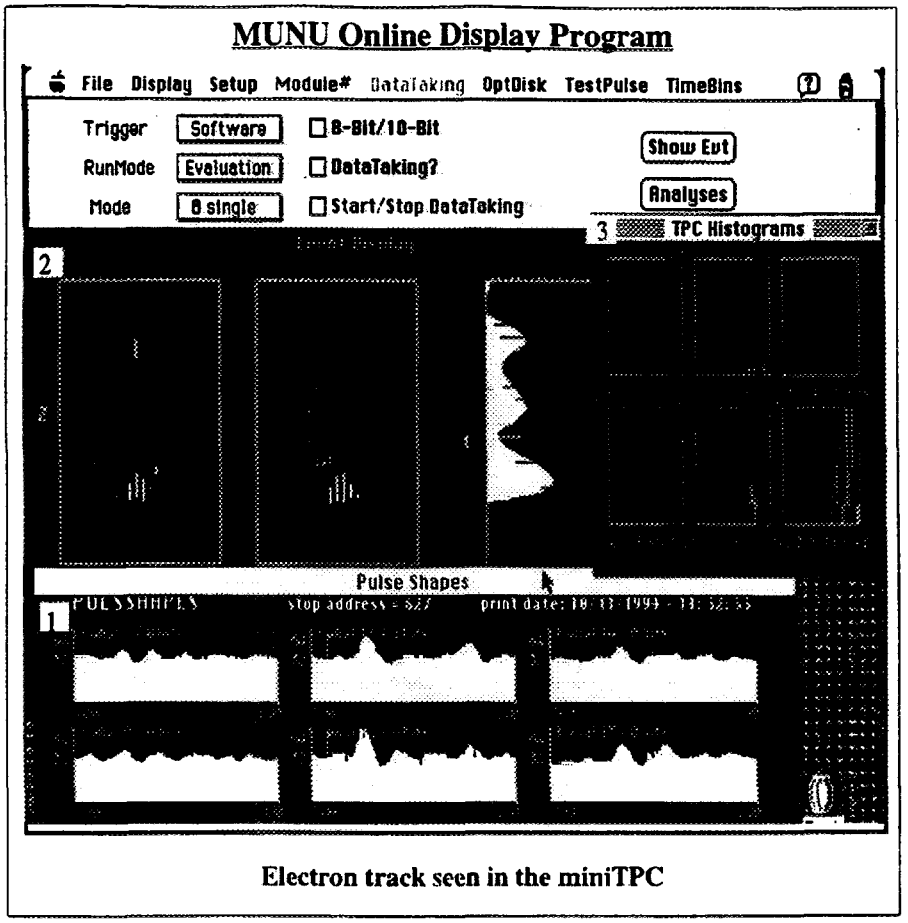

Figure 14: *Electron track seen in the mini TPC.*

- $E > 1.0\ MeV \Longrightarrow \beta$ rejection (50 Hz, 200 μs)
- $E > 5.0\ MeV \Longrightarrow \mu$ rejection (400 Hz, 200 μs)

The expected event rate and the corresponding detector acceptance are summarised in Tab.6 for two energy domains, $0.5 - 1.0\ MeV$ and above $1.0\ MeV$. A hypothetical magnetic moment of 10^{-10} would increase the event rate by $\sim 30\%$.

		$\bar{\nu}_e$ events/day (**year**)	
T[MeV]	Acceptance	$\mu_\nu = 0$	$\mu_\nu = 10^{-10}$
0.5-1.0	0.85	5.3	8.0
		1530	**2400**
≥ 1	0.65	4.2	5.3
		1230	**1560**
σ		9.5	13.4
		Background ~ 3 events/day	

Table 6: *Expected Event Rates[88]*

The MUNU detector presents new features. The energy domain $E_\nu = 0.5 - 1.5\ MeV$ has so far not been explored. The scattering angle θ_e will be measured. As a consequence, background can be measured while reactor is on, by considering events in the backward hemisphere ($\theta_e > 90°$). The data taking will spread over at least one year, giving 5 times more events above $1.5\ MeV$ than observed at Savannah.

Assuming 1 year of data taking and considering only the low energy domain ($0.5 - 1.0\ MeV$), one expects $\pm 3\%$ statistical errors. Systematic uncertainties ($\pm 5\%$) are mainly due to the reactor spectrum ($\pm 3\%$), the reactor power ($\pm 2\%$), and the detection efficiency ($\pm 3\%$).

With a background of about 3 events/day one obtains a sensitivity of

$$\mu_\nu < 3 \times 10^{-11} \mu_B\ ,\quad CL = 90\%$$

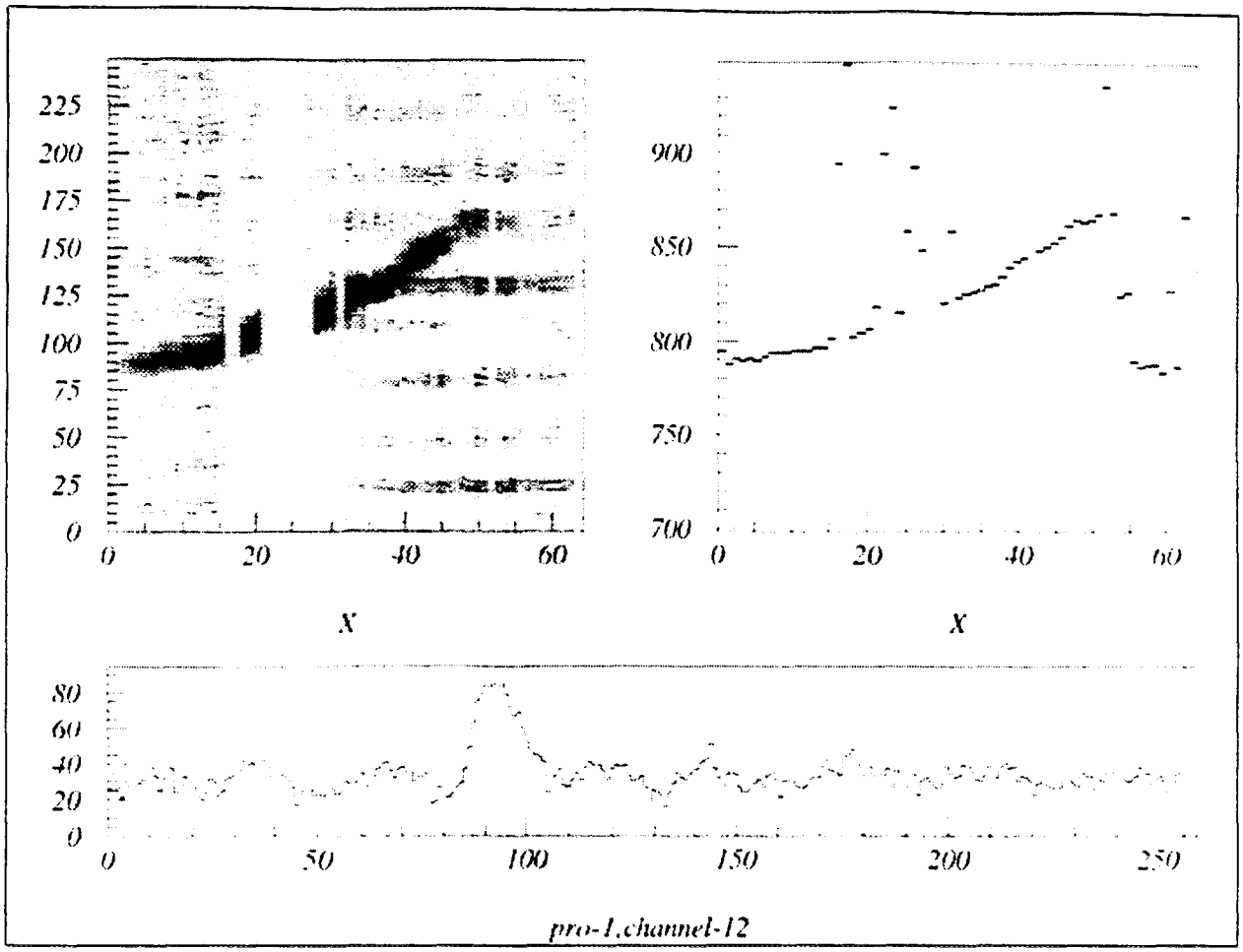

Figure 15: *Muon event seen in a full scale TPC.*

decreasing to $\mu_\nu < 4 \times 10^{-11}\mu_B$, if the background is 4× higher than anticipated. The sensitivity could be improved to

$$\mu_\nu < 2 \times 10^{-11}\mu_B \ , \quad CL = 90\%$$

by considering the following. The use of the energy bin above 1 MeV allows the slope of the reactor spectrum to be extracted, and hence, the systematic uncertainties to be reduced. The angular distribution will be measured. Depending on the background situation the threshold could be lowered to $300 - 350$ keV, and the pressure to 2-3 bar.

On the other hand, assuming a vanishing magnetic moment, the weak mixing angle can be measured, in $\overline{\nu_e}e^-$-scattering at very low energies, with an accuracy

$$\Delta \sin^2 \theta_W = \pm 5\%$$

comparable to that achieved by the CHARM II collaboration in the study of $\nu_\mu e$-scattering[95, 58]

All components of the MUNU detector are ready and tested. Data taking is expected to start by the beginning of 1997. Various features of the detector, like tracking and low background, make MUNU a general multipurpose low energy detector. It can be used to look for double beta decay (see J. Busto, these proceedings) or dark matter[88]. Simulations are being performed to study the feasability of a Super Solar MUNU (SSM), to detect solar neutrinos.

7 Summary and Prospects

To summarise, the neutrino is very important for particle physics, astrophysics and cosmology. It is necessary to study all its properties independently... including its possible electromagnetic interactions.

Several complementary upper limits on neutrino dipole moments and charge radius have been obtained by laboratory experiments at reactors and accelerators, or by using astrophysical arguments. The latter are more stringent but more or less model dependent. It is important to perform more direct measurements, and new experiments, like MUNU, are welcome.

8 Acknoweledgements

I would like to thank the organizers of the Zuoz school, especially Milan Locher, for the warm hospitality and for a pleasant stay in a wonderful place.

References

[1] F. Reines, C.L. Cowan, *Phys. Rev.*, **90**(1953) 492.

[2] C.L. Cowan, H.W. Cruse, F.B. Harrison, A.D. McGuire, F. Reines, *Science*, **124**(1956) 103

[3] M. Goldhaber, L. Grodzins, A.W. Sunyar, *Phys. Rev.*, **109**(1958) 1015.

[4] G. Danby, J.M. Gaillard, K Goulianos, L.M. Lederman, M. Mistry, M. Schwartz, J. Steinberger, *Phys. Rev. Lett.*, 9(1962) 36.

[5] M.L. Perl et al., *Phys. Rev. Lett*, **35**(1975) 1489.

[6] Belesev et al., Phys. Lett.**B350**(1995)263.

[7] Assamagan et al., Phys.Rev.**D53**(1996)6065.

[8] Buskulic et al., Aleph coll., Phys. Lett.**B349**(1995)585.

[9] G. Barbiellini, G. Gocconi, Nature **329** (1987)21.

[10] E. Majorana, Nuovo Cimento **14** (1937) 171.

[11] F. Boehm and P. Vogel, Physics of Massive Neutrinos (Cambridge University Press, 1987/1992)

[12] B. Kayser, Comments Nucl. Part. Phys.**14**(1985)69

[13] J.N. Bahcall, M.H. Pinsonneault, Rev. Mod. Phys.**64**(1992)82.

[14] S. Turck-Chièze, I. LopesRev. Mod. Phys.**64**(1992)82.

[15] B.T. Cleveland et al., Nucl. Phys. (Proc. Supp.)**B38**(1995)47; B.T. Cleveland et al., subm. to Astrophys. J.(1996).

[16] P. Anselmann et al., Phys. Lett.**B357**(1995)237.

[17] J.N. Abdurashitov et al., Nucl. Phys. (Proc. Supp.)**B38**(1995)60.

[18] "Solar neutrino data from Kamiokande" Y. Suzuki et al., Nucl. Phys. (Proc. Supp.)**B54**(1995)47.

[19] R, Davis, in Proc. 7th Work. on Grand Unif., ICONABAN'86, ed. R. Arafune (Singapore: World Scientific)273.

[20] J.N. Bahcall, "Neutrino Astrophysics.", Cambridge University Press, 1989

[21] M.B. Voloshin, M.I. Vytsotskii and L.B. Okun, Sov. Phys. JETP**64**(1986)446.

[22] W. Hampel, these proceedings.

[23] A. Dar, these proceedings.

[24] S. Petcov, these proceedings.

[25] D.S. Oakley et al., Astrophys. J.(1994) **437**,L63

[26] R. L. McNutt Jr, Science **270**(1995)1635

[27] D.S. Oakley, H.B. Snodgrass,hep-ph/9604252, 1996

[28] L. Wolfenstein, Phys. Rev. D17 (1978) 2369; Phys. Rev. D20 (1979) 2634

[29] S.P. Mikheyev, A.Yu. Smirnov, Sov. J. Nucl. Phys. 42 (1986) 913; Sov. Phys. JETP 64 (1986) 4; Nuovo Cimento 9C (1986) 17.

[30] C.S. Lim, W.J. Marciano Phys. Rev. D37 (1988)1368.

[31] W.J. Marciano, A. Sirlin, Electromagnetic properties of neutrinos, Brookhaven,1988.

[32] E. Akhmedov and M. Khlopov, Mod. Phys. Lett. **A3** (1988) 451.

[33] E. Akhmedov and M. Khlopov,

[34] E. Akhmedov Nucl. Phys. **A527** (1991)679.

[35] E. Akhmedov, A. Lanza and S. Petcov, Phys. Lett. **B303** (1992)85

[36] J. Pulido, Phys. Rev.**D48** (1993)1492.

[37] H.Nunokawa, H. MinakataPhys. Lett.**B314** (1993)371

[38] E. Akhmedov, FTUV**94-26** (1994)

[39] C.S. Lim, H.Nunokawa, Astropart. Phys.**4** (1995)63.

[40] W. Pauli, Phys. Today **23** (sept 1978).

[41] P.B. Pal, Inter. J. of Mod. Phys. **A7** (1992) 5387.

[42] J. Pulido, Phys. Rep. **211** (1992) 167.

[43] G. Domogatskii,D. Nadezhin, Sov. J. Nucl. Phys.**12**(1971)678

[44] A.V. Kyuldjiev, Nucl. Phys.**B243**(1984)387

[45] P. Vogel und J. Engel, Phys. Rev. D,**39**(1989)3378

[46] J. Segura, J. Bernabeu, F.J. Botella, J. Penarrocha, Phys. Rev. D49 (1994)1633.

[47] J. Segura, Tesis Doctoral, Universidad de Valecia, Noveiembre 1994,,

[48] J. Bernabeu, S.M. Bilenky, F.J. Botella, J. Segura, Nucl. Phys. B426 (1994)434.

[49] G. DeGrassi, A. Stirlin, W.J. Marciano, Phys. Rev.**D39**(1989)287.

[50] K. Abe et al., Phys. Rev. Lett. **58**(1987)636;

[51] J. Dorenbosch et al., Z. Phys**41**(1989)567.

[52] Ahrens et al., Phys. Rev.**D41**(1990)3297.

[53] Allen et al., Phys. Rev.**D47**(1993)11.

[54] F. Reines, H.S. Gurr and W. Sobel, Phys. Rev. Lett.,**37**(1976)315

[55] G.S. Vidyakin et al., JETP Lett. **49** (1989) 740; G.S. Vidyakin et al., JETP Lett. **55** (1992) 206.

[56] Derbin et al., JETP Lett. **57** (1993) 768(translated from ZETFP **57** 755); Derbin et al., PAN **57** (1994) 222 (transl. from YAF **57** 236)

[57] D.A. Krakauer et al., Phys. Lett.**252B**(1990)177; Phys. Rev.,**44D**(1991)6.

[58] CHARM II collab., P. Vilain et al., Phys. Lett.**B345**(1995)115.

[59] CHARM collab., Dorenbosch et al., Z. Phys.C41(1989)567; Z. Phys.C51(1991)142.

[60] A.M. Cooper-Sarkar et al., Phys. Lett.B280(1992)153.

[61] H. Grässler et al., Nucl. Phys.**B273**(1986)1253.

[62] H. Grotch, R. Robinet, Z. Phys.C39(1988)553.

[63] T.M. Gould, I.Z. Rothstein, Phys. Lett.B333(1994)545.

[64] M. Acciarri et al., Phys. Lett.B346(1995)190.

[65] G. G. Raffelt, Phys. Rep. 198 (1990) 1-113.

[66] J.A. Morgan, Phys. Lett. B102 (1981) 247.

[67] "Upper limit on neutrino electric dipole moments."
J.A. Morgan, D.B. Farrant, Phys. Lett. 128B (1983) 431.

[68] G. Raffelt and D. Dearborn, Phys. Rev. D37 (1988) 549.

[69] G. Raffelt, Phys. Rev. Lett. **64** (1990) 2856.

[70] G. Raffelt, Astrophys. J. 365 (1990)559;

[71] G. Raffelt, A. WeissAstron. Astrophys. 264 (1992)536;

[72] G. G. Raffelt, these proceedings.

[73] G. G. Raffelt, private communication.

[74] M. Catelan et al., Astrophys. J. 461 (1996)231;

[75] G. Raffelt, D. Deaborn, Silk, A. Phys. J. 336 (1989)61.

[76] M. Fukugita, S. Yazaki, Phys. Rev. D36 (1987)3817.

[77] J. M. Lattimer, J. Cooperstein, Phys. Rev. Lett. **61**(1988)23; R. Barbieri, R.N. Mohapatra, Phys. Rev. Lett. **61**(1988)27; I. Goldman et al., Phys. Rev. Lett. **60** (1988) 1789; D. Notzold, Phys. Rev. **D38** (1988) 1658.

[78] A. Goyal, S. Dutta, S.R. Choudhury, Phys. Lett. **B346**(1995)312.

[79] L. Oberauer, Asttropart. Phys. **1**(1993)377; E.L. Chupp et al., Phys. Rev. Lett. **62**(1989)505.

[80] B.W. Lee, R.E. Schrock, Phys. Rev. **D16**(1976)1444; W. Marciano, A.I. Sandra,Phys. Lett.**B67**(1977)303.

[81] M. Baig, J.A. Grifols, E. Masso, Mod. Phys. Lett. **A3**(1988)719

[82] M.B. Voloshin, Sov. J. Nucl. Phys. **481**(1988)225; R. Barbieri, R.N. Mohapatra, Phys. Lett. **218B**(1989)1225; K.S. Babu, R.N. Mohapatra, Phys. Rev. Lett. **63**(1989)228

[83] M. Leurer, N. Marcus, Phys. Lett.**B237**(1990)81.

[84] K.S. Babu, R.N. Mohapatra, Phys. Rev. Lett. **64**(1989)1705

[85] S.M. Barr, E.M. Freire, A. Zee, Phys. Rev. Lett. **65**(1990)2626

[86] B. Kayser, Nucl. Phys. B (proc. suppl.)**19**(1991)177.

[87] M. Voloshin, Nucl. Phys. B (proc. suppl.)**19**(1991)433.

[88] MUNU Collaboration: Grenoble, Münster, Neuchatel, Padova, Zürich, C. Broggini et al., Proposal, LNGS 92-47 (1992) 51 pp.

[89] C. Amsler (MUNU Collab.), Proc. of the 3rd NESTOR Workshop, Pylos, Greece (1993)556.

[90] C. Broggini (MUNU Collab.), Nucl. Phys. B (proc. suppl.)**35**(1994)441.

[91] J. Busto (MUNU Collab.), Proc. XXII Int. Conf. on High Energy Physics, 20-27 July 1994, Glasgow, p.955.

[92] M. Avenier et al. (MUNU Collab.),Contribution to the XVI Conf. of Neutrino Physics and Astrophysics, Eilat, 1994; INSNG 94/56.

[93] R. N. Mohapatra und P. B. Pal, Massive Neutrinos in Physics and Astrophysics (World Scientific, Singapore 1991)

[94] P. B. Pal, University of Oregon, Institute of Theoretical Science, OITS **470** (1991)

[95] D. Geigerat et al., Phys. Lett. **B259**(1991)499.

[96] Particle Data Group, Physical Review **D54/1-I** (The American Physical Society, 1996)1

KARMEN: NEUTRINO SPECTROSCOPY AT ISIS

G. DREXLIN
Institut f"ur Kernphysik I, Forschungszentrum Karlsruhe
D-76021 Karlsruhe, P.O. Box 3640, Germany
E-mail: guido@ik1.fzk.de

ABSTRACT

The Karlsruhe-Rutherford Neutrino Experiment KARMEN at the spallation neutron facility ISIS investigates fundamental properties of neutrinos as well as their interactions with matter. Low energy neutrinos with energies up to 50 MeV emitted by the pulsed ν-source ISIS are detected by a 56 tonne high resolution liquid scintillation calorimeter. Clear ν-signatures allow a reliable search for neutrino oscillations of the type $\nu_\mu \rightarrow \nu_e$ and $\bar{\nu}_\mu \rightarrow \bar{\nu}_e$ as well as a detailed investigation of neutrino-nucleus interactions in an energy range important for astrophysics. We present the results of the KARMEN experiment from data taking in the period from June 1990 - December 1995.

1 Introduction

Despite many attempts in the past sixty years to unravel the nature of the neutrino most of its intrinsic properties such as its rest mass and its possible inner structure resulting in a non-zero magnetic moment are still unknown. The study of fundamental neutrino properties has become a key issue in modern particle physics, nuclear physics and the new field of particle astrophysics. The most promising way to detect a non-zero neutrino mass is the search for *neutrino oscillations* which therefore has very actively been pursued in the past 15 years, however, no unambiguous positive evidence has been reported so far. In the field of particle astrophysics it is especially the investigation of *neutrino-nucleus interactions* which is important for the

understanding of various processes such as the ν-induced elemental synthesis in core-collapse supernovae explosions.

Whereas most neutrino experiments in the past have only been performed with high energy muon neutrinos in the multi-GeV range, precision experiments studying the above issues in neutrino physics can also be carried out with well-defined and copious sources of *low energy neutrinos* in the MeV range. The relevant neutrino energy region of up to 50 MeV is that of 'classical' nuclear physics. At these energies neutrino-nucleus cross sections are typically only of the order of 10^{-42} cm^2. Thus the extremely difficult experimental problem is to measure cross sections which are up to 20 orders of magnitude smaller than those from strong or electromagnetic background processes. In addition, the lack of suitable neutrino sources and the difficulties of high quality detection methods for low energy neutrinos have prevented neutrino physics to become a more systematic and sound working field.

But this situation has now improved due to two technical developments:
a) the completion of new high intensity *pulsed* proton accelerators (neutron spallation sources) providing intense bursts of different species of low energy neutrinos from the decays of pions and muons at rest
b) the possibility to build large volume liquid scintillation detectors with high resolution figures even down to a few MeV of energy deposit, supplemented by efficient background rejection systems.

The spallation neutron source ISIS at the Rutherford-Appleton Laboratory in England constitutes the first high intensity proton accelerator providing a pulsed neutrino source of that kind. Taking full advantage of the unique time structure of the ν-source ISIS, the large volume neutrino calorimeter KARMEN is investigating the fundamental properties of neutrinos via the search for neutrino oscillations in the two appearance modes $\nu_\mu \rightarrow \nu_e$ and $\bar{\nu}_\mu \rightarrow \bar{\nu}_e$. The study of neutrino-nucleus interactions, which is carried out simultaneously, is focused on the observation of charged and neutral current excitations of ^{12}C with special emphasis on the various implications for particle astrophysics. In the following we describe the basic features of the KARMEN neutrino experiment at ISIS [1] before presenting our results from five years of data taking.

2 The ISIS Neutrino Source

The spallation neutron facility ISIS at the Rutherford Appleton Laboratory is the most powerful pulsed neutrino source in operation. Two bunches of protons are extracted from the 800 MeV, 50 Hz proton synchrotron in a single machine cycle.

The DC-equivalent intensity is 200 μA. The beam is dumped in a Ta-D_2O target. Pions, produced in this target are stopped inside the target within 0.1 ns. Negative pions at rest are inevitably captured and absorbed by the target nuclei. Thus the consecutive decay sequences $\pi^+ \rightarrow \mu^+ + \nu_\mu$ and $\mu^+ \rightarrow e^+ + \nu_e + \bar{\nu}_\mu$ with both π^+ and μ^+ decaying at rest, are the ν-generating process of monoenergetic ν_μ (29.8 MeV) and of (ν_e, $\bar{\nu}_\mu$) with continuous energy distributions ranging up to 52.8 MeV ((fig. 1(a)). The neutrino flux is isotropic and of exactly the same intensity for all

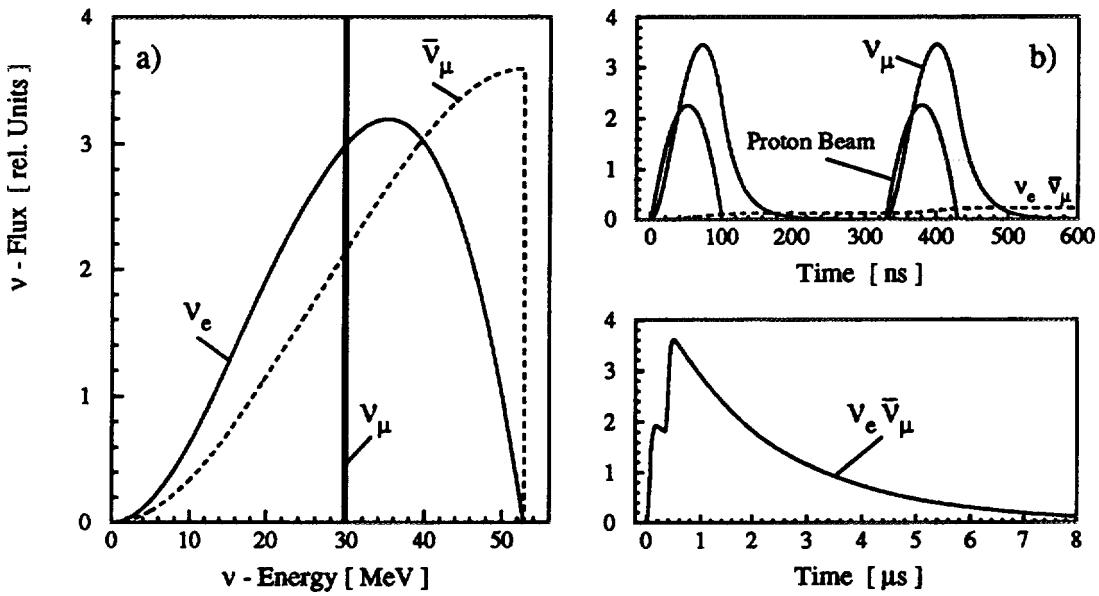

Figure 1: Energy spectra (a) and time structure (b) of the ISIS beam dump neutrino source.

three types of neutrinos. Contamination with $\bar{\nu}_e$ from the $\pi^- \rightarrow \mu^-$ decay chain is limited to 8×10^{-4}.

The beam's inherent time structure is uniquely matched with the different life time of π^+ (26 ns) and μ^+ (2.2 μs) (fig. 1(b)), resulting in high neutrino peak intensity and clear separation of ν_μ-induced reactions from those induced by ν_e or $\bar{\nu}_\mu$. The (ν_e, $\bar{\nu}_\mu$) inherit the decay time constant of the μ^+-decay, a significant identification label for reactions induced by these neutrinos. The accelerator duty cycle allows effective suppression of cosmic ray induced background by five orders of magnitude. This background can be analysed with highest precision during the 20 ms beam pause intervals.

3 The KARMEN Neutrino Spectrometer

The KARMEN detector is a 56 t segmented liquid scintillator calorimeter at a mean distance of 17.5 m (90°) from the beam stop [2]. A matrix structure of 32 rows × 16 columns subdivides the central detector into 512 independent modules. Each module is monitored by two 3-inch phototubes at each end side (fig. 2). Total internal light

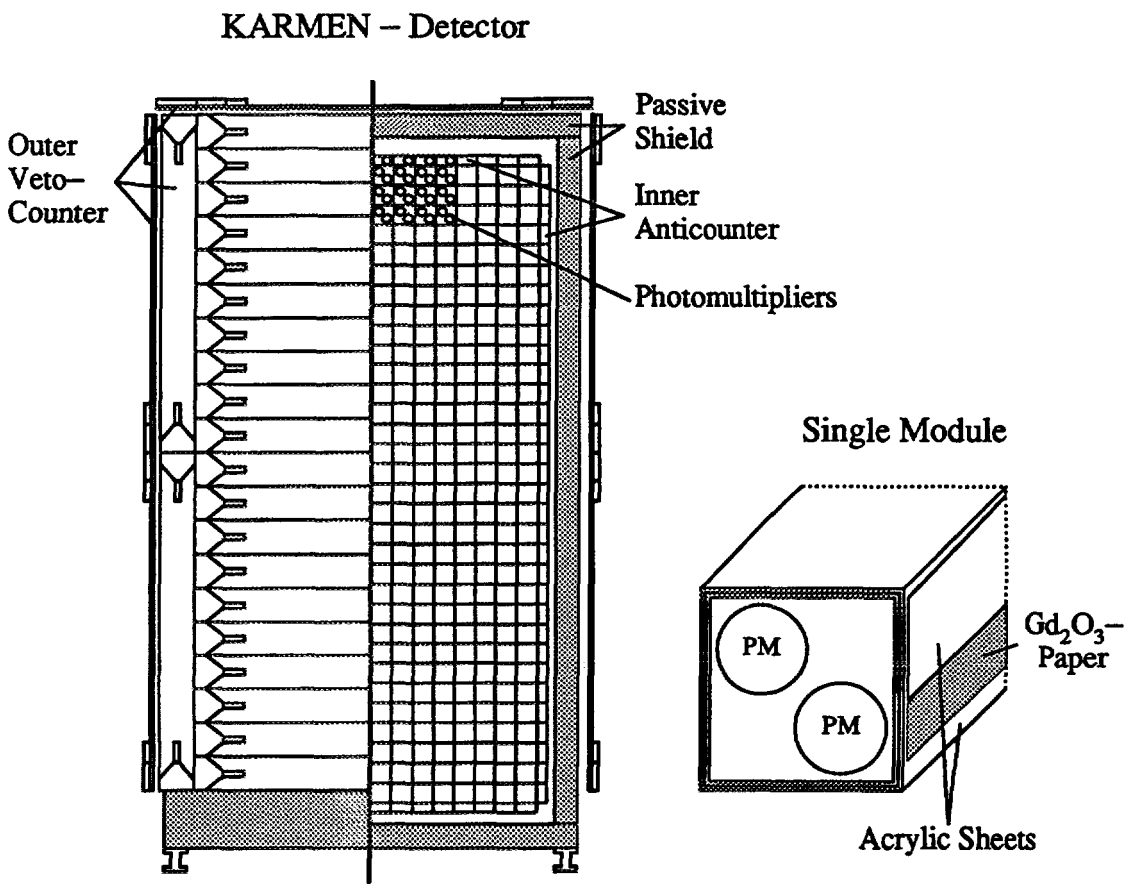

Figure 2: The 56 t high resolution liquid scintillator calorimeter KARMEN

reflection at the module walls is the mechanism of light transport within the modules (fig. 2inset). Gadolinium (Gd_2O_3), deposited in the module's walls, allows neutron detection through the Gd(n,γ) capture reaction releasing on average three gamma quanta with a sum energy of 7.6 MeV.

The liquid scintillator makes up more than 96% of the total mass of the central calorimeter. This essential design feature enables the calorimeter to account for

energy deposits of even less than 2 MeV. The average energy resolution is: $\sigma(E)/E = 11.5\%/\sqrt{E(MeV)}$.
The time resolution is 0.7 ns. A sandwich veto counter system rejecting cosmic muon induced background with 99.9% efficiency encloses the detector. A 7000 t steel blockhouse, lined inside with boracic polyethylene, provides effective shielding against neutrons from the spallation target and against the hadronic component of cosmic rays.

4 Neutrino Nucleus Interactions

The KARMEN liquid scintillation calorimeter consists entirely of hydrocarbons and thus serves as a massive live target of ^{12}C and ^{1}H nuclei for the investigation of various neutrino nuclear interactions. Inelastic scattering of neutrinos by nuclei can proceed either by the weak charged current (exchange of a $W^{\pm}$ boson) or by the weak neutral current (exchange of a Z^0 boson). In both cases the neutrino interaction gives rise to nuclear excitations which can be identified by the subsequent characteristic nuclear deexcitation processes [6].

At beam dump energies charged current reactions upon nuclei can only be induced by electron neutrinos due to energy conservation. An example is the socalled inverse β-decay reaction $\nu_e + {}^{12}C \rightarrow {}^{12}N_{g.s.} + e^-$. This transition, which is observed in the KARMEN experiment with negligible background, allows not only to identify electron neutrinos but also to measure for the first time their energy distribution.

On the other hand neutral current processes can be induced by all neutrino flavours on condition that their energy is above the reaction threshold. At ISIS all three neutrino flavours ($\nu_\mu, \nu_e, \bar{\nu}_\mu$) can induce the neutral current excitation $^{12}C(\nu,\nu')^{12}C^*$ (1^+1; 15.1 MeV) which therefore represents an ideal test case for the principle of flavour universality of the weak neutral current coupling.

In charged current (CC) as well as in neutral current (NC) neutrino scattering the nucleus can be used as a microscopic laboratory for the study of fundamental interactions and symmetries. The well defined change of quantum numbers in the nuclear transitions acts as an effective 'spin-isospin' filter and allows the study of the rather complex spin-isospin structure of the weak hadronic currents. In the charged current as well as in the neutral current excitation of ^{12}C the spin flip ($\Delta S = 1$) selects the axial-vector components of the weak hadronic currents, the change of isospin by one unit ($\Delta T = 1; \Delta T_3 = 0, 1$) correspondingly the isovector components. In this way only one spin-isospin component of the weak hadronic currents contributes in each reaction which thus can be measured with high accuracy.

The astrophysical implications of neutrino-nucleus interactions in the nuclear physics energy range is mainly connected with the new concept of ν-induced elemental synthesis in core-collapse supernovae. Nucleosynthesis in the overlying stellar burning shells of a supernova is induced by inelastic neutrino scattering exciting nuclei above their particle emission threshold. Neutrino scattering may be responsible for the production of most of the galactic abundances of ^{11}B, ^{19}F and various other elements, provided the neutrino interaction rates used in the model calculations are valid. Beam dump neutrinos emitted from the ISIS source are ideally suited to test these ideas, as they are the closest terrestrial analogon of core collapse neutrinos. An interesting example is the reaction $^{12}\mathrm{C}(\nu_e, \mathrm{e}^-)^{12}\mathrm{N}^*$, which, on the one side is contributing to the ν-nucleosynthesis of ^{11}B , and which, on the other side can be measured reliably with the KARMEN experiment, making this reaction a test case for the relative contribution of the socalled 'ν-process' to elemental synthesis [5].

5 The Charged Current Reaction $^{12}\mathrm{C}(\nu_e, \mathrm{e}^-)^{12}\mathrm{N}_{\mathrm{g.s.}}$

The signature of the exclusive charged current reaction $^{12}\mathrm{C}(\nu_e, \mathrm{e}^-)^{12}\mathrm{N}_{\mathrm{g.s.}}$

$$\begin{array}{rcl} \nu_e + {}^{12}\mathrm{C} & \rightarrow & {}^{12}\mathrm{N}_{\mathrm{g.s.}} + \mathrm{e}^- \\ & & \downarrow \\ & & {}^{12}\mathrm{C}_{\mathrm{g.s.}} + \mathrm{e}^+ + \nu_e \end{array}$$

is a position-correlated, delayed coincidence of an electron from the inverse β-decay on ^{12}C within the ν_e time window of $0.5 - 10.5\,\mu$s after beam-on-target and a positron from the subsequent β-decay of $^{12}\mathrm{N}_{\mathrm{g.s.}}$ within the following 36 ms [4]. The Q-value of the initial reaction is $Q = -17.3$ MeV. The ^{12}N-decay, characterized by its lifetime of $\tau = 15.9$ ms and end point energy of $E_0 = 16.3$ MeV, uniquely identifies ν-induced transitions to the ground state of ^{12}N.

After software cuts on time, energy, position-correlation and background subtraction 498.4 ± 22.7 events remain. A fit to the time distribution relative to beam-on-targeet of the electrons with a time constant of $\tau_{exp.} = (2.21 \pm 0.18)\,\mu$s(fig. 3(c)), clearly indicates that these events are due to neutrinos from μ^+-decay. Background contamination (15.7 events) is almost negligible due to the unambiguous signature. The cross section for the charged current reaction averaged over the incident ν_e energy distribution ($0 - 52.8$ MeV) is:

$$< \sigma_{CC}(\nu_e) >_{exp.} \quad = \quad (9.3 \pm 0.4_{(stat.)} \pm 0.8_{(syst.)}) \times 10^{-42} cm^2$$

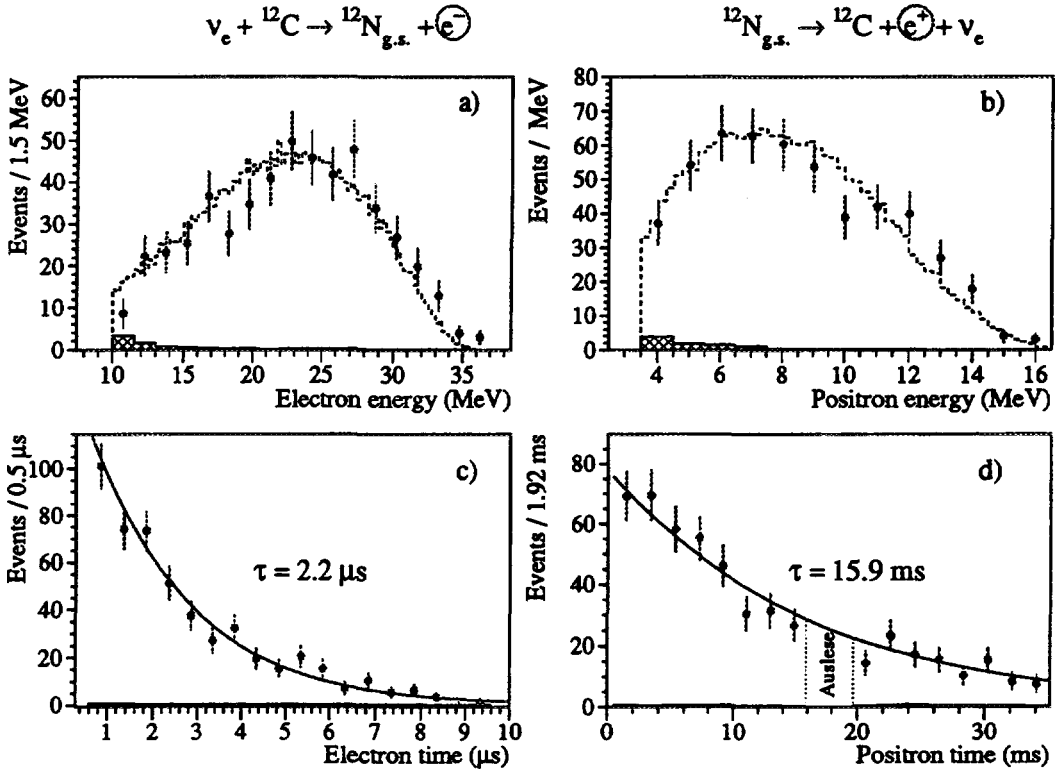

Figure 3: Energy and time distributions of the $^{12}C(\nu_e, e^-)^{12}N_{g.s.}$ reaction

in good agreement with theoretical predictions of $(8.0 - 9.4) \times 10^{-42}\,cm^2$.

The good calorimetric properties of the KARMEN detector also allowed for the first time a measurement of the energy dependence of the $^{12}C(\nu_e, e^-)^{12}N_{g.s.}$ cross section. As the recoil energy transferred to the ^{12}N nucleus is negligible, the neutrino energy E_ν is related to the electron kinetic energy E_{e^-} by $E_\nu = E_{e^-} + 17.3$ MeV. Thus a precise measurement of the electron kinetic energy determines the primary neutrino energy allowing the possibility of *neutrino spectroscopy*. The spectroscopic quality of the measured electron energy spectrum ensures a precise measurement of the spectral shape of ν_e emitted in μ^+-decay. Recently it has been shown that a precise determination of the ν_e shape parameter ω_L (the neutrino analogon to the famous Michel parameter ϱ) is sensitive to the Lorentz structure of muon decay. The experiment will therefore be able to set stringent upper limits on non V-A contributions in muon decay, especially to an interference amplitude of possible (non-standard model) scalar and tensor interactions in muon decay.

6 The Neutral Current Reaction $^{12}C(\nu,\nu')^{12}C^*(1^+,1)$

The neutral current reaction $^{12}C(\nu,\nu')^{12}C^*(1^+,1;15.1\,\mathrm{MeV})$, which has been observed for the first time in this experiment [3], can be induced by all three neutrino flavours present at ISIS. The signal for this excitation ^{12}C is the detection of 15.1 MeV gamma quanta from the decay of the excited $^{12}C^*(1^+,1)$ level. This level decays with a branching ratio of 96% via the emission of a single γ-ray back to the ground state, one therefore expects a clear peak structure around 15 MeV visible energy (fig. 4). The left part of figure 4 shows the energy distribution of neutrino

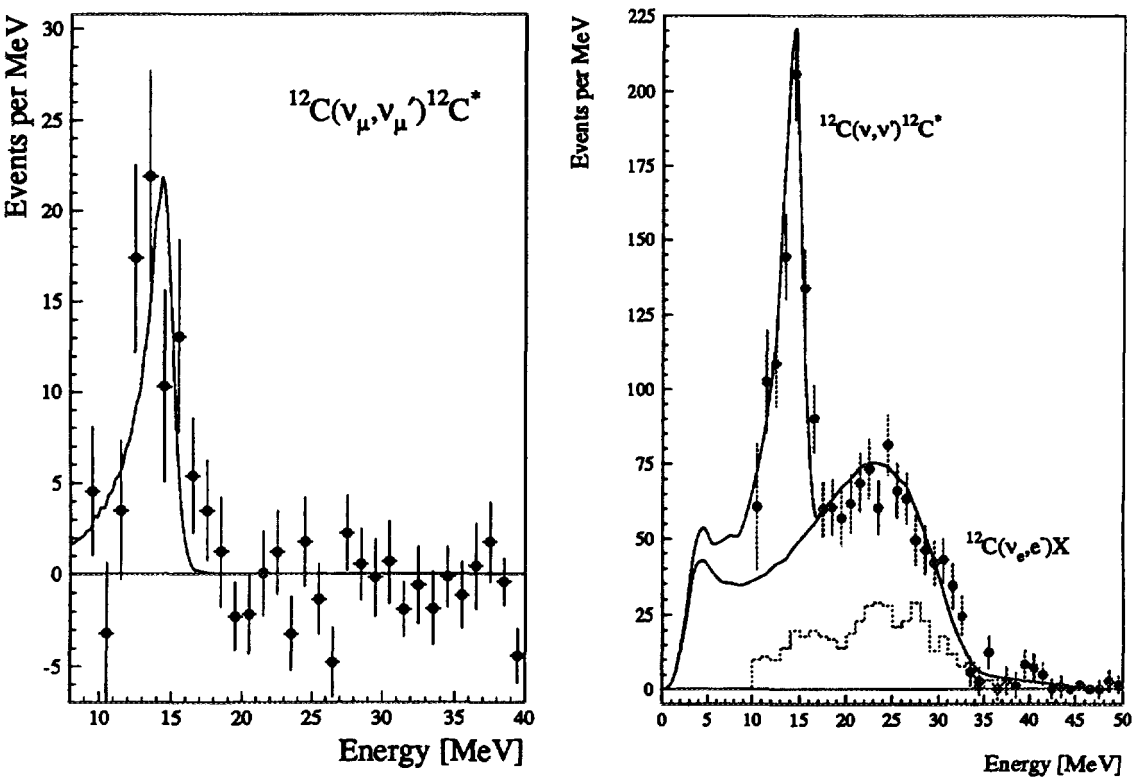

Figure 4: Visible energies of ν-induced single prong events, background subtracted.

induced events remaining after background subtraction in the narrow ν_μ-production time windows $0-100$ ns and $325-425$ ns after beam on target. Statistics for the ν_μ-induced excitation is still low due to the discrete ν_μ energy (29.8 MeV). Nevertheless the cross section for this reaction yields:

$$\sigma_{NC}(\nu_\mu)_{exp.} = (2.5 \pm 0.6_{(stat.)} \pm 0.4_{(syst.)}) \times 10^{-42} cm^2$$

with theoretical predictions of $(2.6-2.8) \times 10^{-42}\,\mathrm{cm}^2$ in good agreement.

The same data set as was used for the $^{12}C(\nu_e, e^-)^{12}N_{g.s.}$ reaction, has been scanned for neutral current events in the extended (ν_e, $\bar{\nu}_\mu$) time window from $0.6 - 90.6\,\mu s$. The energy distribution in the right part of figure 4 is the result of a likelihood analysis on the time distribution relative to beam-on-target of single prong events with an energy greater than 10 MeV, requiring a time signal of $2.2\,\mu s$ for excitations induced by the combined flux of ν_e and $\bar{\nu}_\mu$ and a time independent background. The energy spectrum clearly shows a peak due to the neutral current reaction $^{12}C(\nu, \nu')^{12}C^*(15.1\,MeV)$ in the range $11 - 16$ MeV. The broader underlying distribution has contributions from five reactions: neutrino-electron scattering and the inclusive charged current reactions $^{13}C(\nu_e, e^-)^{13}N$, $^{12}C(\nu_e, e^-)^{12}N_{g.s.}$, $^{12}C(\nu_e, e^-)^{12}N^*$ and $^{56}Fe(\nu_e, e^-)^{56}Co$. The cross section for the neutral current excitation of ^{12}C averaged over the energy spectra of ν_e and $\bar{\nu}_\mu$ is found to be

$$< \sigma_{NC}(\nu_e + \bar{\nu}_\mu) >_{exp.} = (10.9 \pm 0.8_{(stat.)} \pm 0.8_{(syst.)}) \times 10^{-42} cm^2$$

in good agreement with theoretical predictions of $(9.8 - 10.5) \times 10^{-42}\,cm^2$.

7 Search for $\nu_\mu \rightarrow \nu_e$ Oscillations

In the event of $\nu_\mu \rightarrow \nu_e$ oscillations, monoenergetic ν_e's would arise in the ν_μ time window after beam-on-target [7]. The detection reaction is $^{12}C(\nu_e, e^-)^{12}N_{g.s.}$ followed by the β–decay $^{12}N_{g.s.} \rightarrow {}^{12}C + e^+ + \nu_e$. One would therefore expect electrons with a peaked energy spectrum ($E_{e^-} = E_\nu - Q = 29.8 - 17.3 = 12.5$ MeV, see fig. 5a) within the two ν_μ time pulses (fig. 5b). The detection signature also contains the energy of the sequential spatially correlated e^+ (fig. 5c) which follows the e^- with the typical ^{12}N decay time (fig. 5d). The above measured number of CC reactions in the ν_e time window can be used to calculate the expectation of $\nu_\mu \rightarrow \nu_e$ induced CC reactions for $P_{\nu_\mu \rightarrow \nu_e} = 100\%$. Only the different detection efficiencies and the energy dependence of the cross section have to be taken into account to extract the ν-flux and cross section independent expectation of 187.8 oscillation signatures. Applying all cuts (e.g. $10 \leq E_{pr} \leq 14$ MeV; $0 \leq t_{pr} \leq 100$ ns or $325 \leq t_{pr} \leq 425$ ns) only 3 sequences are accepted within the data taken between July 1992 and December 1995. 0.45 ± 0.2 cosmic induced events contribute to the background which is dominated by the small contribution of ν_e's from μ^+–decay within the two 100 ns long ν_μ–time intervals after beam-on-target (1.76 ± 0.2). With a total background of $N_{bg} = 2.21 \pm 0.3$ events, there is no hint for $\nu_\mu \rightarrow \nu_e$ oscillations and an upper limit of the oscillation probability

$$P_{\nu_\mu \rightarrow \nu_e} < 4.8/187.8 = 2.6 \cdot 10^{-2} \qquad (90\%\,CL)$$

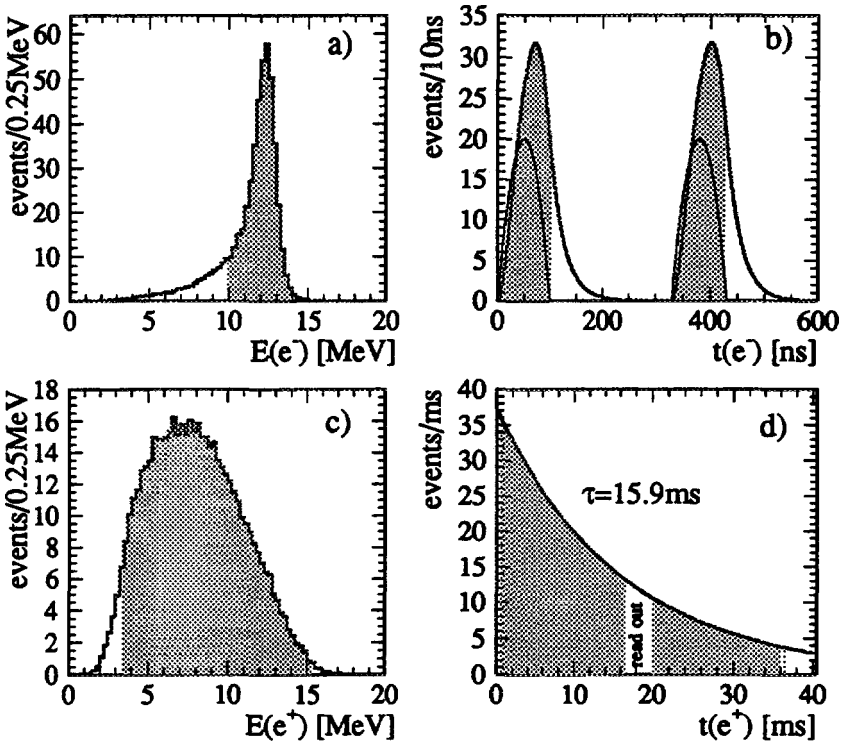

Figure 5: Expected signature for $\nu_\mu \rightarrow \nu_e$ full oscillation:
a) simulated MC energy of prompt event; b) proton pulses and time of prompt event relative to ISIS beam-on-target; c) MC energy of sequential event; d) time difference between prompt and sequential event; shaded areas show the allowed regions of evaluation cuts.

can be extracted following the PDG recommendations. Due to the normalization of the full oscillation expectation this result is very reliable. The background situation is very low so that the sensitivity for this oscillation channel is mainly limited by the relatively small expectation value for full oscillation, i.e. statistics.

8 Search for $\nu_e \rightarrow \nu_x$ Oscillations

The number of sequential events from the CC reaction $^{12}C(\nu_e, e^-)^{12}N_{g.s.}$ with subsequent ^{12}N-decay described in section 2.2 will be decreased in case of $\nu_e \rightarrow \nu_x$, $\nu_x = \nu_\mu, \nu_\tau$ whereas NC reactions $^{12}C(\nu, \nu')^{12}C^*(15.1\ \mathrm{MeV})$ which are also detected with KARMEN remain unchanged. Therefore the ratio of the extracted cross sections $R_{exp} = \frac{\langle\sigma\rangle_{NC(\nu_e+\bar{\nu}_\mu+\nu_\tau)}}{\langle\sigma\rangle_{CC(\nu_e)}} = 1.17 \pm 0.11$ should be increased with $\nu_e \rightarrow \nu_x$. A conservative comparison with theoretical predictions of $R_{theo} = 1.08 \pm 0.02$ doesn't show a statistical significant higher value so that an upper limit of the oscillation probability $P_{\nu_e \rightarrow \nu_x} < 0.197$ ($90\%\,CL$) can be deduced. This limit is nearly inde-

pendent on flux calculations or uncertainties of the theoretical cross section because only their ratios are used [8].

Due to the energy dependence of the oscillation probability not only a reduction of the event rate but also a distortion of the energy spectrum of the prompt e^- and its spatial distribution results from $\nu_e \rightarrow \nu_x$. With the good detector resolution in energy and space, a shape analysis provides even more stringent upper limits for $sin^2(2\Theta)$ in the energy-space sensitive range of $\Delta m^2 = 3 \ldots 30\,\mathrm{eV}^2$ (see fig. 9).

9 Search for $\bar{\nu}_\mu \rightarrow \bar{\nu}_e$ Oscillations

Apart from a small contamination ($\bar{\nu}_e/\nu_e < 6 \cdot 10^{-4}$), $\bar{\nu}_e$'s are not produced in the ISIS target. The detection of $\bar{\nu}_e$'s would therefore indicate oscillations $\bar{\nu}_\mu \rightarrow \bar{\nu}_e$ in the appearance channel. The signature for the detection of $\bar{\nu}_e$'s is a spatially correlated delayed coincidence of positrons from $\mathrm{p}(\bar{\nu}_e, \mathrm{e}^+)\mathrm{n}$ with energies up to $E_{e^+} = E_{\bar{\nu}_e} - Q = 52.8 - 1.8 = 51\,\mathrm{MeV}$ (fig. 6b) and γ emission of either of the two neutron capture processes $\mathrm{p}(\mathrm{n},\gamma)\mathrm{d}$ or $\mathrm{Gd}(\mathrm{n},\gamma)\mathrm{Gd}$ with γ energies of 2.2 MeV or up to 8 MeV, respectively (fig. 6d). The positrons are expected in a time window of 0.5 to 10.5 μs after beam-on-target (fig. 6a). The neutrons from $\mathrm{p}(\bar{\nu}_e, \mathrm{e}^+)\mathrm{n}$ are thermalized and captured typically within $\tau = 120\,\mu\mathrm{s}$ (fig. 6c). The neutron detection efficiency for the analyzed data is 23.8%. The data set remaining after applying all cuts in energy, time and spatial correlation is shown in fig. 7. A prebeam analysis of cosmic ray induced sequences results in an accumulated background level of 11.0 ± 0.2 events per μs in the prompt 10 μs–window (see fig. 7a). The actual rate is $14.7 \pm 1.2/\mu\mathrm{s}$ which corresponds to a beam excess of $2.3\,\sigma$ compared with the prebeam level including ν_e induced CC (8 events) and $\bar{\nu}_e$ contamination (1.1 events). Although the secondary part of the sequences shows the typical signature of thermal neutron capture, the prompt time and energy distribution does not follow the expectation from $\bar{\nu}_\mu \rightarrow \bar{\nu}_e$ oscillation with $\Delta m^2 = 100\,\mathrm{eV}^2$.

To extract a possible small contribution of $\bar{\nu}_\mu \rightarrow \bar{\nu}_e$, the data set is scanned with a two-dimensional maximum likelihood analysis on time and energy distribution of the positrons requiring a 2.2 μs exponential time constant for the e^+ and a time independent cosmic induced background. The measurement of the e^+ energy with spectroscopic quality is highly sensitive to changes in the energy spectrum due to the dependence of the oscillation probability on the mass term Δm^2 (see fig. 8a). The energy distributions of the positrons used in the likelihood analysis therefore have been tested with spectra for Δm^2 in the range from 0.01 to $100\,\mathrm{eV}^2$. The results of this maximum likelihood analysis are shown in fig. 8b.

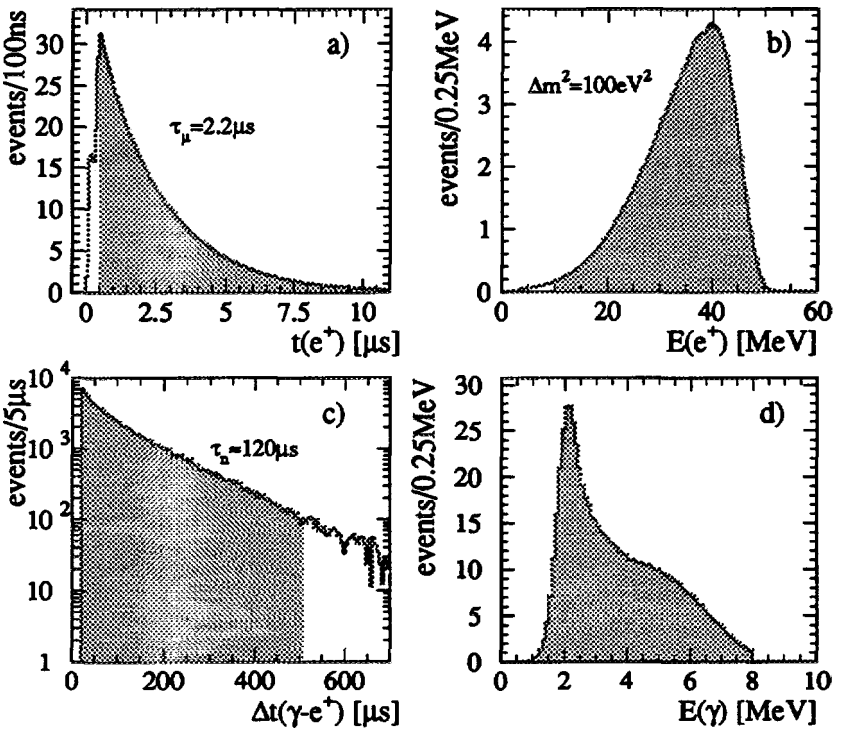

Figure 6: Expected signature for $\bar{\nu}_\mu \rightarrow \bar{\nu}_e$ full oscillation:
a) time of prompt event relative to ISIS beam-on-target; b) MC energy of prompt positron for $\Delta m^2 = 100\,\mathrm{eV}^2$; c) time difference between prompt e^+ and sequential γ's; d) energy of sequential γ's; shaded areas are accepted by evaluation cuts.

Over the entire parameter range of Δm^2 investigated there is no evidence for oscillations resulting in a $90\%\,CL$ upper limit for a possible oscillation signal of 10 to 14 events, depending on Δm^2. This confirms that the beam excess has no oscillation signature in time and energy of the prompt events. Our result can be compared with an expected signal of 6 to up to more than 40 events based on a recently published oscillation probability of $P_{\bar{\nu}_\mu \rightarrow \bar{\nu}_e} = 0.0034$ by LSND [9]. For large Δm^2 we expect at KARMEN 1547 detected oscillation events for full oscillation which results in an upper limit of the mixing angle

$$sin^2(2\Theta) < 11.6/1547 = 7.5 \cdot 10^{-3} \quad \text{for large } \Delta m^2 \qquad (90\%\,CL\,).$$

Fig. 9 shows the KARMEN exclusion curves in the parameter space of Δm^2 and $sin^2(2\Theta)$ in a two neutrino flavor oscillation calculation for the appearance channels $\nu_\mu \rightarrow \nu_e$ and $\bar{\nu}_\mu \rightarrow \bar{\nu}_e$ in comparison with some other results of ν–oscillation searches at accelerators and reactors.

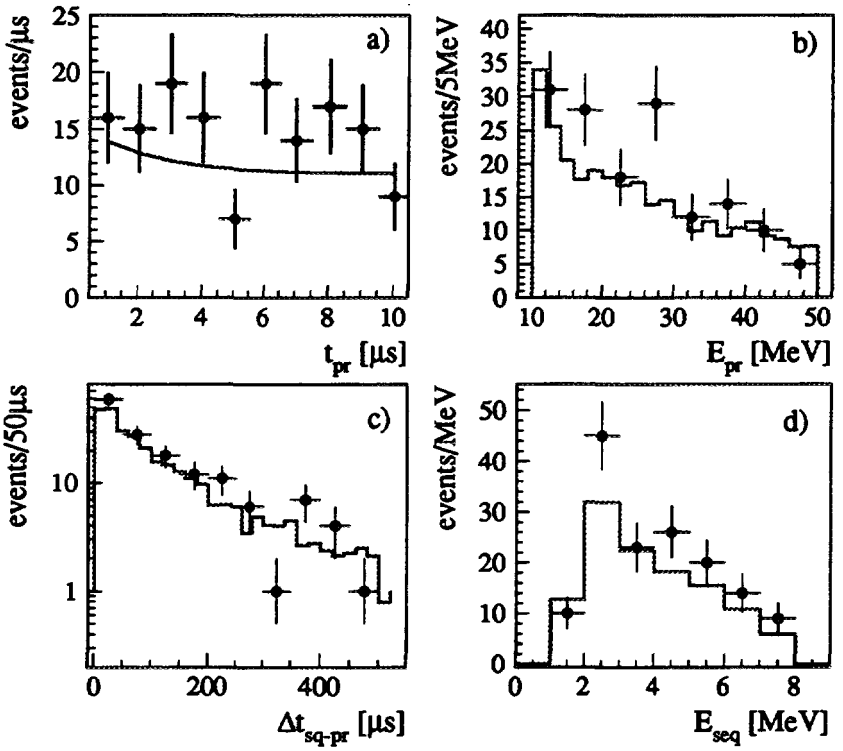

Figure 7: Time (a,c) and energy (b,d) distribution of reduced sequences; lines and histograms represent the pre-beam background (11.0 events per μs) plus ν_e-induced CC events and $\bar{\nu}_e$-contamination.

10 KARMEN Upgrade

Whereas the sensitivity for $\nu_\mu \rightarrow \nu_e$ oscillations is essentially limited by statistics, the KARMEN sensitivity in the $\bar{\nu}_\mu \rightarrow \bar{\nu}_e$ channel can be dramatically increased by the reduction of the small but dominant cosmogenic background (see fig. 7). Detailed investigations and MC simulations showed that this background is induced by cosmic muons being stopped or undergoing inelastic scattering in the iron blockhouse which surrounds the KARMEN detector and veto system. Energetic neutrons emitted in these processes can penetrate deeply into the detector without triggering the veto system, thus producing an event sequence of prompt recoil protons followed by the capture of the then thermalized neutrons. To mark the original muons in the vicinity of the detector, a further active veto layer within the blockhouse, 1 m away from the existing shield, is being built since the beginning of 1996 [10]. All sides of the detector will be covered by plastic scintillator bars with an overall surface of 300 m^2. This new veto system will reduce the cosmogenic sequential background by a factor of 40.

In addition to this veto system, an increase of the neutron detection efficiency

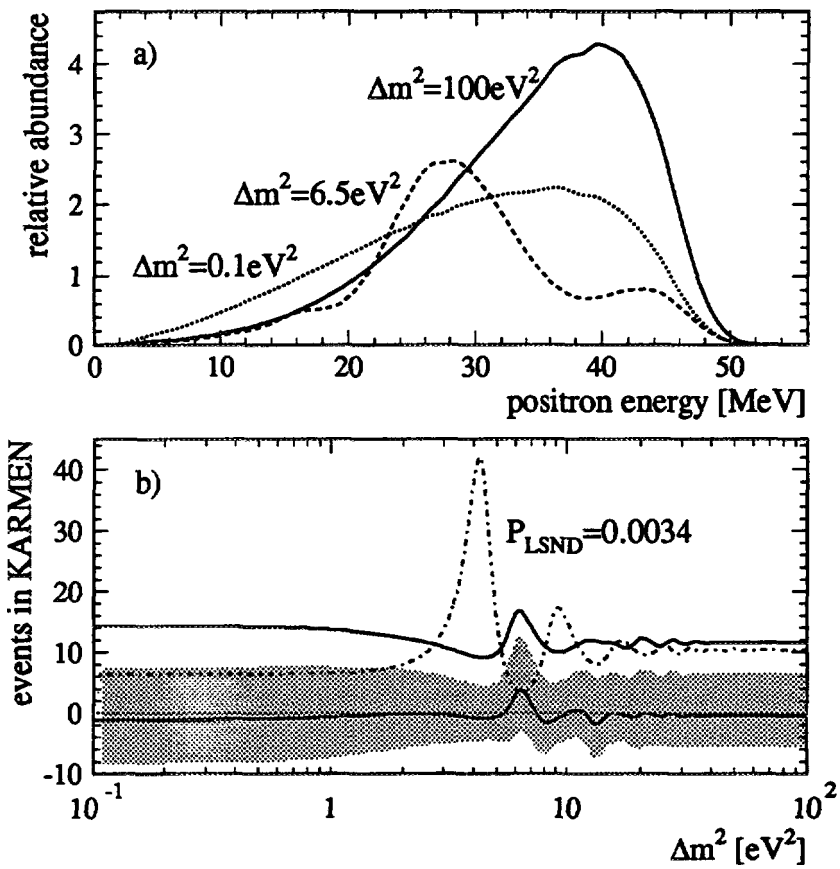

Figure 8: a) Examples of expected e^+–spectra (visible energy including detector response) for different oscillation parameters Δm^2; b) likelihood-fit results depending on Δm^2; the shaded area represents the 1σ–error band around the best fit values for $\Delta m^2 = 0.01 \ldots 100\,\mathrm{eV}^2$; the solid line above the shaded band shows the 90% CL upper limit from KARMEN, the broken line the expected event numbers in KARMEN based on the LSND oscillation evidence.

as well as improvements of the trigger system are envisaged. After two years of further measuring time, the KARMEN sensitivity for $\bar{\nu}_\mu \rightarrow \bar{\nu}_e$ is expected to cover the whole parameter region of evidence suggested by LSND. Fig. 9 also shows the expected exclusion curve from the upgraded KARMEN experiment if no oscillation signal will be found. The veto upgrade will also increase the signal to background ratio in the investigation of the recently published anomaly in the time distribution of ν–induced single prong events.

The KARMEN experiment has found no positive evidence for ν–oscillations in neither of the investigated channels $\nu_\mu \rightarrow \nu_e$ and $\bar{\nu}_\mu \rightarrow \bar{\nu}_e$ or $\nu_e \rightarrow \nu_x$. The upper limit for $\nu_\mu \rightarrow \nu_e$ is very reliable due to the spectroscopic measurement of the ν_e–flux from μ^+–decay at ISIS and the nearly background–free $^{12}\mathrm{C}\,(\nu_e, \mathrm{e}^-)\,^{12}\mathrm{N}_{\mathrm{g.s.}}$ detection re-

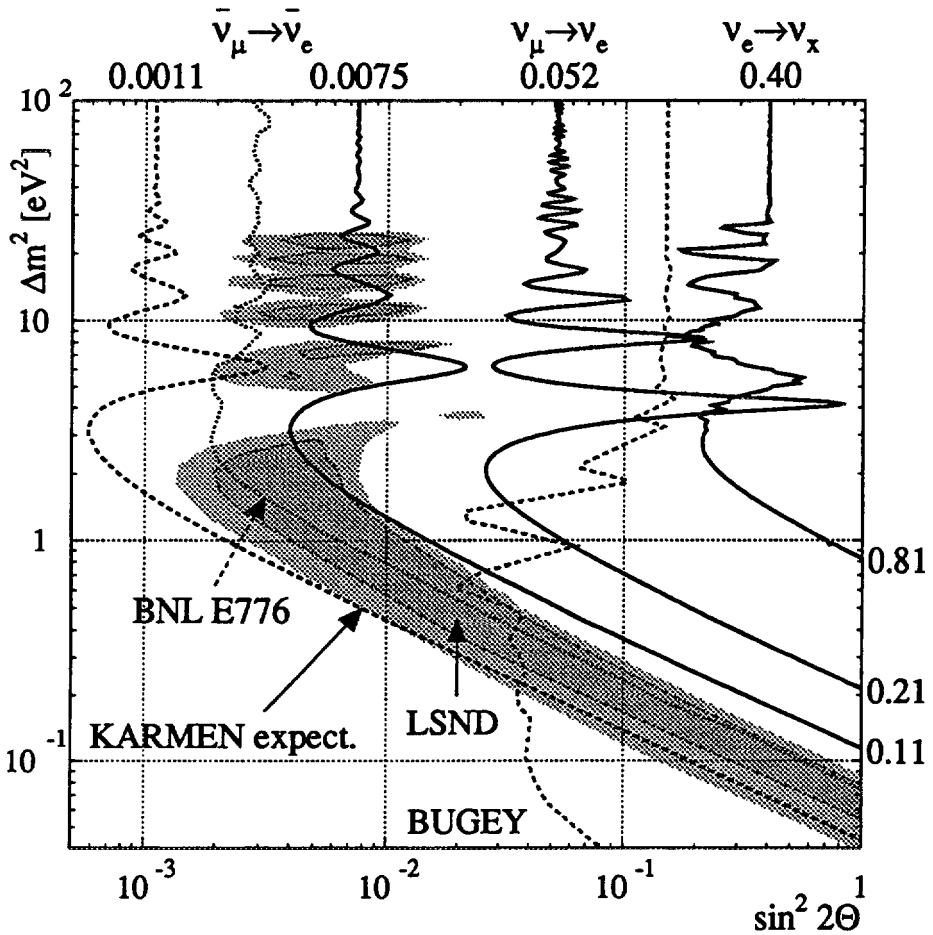

Figure 9: 90% CL exclusion curves and limits for $\Delta m^2 = 100\,\mathrm{eV}^2$, $sin^2(2\Theta) = 1$ from KARMEN for $\nu_\mu \to \nu_e$, $\bar{\nu}_\mu \to \bar{\nu}_e$ and $\nu_e \to \nu_x$ as well as the expected sensitivity for $\bar{\nu}_\mu \to \bar{\nu}_e$ after the upgrade; oscillation limits from BNL E776 and Bugey; LSND evidence is shown as shaded areas (90% CL and 99% CL areas respectively).

action. The sensitivity of the search for $\bar{\nu}_\mu \to \bar{\nu}_e$ is actually limited by cosmogenic background, but will be increased substantially by the current upgrade of the experiment. A sensitivity of $sin^2(2\Theta) \approx 1 \cdot 10^{-3}$ for large Δm^2 will be reached by the end of 1998.

Acknowledgement

This work was supported, in part, by the Bundesministerium für Bildung, Wissenschaft, Forschung und Technologie.

References

[1] B. Zeitnitz, *Prog. Part. and Nucl. Physics* **13** (1985) 445.

[2] G. Drexlin et al., *Nucl. Instr. Meth.* **A 289** 490-495 (1990).

[3] B. Bodmann et al., *Phys. Lett.* **B 267** 321-324 (1991).

[4] B. Bodmann et al., *Phys. Lett.* **B 280** 198-203 (1992).

[5] S. E. Woosley et al., *Astrophys. J.* **356** 272-301 (1990).

[6] B. Zeitnitz, *Prog. Part. Nucl. Phys.* **32** (1994) 351.

[7] G. Drexlin, *Prog. Part. Nucl. Phys.* **32** (1994) 375.

[8] K. Eitel et al., *Proc. of the XIIIth Rencontres de Blois*, June,8-12 1996, to be published

[9] C. Athanassopoulos et al., *Phys. Rev. Letters* **75** (1995) 2650.
C. Athanassopoulos et al., *Phys. Rev. Letters* **77**, (1996) 3082.

[10] G. Drexlin, B. Zeitnitz *Proposal for an Upgrade of the KARMEN Veto System*, Internal KARMEN Report

Search for a neutral particle of mass 33.9 MeV in pion decay

M. Daum, PSI, Paul-Scherrer-Institut, CH-5232 Villigen-PSI, Switzerland.

Abstract

We have measured the muon momentum distribution in charged pion decay in flight in order to search for a small branching fraction η of pion decays $\pi^+ \to \mu^+ + X$, in which a heavy neutral particle X with a mass of 33.9 MeV would be emitted. Such a particle was postulated by the KARMEN collaboration as a possible explanation for an anomaly in their time-of-flight spectrum. In a first experiment we found an upper limit of $\eta \leq 2.6 \cdot 10^{-8}$ at a confidence level of 95 %.

Introduction

Recently an anomaly in the time distribution of neutrinos from a pulsed beam-stop source was reported by the KARMEN collaboration [1], with a speculative explanation that these events could originate from a rare pion decay process,

$$\pi^+ \to \mu^+ + X, \tag{1}$$

where X is a heavy neutral particle with a mass of 33.9 MeV. The KARMEN collaboration estimated values of the branching fraction of this decay mode down to $2 \cdot 10^{-16}$, depending on the lifetime τ_X of such a particle. Barger et al. [2] pointed out that part of this range can be excluded by consideration of other experiments. They determined the allowed range for the branching fraction to be between $6 \cdot 10^{-5}$ and $3 \cdot 10^{-8}$. A few weeks later they corrected part of their earlier findings concerning mainly the X-particle as an isosinglet (sterile) neutrino to include neutral current contributions in addition to the charged current ones [3]. For this special case, i.e. if the X-neutrino is mainly isosinglet (sterile), the branching fraction may be as low as about 10^{-13}.

Very recently, Choudhury and Sarkar[4] considered the hypothesis that the KARMEN anomaly is due to the production of a light photino (or Zino) which decays radiatively. In this case the branching fraction of the decay (1) would be larger than about $6 \cdot 10^{-9}$.

Kinematics of pion decay

According to Ref. [1] the flight time of the hypothetical X-particles for a path of 17.5 m is $(3.60 \pm 0.25)\,\mu$s. This, together with the pion and muon masses of Ref. [5], corresponds to a rest mass of

$$m_X = 33.9057 \pm 0.0009\,\text{MeV}, \tag{2}$$

which is very close to the mass difference between the charged pion and the muon, $m_{\pi+} - m_{\mu+} = 33.91157 \pm 0.00067$ MeV. Because of the small muon kinetic energy from such a decay mode, these particles could not have been detected in heavy neutrino searches with pions decaying at rest [6]. However, for the decay in flight, the small Q-value has several advantages: firstly, the velocity of the muon is very close to the velocity of the original pion ($p_\mu \approx p_\pi \cdot m_\mu / m_\pi$), secondly, the flight direction of the muon differs only slightly from that of the pion, and thirdly, the specific energy loss of the muon is almost the same as that of its parent pion. This enables one to use the beam-line itself as a spectrometer to separate the decay muons from other particles as well as muons originating from the main π^+-decay mode. An added advantage is that pions themselves can be used to set up counter thresholds and timing in order to calibrate the system for optimal detection of muons from the decay (1).

Experimental investigations

In 1995 two measurement of the momentum spectrum of muons from π^+-decay in flight were performed at PSI. Bilger et al. [7] used the decay in flight, and the Low Energy Pion Spectrometer (LEPS) with a momentum resolution of $\Delta p/p$=0.1 % and an angular acceptance of 150 mrad and found an upper limit for the decay (1) of $7 \cdot 10^{-8}$ with 95 % confidence. In our experiment [8] we used the high intensity pion-channel πE1 at PSI, together with a scintillator hodoscope. As a result the hypothesis of a heavy neutrino could not be confirmed but an upper level of $2.6 \cdot 10^{-8}$ with 95 % confidence was set.

The pion beam

In our set-up we took advantage of the fact that a "quadrupole channel", i.e. a beam-line consisting of dipoles and quadrupoles only, accepts muons preferably in the forward or backward direction in the pion center-of-mass system. The momenta of these muons differ strongly from those of the decay (1), whereas the muons from the main decay mode which are emitted sideways are suppressed because of the limited angular acceptance of the beam-line. The lay-out of the experiment is shown in Fig. 1.

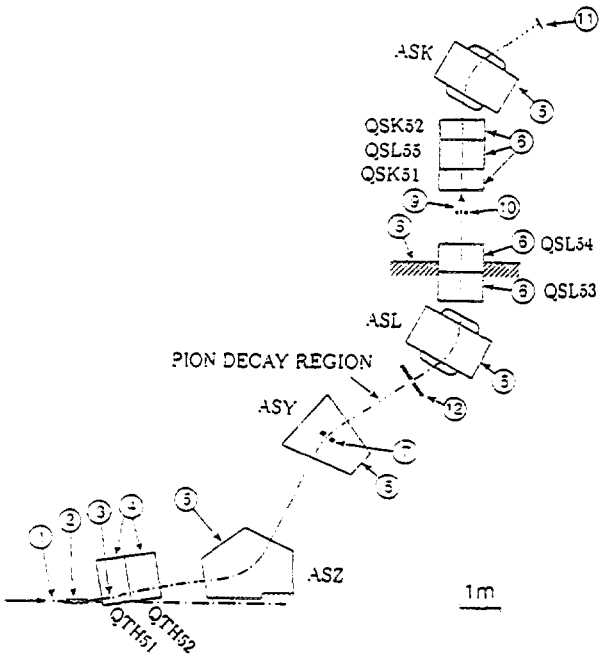

Figure 1:
Experimental set-up. 1) central trajectory of 590 MeV proton beam; 2) pion production target (graphite, not to scale); 3) central trajectory of pion beam; 4) half-quadrupole magnets; 5) dipole magnets; 6) quadrupole magnets; 7) collimator defining the beam momentum acceptance; 8) concrete shield of proton channel; 9) scintillation counters S0, S1; 10) lead collimator; 11) scintillation counter hodoscope; 12) acceptance limiting collimator.

The beam-line consists of three parts: (i) The first part from the pion production target to the dipole magnet ASY, used to transmit the π^+. (ii) The pion decay region between the dipole magnets ASY and ASL. (iii) The muon transmitting and analyzing part from the dipole magnet ASL to the hodoscope.

Positive pions of 120.0 MeV/c with a momentum spread of 1.5 % (fwhm), defined by the collimator opening at the dispersive focus in the dipole magnet ASY, were used (Fig. 1). The momentum choice was governed by the need for a good particle (positrons, muons, pions) separation in time-of-flight at the point of detection. About 1/3 of the pions entering the decay region between the two dipole magnets ASY and ASL (cf. Fig 1.) decay in it. By tuning the whole beam-line to pions of 120.0 MeV/c a measured intensity of $1 \cdot 10^7$ π^+/s at a primary proton current of 1 mA was achieved at the initial point of detection (pt. 9, Fig. 1).

At a pion momentum of 120.0 MeV/c and a momentum spread of 1.5 % (fwhm) muons from the decay of Eq. (1) have a momentum distribution centered at 90.8 MeV/c with a width of 1.8 MeV/c (fwhm). Their emission angle with respect to the pion in the laboratory system is $0 \leq \theta \leq 6$ mrad whereas muons of about 90.8 MeV/c from normal pion decay have a decay angle close to the maximum of 334 mrad.

During the data-taking the first part of the beam-line up to the decay region was tuned to 120.0 MeV/c, with the quadrupole doublet (QTH51, QTH52) set to focus pions onto the momentum defining slit at the center of dipole ASY. The last part of the beam-line after the decay region

was set to momenta around 91 MeV/c (see below). The quadrupole doublet (QSL53, QSL54) was set to focus muons from the decay (1) onto a counter telescope (S0, S1) (items 9 and 10, Fig. 1).

The particles downstream of the telescope passed a spectrometer consisting of three quadrupoles and a dipole magnet with a deflection angle of 50^0 and a dispersion of 2 cm/%. A hodoscope placed at the end of the beam-line and consisting of 10 plastic scintillation counters, each 3 cm wide, 17 cm high and 5 mm thick, was used for the momentum analysis.

Time-of-flight distributions

The time-of-flight separation of the particles was checked by tuning the whole beam-line to 120.0 MeV/c. The positrons, muons and pions from the production target to the telescope (S0, S1) take respectively 53, 71 and 81 ns, and can be clearly separated using the 50 MHz radio-frequency of the accelerator (see Fig. 2a).

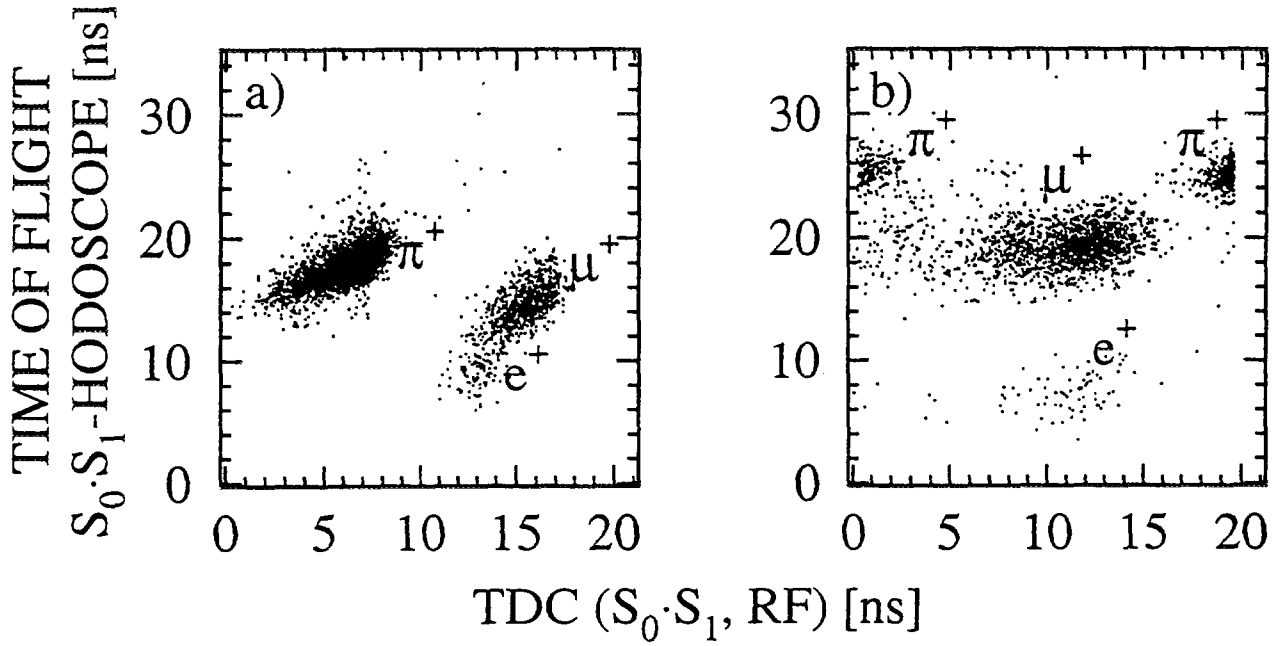

Figure 2:
a) Two-dimensional event distribution. All beam elements are set for 120.0 MeV/c. Horizontal axis: time-of-flight of the particles in the beam-line from the pion production target to the scintillation counters S0 and S1. Start signal is the coincidence S0·S1, stop signal is RF, the 50 MHz radio-frequency signal of the cyclotron. Time increases to the left. The absolute flight times are 53, 71 and 81 ns for positrons, muons and pions, respectively. Vertical axis: time-of-flight of the particles from the start counters S0 and S1 to one of the central hodoscope counters. Muons from the decay mode of Eq. (1) are expected to appear in the pion region of this plot when the second part of the beam-line is set to momenta around 91 MeV/c.
b) As Fig. 2a). Here the first part of the beam is set to 120.0 MeV/c and the second part to 91.0 MeV/c.

The corresponding distributions of the observed particles in which the beam-line from ASL to the hodoscope was set to a momentum of 91.0 MeV/c, corresponding to a the search for the X-particles, are displayed in Fig. 2b. There are three separate distributions which can be attributed to pions, muons, and positrons, respectively. Events around 0 to 2 and 18 to 20 ns on the horizontal and 24 to 27 ns on the vertical scale originate from pions, which fly with a momentum of 120.0 MeV/c from the target to the momentum slit in ASY. There they undergo slit scattering, lose about 29 MeV/c and follow the beam-line up to the hodoscope. Scattered positrons are found around 13 ns (horizontal scale) and 8 ns (vertical scale).

Muons appear between 15 and 23 ns on the vertical scale. Events between 10 and 15 ns on the horizontal scale can be attributed to muons which originate from pion decays in the vicinity of the

pion production target (cloud muons) and move with a momentum of about 120 MeV/c along the first part of the beam-line. Again at the momentum slit they are scattered, so that they continue with about 91 MeV/c and are accepted by the second part of the beam-line. All these events can be clearly separated by time cuts from candidate X-events. The candidates are expected to show up in the muon band (vertical scale 15 to 23 ns) on the horizontal scale between 5 and 8 ns, i.e. approximately in those channels in which pions show up in Fig. 2a. Moreover, X-candidates should produce a peak in the hodoscope counters.

Interpretation of the data

In order to search for such a peak we scanned the beam momentum in the second part of the beam-line, i.e. from ASL onwards. One scan consisted of 17 runs corresponding to the 17 momentum settings between 87.0 and 95.0 MeV/c in steps of 0.5 MeV/c. In total, we performed 7 such scans. As a normalization monitor we used the "proton signal" of the accelerator, a monitor proportional to the proton beam intensity. A run consisted of registering events for 1000 seconds at 1 mA of proton beam.

A peak produced by the hypothetical decay (1) would shift systematically with the hodoscope counter number. The position and the shape of such a peak were predicted from scans with pions and "cloud muons". In these scans the first part of the beam-line was set to 120.0 MeV/c for pions and to 90.8 MeV/c for muons, respectively. The second part was then scanned for pions between 118.0 and 122.0 MeV/c and for muons between 88.0 and 93.0 MeV/c in steps of 0.5 MeV/c.

The summed candidate X-muon events of all scans in one of the central hodoscope counters are displayed in Fig. 3. In our data, no peak is visible. As a study with DECAY TURTLE showed, the events in Fig. 3 are consistent, within fairly large uncertainties, with being due to muons which were emitted by pions in the decay region and were scattered at the apertures of the beam-line elements, mainly at the acceptance limiting collimator (item 12, Fig. 1).

From the scans with pions and cloud muons we know that in the hodoscope counters 1, 2, 9, and 10 only very few X-muon candidates can appear. We used the momentum scans of these hodoscope counters for the estimation of the background and found a hyperbola as the best fitting function. Such hyperbolas were also fitted to the data of the hodoscope counters 3 to 8 together with a distribution for the hypothetical X-muon candidates.

The height of the distribution predicted for an assumed branching fraction of 10^{-7} was multiplied by a parameter α which was varied in steps of 0.1 between -1 and +1. For each value of α the data were fitted by the hyperbola plus the expected distribution for muons from the decay (1), with five free parameters and typically 11 degrees of freedom.

Experimental results

The summed χ^2 of all scans for the hodoscope counters 3 to 8 is displayed in Fig. 4. From the parabola fitted to the χ^2-distribution of Fig. 4, we find the branching fraction to be

$$\eta = \frac{\Gamma(\pi^+ \to \mu^+ + X)}{\Gamma(\pi^+ \to \mu^+ + \nu_\mu)} = (-0.40 \pm 0.23) \cdot 10^{-7}; \tag{3}$$

the uncertainty corresponds to one standard deviation. From this, using the "Bayesian approach" described in Ref. [5] (probability function is set to zero for negative, i.e. unphysical values of η) we find an upper limit of

$$\eta \leq 2.6 \cdot 10^{-8} \text{ (c.l. } = 95\,\%). \tag{4}$$

This value is lower than the upper limit of $7 \cdot 10^{-8}$ (c.l. $= 95\,\%$) found by Bilger et al. [7] who had a significantly smaller total number of useful pions.

Outlook

Due to the lack of an appropriate vaccum system and the background from slit scatterring the experiment can be improved considerably and a measurement with an optimized set-up will result in a

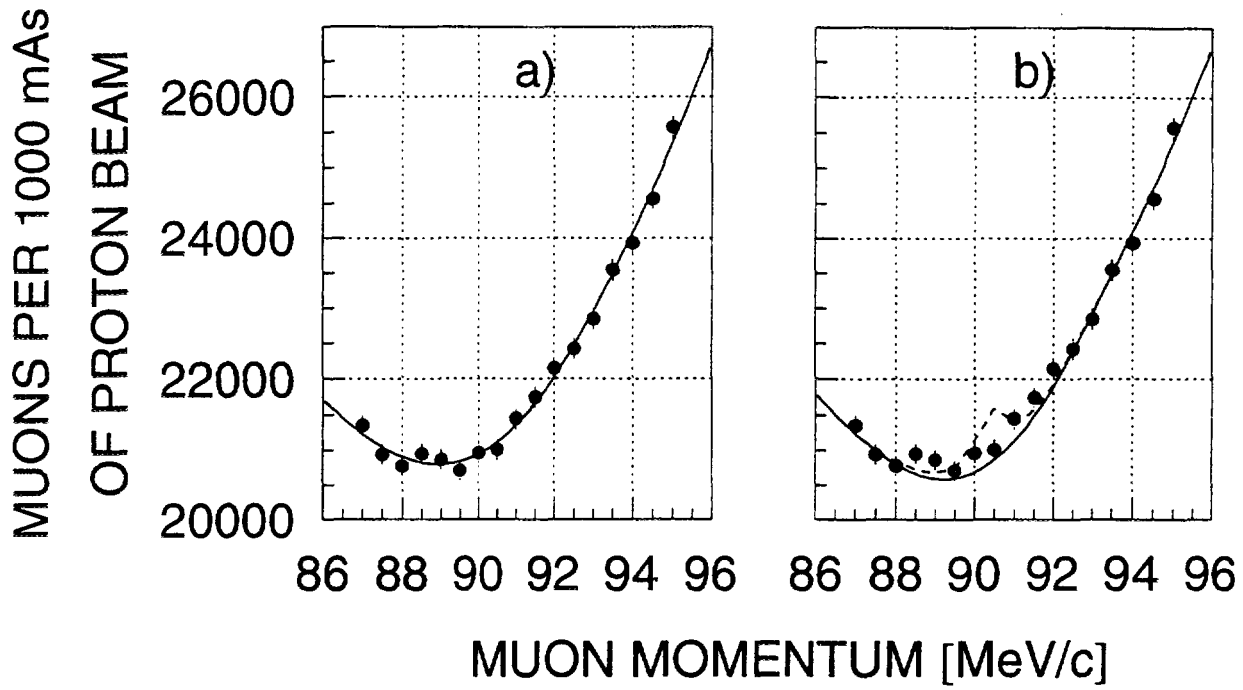

Figure 3:
Muon events in one of the central hodoscope counters. The uncertainties are about equal to the size of the dots.
a) The curve is a hyperbola fitted to the points from momenta 87.0 to 95.0 MeV/c; the χ^2 is 10.0 for 12 degrees of freedom.
b) Here the dashed curve is a fit of a hyperbola plus a peak from the hypothetical decay $\pi^+ \to \mu^+ + X$ with a branching fraction of $2{\cdot}10^{-7}$; the χ^2 of the fit is 31.3 for 12 degrees of freedom. The solid curve is the hyperbola without the additional peak.

much higher sensitivity. The main difference is that the decay region starts behind the dipole magnet ASL1, i.e. when the phase space of the beam is well defined and where we have no passive collimators close to the cental trajectory of the beam. In this way we avoid the background from slit scattering at openings very close to the beam emittance. From studies with the computer program TURTLE [9] it was found that these scattered particles were the reason for most of the background in the old experiment (see discussion of Fig. 2b above).

With these improvements we should be able to reach the level of background originating from the radiative pion decay $\pi^+ \to \mu^+ + \nu_\mu + \gamma$, which is of the order of 10^{-10} in the momentum range of interest. The distribution of the background from radiative decay should be, however, flat, i.e. it should not show any significant peak structure around $p_\mu \approx p_\pi \cdot m_\mu/m_\pi$.

References

[1] KARMEN collaboration, B. Armbruster et al., Phys. Lett. B 348 (1995) 19.

[2] V. Barger et al., Phys. Lett. B 352 (1995) 365.

[3] V. Barger et al., Phys. Lett. B 356 (1995) 617.

[4] D. Choudhury and S. Sarkar, Phys. Lett. B 374 (1996) 87.

[5] Particle Data Group, Phys. Rev. D50 (1994) 1280.

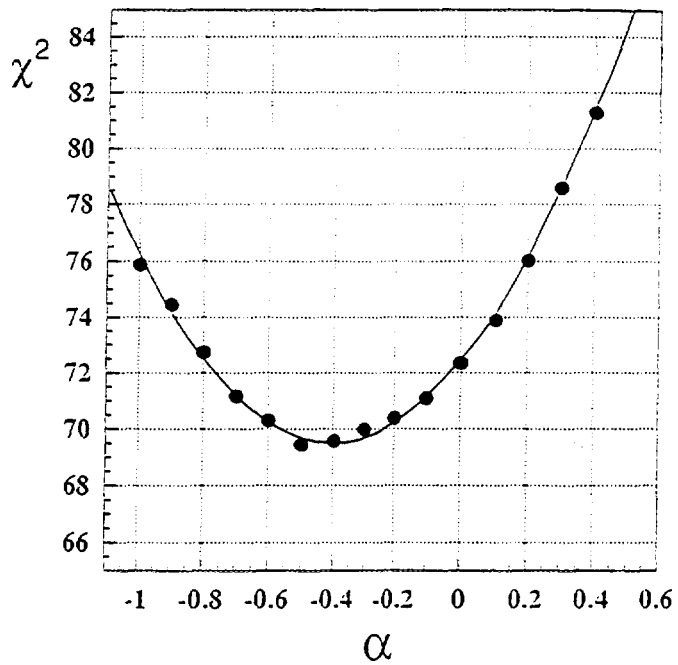

Figure 4:
χ^2 for the summed momentum scans of the hodoscope counters 3 to 8, as a function of $\alpha \equiv \eta/10^{-7}$, where η is the assumed branching fraction for the decay (1). The total number of degrees of freedom is 66. The solid curve is a parabola fitted to the data points.

[6] M. Daum et al., Phys. Rev. D36 (1987) 2624, and
R. Abela et al., Phys. Lett. B 105 (1981) 263.

[7] R. Bilger et al., Phys. Lett. B 363 (1995) 41.

[8] M. Daum et al., Phys. Lett. B 361 (1995) 179.

[9] K. L. Brown and Ch. Iselin, CERN report 74-2 (1974).

Direct Measurements of Neutrino Masses

E. Holzschuh

Physik-Institut der Universität Zürich, CH-8057 Zürich

1. Introduction

In this lecture I discussed direct measurements of the masses of the three known neutrinos. With 'direct' I mean the analysis of the kinematics of suitable decays. There are other types of experiments which are sensitive to effects of non-zero neutrino masses. Double beta decay has been discussed by J. Busto and oscillation experiments by L. Camilleri at this school. A general review of the status of the neutrino mass is given in [1] which contains also many references. For reviews about the tritium experiments I refer to the references [2, 3]

In the next two sections I briefly review recent measurements of the tau and the muon neutrino mass. The main part of the lecture was devoted to the tritium experiments and is presented in section 4.

2. The τ–Neutrino Mass

Tau leptons are produced in pairs at $e^+ e^-$ storage rings. Recent results have been reported by the ARGUS collaboration at DESY [4], by the CLEO collaboration at Cornell [5], and by the ALEPH collaboration at CERN [6]. Events are selected where one tau from the produced pair makes a simple decay, e.g.

$$\tau^+ \longrightarrow e^+ \, \nu_e \, \overline{\nu}_\tau \quad \text{or} \quad \mu^+ \, \nu_\mu \, \overline{\nu}_\tau$$

and the other tau decays into many pions, i.e.

$$\tau^- \longrightarrow n \, \pi^{+,-,0} \; \nu_\tau,$$

where n is 5 or 6. Such events are very rare when compared with decays into three pions. The idea is to convert as much decay energy into restmass as possible. In that way the sensitivity to the restmass of the ν_τ is maximized.

The measured quantities used in the analysis are the beam energy, the mass of the tau m_τ, and energies E_i and momenta $\vec{p}_i$ of the n pions. Using 4–momentum conservation

$$p_\tau = \sum_i p_i + p_\nu$$

the invariant mass of the pions can be related to the mass of the tau-neutrino.

$$\begin{aligned} m^2_{n\pi} &= \Big(\sum_i p_i\Big)^2 = \Big(\sum_i E_i\Big)^2 - \Big(\sum_i \vec{p}_i\Big)^2 \\ &= m^2_\tau + m^2_{\nu_\tau} - 2 m_\tau E^0_\nu \end{aligned}$$

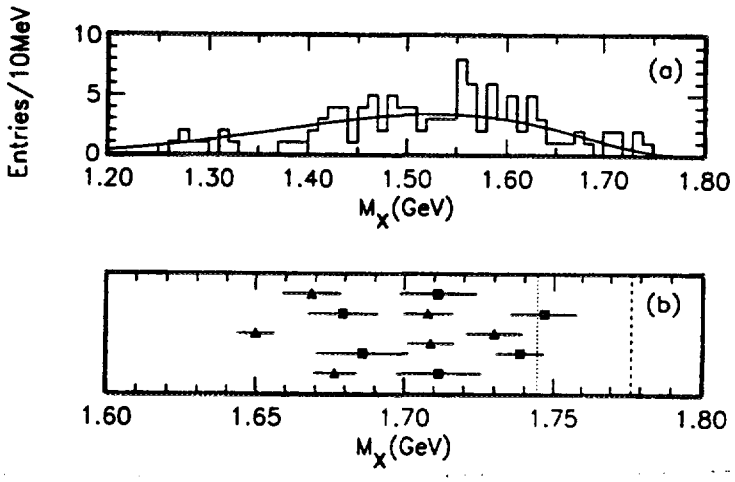

Figure 1: Measured events from CLEO. The invariant mass is denoted $M_X = m_{n\pi}$.

Table 1: Results for the tau neutrino mass from resent experiments.

Events observed	Upper limit (MeV), 95%CL	Collaboration
20	31	ARGUS [4]
113	32.6	CLEO [5]
25	24	ALEPH [6]

Here E_ν^0 is the energy of the tau-neutrino in the rest frame of the decaying tau. With $E_\nu^0 \geq m_{\nu_\tau}$ we obtain a kinematic limit

$$m_{n\pi} \leq m_\tau - m_{\nu_\tau}$$

The distribution of $m_{n\pi}$ is not known exactly. However, it is argued that the distribution should be sensitive to m_{ν_τ} only close to the kinematic limit and there the shape of the distribution is dominated by the phase space factor. The data from CLEO are shown in figure 1.

The results are summarized in table 1. One notes that CLEO has about the same upper limit as ARGUS although they observed much more events. This is because the distribution of $m_{n\pi}$ is broad and most events provide no information about m_{ν_τ}. One event close to the kinematic limit, where the expected distribution drops rapidly to zero, may easily dominate the final result. ARGUS has such events whereas CLEO does not. The background analysis of both collaborations show that the expected number of misidentified events should be much smaller than one.

The ALEPH collaboration performed a different analysis. In addition to $m_{n\pi}$ they used also the sum of the pion energies as a second variable in the analysis giving a much better upper limit. They report that their upper limit would rise to 40 MeV if only $m_{n\pi}$ would be used. There is no obvious reason why ARGUS and CLEO could not do the same analysis and it would be interesting to see the result.

3. The μ–Neutrino Mass

All recent measurements of the mass of the muon neutrino have been performed at PSI [7, 8]. The latest experiment has been presented by P. Kettle at this school and here I give only a short summary.

Studied is the pion decay at rest.

$$\pi^+ \longrightarrow \mu^+ \nu_\mu$$

Using 4-momentum conservation $p_\pi = p_\mu + p_\nu$ it is easy to derive a formula for the mass of the muon neutrino.

$$m_{\nu_\mu}^2 = m_\pi^2 + m_\mu^2 - 2m_\pi\sqrt{m_\mu^2 + p_\mu^2}$$

Hence the masses of the pion and muon and the 3-momentum of the muon are needed. As the formula above involves the difference of large numbers high precision measurements are necessary. The result for the muon momentum is

$$p_\mu = 27\,792\,000 \pm 110\,\mathrm{eV/c},$$

a 3.7 ppm measurement. Whereas the mass of the muon is known with sufficient precision there has been a longstanding problem with the pion mass. It is now believed to be solved [8]. The upper limit for the muon neutrino mass is given by

$$m_{\nu_\mu} < 170\,\mathrm{keV} \quad (90\ \%\ \mathrm{CL}).$$

Considering the precision required for this result, significant improvements are certainly difficult to achieve.

4. The Electron–Neutrino Mass

The best direct limits for the mass of the electron neutrino have traditionally been obtained from studies of the beta decay of tritium.

$$^3\mathrm{H} \longrightarrow {}^3\mathrm{He}^+ \ e^- \ \bar{\nu}_e$$

For the decay of a bar nucleus, the energy distribution of the decay electrons is given by

$$N(E) := \frac{dN}{dE} \sim F(Z,W)pW\varepsilon^2\sqrt{1 - \frac{m_{\nu_e}^2}{\varepsilon^2}}, \quad \varepsilon \geq m_{\nu_e}$$

where $\varepsilon = E_0 - E$ is the neutrino energy, $W = E + m_e$, and $E_0 \approx 18.6$ keV is the endpoint energy (for $m_{\nu_e} = 0$). The Fermi function $F(Z,W)$ is a phasespace correction, taking into account the deceleration in the Coulomb field of He^{++} $(Z = 2)$. The complete spectrum of tritium is shown in figure 2. The spectrum is sensitive to a non-zero neutrino mass only close to the endpoint, i.e. for small neutrino energies. This is shown in the inset.

Table 2: Results for the electron neutrino mass from recent experiments. The column $m_{\nu_e}^2$ (all data) gives the results when all measured data are analysed. The upper limit (UL) is at 95% confidence level.

Experiment	Source	$m_{\nu_e}^2$ (eV^2)	$m_{\nu_e}^2$ (all data)	UL (eV)
Los Alamos [9]	T_2 gas	$-147 \pm 68 \pm 41$	-230	9.3
Zürich [10]	CHT monolayer	$-24 \pm 48 \pm 61$	same	11
Mainz [11]	frozen T_2	$-39 \pm 34 \pm 15$	-120	7.2
Livermore [12]	T_2 gas	$-130 \pm 20 \pm 15$	same	–
Troitsk [13]	T_2 gas	-22 ± 5	-60	4.35

The physical parameters of the spectrum are the neutrino mass m_{ν_e} and the endpoint energy. The latter is related to the atomic mass difference of tritium and ^{3}He which however is not known with sufficient accurary. Hence tritium data are analysed with E_0 treated as a free parameter. This should be contrasted with the tau neutrino experiments in section 2 where the endpoint (the kinematic limit) was used in the analysis. With tritium information for the neutrino mass m_{ν_e} comes only from the spectrum shape and the measured quantity is the mass squared $m^2_{\nu_e}$ and not the mass. It is accepted practice that $m^2_{\nu_e}$ is allowed to take on negative values. This may occur due to statistical fluctuations and has no physical meaning. Of course if a result is strongly negative we may suspect that there is a systematic error.

The results from recent experiments are summarized in table 2. The values in the column labeled $m^2_{\nu_e}$ are denoted best estimates in the cited references. Obviously all results are negative, some quite significantly. This is not the whole story. In the next column I have listed the results provided *all* measured data are included in the analysis. These values, when applicable, are even more negative. The obvious conclusion to be drawn is that something must be wrong either with the experiments or with the interpretation of the data, i.e. the fitted model. In the following I will briefly discuss what it could be.

The beta decay of tritium is a superallowed transition between two mirror nuclei with isospin $T = 1/2$. The ft–value is 1135 s, similar as for neutron decay. Hence one does not expect that some complicated nuclear effects are affecting the spectrum shape. Because of the small decay energy recoil effects should also be negligible.

The Fermi function can be computed exactly only for a point-like nucleus. The correction for the finite size of the nucleus is of order 10^{-4} for tritium and depends only weakly on energy. If taken into account in the analysis this correction is found to be negligible.

Radiative corrections (QED) for beta decay has been calculated to first order in the fine structure constant α. As we are only interested in the shape, it can be written in the form

$$S = 1 + \frac{\alpha}{2\pi} O\Big(\ln \frac{2\varepsilon}{m_e}\Big).$$

There is a logarithmic singularity right at the endpoint (for $m_{\nu_e} = 0$), which however is only present in the correction and not in the spectrum. Also this correction has a small effect on the fitted value of $m^2_{\nu_e}$.

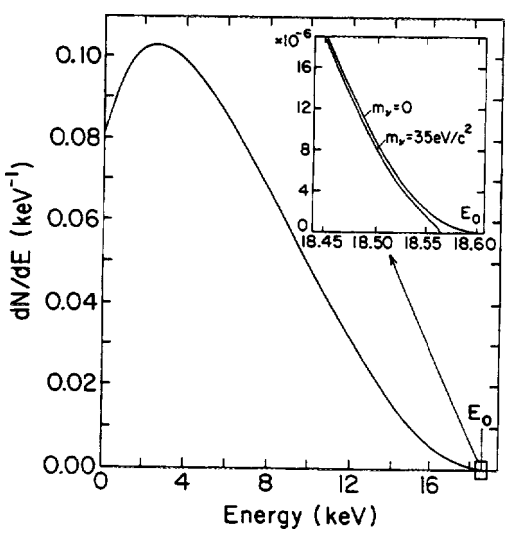

Figure 2: Beta spectrum of tritium.

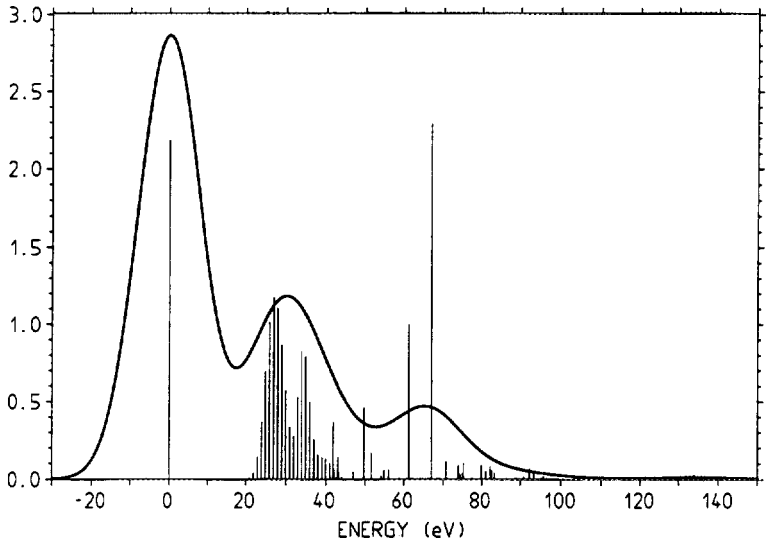

Figure 3: Transition probabilities to electronic final states in the decay of T_2. The solid line is the same distribution but convoluted with a Gaussian with 17 eV FWHM.

In the analysis of all tritium data so far, it was assumed that the electron neutrino is created in a mass eigenstate. With neutrino mixing and with a certain choice for the mass eigenvalues, one can produce noticeable distortions in the measured range of a tritium spectrum. However, all groups with strongly negative $m^2_{\nu_e}$ values say that such a model does either not fit the data or gives inconsistent results.

In experiments tritium is bound to some molecule R–T, which may be excited during the decay. Hence we have a multi-channel process

$$\text{R–T} \longrightarrow (\text{R–He}^+)_n \;\; e^- \;\; \bar{\nu}_e$$

where n denotes quantum numbers of the product molecule (which may be unbounded). It is easy to see that this process is fast compared with the orbital frequencies of the bound electrons, i.e.

$$\frac{T_{\text{escape}}}{T_{\text{orbit}}} = \frac{a_{\text{B}}/v}{2\pi a_{\text{B}}/(\alpha c)} = \frac{1}{2\pi}\frac{\alpha}{v/c} \approx 4 \times 10^{-3}$$

and the sudden approximation should be applicable. The transition probabilities to a final state n are then given by overlap matrix elements

$$W_{0n} = |\langle \Psi_0(\text{R–T}) | \Psi_n(\text{R–He}^+) \rangle|^2$$

Extensive computations have been performed using the sudden approximation. Figure 3 shows the result for the T_2 molecule [14]. The transition probability from ground state to ground state is 57.4%. It is believed that within the framework of the sudden approximation, the accuracy of the computations for T_2 is actually better than needed for the present experiments.

We should now ask for the validity of the sudden approximation. The magnitude of the leading order correction is determined by a small time parameter (also called the Sommerfeld parameter)

$$\eta = \frac{\alpha}{v/c} = 2.63 \times 10^{-2}.$$

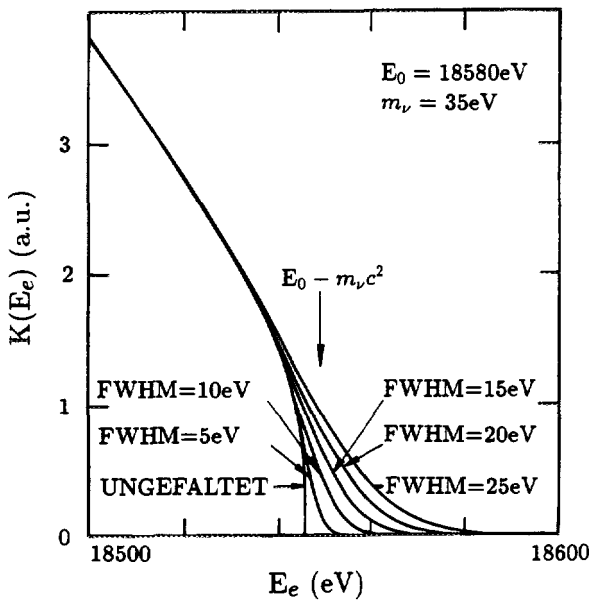

Figure 4: Kurie plot for an assumed neutrino mass $m_{\nu_e} = 35$ eV and for several widths of the resolution function.

The same parameter determines also the size of the matrix elements and the leading order correction is thus

$$\delta W_{0n} \sim O(\eta^2) = 7 \times 10^{-4}.$$

This is a factor of 30 to 70 smaller than what would be required to 'explain' the experimental results for T_2, i.e. making $m^2_{\nu_e}$ compatible with zero. Calculations have been performed for the T atom by several workers. In this case a 'accidental' cancelation occur making the corrections even smaller. For example the correction for the ground state probability is $\delta W_{00} = -2 \times 10^{-4}$ to be compared with the sudden approximation value $W_{00} = 0.702$.

I should mention two more things. Presently there is a project [15] to calculate corrections to the sudden approximation for the T_2 molecule and one should not draw far reaching conclusions before this difficult task is completed. In a recent diploma thesis a different approach was used [16]. Assuming an initial wave function for the electron created in the decay, the time dependent Schrödinger equation for the T atom was solved numerically. An amazingly large correction $\delta W_{00} \approx -0.05$ was found. This work *must* be checked independently.

There are many experimental effects which must be properly taken into account to avoid systematic errors. Here I mention just two and refer to [2] for a more thorough discussion. Figure 3 shows the endpoint region of the tritium spectrum as a Kurie plot, defined by

$$K(E) = \sqrt{N(E)/(FpW)}.$$

Far below the endpoint, $K(E)$ should be a straight line. At the kinematic limit $E_0 - m_{\nu_e}$ and for infinite resolution, $K(E)$ drops to zero with a vertical slope if $m_{\nu_e} > 0$. This signature of a nonzero neutrino mass gets more and more diminished with increasing width of the resolution function. This is not a problem if properly taken into account. However, if the assumed resolution function is too narrow, a fit gives a smaller value of $m^2_{\nu_e}$, becoming negative if the expected value is close to zero. This is an example of a general rule. If any of the distributions needed for the analysis is erroneously taken to be too narrow, the fitted value of $m^2_{\nu_e}$ is shifted in the negative direction.

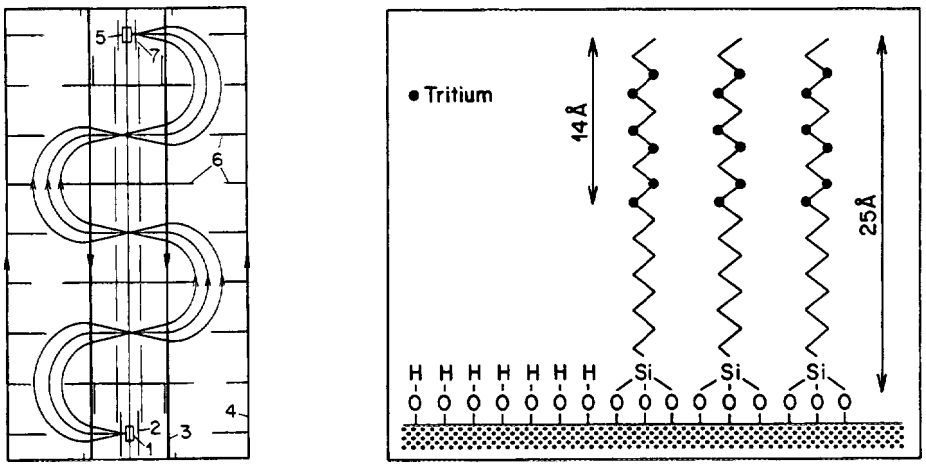

Figure 5: Left: Cross section of the Zürich spectrometer. Source 1, grids 2,7 current conductors 3,4, detector 5, baffles 6. The distance between source and detector is 2648 mm. Right: Model of the monolayer tritium source.

Tritium sources must be thin, in fact so thin that the probability for one inelastic interaction in the source is a small number. It is not sufficient to know the average energy loss, the whole distribution is needed. This is a problem which in my view has not always been appreciated. One reason is that the energy loss distribution has a very extended tail which is difficult to measure and for which theoretical extrapolations may be even more suspect.

In the following I briefly discuss the various tritium experiments. It is of course not possible here to go into any details and I refer to the original publications (see table 2).

Figure 5 (left) shows a cross-section of the spectrometer used in the Zürich experiment. It is of the Tret'yakov type. Electrons from the source are focused onto the detector in a toroidal magnetic field in four 180° bends. The tritium data were taken by stepping a high voltage applied to the source at fixed magnetic field. The resolution was 17 eV FWHM. A model of the tritium source is shown on the right side of figure 5. It was produced by chemically growing a monolayer of hydro-carbon chains on a suitable surface. There are six tritium atoms per molecule. This source is distinguished by its well defined structure and its very small thickness. Only 2% of the detected electrons had made an inelastic interaction in the source layer.

Data were recorded from 920 eV below to 180 eV above the endpoint. The results indicate a high degree of internal consistency of the data. This is shown in figure 6. Plotted are the fitted neutrino mass squared and endpoint energy as a function of a energy E_{cut} below which the data points were excluded from the fit for this test. Within a narrow band of statistical fluctuations the parameters are independent of E_{cut} as it should be. For the final result in table 2 all data were used.

The first experiment using a gaseous tritium source was performed in Los Alamos. A schematic of the set-up is shown in figure 7. The experiment in Livermore is similar. The source consists of a long tube. Tritium gas enters the tube in the middle and streams to the ends where it is pumped away by large mercury diffusion pumps. The tritium gas is recycled through a palladium foil. Decay electrons are transported in a strong longitudinal magnetic field from the source tube into a Tret'yakov type spectrometer. The energy resolution was about 22 eV for the Los Alamos and 18 eV FWHM for the Livermore experiment. The fraction of electrons making an inelastic interaction before leaving the source tube, was also similar, being 8.5% (Los Alamos) and 12% (Livermore).

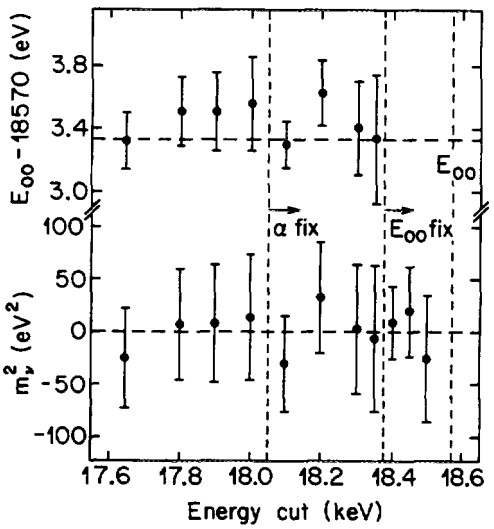

Figure 6: Fitted neutrino mass squared and endpoint energy when data points below the energy E_{cut} are excluded from the fit.

The Livermore group finds an anomalous bump in their spectrum close to the endpoint which seemingly cannot be accounted for by experimental effects. As a consequence they did not publish an upper limit for m_{ν_e}.

The groups in Mainz and Troitsk (Moscow) use instruments which they call solenoid retarding spectrometers with adiabatic magnetic collimation. The set-up from Mainz is shown in figure 8. The source is located in a strong magnetic field B_i. The electrons emitted in the forward direction spiral along the field lines into a large vacuum tank where the magnetic field drops to a small value B_f, typically $B_f/B_i = 1/3000$. The adiabaticity theorem shows that most of the transverse energy $E_{i\perp}$ at the source is converted into longitudinal energy

$$E_{f\parallel} = E_i - \frac{B_f}{B_i} E_{i\perp}.$$

At the centre of the tank, a electrostatic potential barrier is generated by a set of cylin-

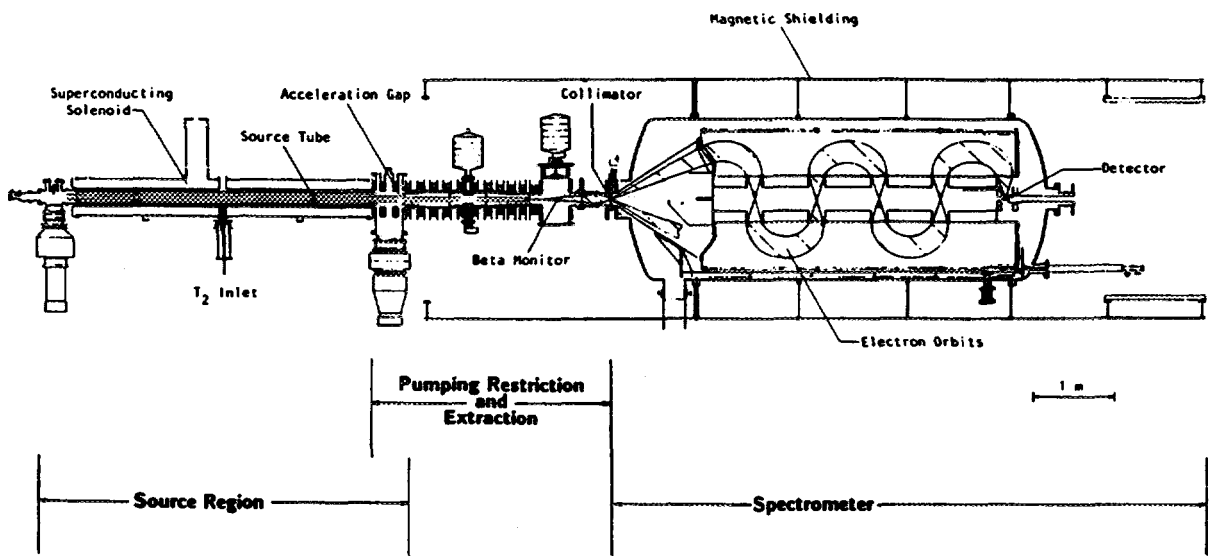

Figure 7: Overview of the Los Alamos tritium experiment. The overall length of the apparatus is 16 m.

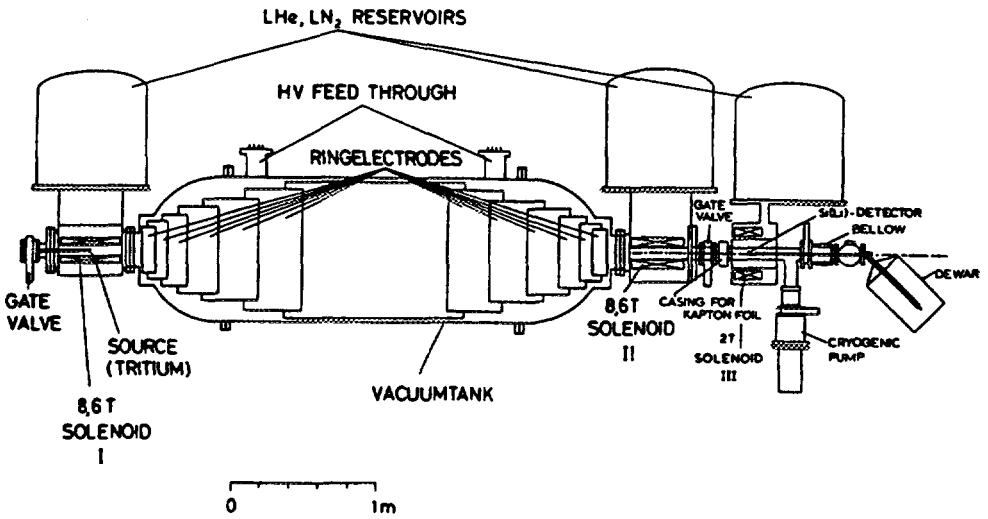

Figure 8: Schematic view of the Mainz retarding spectrometer.

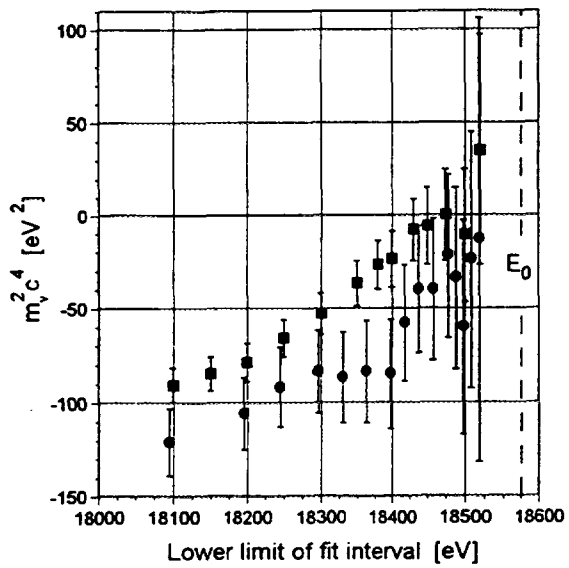

Figure 9: Fitted $m^2_{\nu_e}$ as a function of the data range for two runs (dots and squares) from the Mainz experiment.

drical high voltage electrodes. Electrons with sufficient energy pass the barrier and are reaccelerated and focused onto a detector, all other electrons returning to the source. Hence the integral of a spectrum is measured. The energy resolution, defined as the energy range over which the transmission curve drops from one to zero, was 6 eV at Mainz and 3.7 eV at Troitsk.

The source at Mainz was frozen tritium whereas a gaseous source was used at Troitsk with a set-up similar to Los Alamos. From the information given in the publications the fraction of electrons interacting in the source, can be estimated. I find 13% for Mainz and 16% to 26% for Troitsk (rather thick source).

Both groups have collected data with very high statistical power. Unfortunately, the fitted $m^2_{\nu_e}$ have highly significant negative values if all measured data are used and moreover show an unphysical dependence on the energy range. In addition a step-like distortion (corresponding to a line in a differential spectrum), about 10 eV below E_0, seems to be present in the Troitsk data. It is unclear to me whether this is something

interesting or just an experimental artifact.

Conclusion

The direct measurements have so far given no indication for a nonzero (positive) mass of any of the three known neutrinos. The experiments measuring the tau and the muon neutrino are good shape. The tritium experiments are in an unfortunate situation. It is unclear to me whether the problems are experimental or theoretical or a combination of both. The electronic final states distribution have been calculated, but the results have never been tested experimentally. The most important question to be answered is about the validity of the sudden approximation.

References

[1] G. Gelmini and E. Roulet, Rep. Prog. Phys. 58, 1207, 1995.

[2] E. Holzschuh, Rep. Prog. Phys. 55, 1035, 1992.

[3] E.W. Otten, Nucl. Phys. B (Proc.Suppl.) 38, 26, 1995.

[4] ARGUS Collaboration, Phys. Lett. B 292, 221, 1992.

[5] CLEO Collaboration, Phys. Rev. Lett. 70, 3700, 1993.

[6] ALEPH Collaboration, Phys. Lett. B 349, 585, 1995.

[7] K. Assamagan *et al.*(PSI), Phys. Lett. B 335, 231, 1994.

[8] K. Assamagan *et al.*(PSI), Phys. Rev. D 53, 6065, 1996.

[9] R.G.H. Robertson *et al.*(Los Alamos), Phys. Rev. Lett. 67, 957, 1991.

[10] E. Holzschuh *et al.*(Zürich), Phys. Lett. B 287, 381, 1992.

[11] Ch. Weinheimer *et al.*(Mainz), Phys. Lett. B 300, 210, 1993.

[12] W. Stoeffl and D.J. Decman (Livermore), Phys. Rev. Lett. 75, 3237, 1995.

[13] A.I. Belesev *et al.*(Troitsk), Phys. Lett. B 350, 263, 1995.

[14] O. Fackler *et al.*, Phys. Rev. Lett. 55, 1388, 1985.

[15] A. Saenz, University of Konstanz, Germany, private communication.

[16] T. Rohde, Diploma Thesis, University of Giessen, Germany.

UPPER LIMIT OF THE MUON-NEUTRINO MASS AND CHARGED-PION MASS FROM THE MOMENTUM ANALYSIS OF A SURFACE MUON BEAM

PRESENTED ON BEHALF OF THE $P_{\mu+}$COLLABORATION BY

PETER-RAYMOND KETTLE
Paul-Scherrer-Institut, CH-5232 Villigen-PSI, Switzerland.
E-mail: kettle@psi.ch

ABSTRACT

Using a surface muon beam and a magnetic spectrometer equipped with a position-sensitive detector, we have measured the muon momentum from pion decay at rest $\pi^+ \rightarrow \mu^+\nu_\mu$, to be $p_{\mu+} = (29.79200 \pm 0.00011) MeV/c$. This value together with the muon mass and the favoured pion mass leads to an upper limit of 0.17 MeV (90% CL) for the muon-neutrino mass.

1. Introduction

The question of whether neutrinos have non-zero masses is of fundermental importance in both particle physics and cosmology. The main quantity to be determined from the present experiment is the muon-neutrino mass m_{ν_μ}. This mass is derived from three quantities: the momentum $p_{\mu+}$ of muons originating from the decay $\pi^+ \rightarrow \mu^+\nu_\mu$ at rest ($p_{\mu+}$ ≈29.79 MeV/c, measured in this experiment) and the masses of the negative pion $m_{\pi-}$ and the muon $m_{\mu+}$ (measured in other experiments). Assuming the validity of the CPT-theorem and four-momentum conservation in the decay of the pion, leads to an expression for the squared muon-neutrino mass, which is based only on the above three quantities:

$$m_{\nu_\mu}{}^2 = m_{\pi-}{}^2 + m_{\mu+}{}^2 - 2m_{\pi-}(m_{\mu+}{}^2 + p_{\mu+}{}^2)^{1/2}. \quad (1)$$

A new method employing a surface muon beam (a beam of muons originating from the decay of π^+-mesons at the surface of a pion production target) was chosen, which gives significant advantages compared to our previous method using a π^+-beam stopped in a scintillator [1]. The main advantage being that the density of muons in phase space is four orders of magnitude higher than previously.

2. Experimental Method and Set-up

In the present method protons with a kinetic energy of 590 MeV, from the PSI isochronous cyclotron produce π^+-mesons in a graphite target. A fraction of these pions, which decay nearly at rest and at the surface of the target, produce muons which have their momentum vector such that they can be accepted by the ~ 1% wide momentum band of the πE1 beam-line, c.f. Fig.1. A Wien filter is used to suppress the positron contamination in the beam. The selected muons are focussed onto the

centre of the collimator A (width 0.12mm, height 10mm, thickness 0.3mm), one of a set of three copper collimators, placed inside the homogeneous field of the spectrometer magnet. The collimators B (width=height=10mm) and C (width 14mm, height 10mm) define respectively the horizontal and vertical angular acceptance.

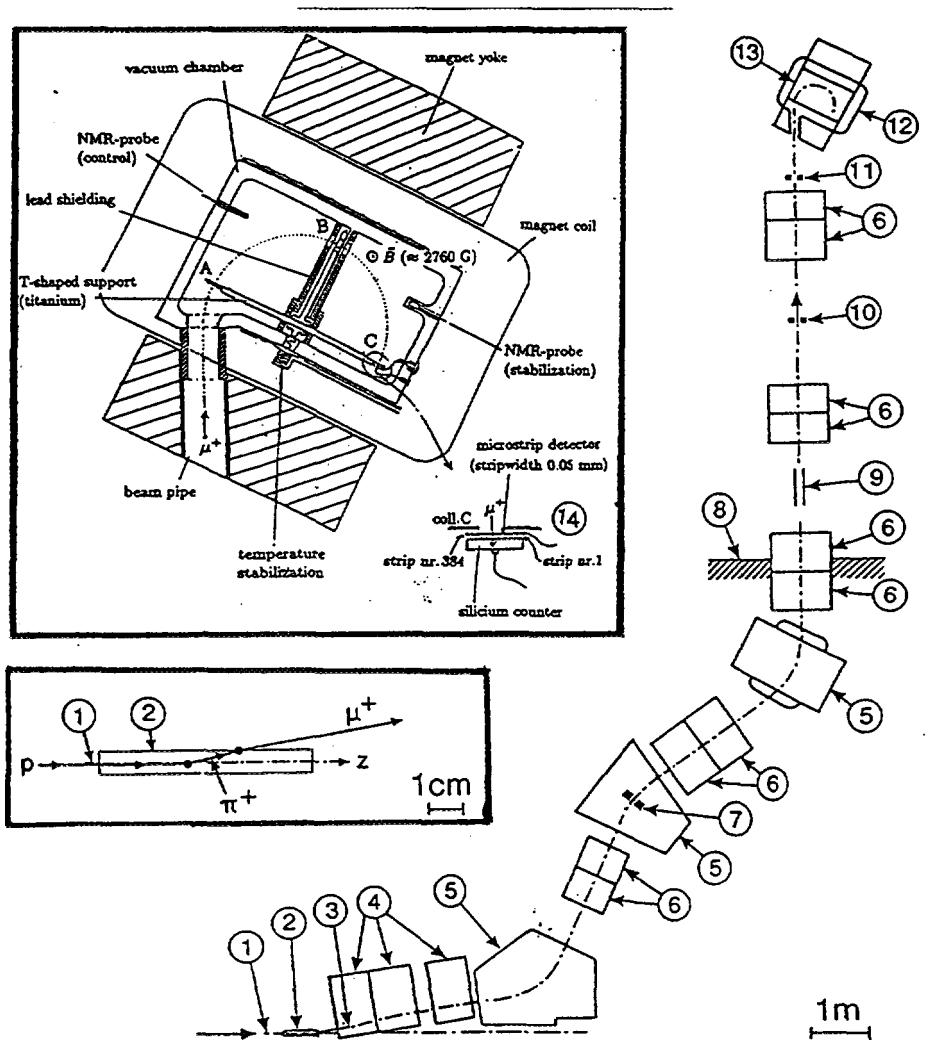

Fig. 1. Experimental set-up: 1) Central trajectory of 590MeV proton beam; 2) pion production target(graphite); 3) central trajectory of muon beam; 4) half-quadrupole magnets; 5) dipole magnets; 6) quadrupole magnets; 7) collimator defining the beam momentum acceptance; 8) concrete shielding of proton channel; 9) crossed-field particle separator(Wien filter); 10) lead collimator; 11) remotely movable collimator system (normally open); 12) magnetic spectrometer; 13) pole of spectrometer; 14) muon detectors (silicon microstrip and single silicon surface barrier detectors); A,B,C copper collimators.

These are chosen such that the spectrometer accepts only the central, almost uniformly populated part of the beam phase space. The angular distribution of the muons is measured by means of a remotely movable set of horizontal and vertical slits, placed 1.5m upstream of collimator A and two small scintillators on either side of the collimator opening. The muons are detected after passing collimator C by means of two silicon detectors, one a microstrip detector placed just in front of a large silicon surface barrier detector.

Forty-four momentum spectra (each consisting of the distribution of hits in the microstrip detector) were recorded at six different magnetic field settings (275.4–276.4 mT), spaced closely about the corresponding initial decay momentum of 29.79 MeV/c. Figure 2 shows such a spectrum taken at a spectrometer setting of 275.5 mT. The sharp edge, indicated by c) in Fig.2 is due to decay muons which originate at the surface of the graphite production target. The distribution between c) and g) contains muons from stopped pion decays inside the target. The peak at d) originates from energy-loss straggling of the muons. The flat distribution at b) comes from 'cloud' muons i.e. muons from π^+-decay in flight. The momentum band transmitted by the πE1-channel corresponds to the part between a) and e). Where as the distribution at f) is predominantly due to muons scattered on the jaws of the collimators.

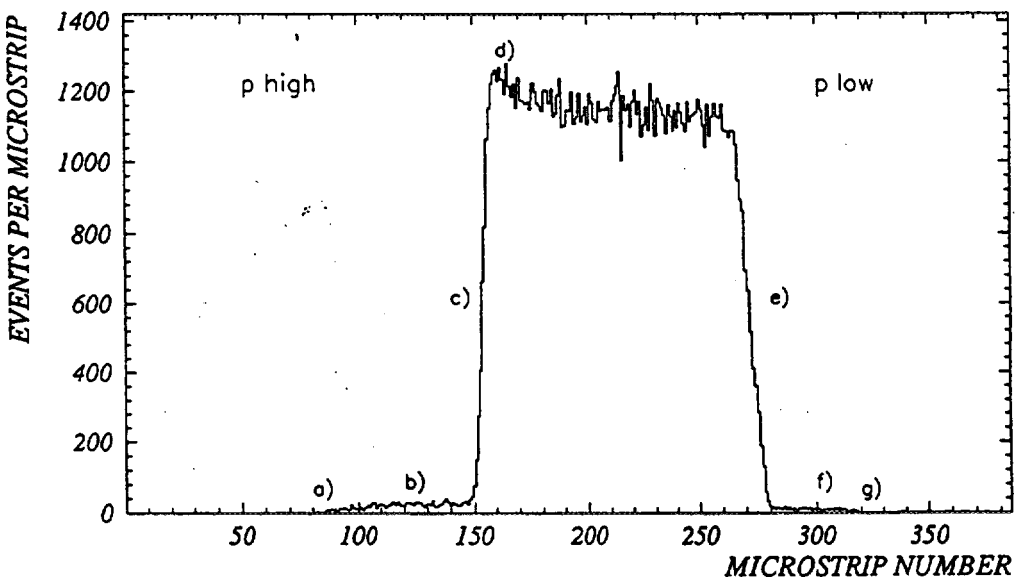

Fig. 2. Experimental Microstrip Spectrum taken at a spectrometer field of 275.5mT

3. Results

The measured muon momentum spectra, obtained from the microstrip detector are fitted to Monte-Carlo generated spectra, taking into account: the spatial distribution of pions in the target, their kinetic energy distribution in graphite just prior to their decay and the muon energy-loss on exiting the target. The magnetic field-map of the spectrometer and the precisely measured distances of the collimators and the microstrip detector to one another are also used.

The resulting momentum p_{μ^+} [2], based on the spectra taken in 1993 is

$$p_{\mu^+} = 29.79200 \pm 0.00011 \text{ MeV/c}. \quad (2)$$

This value together with the μ^+-mass [3] and the two possible solutions (A & B) of the π^--mass from the recent re-analysis [4] of the pionic X-ray measurement of

Jeckelmann et al. leads to two solutions for the squared muon-neutrino mass. This is based on the assumptions of $m_{\pi^-} = m_{\pi^+}$, as implied by the CPT-theorem and energy and momentum conservation in π^+-decay. The $m^2_{\nu_\mu}$-dependence on the charged pion mass is illustrated in Fig.3, together with the two solutions of the Jeckelmann et al. pion mass. If one excludes solutions where the neutrino would be a 'tachyon' i.e. have a negative squared mass, then only the upper of the two solutions (elliptical overlapping regions) remains, since this extends into the region of positive $m^2_{\nu_\mu}$-values ('physical' region). The lower solution is excluded by 6 standard deviations. Thus a squared neutrino mass of

$$m^2_{\nu_\mu} = -0.016 \pm 0.023 \text{ (MeV)}^2 \tag{3}$$

is obtained. By setting the probability density function to zero outside the 'physical' region (Bayesian approach) one obtains

$$m_{\nu_\mu} \leq 0.17 \text{ MeV} \quad (90\%\text{CL}) \tag{4}$$

and a combined pion mass (Jeckelmann 94B and Assamagan 96) of

$$m_{\pi^\pm} = 139.57037 \pm 0.00021 \text{ MeV}. \tag{5}$$

This gives a somewhat smaller error than Jeckelmann 94B alone because only the right–hand upper ellipse extends into the physical region.

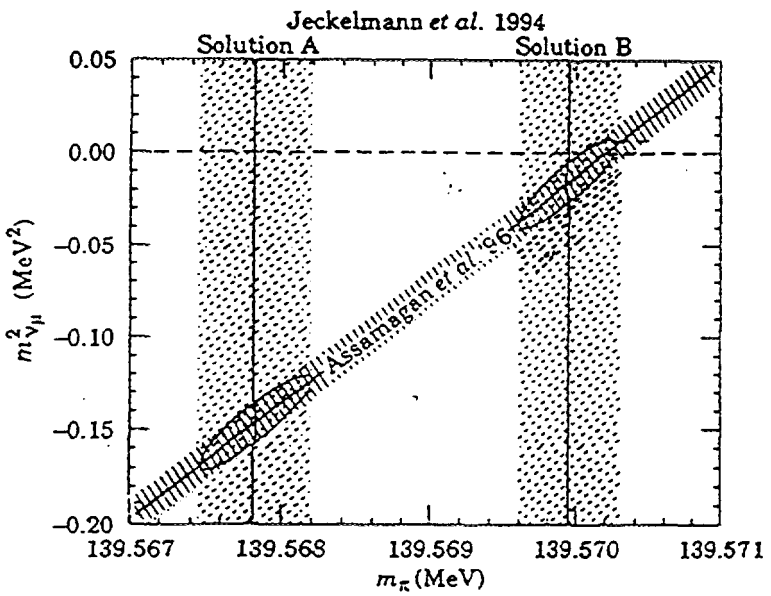

Fig. 3. Allowed regions of the $(m^2_{\nu_\mu}, m_\pi)$ plane; shaded bands correspond to $\pm$ 1σ.

The uncertainty of $m^2_{\nu_\mu}$ in equation 3 is dominated by the pion-mass uncertainty which at present has a relative uncertainty of 2.5 ppm [4]. A new pion-mass measurement, at present underway at PSI, hopes to reduce this relative uncertainty to 1 ppm [5]. Fig.4 shows how the upper limit of $m_{\mu\nu}$, given in equation 4, varies with the relative uncertainty of the pion-mass measurement (assuming the p_{μ^+}-value of equation 2 and the muon mass stay the same). Shown are the two cases, one where the central value of the pion-mass stays at its present value, yielding a slightly negative value for $m^2_{\nu_\mu}$ (equation 3) and the other case where the pion-mass value gives a central value of $m^2_{\nu_\mu}$ equal to zero.

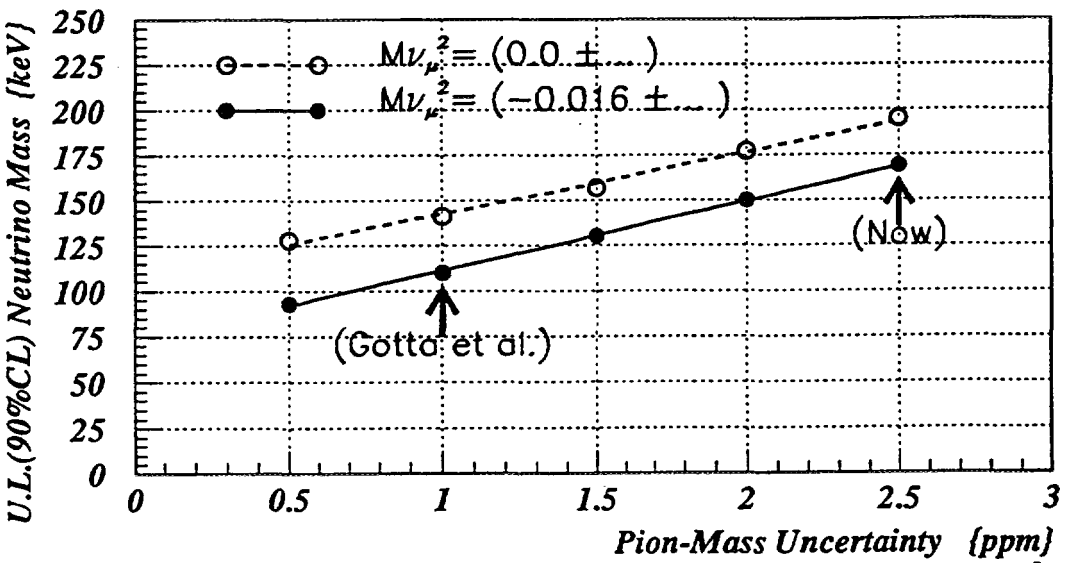

Fig. 4. Upper limit of m_{ν_μ} versus relative uncertainty of pion-mass

4. References

1. M. Daum et al., *Phys. Lett.* **B265** (1991) 425.
2. K. Assamagan et al., *Phys. Rev.* **D 53** (1996) 6065.
3. Particle Data Group, *Phys. Rev.* **D 54** (1996) 1.
4. B. Jeckelmann et al., *Phys. Lett.* **B 335** (1994) 326.
5. D. Gotta et al., *PSI-proposal R-94-01.*

SUMMER SCHOOL ON PHYSICS WITH NEUTRINOS, AUGUST 4 - 10, 1996

Schedule	Monday, Aug. 5	Tuesday, Aug. 6	Wednesday, Aug. 7	Thursday, Aug. 8	Friday, Aug. 9
08.30 - 10.00	Petcov	Raffelt	Dar	Janka	Camilleri
10.00 - 10.30	Coffee				
10.30 - 12.00	Raffelt	Petcov	Janka	Hampel	Steinberger
12.15	Lunch				
13.00 - 16.15		extra seminars			
16.30 - 17.00	Coffee				
17.00 - 18.15	Jetzer	Busto	Hampel	Caldwell	
18.30	Dinner				19.00
20.00-(20.45) - 21.30	Holzschuh/ Ould-Saada	Drexlin/ Daum	extra seminars	Straumann	Conf. Dinner

List of Topics

Zuoz Summer School on „Physics with Neutrinos"

Zuoz, August 4 - 10, 1996 (Aug. 4 and 10 are days of travel)

L = Lecture / S = Seminar / ES = Extra Seminar

	Solar Neutrinos	
S. PETCOV	Neutrinos Beyond the Standard Theory	2 L
A. DAR	Standard Physics Solution to the Solar Neutrino Problem?	1 L
W. HAMPEL	Solar Neutrino Experiments	2 L
	Oscillations	
D.O. CALDWELL	LSND Results and their Implications	1 L
L. CAMILLERI	Neutrino Oscillation Experiments	1 L
	Neutrinos and Astrophysics	
G.G. RAFFELT	Neutrino Masses in Astrophysics and Cosmology	2 L
H.-Th. JANKA	1. Neutrinos from Type-II Supernovae and the Neutrino-driven Supernova Mechanism	1 L
	2. Numerical Models of Protoneutron Stars and Type-II Supernovae - Recent Developments	1 L
Ph. JETZER	Neutrinos and Dark Matter in Galactic Halos	1 L
	History	
N. STRAUMANN	Early History of Gauge Theories and Weak Interactions	1 L
	Neutrino Properties	
J. BUSTO	Experiments on Double Beta Decay	1 L
F. OULD-SAADA	Electromagnetic Properties of Neutrinos	1 S
G. DREXLIN	KARMEN: Neutrino Spectroscopy at ISIS	1 S
M. DAUM	Search for a Neutral Particle of Mass 33.9 MeV in Pion Decay	1 S
E. HOLZSCHUH	Direct Measurements of Neutrino Masses	1 S
	Extra Seminars on Wednesday:	
A. DAR	Extinction of Life by Neutron Star Fusion	1 ES
J. STEINBERGER	Measurement of Rb	1 ES

Short Seminars on Tuesday:

P.-R. KETTLE	Upper Limit of the Muon-Neutrino Mass and Charged-Pion Mass from the Momentum Analysis of a Surface Muon Beam	1 ES
E. KOLBE	Neutrino Scattering on ^{12}C and $^{16}0$	1 ES
J. SCHWIEGER	Pauli Effects in Double Beta Decay	1 ES
T. KOSMAS	Neutrino Mixing in μ-e-Conversion	1 ES
A. HUSAIN	Neutrino Spin Flip in Collapsing Stars	1 ES
N. MUKHOPADHYAY	Neutrino Excitation of Delta Resonance	1 ES

List of speakers

BUSTO Jose, Université de Neuchâtel, Physics Dept., CH-2000 Neuchâtel, Switzerland

CALDWELL David O., University of California, Physics Dept., USA Santa Barbara CA 93106, USA

CAMILLERI Leslie, CERN/PPE, CH-1211 Genève 23, Switzerland

DAR Arnon, Technion, IL-32000 Haifa, Israel

DAUM Manfred, Paul Scherrer Institut, CH-5232 Villigen-PSI, Switzerland

DREXLIN Guido, Forschungszentrum Karlsruhe, Inst. f. Kernphysik I, D-76021 Karlsruhe, Germany

HAMPEL Wolfgang, Max-Planck-Inst. f. Kernphysik, D-69029 Heidelberg, Germany

HOLZSCHUH Eugen, Uni Irchel, Physik Institut, CH-8057 Zürich, Switzerland

JANKA Hans-Thomas, Max-Planck-Institut f. Astrophysik, D-85740 Garching, Germany

JETZER Philippe, Paul Scherrer Institut, CH-5232 Villigen-PSI, Switzerland

OULD-SAADA Farid, Uni Zürich, Physik Institut, CH-8057 Zürich, Switzerland

PETCOV Serguey, SISSA, I-34014 Trieste, Italy

RAFFELT Georg G., MPI f. Physik, D-80805 München, Germany

STEINBERGER Jack, CERN/PPE-LE, CH-1211 Genève 23, Switzerland

STRAUMANN Norbert, UNI Irchel Theor. Physik, CH-8057 Zürich, Switzerland

List of participants

ANNIS Patrio, CERN PPE, CH-1211 Genève, Switzerland

ASTE Andreas, Uni Zürich, CH-8057 Zürich, Switzerland

BALL Patricia, CERN Theory Division, CH-1211 Genève, Switzerland

BARENBOIM Gabriela, Dept. de Fisica Teorica, E-46100 Burjasot - Valencia, Spain

BARNETT Irene, Paul Scherrer Institut, 5232 Villigen PSI, Switzerland

BENSLAMA Kamal, University of Lausanne, Inst. de Physique, CH-1015 Dorigny/Lausanne, Switzerland

CARLOGANU Cristina, Niels Bohr Institute, DK-2200 Copenhagen, Denmark

CONTI Davide, Inst. für Teilchenphysik ETH Hönggerberg, CH-8092 Zürich, Switzerland

CUYPERS Frank, Paul Scherrer Institut, F1-Theoriegruppe, CH-5232 Villigen PSI, Switzerland

DANIELS David, Harvard University, High Energy Physics Laboratory, USA- Cambridge MA 02138, USA

DEGAUDENZI Hubert, Institute de Physique Nucleaire, CH-1522 Lucens, Switzerland

DEUTSCH Jules, Centre de Physique Nucléaire, Univ. Catholique de Louvin, B-1348 Louvain la Neuve, Belgium

DEVIDZE Gela, Joint Institute for Nuclear Research JINR, Lab. of Theoretical Physics, GUS-141980 Dubna, Moscow Region, Russia

EGGER Johny, Paul Scherrer Institut, F1, CH-5232 Villigen PSI, Switzerland

FETSCHER Wulf, Paul Scherrer Institut, CH-5232 Villigen PSI, Switzerland

GREULACH Martin, Univ. Kaiserslautern, Fachbereich Physik, D-67663 Kaiserslautern, Germany

GRGIC Gordana, Institut de Physique de l'universite de Neuchatel, CH-2000 Neuchâtel, Switzerland

HEEGER Karsten M., University of Washington, Dept. of Physics, USA-WA98195 Seattle, USA

HERRMANN Torsten, Paul Scherrer Institut, F1-Theoriegruppe, CH-5232 Villigen PSI, Switzerland

HUNDERTMARK Stephan, DESY Institute for High Energy Physics, D-15738 Zeuthen, Germany

HUSAIN Athar, Department of Physics, Quaid-i-Azam University, PAK- Rawalpindi, Pakistan

IANNI Aldo, Lab. Nazionali del Gran Sasso, Ist. Naz. di Fisica Nucleare, I-67010 Assergi AQ, Italy

JÜNGER Peter, Univ. Erlangen-Nürnberg, Physik Inst. Abt. 4 Gr. KARMEN, Zi. 214, D-91058 Erlangen, Germany

JUNKER Klaus, Paul Scherrer Institut, F1-Theoriegruppe, CH-5232 Villigen PSI, Switzerland

KEIL Wolfgang, Max-Planck-Institut für Astrophysik, D-85740 Garching, Germany

KERÄNEN Petteri, Univ. of Helsinki, Dept. of Physics, Theory Division, FIN-00014 Helsinki, Finland

KETTLE Peter-Raymond, Paul Scherrer Institute, F1, CH-5232 Villigen PSI, Switzerland

KOLBE Edwin, Institut für Physik der Univ. Basel, CH-4056 Basel, Switzerland

KOSMAS Theocharis, Institute of Theoretical Physics, D-72076 Tübingen, Germany

KUNZ Christine, Paul Scherrer Institut, F1-Theoriegruppe, CH-5232 Villigen-PSI, Switzerland

LOCHER Milan, Paul Scherrer Institut, F1-Theoriegruppe, CH-5232 Villigen PSI, Switzerland

MANEIRA Carvalho José, INFN-Sezione di Milano - Sezione Particelle Elementari, I-20133 Milano, Italia

MARKUSHIN Valeri, Paul Scherrer Institut, F1-Theoriegruppe, CH-5232 Villigen PSI, Switzerland

MONTANINO Daniele, Univ. di Bari, Dipartimento di Fisica, I-70126 Bari, Italy

MORGAN David, College of William and Mary, Dept. of Physics, USA- Williamsburg, VA 23187, USA

MUKHOPADHYAY Nimai, Physics Dept., Rensselaer Polytechnic Institutute, Troy, NY 12180-3590 New York, USA

PALERMO Luca, Physik Institut UNI Irchel, CH-8057 Zürich, Switzerland

PEPPINO Giaritta, Physik Institut UNI Irchel, CH-8057 Zürich, Switzerland

PLUQUET Alain, DSM/Dapnia/SPP, F-91191 Gif sur Yvette Cedex, France

RATHOUIT Patrick, CEA SACLAY DAPNIA/SphN, F-91191 Gif-Sur-Yvette cedex, France

RIGHINI Pierpaolo, INFN Sezione di Cagliari, I-09127 Cagliari, Italy

ROSENFELDER Roland, Paul Scherrer Institut, F1-Theoriegruppe, CH-5232 Villigen PSI, Switzerland

ROSSI Claudia, Dipartimento di Fisica e INFN, I-67010 Coppito (AQ), Italy

ROSSWOG Stephan, Institut für Physik der Univ. Basel, CH-4056 Basel, Switzerland

SALATHÉ Andreas, Physik Institut UNI Irchel, CH-8057 Zürich, Switzerland

SCHOTTMÜLLER Jörg, Paul Scherrer Institut, F1 (1111), CH-5232 Villigen PSI, Switzerland

SCHWIEGER Jörg, Institute of Theoretical Physics, D-72076 Tübingen, Germany

SCIALOM David, UNI Irchel, Inst. f. Theor. Physik, CH-8057 Zürich, Switzerland

STOCKINGER Peter, Institut für Theoretische Physik der Universität Wien, A-1090 Wien, Austria

THIELEMANN Friedel, UNI Basel, Theor. Physik, CH-4056 Basel, Switzerland

VON ROTZ Stefan, Paul Scherrer Institut, F1-Theoriegruppe, CH-5232 Villigen PSI, Switzerland

VOROBEL Vit, Charles University, Faculty of Mathematics and Physics, Dept. of Nuclear Physics, TCH-18000 Praha-8, Czech Republic

VUOPIONPERÄ Raimo, Univ. of Helsinki, SEFT, Research Institute for High Energy Physics, FIN-00014 Helsinki, Finland

WALTER Hans-Christian, Paul Scherrer Institut, F1, CH-5232 Villigen PSI, Switzerland

WEBER Peter, Paul Scherrer Institut, CH-5232 Villigen PSI, Switzerland

WENK Philipp, Physik Institut UNI Irchel, CH-8057 Zürich, Switzerland

WIAUX Vincent, Institut de Physique Nucleaire, Univ. Catholique de Louvain, B-1348 Louvin-La-Neuve, Belgium

ZHENG Hanqing, Paul Scherrer Institut, F1-Theoriegruppe, CH-5232 Villigen PSI, Switzerland

PAUL SCHERRER INSTITUT

Paul Scherrer Institut
CH-5232 Villigen PSI
http://www.psi.ch

Phone 056 310 21 11
Fax 056 310 21 99